ILLINOIS CENTER FOR TRANSPORTATION

Report No. FHWA-ICT-26-006

Development of a Pavement Friction Management Program

Run Hu
Renan Santos Maia
Babak Asadi
Ramez Hajj
Yanfeng Ouyang
Priscilla Tobias
Hao Wang

ICT Project R27-264

May 2026

ISSN: 0197-9191
ICT Series Report No. 26-006
https://doi.org/10.36501/0197-9191/26-006

TECHNICAL REPORT DOCUMENTATION PAGE

1. Report No.	2. Government Accession No.	3. Recipient's Catalog No.
FHWA-ICT-26-006	N/A	N/A

4. Title and Subtitle	5. Report Date
Development of a Pavement Friction Management Program	May 2026
	6. Performing Organization Code N/A

7. Authors	8. Performing Organization Report No.
Run Hu, Renan Santos Maia, Babak Asadi (https://orcid.org/0000-0002-4946-8793), Ramez Hajj (https://orcid.org/0000-0003-0579-5618), Yanfeng Ouyang (https://orcid.org/0000-0002-5944-2044), Priscilla Tobias, and Hao Wang	ICT-26-006 UILU-2026-2006

9. Performing Organization Name and Address	10. Work Unit No.
Illinois Center for Transportation Department of Civil and Environmental Engineering University of Illinois Urbana-Champaign 205 North Mathews Avenue, MC-250 Urbana, IL 61801	N/A **11. Contract or Grant No.** R27-264

12. Sponsoring Agency Name and Address	13. Type of Report and Period Covered
Illinois Department of Transportation (SPR) Bureau of Research 126 East Ash Street Springfield, IL 62704	Final Report 9/1/23–5/31/26 **14. Sponsoring Agency Code**

15. Supplementary Notes

Conducted in cooperation with the U.S. Department of Transportation, Federal Highway Administration.
https://doi.org/10.36501/0197-9191/26-006

16. Abstract

This project aims to develop a comprehensive framework for statewide pavement friction management and safety-oriented decision-making for IDOT. The project was structured into several key tasks. First, a literature review was conducted to synthesize existing research on pavement friction measurement, friction-crash relationships, investigatory levels, and friction-based treatment strategies. Second, a survey and an assessment of current agency practices were carried out to understand how friction data are collected, processed, and incorporated into project selection and maintenance decisions across peer states. Third, statewide friction data were compiled, cleaned, and spatially integrated into databases for roadway and intersection peer groups to evaluate friction coverage, measurement density, and variation across facility types. Fourth, safety performance functions were developed with explicit consideration of pavement friction and other roadway and intersection characteristics to support risk-based safety evaluation. In parallel, a new life cycle cost analysis (LCCA) framework was established to integrate friction and other pavement surface condition measures (such as the IDOT Condition Rating Survey) into a unified treatment selection model, explicitly accounting for pavement deterioration, treatment effectiveness, and traffic loading. This LCCA framework was further extended to network-level site screening and prioritization through a decision-tree-based approach. In addition, IDOT-specific aggregate policy was assessed with an emphasis on incorporating friction performance into mixture design considerations. Digital image processing techniques, including the Aggregate Imaging Measurement System, have been previously applied to characterize the angularity and surface texture of Illinois aggregates and their degradation under simulated polishing. Morphological indices derived from these prior investigations were compiled and used as inputs for friction prediction modeling, supporting a more proactive, material-level approach to pavement safety performance. The tasks' outcomes were synthesized into a schematic design of the Illinois friction management system. Finally, educational materials were developed to support statewide training on fundamental pavement friction management concepts. Overall, the project establishes a practical, data-driven foundation for integrating friction performance into safety analysis, material selection, and maintenance planning.

17. Key Words	18. Distribution Statement
Pavement Friction, Traffic Safety, Safety Performance Functions, Crash Modification Factors, Pavement Management, Preservation Treatment, Decision Trees, Aggregate, Network Screening	No restrictions. This document is available through the National Technical Information Service, Springfield, VA 22161.

19. Security Classif. (of this report)	20. Security Classif. (of this page)	21. No. of Pages	22. Price
Unclassified	Unclassified	88+ appendices	N/A

ACKNOWLEDGMENT, DISCLAIMER, MANUFACTURERS' NAMES

This publication is based on the results of **ICT-R27-264: Development of a Pavement Friction Management Program**. ICT-R27-264 was conducted in cooperation with the Illinois Center for Transportation; the Illinois Department of Transportation; and the U.S. Department of Transportation, Federal Highway Administration.

Members of the Technical Review Panel (TRP) were the following:

- John Senger, TRP Chair, Illinois Department of Transportation
- David Adedokun, Federal Highway Administration
- Katherine Beckett, Illinois Department of Transportation
- Doug Keirn, Illinois Department of Transportation
- Todd Schmidt, Federal Highway Administration
- Michael Short, Illinois Department of Transportation
- Dylan Specht, Illinois Department of Transportation
- Jewell Stone, Illinois Department of Transportation
- William Warfel, Illinois Department of Transportation

EXECUTIVE SUMMARY

This project developed a comprehensive framework to support statewide pavement friction management and safety-oriented treatment decision-making for the Illinois Department of Transportation (IDOT). Pavement friction is a critical surface characteristic that directly influences vehicle braking and steering performance, particularly under wet conditions. Maintaining adequate friction is therefore an important component of roadway safety management. The primary objective of this study was to establish a data-driven methodology that integrates pavement friction into safety analysis, pavement treatment and material selection considerations, and pavement asset management.

The study was organized into several major tasks. First, an extensive review of existing research was conducted to synthesize current knowledge related to friction measurement technologies, friction's impacts on safety, friction investigatory levels used by transportation agencies, and friction-related pavement preservation treatments. In addition, a survey and assessment of current agency practices were carried out to understand how friction data are collected, processed, and incorporated into pavement management and project prioritization across peer states. These activities provided a foundation for identifying gaps in existing practices and opportunities for improving friction management in Illinois.

Statewide friction data were then compiled and integrated with roadway and intersection inventory, crash records, and preservation histories into comprehensive databases. These datasets allowed the research team to evaluate friction data coverage, measurement density, and spatial-temporal variations across different facility types and pavement conditions. The integrated databases served as the foundation for subsequent safety analysis and pavement management.

Safety performance functions and crash modification factors were developed with explicit consideration of pavement friction and other roadway and intersection characteristics. These models were used to evaluate the relationship between friction levels and crash risk and to support safety assessments across the roadway network. The safety analysis demonstrated how friction information can be incorporated directly into safety analysis to identify locations where friction-related risks may be elevated.

To support treatment selection and planning, the study developed a life cycle cost analysis framework that integrates safety performance indicated by friction with Condition Rating Survey (CRS), another pavement surface condition measure used by IDOT. The framework explicitly accounted for deterioration of pavement conditions, treatment effectiveness, heterogeneities across different traffic load levels, and pavement facility types. This approach enabled a joint consideration of both pavement friction and other pavement surface characteristics (e.g., CRS) when determining optimal treatments. The framework was further extended to support network-level site screening and treatment prioritization through a decision-tree-based methodology designed to assist agencies in identifying locations where treatments could provide the greatest improvements to both safety and pavement conditions.

The project also evaluated Illinois aggregate polices with respect to their influence on pavement friction performance. Conventional asphalt mixture design practices primarily focus on volumetric properties and mechanical performance, while friction performance is typically evaluated only after construction. The research team examined how aggregate characteristics influence pavement friction and explored opportunities to incorporate friction considerations earlier in the mixture design process. Digital image processing techniques, including the Aggregate Imaging Measurement System (AIMS), have previously been used to characterize aggregate angularity and surface texture and to evaluate how these characteristics change under simulated polishing. Morphological indices derived from these prior investigations were compiled and used to support friction prediction modelling and to assess the potential implications for aggregate selection policies. The results showed that aggregate source and gradation play important roles in determining friction performance, and incorporating friction-related considerations into aggregate selections and policies could potentially benefit sites with high friction demand.

Building upon these findings, the project synthesized the outcomes of the research tasks into a conceptual design for a statewide pavement friction management system for Illinois. The proposed framework demonstrates how friction data can be systematically incorporated into safety evaluations, aggregate selections, pavement management decisions, and future friction measurements. The project also developed educational materials to support statewide training and knowledge transfer on pavement friction management strategies and practices. Overall, the project provided a practical and data-driven foundation for integrating pavement friction considerations into IDOT's safety and pavement management processes. The framework developed through this research provides guidance for long-term pavement performance evaluations, proactive treatment decisions, and aggregate policy development across the Illinois highway network.

TABLE OF CONTENTS

LIST OF FIGURES

LIST OF TABLES

CHAPTER 1: INTRODUCTION

INTRODUCTION AND RESEARCH OBJECTIVE

The Illinois Department of Transportation (IDOT) has set a goal of driving traffic-related fatalities and severe injuries toward zero. In the past decades, IDOT has made many progressive efforts to systematically improve the safety of its roadway systems. For example, IDOT developed and updated network-level safety performance functions (SPFs) and crash modification factors (CMFs) for various roadway and intersection peer groups to understand the statistical relationships among traffic volumes (i.e., risk exposure), geometric design features, crash severity type, and crash density (number of crashes per unit of time, per unit roadway length, or per intersection). The SPFs and CMFs and the associated Empirical-Bayesian analyses (Hauer, 1992; Hauer et al., 2002) allow IDOT to calculate the potential for safety improvements values for each roadway segment and intersection. Illinois' efforts in developing its own SPFs and CMFs (Tegge et al., 2010; Tegge & Ouyang, 2009) have successfully led to:

- The development of Safety Tiers and Safer Roads Index (SRI) ratings (e.g., critical, high, medium, low, minimal) for the Highway Safety Improvement Program.
- Development and implementation of state-of-the-art safety analysis tools (such as crash analysis tools).
- IDOT's implementation of *Highway Safety Manual* crash prediction tools, Safety Analyst, and the Interactive Highway Safety Design Model.
- Economic analysis programs, among many others, that help IDOT prioritize their safety projects.

Pavement friction is widely considered an important factor that contributes to the reduction of fatal and serious injury crashes, especially those related to run-off-the-road crashes, rear-end crashes, and wet-surface crashes near intersections, curves, and steep grades. The amount of available friction as well as the amount of friction needed, otherwise known as friction demand, are essential to safety performance. The available pavement friction is influenced by many factors including the type and texture of surface treatment, aggregate type and source, construction methods, and age of surface. Friction demand varies based on classification of roadways, geometric design, environment, and traffic conditions. Higher values of pavement friction can help compensate for deficient geometric designs and maintain traction of vehicles within the intended lane (Lenzo, 2022). Degradation of pavement friction, especially at a rate faster than anticipated, will negatively influence safety performance. Hence, a pavement friction management program that provides for regular collection of network-level friction data, monitors pavement friction and material performance, establishes investigatory friction thresholds, and includes proactive maintenance with the aim of improving pavement friction can be very beneficial for asset management and safety performance. This can also serve as the basis for screening and prioritization of pavement preservation and resulting safety enhancements.

Illinois does not currently have a well-defined policy for routine friction measurements, monitoring and improvement of pavement friction, or guidelines for the use of potential friction treatments. In addition, existing safety analyses in Illinois have not sufficiently addressed the impacts of pavement friction on traffic safety, nor has the effectiveness of pavement friction treatments in reducing crashes been assessed quantitatively. A few peer states (e.g., Kentucky, Virginia, North Carolina, Florida, and Texas) have made pioneering efforts on developing pavement friction management systems. However, their empirical relationships between pavement surface friction and crash risk cannot be directly used for Illinois because of variations from state to state and even across locations within the same state. These factors make the development of a statewide friction management program necessary in Illinois. To support the development of such a framework, this project builds upon an extensive literature review on pavement friction management and related topics. Previous studies have examined pavement friction evaluation technologies, friction investigatory levels, the effectiveness of different pavement surface treatments in restoring pavement friction, and the relationships between pavement friction, roadway characteristics, and crash risk. In addition, the influence of pavement materials and surface texture on friction performance has been widely investigated in both laboratory and field studies. A literature review of these topics—including friction measurement methods, preservation treatments, safety benefits of friction, and the impacts of pavement materials and surface characteristics—is provided in Appendix A.

The objective of this project is to develop a comprehensive, network-level pavement friction management program for Illinois that provides opportunities to develop safer roadways for the traveling public. This program will build upon traffic, safety, and pavement data collection and statistical modeling to establish a systematic investigatory decision-tree procedure that evaluates the safety performance of a roadway site and estimates the potential safety benefit of installing surface treatments that provide the necessary levels of friction. SPFs and CMFs are developed for a range of crash types (e.g., wet-weather and run-off-the-road crashes), severity types (e.g., K, A, and B), roadway site types (e.g., curves and intersections on state maintained and/or municipal roads) and roadway facility types (i.e., roadway peer groups defined by functional class, traffic level, and geomety), where Illinois-specific friction measurement (skid number and later the new vision-based friction device) are explicitly incorporated in addition to traditional variables such as traffic volume, curve radius, and cross-sectional lane and shoulder widths. The SPFs and CMFs will then be used in a decision-tree framework that bridges gaps between pavement treatments and safety performance to ensure adequate friction for each type of site scenario. The analysis will help IDOT to establish a data-driven, safety-based friction management program that helps select and justify appropriate friction treatments for use on Illinois roadways as well as update its friction aggregate policy (Chapter 53 of the *Bureau of Design and Environment Manual*). The specific objectives of this project include the following items:

- Provide recommendations to the current friction collection program for safety needs.
- Quantify the impact of friction on traffic safety using statistical analysis of crashes, traffic, and roadway data.
- Establish investigatory friction thresholds for various roadway site types and facility types.

- Develop decision trees for choosing the proper treatments to improve friction and refine friction aggregate policy in current IDOT specifications.

- Develop and demonstrate a prototype of a friction management program of Illinois.

FUNDAMENTAL CONCEPTS OF PAVEMENT FRICTION

Tire-pavement friction refers to the forces developed at the interface between a vehicle tire and the road surface during braking, steering, and acceleration maneuvers. Two principal mechanisms govern these forces: adhesion and hysteresis. Adhesion arises from molecular bonding in areas of actual contact where local pressures are sufficiently high. Hysteresis reflects the energy dissipated as the viscoelastic tire rubber deforms over surface asperities during a sliding motion (Kogbara et al., 2016; Wang et al., 2014). Surface texture describes the variation of pavement surface elevation across different spatial scales, commonly quantified along the vertical (z-axis) dimension, which plays a key role in governing these friction mechanisms. The classification of texture scales follows a widely adopted framework based on texture wavelength (λ) and vertical amplitude (A), which distinguishes four regimes: microtexture, macrotexture, megatexture, and unevenness (roughness). Table 1 summarizes the wavelength and amplitude limits for each regime (Hall et al., 2009; Wambold et al., 1995).

Table 1. Texture Scales and Wavelength/Amplitude Classification Limits

Scale	Wavelength and Amplitude Limits
Microtexture	$\lambda < 0.5$ mm; $A < 0.5$ mm
Macrotexture	$0.5 < \lambda < 50$ mm; $0.1 < A < 20$ mm
Megatexture	$50 < \lambda < 500$ mm; $0.1 < A < 50$ mm
Unevenness (Roughness)	500 mm $< \lambda <$ 50 m

Of the four texture scales described above, microtexture and macrotexture have the largest impact on tire-pavement friction and are the most critical for pavement friction management. Microtexture, controlled by aggregate mineralogy and surface roughness at the fine scale, governs the adhesion component and is therefore most influential at low sliding speeds. Macrotexture, driven by aggregate gradation and particle morphology (angularity and shape), contributes to hysteresis and is critical at moderate-to-high vehicle speeds by providing surface drainage pathways that evacuate water from the tire contact patch, limiting the formation of continuous water films and preventing hydrodynamic lubrication effects (Hall et al., 2009; Henry, 2000; Wang et al., 2020).

Skid resistance refers to the ability of a pavement surface to provide adequate friction under braking and steering demands, particularly under wet conditions. When water accumulates at the tire-pavement interface, available friction is reduced substantially due to lubrication effects. In severe cases, a buildup of hydrodynamic pressure may partially or fully separate the tire from the pavement surface, known as hydroplaning. Effective skid resistance therefore requires adequate macrotexture to promote rapid water drainage and sufficient microtexture durability to maintain adhesion over the service life of the surface. From a safety perspective, skid resistance is a functional performance

attribute linked to braking distance, vehicle maneuverability, and crash risk under wet-weather conditions. The long-term evolution of friction on asphalt pavements is strongly influenced by aggregate type, mixture category, and the selection of preservation treatments, making aggregate material policy a critical lever in friction management programs.

CHAPTER 2: ASSESSMENT OF IDOT FRICTION COLLECTION METHOD AND POLICY

STATE OF PRACTICE ON PAVEMENT FRICTION MANAGEMENT

Pavement Friction Management

Efficient pavement management is crucial for ensuring traffic safety, reducing maintenance costs, and extending the lifespan of transportation infrastructure. Pavement friction management (PFM) plays a pivotal role by systematically assessing and optimizing the friction between vehicle tires and roadways. Friction directly impacts a driver's ability to steer, brake, and maintain control of the vehicle. By incorporating PFM into broader road maintenance strategies, transportation authorities can significantly decrease the incidence and severity of traffic accidents, enhance the overall driving experience, and effectively address the immediate and long-term safety concerns associated with road usage. The AASHTO (2008) *Guide for Pavement Friction* emphasizes the importance of maintaining optimal road safety through several key recommendations. It advocates for routine friction testing and systematic collection of crash data to ensure road conditions are continuously monitored. Furthermore, the guide suggests identifying specific locations where friction levels fall below investigatory thresholds, as well as areas where friction is below intervention levels or where there is a high incidence of wet-weather crashes. Based on these assessments, agencies can then develop, prioritize, and implement targeted friction treatments.

The AASHTO (2008) *Guide for Pavement Friction* also states that friction demand categories should be established logically and systematically based on highway alignment, highway features/environment, and traffic characteristics. The number of demand categories should be kept reasonably small so that enough PFM sections are available for each category from which to define investigatory friction levels. The primary steps of PFM can be summarized as follows:

- Divide the network into groups according to friction needs (friction demand categories).
- Collect friction, texture, crash, traffic, and other data.
- Analyze the data to explore investigatory and intervention threshold levels for pavement friction and texture.
- Evaluate and select friction treatments.

Data Collection

At the network level, PFM involves categorizing road sections based on alignment, environmental factors, and traffic characteristics that are directly or indirectly relevant to safety. Relevant factors for categorization include traffic volume, road classification, surface type, road age, friction, macrotexture, road geometry (including cross-slope, superelevation, vertical grade, and curvature), and crash data (both in dry and wet conditions). The two most common pavement friction measurements are the longitudinal friction coefficient, which is measured using fixed slip devices

such as the GripTester and Locked-Wheel Skid Tester (LWST), and the sideway force coefficient, measured using devices such as the Sideway-force Coefficient Routine Investigation Machine (SCRIM).

Pavement friction is significantly influenced by two key surface characteristics: microtexture and macrotexture. Microtexture, which is crucial for tire-pavement interaction at the microscopic level, is difficult to measure, and it is usually assessed using the British Pendulum Tester. Macrotexture, which affects water drainage and friction at higher speeds, is measured through different approaches. Volumetric methods like the sand patch test, laser methods including the Circular Track Meter and Surface Texture Analyzer, and high-speed devices that utilize single-spot or line lasers are commonly employed (Tobias et al., 2023). Seasonal weather changes significantly impact pavement friction. In regions like the United Kingdom and the United States, friction testing primarily occurs during summer, when friction levels are lower. Given resource limitations and optimal testing periods correlating with higher crash instances, a cyclical testing approach is advisable, where different network portions are tested biennially (de León Izeppi et al., 2017).

Data Analysis

An analytical approach should be taken to establish empirical friction thresholds tailored to each friction demand category, using comprehensive crash rate data. This analysis should encompass total crash rates, rather than exclusively focusing on wet/dry crash distinctions, to capture the full spectrum of interactions between crashes and the two critical surface properties: friction and macrotexture. This all-encompassing perspective is essential for divided and undivided roadways as well as for segments characterized by eventful or uneventful histories, ensuring a holistic understanding of the factors contributing to roadway safety (de León Izeppi et al., 2017).

A detailed analysis was conducted using data from continuous pavement friction measurement (CPFM) collected across five states (Florida, North Dakota, Texas, Virginia, and Washington) to evaluate friction performance, data coverage characteristics, and their implications for safety assessment and treatment prioritization. The data served as the foundation for developing safety performance functions (SPFs) through regression modeling. These SPFs were used to create crash modification factors (CMFs) or crash modification functions (CMFx). Figure 1 shows CMFx for various roadway facility types. The impact of friction on crashes is quite significant on urban arterials and rural multilane highways. In these types of facilities, a 10-point increase in SFN40 (sideway force number with measuring speed adjusted to 40 mph) can result in a 23% to 25% reduction in crashes (Flintsch et al., 2023).

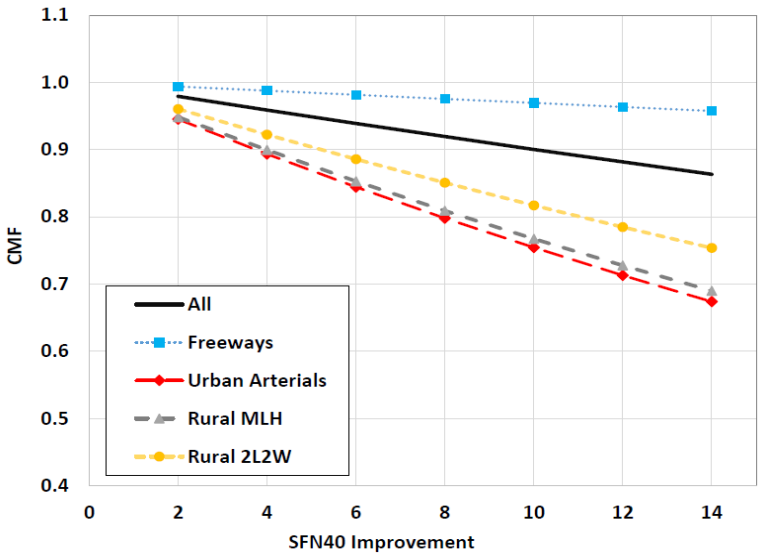

Figure 1. Graph. Correlation between CMFx and friction improvement (SFN40 from SCRIM) on different roadway facility types (Flintsch et al., 2023).

The primary purpose of these models is to quantify the impact of changes in pavement friction on road safety performance. By understanding these relationships, the analysis helps in assessing the cost-effectiveness of investments in pavement friction improvements, and the performance or investigatory thresholds for friction based on roadway type and category can be established. The analysis confirmed a strong statistical association between pavement surface frictional properties (friction and macrotexture) and crash rates. The AASHTO (2008) *Guide for Pavement Friction* outlines three methods for establishing investigatory and intervention friction levels.

i. **Using Historical Pavement Friction Data Only**: The investigatory level is set at the pavement friction value where friction loss begins to increase at a significantly faster rate. The intervention level is then set at a certain amount/percentage below (Method 1).

ii. **Using Both Historical Pavement Friction Data and Crash Data**: The investigatory level is set corresponding to a large change in friction loss rate, while the intervention level is set where there is a significant increase in crashes (Method 2).

iii. **Using Pavement Friction Distribution and Crash Rate–Friction Trend**: Plot a histogram of pavement friction and current wet-to-dry crash ratio for a given friction demand category. Determine the mean pavement friction and standard deviation. Set the investigatory level as the mean friction value minus 1.5 or 2.0 standard deviations and adjust to where wet-to-dry crashes begin to increase considerably. The same approach is used to determine the intervention level where the standard deviations are minus 2.5 or 3.0 (Method 3).

The typical analytical approaches for Method 3 are described as follows and illustrated in Figure 2:

1. **Network Friction Distribution Analysis**: Develop histograms or cumulative distribution plots of statewide (or category-specific) friction values to understand the typical distribution and identify percentile-based candidate thresholds for further evaluation.

2. **Wet-to-Dry Crash Ratio Evaluation**: Analyze the relationship between measured friction levels and the wet-to-dry crash ratio. Friction values associated with noticeable increases in crash ratios can be used to identify candidate investigatory or intervention levels.

3. **Wet Crash Frequency vs. Friction Level Analysis**: For each roadway category, estimate the mean friction level and standard deviation (Figure 2). Investigatory level is typically set near the mean minus 1.5 to 2.0 standard deviations, adjusted to the observed friction level at which wet crash frequencies begin to rise. Intervention level is typically set near the mean minus 2.5 to 3.0 standard deviations, indicating friction levels consistently associated with significantly elevated crash risk.

4. **Climate- or Facility-Stratified Threshold Determination**: Conduct analyses separately for different climate regions, functional classifications, or event sites (e.g., curves, ramps, intersections). This allows agencies to adopt friction thresholds tailored to specific operating and environmental conditions.

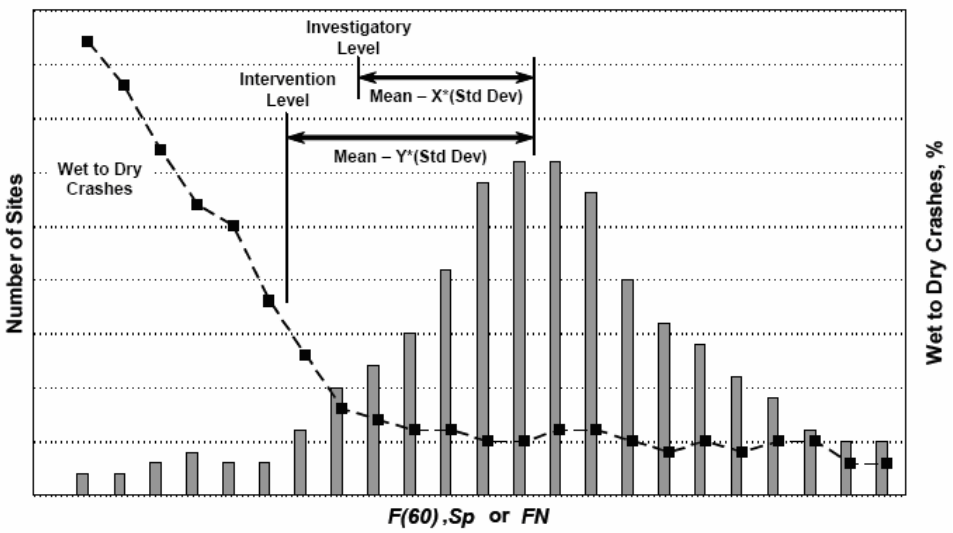

Figure 2. Graph. Establishing friction levels using pavement friction distribution and crash rate friction trend.

Friction Threshold Levels Used by State Agencies

In the last 10 years, federal and state DOTs have made attempts to develop or quantify the relationship between friction/texture and crash occurrence. Different measurements, data collected, and analysis techniques will generate different thresholds.

Illinois DOT

In Illinois, according to IDOT PTA-T3 (effective as of October 1996 and revised in February 2005), friction testing is performed using a locked-wheel skid tester at 40 mph, assessing the friction with a treaded tire in the left wheel path (FNt) and a smooth tire in the right wheel path (FNs). The state has delineated four categories for testing: all sites with wet-weather accidents, selected new construction

and rehabilitation sites, biennial retesting of previous sites, and sites based on special requests. The main factors affecting friction are the age of the surface course, traffic volume, seasonal variations, and vehicle speed. The guidelines for assessing friction related to wet-weather accidents are listed as follows (specific evaluation is needed considering traffic demands and road geometries):

1. FNt ≤ 30 or FNs ≤ 15, friction may be a factor.
2. FNt > 30 and 16 ≤ FNs ≤ 25, or 31 ≤ FNt ≤ 35 and FNs >25, uncertain.
3. FNt > 35 and FNs > 25, friction may not be a factor.

Ohio DOT

In a study commissioned by the Ohio Department of Transportation, Larson et al. (2008) analyzed the results from locked-wheel friction testing alongside wet-weather crash data. The friction tests, conducted across 90 pavement sections statewide in 2007, measured friction using both ribbed (FN40R) and smooth tires (FN40S). The study primarily focused on developing correlations between the wet-to-total crash ratio and various factors such as friction number (FN), macrotexture, speed gradient, average annual daily traffic (AADT), and the International Roughness Index (IRI). The findings are summarized in Table 2, which provides recommended values based on the data analysis.

Table 2. Recommended Intervention (Minimum) and Investigatory (Desirable or Target) Friction, Texture, and Roughness Levels by Ohio DOT (Larson et al., 2008)

Check	Variable	Intervention Level	Investigatory Level
1	a. If wet/total crash rate, and	≥ 35 percent	≥ 25 percent
1	b. Annual average number of wet pavement crashes (2- or 3-year average), then	> 3 for rural settings > 5 for urban settings	> 2 for rural settings > 3 for urban settings
1	c. Check minimum friction number	FN40Rmin < 32 or FN40Smin < 23	FN40Rmin < 42 or FN40Smin < 32
2	Minimum macrotexture		< 0.04 in (1.0 mm) (sand patch) (Based on UK criteria)
3	Roughness spikes based on 20 ft (6.1 m) sliding base length	Use the current Ohio DOT requirements	300 in./mi (4.7 m/km)

* Notes:

- Sections meeting the check 1a and 1b criteria are then friction tested to determine if poor skid resistance is the likely cause of the crashes. If all three variable criteria for check 1 are met, then a skid-resistant overlay should be planned without the need for any further evaluations. A skid-resistant overlay with non-carbonate aggregate will likely be very cost-effective.
- The minimum macrotexture depth is based on the French criteria in LCPC Bulletin Special Issue #255 on Skid Resistance (Dupont & Bauduin, 2005).
- Proactive approach: Desirable or target (investigatory level) criteria where low friction, texture, or spikes in roughness may be contributing to increased numbers of wet pavement and total crashes.

Maryland State Highway Administration

In Maryland, initiating a PFM program began with demarcating the pavement network, which involved defining site categories and setting the friction levels relevant to the Maryland State Highway Administration's pavement network (Speir et al., 2009). Table 3 shows the recommended site categories and their corresponding friction levels, which are integral for conducting both network- and project-level friction analyses. The friction level was tested by LWST with a standardized ribbed tire.

Table 3. Friction Levels for Implementation (Speir et al., 2009)

Site Category	Site Description	Threshold FN	Investigatory FN	Intervention FN	Demand Category
1	Approach railroad crossings, traffic lights, pedestrian crossings, stop and give way controlled intersections (SH only).	55	50	45	High
2	Curves with radius=<250 m, downhill gradients > 10% and > 50 m long, freeway/highway on/off ramp.	50	45	40	High
3	Approach to intersections, downhill gradients 5% to 10%.	45	40	35	High
4	Undivided highways without other geometric constraints that influence frictional demand	40	35	30	Low
5	Divided highways without any other geometrical constraints that influence frictional demand.	35	30	25	Low

United Kingdom

England originally developed SCRIM, and the skidding standards were revised based on SCRIM data of the whole trunk road network in 2004, in which a link between accident risk and skid resistance was made (Viner et al., 2005). Table 4 is a modification of the investigatory levels (and ranges for some site categories) currently used in the UK.

Table 4. Friction Demand Categories and Investigatory Levels (30 mph) in the UK (Viner et al., 2005)

Code	Road Classification Definitions	0.30	0.35	0.40	0.45	0.50	0.55	0.60	0.65
A	Motorways (interstate highways)	✓	✓						
B	Dual carriageways non-event (divided highways non-event)	✓	✓	✓					
C	Single carriageways non-event (two-lane roads non-event)		✓	✓	✓				
Q	Dual carriageways (all purpose)—minor junctions (divided highway intersection/roundabout approaches)				✓	✓	✓		
K	Approaches to pedestrian crossings and other high-risk situations					✓	✓		
R	Roundabouts					✓	✓		
G1	Gradients 5%–10%, longer than 50 m (slopes 5%–10%, longer than 160 ft)					✓	✓		
G2	Gradients ≥ 10%, longer than 50 m (slopes ≥ 10%, longer than 160 ft)					✓	✓	✓	
S1	Bend radius < 500 m — dual carriageway (curve radius < 1,600 ft — divided highways)					✓	✓		
S2	Bend radius < 500 m — single carriageway (curve radius < 1,600 ft — two-lane highways)					✓	✓	✓	

* Notes:

- In the UK, SCRIM results are normally reported as SCRIM coefficient values, equal to the SCRIM Reading multiplied by 0.0078.
- "Non-event" tangent segments are defined as roadway sections without intersections, without horizontal curves sharper than 1,600 ft (500 m) radius, and without longitudinal grades exceeding 5%.
- A reduction of 0.05 is allowed for categories A, B, C, G2, and S2 in low-risk situations (e.g., low traffic levels or risk is well mitigated, or a low incidence of accidents has been observed), as indicated by the pink check marks.

Washington State

Washington State has adopted the use of SCRIM data to refine its analysis of friction thresholds (de León Izeppi et al., 2017). They process SCRIM data into discrete 0.1 mile segments, categorize the data based on friction demands, and establish investigatory thresholds. This systematic approach aligns with Method 3 from the AASHTO (2008) *Guide for Pavement Friction*. The thresholds of SCRIM friction and macrotexture are shown in Table 5.

Table 5. SCRIM Friction and Macrotexture Threshold Results (de León Izeppi et al., 2017)

Roadway Type	SR Investigatory Level	MPD Investigatory Level (mm)
Divided	30-35	0.5-0.7
Undivided	50-55	0.7
Curves	50-55	0.7
Intersections	55-60	NA

FHWA Study

In an FHWA study conducted by Flintsch et al. (2023), microtexture is represented by SCRIM friction (SFN40), and macrotexture is characterized by the mean profile depth (MPD). The friction, macrotexture, and roadway geometry data were collected with SCRIM equipment. The network in this study includes 55,677 0.1-mile roadway segments in five states (Florida, Indiana, Texas, North Dakota, and Washington). The research team employed a graphical assessment (Figure 3), which used observed crash rates per 100 MVMT (100 million vehicle miles traveled) for different friction levels, to identify different investigatory levels (Table 6).

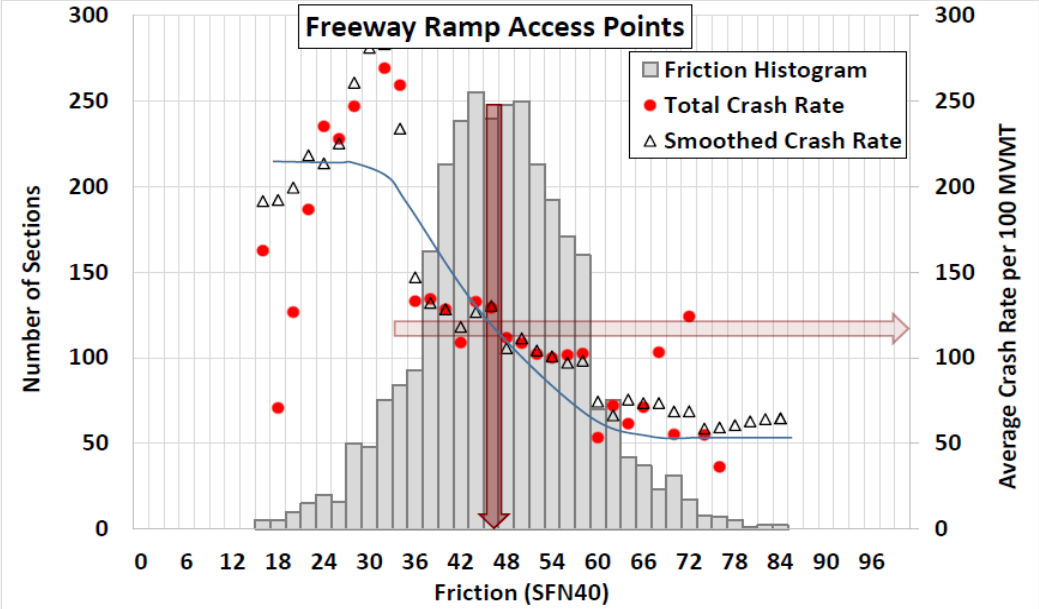

Figure 3. Graph. Friction distribution, crash rates, and estimated thresholds for freeway ramp access points (Flintsch et al., 2023).

Table 6. Summary of Threshold Analysis (Flintsch et al., 2023)

Roadway Facility Type	Site Type	Suggested FN40	Graphic Threshold
Freeways	Tangents	40	36-38
	Curves	45	42-44
	Ramp Access	45	44-46
Rural Multilane Roadways	Divided Tangents	50	48-50
	Undivided Tangents	50	48-50
	Curves	55	54-56
	Intersections	55	54-56
Rural Two-Lane, Two-Way Roadways	Tangents	50	48-50
	Curves	55	54-56
	Intersections	60	54-56
Urban and Suburban Arterials	Divided Tangents	50	48-50
	Undivided Tangents	50	48-50
	Curves	50	48-50
	Intersections	55	54-56

*Graphic threshold is the value obtained by the graphical assessment.

SURVEY RESULTS ON PAVEMENT FRICTION MANAGEMENT PROGRAM

Survey Results of Peer States

Pavement Friction Measurement

1. Michigan, South Carolina, Ohio, Texas, and Pennsylvania DOTs have a pavement friction management program, while Connecticut and Illinois DOTs currently do not have one.
2. Michigan DOT collects friction entirely with LWST every two years since 2012 and will collect continuous friction with ARRB iSAVE in 2024.
3. South Carolina DOT collects friction data with Dynatest 1295 LWST and tests every 1/3 miles. The agency collects data every three years on interstates and every six years on primary routes.
4. Texas DOT collects friction data with Dynatest 1295 LWST. It collects 50% of interstate and 25% of all other road systems annually, collected at 50 mph at 0.5-mile intervals.
5. Pennsylvania and Ohio DOTs only collect friction data by request.
6. Michigan DOT collects friction on the right-most lanes, Texas and South Carolina DOTs test the outside lane, and Ohio and Pennsylvania DOTs test all lanes.
7. Other than friction data, Michigan DOT also collects texture and roadway geometrics, Ohio and Texas DOTs also collect macrotexture data, PennDOT just started to collect horizontal curve, vertical curve, grade, and cross-section data using video log contract.
8. Except Texas DOT, no respondents developed SPFs using friction data or integrated friction data into project prioritization processes or asset management processes.
9. The respondents provided additional lessons on pavement friction management: (i) properly geolocate and reference friction test data and (ii) perform annual calibration and correlation for LWST data.

Pavement Treatment Selection

1. Major considerations in selecting pavement treatments mentioned by respondent DOTs: surface condition, traffic volume, facility type, cost, life cycle, and friction.
2. Pavement friction treatments used by respondent DOTs: chip seals, scrub seals, microsurfacing, high friction surface treatment (HFST), ultra-thin bonding wearing course (UTBWC), diamond grinding, and hot-mix asphalt (HMA) overlay.
3. Pennsylvania DOT conducted before-and-after analysis to quantify the effectiveness of treatment in crash reduction using CMFs for HFST over 500 locations.
4. Pennsylvania DOT established some policies about treatment selection such as safety warrants.

Decision-Support Computer Programs

1. None of the responding DOTs have a computer program to do cost-benefit analysis of pavement friction treatment, except PennDOT, which has an analysis tool available on PennDOT's safety infrastructure website.
2. None of the responding DOTs have a computer program or decision-tree software to assist with decision-making on pavement friction treatment selection.

Survey Results of IDOT Districts

Pavement Friction Measurement

1. The IDOT Central Office coordinates and schedules friction data testing for individual districts, as the districts usually do not have friction testing equipment. District 1 mentioned that the frequency of pavement friction data collection is the first season after construction and subsequentially every other year.
2. Recommendations from District 1: Create a site where all friction data can be accessed as it becomes available. Understand that a program works literally and may not consider history. Keep a record of crash locations that benefit from mix changes so future contracts maintain the friction mix rating, reverting to lower rated mixes would lead to resurgence of crashes/incidents. Always keep lines of communications open with construction reviewers, they are usually working in that area for many years and have insight that is not recorded on tests. Anything that is developed should also allow for district recommendations. Programs may have a broad focus to fit all districts and not address distinct local issues such as equipment availability and pavement composition.

Pavement Treatment Selection

1. In terms of the major considerations for selecting pavement treatment, District 1 mentioned treatment selection is a combination of traffic data, previous mix placed, type of business in that area and roadway geometry, Bureau of Traffic requests for higher friction treatments, and work limits. Districts 2 and 3 mentioned it is typically determined based on the roadway conditions and is largely governed by Transportation Asset Management Plan (TAMP) policies in the *Bureau of Design and Environment Manual*. District 6 mentioned life cycle, facility type, and cost, and District 2 also mentioned traffic volume, cost, and crash data.
2. For treatments in practice and their longevity, districts mentioned microsurfacing (5 or 7 to 10 years), chip seal and cape seal (7–10 years), HFST (10 years, requested by the Bureau of Traffic), HMA overlay/resurfacing (10/15~20 years), thin overlay and diamond grinding (5–10 years).
3. No district has done before-and-after analysis to quantify the treatment effectiveness in crash reduction, but District 1 mentioned durability issues with microsurfacing.

Decision-Support Computer Programs

1. None of the districts currently have a computer program or decision-tree software to do cost-benefit analysis or decision-making on treatment prioritization.

Stakeholder Interview Notes

The Federal Highway Administration (FHWA, 2017) is encouraging the use of CPFM for safety analysis instead of LWST for several reasons and is providing resources to support CPFM practices:

1. LWST does not provide enough information to properly conduct network-level analysis, and it cannot tell the complete picture of a whole highway network.

2. LWST cannot be used in high-stress areas such as intersections or ramps.

3. LWST is a discrete test (three locks per mile) and therefore does not provide 100% coverage compared to SCRIM.

FHWA mentioned most states have certain levels of PFM, but every state should treat PFM differently to fit specific conditions. A PFM toolbox is suggested to be built to include a variety of pavement treatments that improve pavement friction instead of only HFST, where agencies should consider different perspectives such as how they are fitted into benefit-cost analysis, the life cycle, and the effectiveness based on the context. FHWA also suggests DOTs implement a PFM program with a smaller scale (district-level) first. Careful consideration is recommended when deciding whether to acquire a SCRIM vehicle or contract one, because a large SCRIM vehicle requires a CDL license and is difficult to maintain and calibrate. A key aspect of measuring continuous pavement friction and implementing a PFM program is the ability to identify and flag locations that require further investigation, allowing for a proactive approach in addressing potential issues.

Pioneer Efforts from VTTI, KYTC, and NCDOT

The Virginia Tech Transportation Institute (VTTI) and Kentucky Transportation Cabinet (KYTC) have been actively involved in network-level continuous pavement friction measurement. VTTI has measured 7,000 miles using a SCRIM device at 40 mph, with data being averaged over 0.1-mile sections. KYTC has focused on higher-type roads such as interstates and state primary routes, collecting approximately 15,000 lane-miles per year using SCRIM. KYTC's approach includes collecting CPFM data in one direction one year and in the opposite direction the following year. Beyond measuring continuous friction, both VTTI and KYTC also collected other relevant roadway characteristics using SCRIM, including texture (reported as mean profile depth, MPD), curve radius, grade, and cross slope.

Regarding the correlation between SCRIM and LWST data, KYTC reported a strong correlation between SCRIM, LWST, and dynamic skid tester data (Hacker et al., 2023). VTTI noted that SCRIM data are more closely related to ribbed tire LWST measurements than to those using a smooth tire (de León Izeppi et al., 2019). In terms of friction-related safety analysis, both VTTI and KYTC have worked on developing SPFs for different site categories based on CPFM data. KYTC has integrated CPFM data analysis into their HFST project by assigning safety scores to sites and ranking them by ROI

to prioritize treatment, with significant improvements observed on state primary and secondary routes. VTTI used CPFM data to identify friction investigatory levels for different roadway facility types, primarily based on graphical interpretations of crash rates (de León Izeppi et al., 2016; Hamilton & Coley, 2021).

North Carolina DOT recently collaborated with Virginia DOT and VTTI for research projects exploring CPFM as a tool for pavement friction management programs. North Carolina DOT is planning to initialize CPFM data collection for around 5,000 miles of roadway in both directions of travel for full control facilities, then they plan to focus on rural two-lane primary routes. The agency is currently working on research projects related to CPFM data analysis to determine how crash risk is related to friction. They observed correlation between SCRIM, LWST, and Skidometer BV11 and strong correlation between cross slopes and crashes (Underwood et al., 2023).

Lessons from WDM's Data Collection

WDM is a UK-based company that utilizes CPFM and asset management strategies to proactively manage crash risks where friction is involved and help with evaluating friction degradation, friction levels, and related issues over time. WDM mentioned the key difference between other countries and the US regarding pavement friction management is the presence of long-standing policies that guide prioritization and resources when pavements are approaching investigatory or demand levels (Tobias, 2023). Several tools for the safety side have been developed to bridge the gap, such as SPFs, friction and texture investigation thresholds, friction demand levels, and prioritization lists. The authors also highlighted the challenge of determining whether friction improvements should always be tied directly to observed safety issues, a perspective that tends to promote a reactive approach. Instead, they advocated for more proactive strategies that integrate pavement friction management into the routine processes of designing, constructing, and maintaining roadways. The study further notes that several states have recognized the potential benefits of continuous friction measurement equipment such as SCRIM and are exploring its implementation, including Missouri and Maryland. A key lesson emphasized by the authors is the importance of well-designed data management systems within DOT agencies to ensure the accuracy, consistency, and long-term reliability of friction data.

Florida DOT's Practice

Florida's pavement friction management program, developed through Florida DOT District 7 and the University of South Florida, aims to explicitly link high-resolution friction data to crash-based safety analysis and project prioritization. Friction (SR40), macrotexture (MPD), and roughness (IRI) are collected using SCRIM and processed at a detailed spatial scale. The highway network is categorized into homogeneous groupings (e.g., tangents with radius ≥ 2000 ft, short and long curves with radius < 2000 ft, urban signalized intersections) to account for geometric effects. SPFs are further developed to quantify how changes in those factors (e.g., AADT, SR30, MPD, IRI, crack, grade) affect crash frequency. Investigatory levels (ILs) are defined to flag potentially problematic sites. For example, locations where friction below a certain IL and with at least 10% or more wet crashes in the past 3–5 years are advanced to Tier 2 and Tier 3 for formal treatment assessment.

For treatment selection and prioritization, Florida enhances the traditional resurfacing prioritization procedure (based on cracking, rutting, and ride quality) by incorporating a friction-based performance ranking. Roadway segments are divided into uniform 0.1-mile subsections, and then the friction rating (FR) is calculated for each subsection based on averge SR40, ILs, and maximum and minimum values of SR40. A graphical representation of FR calculations is shown in Figure 4. These two independent rankings—the original pavement condition ranking and FR—are merged using a reciprocal rank fusion algorithm to create a combined priority index. Treatment decisions are further determined through a benefit-cost ratio framework. In summary, Florida DOT proposed a network-level screening procedure driven by both structural need and friction-related safety risk.

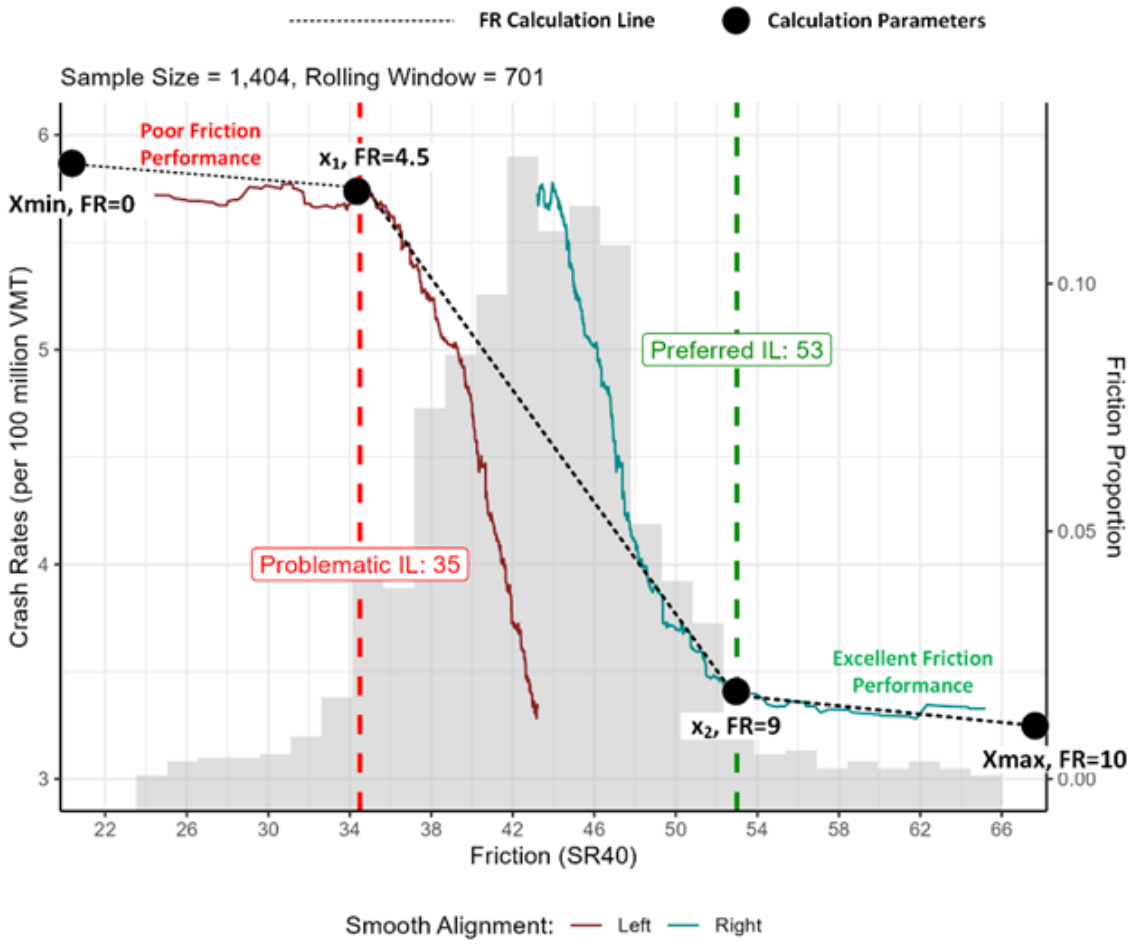

Figure 4. Graph. Graphical representation of friction rating calculation in Florida.

ANALYSIS OF FRICTION AND CRASH DATA AT IDOT

LWST Data Collection and Compilation

The existing friction data managed by IDOT is "Friction Database 2.5 – 2022.accdb," which contains tables of annual LWST friction records from 2012 to 2022, as illustrated in Figure 5. These tables include important information needed for detailed analysis such as the adjusted friction number, left or right wheel used for data collection, date of collection, and the latitude-longitude coordinates. The friction data are further merged with IDOT's Roadway Inventory GIS Database, where roadway segments are categorized into a set of roadway facility peer groups. Data analysis is conducted to (1) show the spatial and temporal pattern of LWST friction data across various roadway peer groups of different functionalities, (2) help determine the blind spots of friction data collection, (3) recommend a customized data collection frequency for different peer groups, and (4) explore the possibility of developing new site categories for pavement friction.

00_Detail

ID	Contract #	ID #	Suff	DIR	Lar	LOG	T	RA\	Adj Fi	SPD	FLOW	Wheel	TDATE	CREV	SYS	R/U	TTIME	Remarks	Latitude	Longitude
6759	74056	120363	0	East(+)	T1	0.01	1	32.7	31	35.6	29.5	Right	8/22/2012	DS	2/2	URBAN	1:26:48 PM		38.37945123	-88.39544645
6760	74056	120363	0	East(+)	T1	0.156	2	37	37	40.3	31.6	Left	8/22/2012	DS	2/2	URBAN	1:26:48 PM		38.37912753	-88.39282207
6761	74056	120363	0	East(+)	T1	0.273	3	23.4	23	40.2	30.9	Right	8/22/2012	DS	2/2	URBAN	1:26:48 PM		38.37866149	-88.39077826
6762	74056	120363	0	East(+)	T1	0.379	4	39.1	39	40.4	31.3	Left	8/22/2012	DS	2/2	URBAN	1:26:48 PM		38.37840786	-88.38887517
6763	74056	120363	0	East(+)	T1	0.455	5	20.1	21	41.4	32	Right	8/22/2012	DS	2/2	URBAN	1:26:48 PM		38.37835859	-88.387477
6764	74056	120363	0	East(+)	T1	0.52	6	32.8	33	41.1	31.7	Left	8/22/2012	DS	2/2	URBAN	1:26:48 PM		38.37836229	-88.38629962
6765	74056	120363	0	East(+)	T1	0.619	7	29.9	30	39.4	30.6	Right	8/22/2012	DS	2/2	URBAN	1:26:48 PM		38.37836798	-88.38448567
6766	74056	120363	0	East(+)	T1	0.754	8	31.9	30	36.1	28.1	Left	8/22/2012	DS	2/2	URBAN	1:26:48 PM		38.37836813	-88.38200386
6767	74056	120363	0	East(+)	T1	0.843	9	29.5	27	33.9	26.9	Right	8/22/2012	DS	2/2	URBAN	1:26:48 PM		38.3785561	-88.3804145
6768	74056	120363	0	East(+)	T1	0.916	10	36.5	34	34.4	27.7	Left	8/22/2012	DS	2/2	URBAN	1:26:48 PM		38.37874292	-88.37911861
6769	74056	120363	0	East(+)	T1	0.995	11	27.7	26	35.5	27.6	Right	8/22/2012	DS	2/2	URBAN	1:26:48 PM		38.37873376	-88.37767274
6770	74056	120363	0	East(+)	T1	1.07	12	36.5	34	34.4	27.4	Left	8/22/2012	DS	2/2	URBAN	1:26:48 PM		38.37873215	-88.37631259
6771	74056	120363	0	East(+)	T1	1.144	13	29	27	35.2	27.8	Right	8/22/2012	DS	2/2	URBAN	1:26:48 PM		38.37872139	-88.37495909
6772	74056	120363	0	East(+)	T1	1.209	14	33.9	32	35.5	28.1	Left	8/22/2012	DS	2/2	URBAN	1:26:48 PM		38.37871851	-88.37375751
6773	74056	120363	0	East(+)	T1	1.27	15	23.5	22	36.6	28.6	Right	8/22/2012	DS	2/2	URBAN	1:26:48 PM		38.37871596	-88.37264198
6774	74056	120363	0	East(+)	T1	1.35	16	32	31	36.5	28.6	Left	8/22/2012	DS	2/2	URBAN	1:26:48 PM		38.37870824	-88.37118953
6775	74056	120363	0	East(+)	T1	1.407	17	23.6	22	35.3	28.1	Right	8/22/2012	DS	2/2	URBAN	1:26:48 PM		38.37870498	-88.37013168

Figure 5. Graph. Sample friction data from IDOT's friction database.

Table 7 compares the total mileage of each peer group versus the total LWST-tested mileage from 2012 to 2022. Given that LWST is a discrete testing method, the following approach is employed to approximate the coverage of friction data collection. The coordinate information is used to match friction data with specific highway segments and defined a LWST-tested segment as any highway segment with at least one available friction record from 2012 to 2022. To avoid double-counting, friction data collected on the same roadway segments across different years were removed from the calculation. Additionally, the total number of tests during the 11-year period is recorded for each peer group, and the average number of tests per mile per year for each peer group is calculated to improve the interpretability of friction data collection results. The results indicate satisfactory LWST coverage across the network from 2012 to 2022, with all peer groups having at least one-third of their roadways covered by at least one friction record during this period. For some peer groups, such as rural freeways and urban freeways with four lanes, the coverage is around two-thirds of their total length.

Table 7. Summary of Illinois LWST Friction Data Collection Results on Different Roadway Peer Groups from 2012 to 2022

Roadway Peer Group	Length (mile)	Tested Length 2012–2022 (mile)	Percentage 2012–2022 (%)	Number of Tests 2012–2022	Number of Test per Mile per Year (#/mile/yr)
Rural Freeway, Four Lanes	2,831	2,240	79	39,763	1.61
Rural Freeway, Six+ Lanes	62	49	79	1,316	2.46
Rural Multilane Divided Highway	404	185	46	9,759	4.80
Rural Multilane Undivided Highway	39	13	35	1,417	9.55
Rural Two-Lane Highway	18,574	7,367	40	450,828	5.56
Urban Freeway, Four Lanes	1,270	912	72	28,833	2.87
Urban Freeway, Six Lanes	687	452	66	13,552	2.69
Urban Freeway, Eight Lanes	150	61	41	2,292	3.39
Urban Multilane Divided Highway	2,504	930	37	65,796	6.43
Urban Multilane Undivided Highway	1,917	804	42	79,836	9.03
Urban One-Way Arterial	384	140	36	8,844	5.75
Urban Two-Lane Highway	5,895	2,240	38	194,023	7.88

Spatial and Temporal Distribution of LWST Friction Data

Figure 6 shows the spatial distribution of tested highway segments in Illinois in 2022, which indicates robust annual coverage of friction tests. While annual LWST data collection does not encompass all roadways, it is strategically conducted across the state, focusing on key roadways that connect various counties or districts, and certain roadway segments undergo repeated friction testing over multiple years. This repeated data collection forms a valuable foundation for detailed time-series analysis, such as how annual variations in friction relate to factors such as traffic load, weather conditions, pavement treatments, and more. These statistics underscore the significant efforts made in LWST data collection over the past decade.

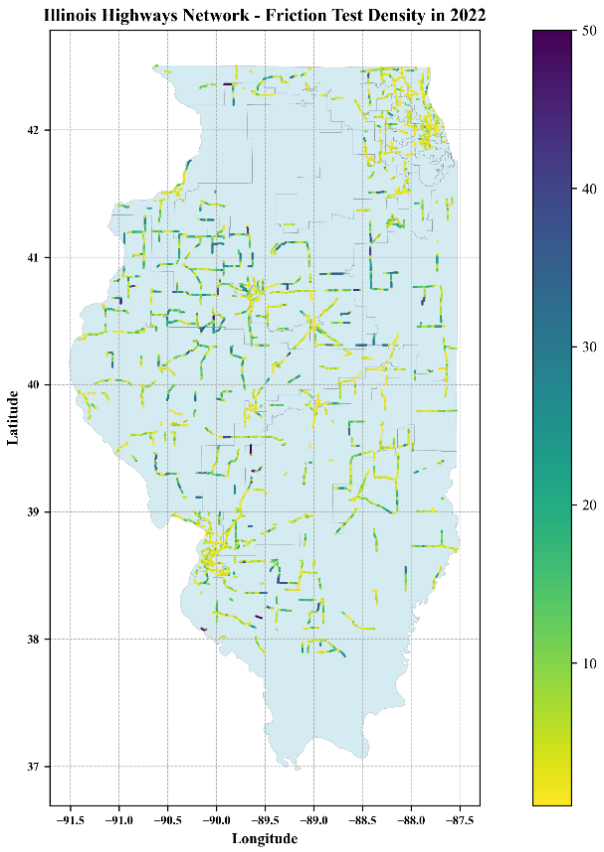

Figure 6. Map. Spatial representation of LWST collection density map in 2022.

It is important to note, however, that LWST performs one or two tests per mile, resulting in only a limited portion of the pavement surface being tested (Tobias et al., 2023). Hence, LWST data typically cannot accurately represent pavement conditions across all locations in a roadway segment, and as a result, using LWST data to represent the average friction condition of roadway segments may not always provide a highly accurate depiction. From the approximation of the average number of tests per mile per year, all peer groups have an average number less than 10 points per mile per year, with freeways having the least tests. Note that the analysis methodology relies heavily on the accuracy of the coordinates used for spatial matching with highway segments. Therefore, precise latitude and longitude data for friction measurements are essential to ensure reliable results. To enhance future analysis, it would be beneficial to record friction data alongside detailed roadway information, such as peer group, facility type, and whether the data were collected on tangents, curves, ramps, or intersections. This approach would significantly improve data utilization and aid in identifying problematic sites more effectively.

The spatial distributions of 2012–2021 friction data as a density map are shown in Appendix B. A lighter color (yellow) represents fewer tests on roadway segments, while a darker color (purple) shows denser tests. The distributions from 2012 to 2022 show a strong sparsity of data collection. Most tested roadway segments have the number of tests less than 10, while only a small portion of them experienced more than 20 tests per year. Figure 7 illustrates the variation of average friction

number across different peer groups over time, with fluctuations around the value of 40. Most peer groups show a relatively stable trend with slight improvements in average friction number across the years. However, significant fluctuations are observed between 2018 and 2020, with a minor peak in 2021 for most peer groups. These peaks could indicate major network-level maintenance activities, particularly for rural two-lane highways and urban multilane divided highways. However, the sharp increase in average friction observed in 2019 for some peer groups, such as four-lane urban/rural freeways and six-lane urban freeways, appears unrealistic. These surges are most likely due to the limited amount of friction data collected and the resulting bias during the COVID-19 pandemic.

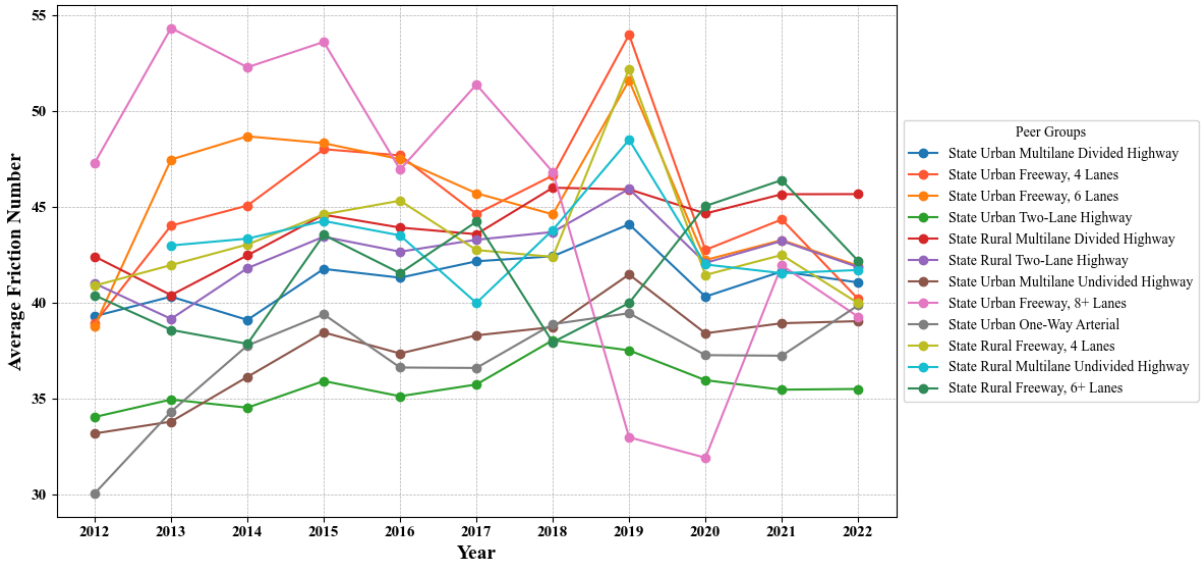

Figure 7. Graph. Average friction number per year for all peer groups.

Figure 8 and Figure 9 highlight two peer groups that lack friction data collection and provide less reliable results. As observed from Figure 8, significantly less friction data was collected in 2019 compared to other years on four-lane urban freeways. Additionally, urban freeways with eight or more lanes show the greatest fluctuation pattern. Closer inspection of its annual friction distribution in Figure 9 reveals that this variability is also due to the limited friction data collected on this peer group. This finding highlights the importance of comprehensive friction data collection to provide an accurate understanding of friction variations across the network.

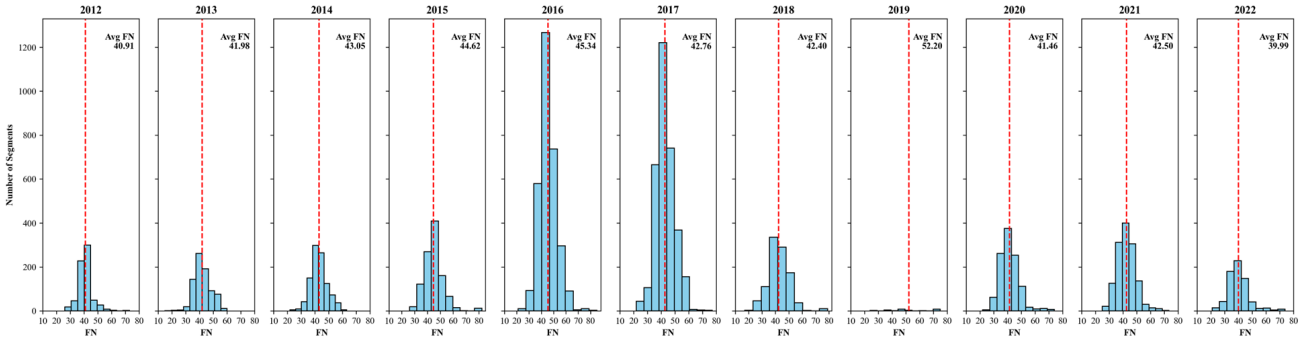

Figure 8. Histogram. Annual friction distribution for four-lane urban freeways.

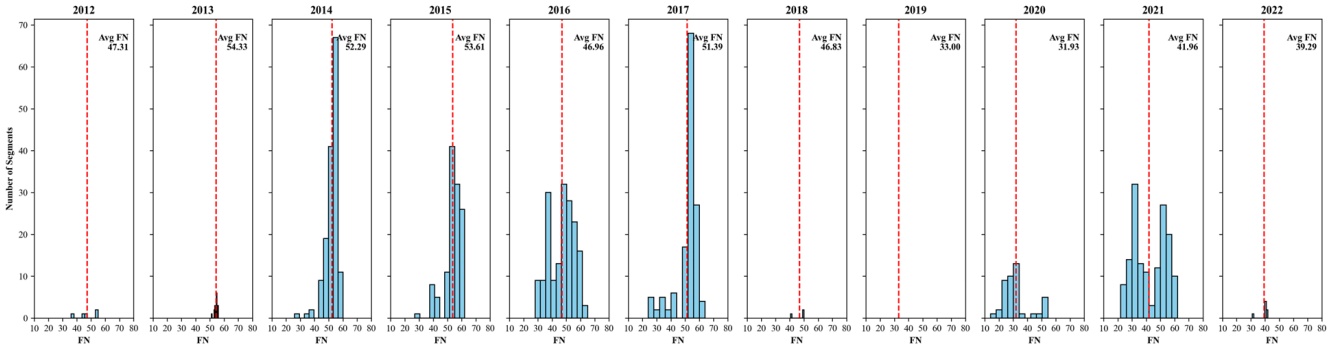

Figure 9. Histogram. Annual friction distribution for urban freeways with eight or more lanes.

Figure 10 and Figure 11 show histograms for the two most extensively tested peer groups: urban and rural two-lane highways. These groups provide the most reliable analysis due to their extensive data. The friction values for both peer groups exhibit minor fluctuations but remain generally stable over the 10-year period, with a slight upward trend. For both peer groups, there are noticeably higher average friction values in certain years such as 2015 and 2017. This may indicate maintenance activities around those years but may also reflect differences in the roadway segments selected for measurement. Most of the roadway segments have friction numbers concentrated around the average number, with few segments showing extremely low values (below 20) or exceptionally good conditions (above 60). This annual friction distribution, resembling a normal distribution, remains consistent over the years, which may suggest a stable friction condition for them.

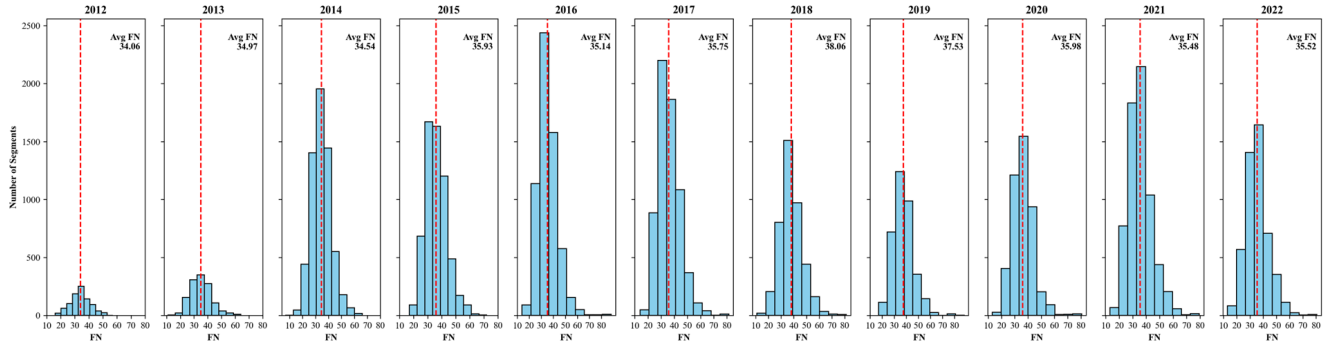

Figure 10. Histogram. Annual friction distribution for urban two-lane highways.

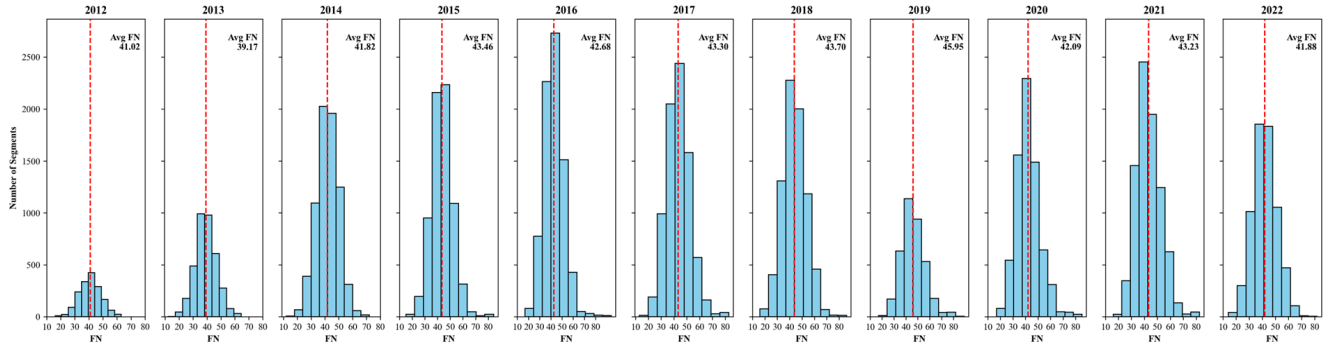

Figure 11. Histogram. Annual friction distribution for rural two-lane highways.

Additional Friction Data from SCRIM

In fall 2025, approximately 2,000 miles of friction data were collected using a SCRIM truck across highway networks primarily in Illinois District 6, with a smaller portion in District 5. The primary objective was to mitigate the limited friction data coverage within several roadway peer groups, particularly those representing intersections. Figure 12 illustrates the spatial distribution of the 2025 Illinois SCRIM data across roadway and intersection peer groups. Table 8 provides a quantitative summary of friction data coverage by peer groups. First, SCRIM data were calibrated to collect one measurement approximately every 10 m, which produces a higher spatial resolution than that of traditional LWST data. This dense sampling captures detailed friction conditions not only along roadway segments, but also within braking and turning zones at intersections. At the roadway level, rural two-lane highways account for the largest share of segments with friction data (4,620 segments covering 1,233 miles), indicating that SCRIM coverage is most extensive for this facility type. In contrast, rural and urban freeways include fewer segments but exhibit longer average segment lengths and generally higher average friction numbers. Overall, rural divided highways and freeways tend to show higher average friction levels than urban two-lane highways and arterial roads. A similar pattern is observed for intersection peer groups (Table 9). Rural minor-leg stop control intersections receive the largest number of friction observations, consistent with their dominant share in the statewide inventory. The 2025 CPFM survey also provides meaningful coverage for several urban intersection peer groups. In general, rural intersections exhibit higher average friction values than urban intersections.

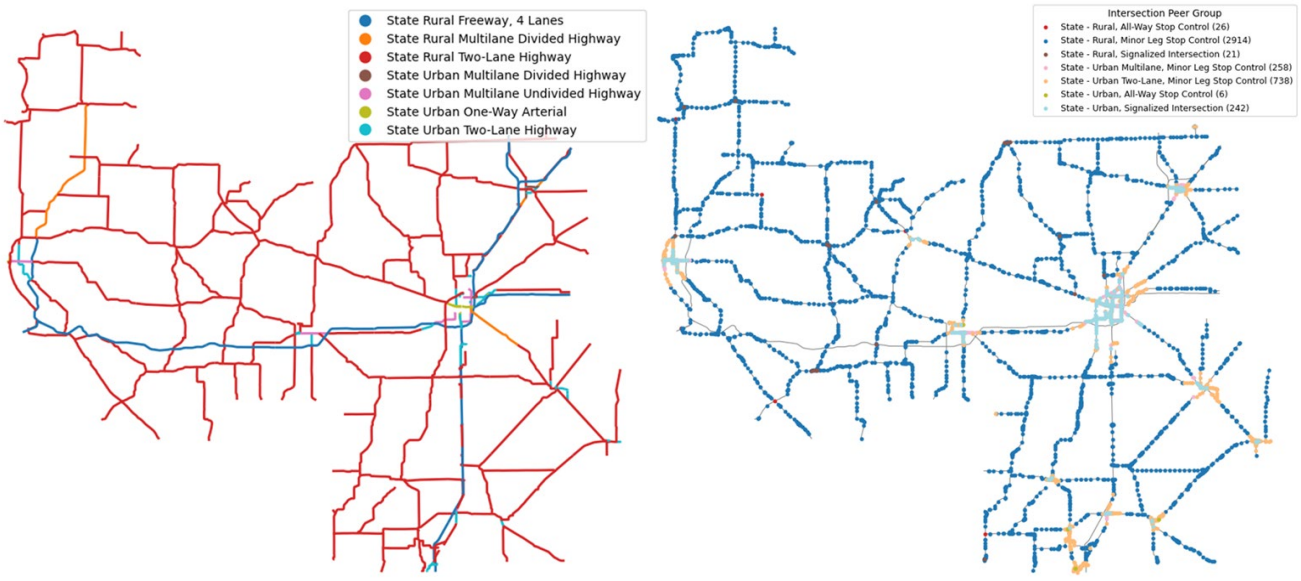

Figure 12. Map. Spatial distribution of 2025 SCRIM data over roadway and intersection peer groups in IDOT district 6.

Table 8. SCRIM Friction Data Coverage Summary by Roadway Peer Group

Peer Group	CPFM # of Segments	Mileage (mi)	Avg. Segment Length (mi)	Avg. Friction	Avg. # of Records per Segment	LWST 2012–2022 # of Intersections
State Rural Two-Lane Highway	4,620	1,233	0.267	57	44.8	28,924
State Urban Two-Lane Highway	1,609	186	0.116	49	15.8	17,570
State Rural Freeway, Four Lanes	295	125	0.424	58	50.0	8,314
State Rural Multilane Divided Highway	485	69	0.142	66	22.8	1,242
State Urban Multilane Divided Highway	655	43	0.065	55	11.2	8,145
State Urban Multilane Undivided Highway	384	31	0.080	50	11.5	2,210
State Urban Freeway, Four Lanes	143	24	0.166	59	23.0	1,154
State Urban One-Way Arterial	94	8	0.087	49	12.9	1,002
State Urban Freeway, Six Lanes	7	1	0.183	55	16.7	129
State Rural Multilane Undivided Highway	7	1	0.153	62	27.1	91
State Rural Freeway, Six+ Lanes	6	1	0.140	63	20.5	3,256

Table 9. SCRIM Friction Data Coverage Summary by Intersection Peer Group

Intersection Peer Group	CPFM # of Intersections	Avg. Friction	Avg. # of Records per Intersection	LWST 2012–2022 # of Intersections
State Rural, Minor Leg Stop Control	2,625	55	9.2	17,774
State Urban Two-Lane, Minor Leg Stop Control	625	45	3.0	12,058
State Urban Multilane, Minor Leg Stop Control	191	52	2.7	8,588
State Urban, Signalized Intersection	230	48	14.4	6,277
State Urban, All-Way Stop Control	22	45	6.0	457
State Rural, All-Way Stop Control	1	40	1.0	214
State Rural, Signalized Intersection	17	52	16.6	112

In summary, incorporating SCRIM data significantly enhances the quality of the safety analysis, primarily through improved spatial resolution. Measurements collected at approximately 10 m intervals provide far denser coverage than the limited records per mile available from LWST. This high-resolution friction information allows for more accurate representation of pavement surface conditions across both roadway segments and intersections. In addition, the increased number of observations supports more stable and reliable model estimation in subsequent safety analyses.

Crash Data Analysis

Comparative analysis of crash rates per mile across all peer groups from 2017 to 2022 is shown in Figure 13. Each bar represents the sum of crash rate per mile for a specific crash severity between the six-year period. The bars are split into two segments, with the left segment in a darker color representing crash rate under wet conditions and the right lighter color representing crash rate under dry conditions. The x-axis is on a logarithmic scale for a clearer comparison across a wide range of crash rates. For all urban peer groups and most rural peer groups, crash rates are higher under wet conditions than dry conditions. The crash rates vary greatly among peer groups, with urban freeways showing higher crash rates per mile, partly due to higher traffic volume and speeds. However, these peer groups have fewer LWST friction records, mainly due to the challenges of deploying LWST in freeways. This discrepancy highlights the need for comprehensive friction data collection and safety analysis on urban freeways to optimally apply the pavement friction management program to enhance safety.

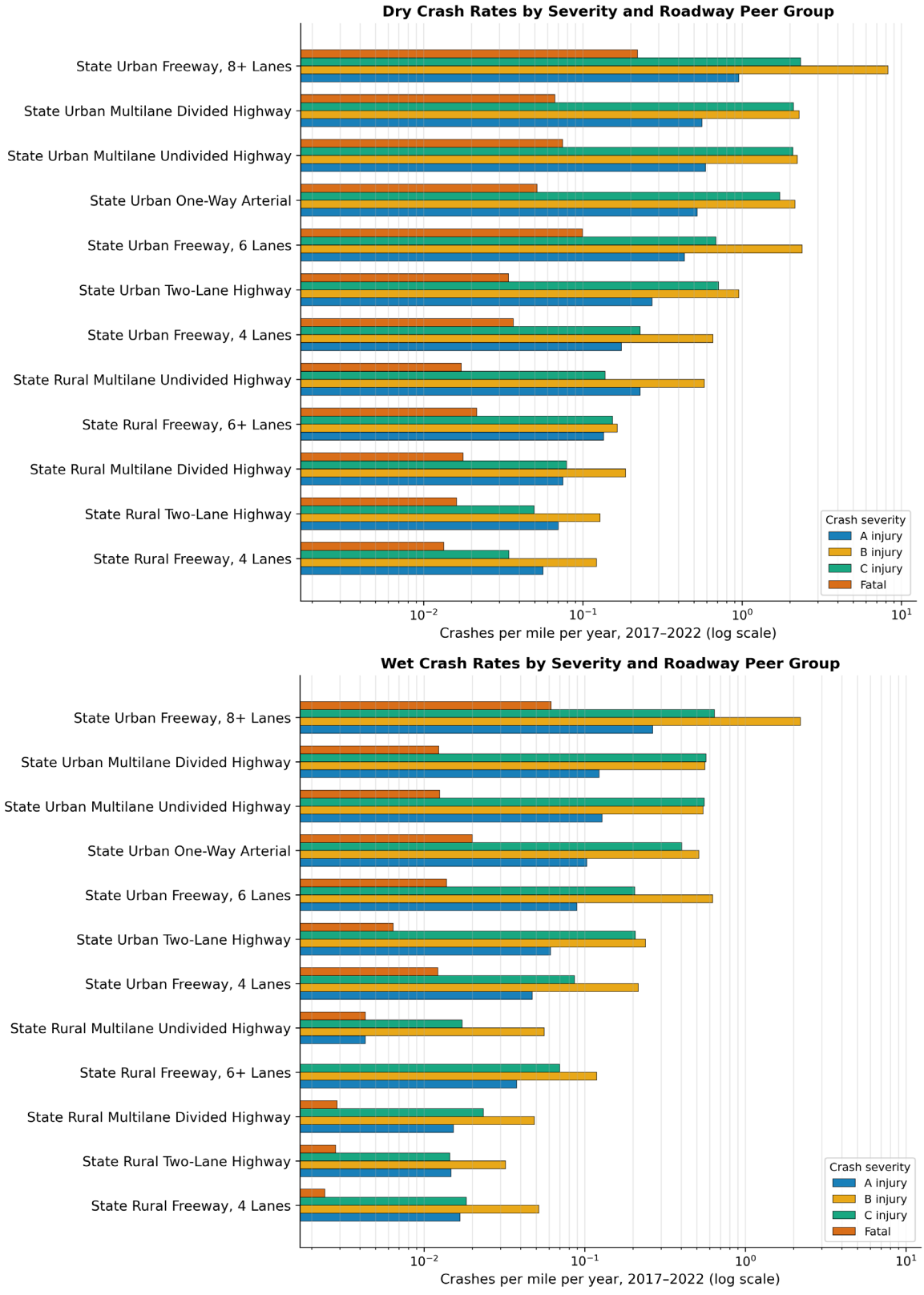

Figure 13. Graph. Comparisons of total crash rates per mile (categorized by severity and dry/wet conditions) for all peer groups from 2017 to 2022.

RECOMMENDATIONS FOR CURRENT IDOT FRICTION COLLECTION PROGRAM

In summary, the friction database and roadway inventory database provided by IDOT were used to conduct a comprehensive analysis of friction data collection practices in Illinois. Geographic information associated with the friction measurements was used to spatially match friction data with roadway peer groups and to evaluate the temporal and spatial patterns of friction across these groups. In addition, a comparative analysis of crash rates among the peer groups was performed to help identify potential gaps in coverage and highlight locations where friction-related safety issues may exist across the Illinois highway network. The following recommendations are provided to IDOT regarding friction data collection.

1. Comprehensive friction data collection forms the foundation for reliable safety analysis and informed decision-making. Because the LWST is a non-continuous friction measurement method, it may not fully represent the overall surface friction conditions of roadway segments. Variability in LWST measurements may occur at different locations within the same segment. This is evidenced by instances where no pavement treatment was applied, yet friction values increased from one year to the next. Therefore, the application of appropriate statistical analysis methods is recommended when processing friction data collected using LWST.

2. Facility type identification is currently limited within the friction database. Based on the available data, it is difficult to determine the specific facility type where friction measurements were collected (e.g., highway tangents, horizontal curves, ramps, or intersections), even though friction demand is typically higher for curves, ramps, and intersections. It is recommended that facility type information be explicitly recorded either during friction data collection or within the roadway inventory database. While this information is not typically required for LWST measurements, which are usually conducted on tangents, it will become increasingly relevant as additional friction data sources are incorporated.

3. Spatial coverage of friction data across the network is inconsistent. Some roadway segments have been tested repeatedly over several years, while others have little or no friction data available. Increasing data collection efforts on segments with limited historical friction measurements is recommended to better analyze temporal variations within roadway peer groups and to understand long-term friction performance trends across different pavement surface types.

4. Urban freeway peer groups currently lack sufficient friction data due to the operational challenges associated with performing LWST testing on high-speed and high-volume facilities. However, these facilities exhibit some of the highest crash rates per mile among the peer groups analyzed. Expanding friction data collection on these facilities is recommended to support more reliable safety analysis and network-level decision making.

5. Continuous friction measurement technologies present an opportunity to enhance friction monitoring. A pilot project has been conducted in Illinois to collect friction data using

SCRIM at selected roadway segments as part of an FHWA pooled fund project. It is recommended to evaluate the relationship between friction measurements obtained using LWST and SCRIM at the same locations. Additionally, friction measurements on curved segments should be collected using continuous friction measurement equipment to better assess friction demand and safety needs on facilities where friction plays a critical role in vehicle control.

CHAPTER 3: DATA COLLECTION AND PROCESSING

SUMMARY OF COLLECTED DATABASE

IDOT provided most of the datasets used for the development of safety performance functions (SPFs). These datasets include information on the roadway segments, intersections, crash records, preservation history, and pavement friction measurements. Some of the datasets were also provided by IDOT's consultants and contractors. The following section provides a detailed description of each collected dataset and the methodology to process and combine the datasets.

Roadway Inventory Data

The roadway inventory data T2HWY20222.shp is public and available at the Illinois Highway Information System website. It is in GIS format and includes various fields related to roadway geometry and traffic information. The most relevant fields for safety analysis and decision-making are (i) annual average daily traffic (AADT), (ii) begin mile, (iii) end mile, (iv) road name, (v) county, (vi) functional class, (vii) inventory key route ID, (viii) median type, (ix) median width, (x) number of lanes, (xi) lane width, (xii) shoulder type, (xiii) shoulder width, (xiv) segment length, (xv) surface type, (xvi) access control type, (xvii) township, (xviii) urban code, (xix) International Roughness Index (IRI), (xx) Condition Rating Survey (CRS), (xxi) geometry, and (xxii) coordinates. These fields will be explicitly considered throughout the safety analysis, and other important roadway features (e.g., grade, curvature, cross-slope, etc.) will be considered if available.

Intersection Data

IDOT provided the intersection dataset (ST2020_Intersections.shp), which includes information of where intersections are located and the traffic characteristics of each intersection. This dataset includes 98,193 intersections, which are a subset of all intersections in Illinois. Each intersection is categorized into the following pre-defined peer groups: (i) rural minor leg stop control, (ii) rural signalized intersection, (iii) rural all-way stop control, (iv) urban two-lane minor leg stop control, (v) urban multilane minor leg stop control, (vi) urban signalized intersection, and (vii) urban all-way stop control.

The geometric characteristics of both the major and minor approaches at each intersection were obtained by merging the intersection database with the corresponding roadway segments. The most relevant information contained in this dataset includes (i) intersection geometry, (ii) coordinates (latitude and longitude), (iii) AADT of the major road, (iv) AADT of the minor road, (v) intersection peer group, (vi) major road name, and (vii) minor road name.

Crash Data

Similar to the roadway inventory data, the crash datasets (Crashes_2017.gdb–Crashes_2022.gdb) are publicly available through the Illinois Highway Information System in GIS format. These datasets contain records of all reported crashes in Illinois from 2017 to 2022. Each crash is classified into five severity categories: (i) K—fatal crash, (ii) A—incapacitating injury, (iii) B—non-incapacitating injury, (iv) C—possible injury, and (v) property damage only (PDO) or no injury. Additional fields provide

detailed information to further characterize each crash, including whether the crash is intersection-related, the primary cause of the crash, the road surface condition (e.g., ice, snow or slush, wet), and the lighting condition. These attributes allow for more detailed safety analyses under specific roadway and environmental conditions. The most relevant fields considered in this study include (i) crash severity, (ii) intersection-related indicator, (iii) crash coordinates, (iv) type of first crash, (v) crash cause, and (vi) road surface condition. Note that not all listed fields are used in the current safety analysis. Subsequent sections of this report describe in detail how these variables are incorporated into the analysis.

Friction Data

The friction dataset integrates measurements from multiple sources. The primary data source for this study is the Locked-Wheel Skid Tester (LWST) database, which provides long-term, standardized friction measurements. To supplement these data and improve the spatial resolution of the safety analysis, additional continuous friction measurements were collected using SCRIM in 2023 and 2025. Macrotexture data were also obtained. These data, however, were not directly incorporated into the crash-based safety modeling in the current phase of the project.

LWST

The database Friction_database_2.5 – 2022.accdb contains friction records collected using the LWST for both the left wheel (ribbed tire) and the right wheel (smooth tire) from 2011 to 2022. All friction values were calibrated to a standard testing speed of 40 mph to ensure consistency across measurements. In addition to friction measurements, the database also includes information on the pavement surface mixture (e.g., aggregate type and mix type). The most relevant fields include (i) friction number, (ii) wheel type, (iii) test speed, (iv) coordinates, and (v) surface type.

SCRIM

To improve the spatial resolution and reliability of the safety analysis, IDOT contracted the Virginia Tech Transportation Institute to conduct continuous friction measurements using SCRIM in 2025. The SCRIM dataset covers approximately 1,850 miles within Illinois District 6. Friction measurements were aggregated at 0.1-mile intervals, providing finer spatial resolution compared to the point-based measurements obtained with the LWST. This level of resolution enables a more detailed evaluation of friction conditions along roadway segments and at intersections. All measurements were calibrated to a standard testing speed of 40 mph. The most relevant fields include (i) friction number, (ii) mean profile depth (mm), (iii) grade, (iv) cross-slope, (v) curvature, and (vi) coordinates.

Macrotexture

Macrotexture data consist of a pilot measurement conducted in District 6 in 2022 and a statewide survey completed in 2023. Although the data were not directly incorporated into the safety modeling in this phase of the project, macrotexture provides important complementary information on pavement surface performance. In addition, the data may support future studies aimed at identifying relationships between surface texture and pavement friction. The most relevant fields include (i) pavement type, (ii) mean texture depth (mm), and (iii) coordinates.

Preservation History Data

The preservation history dataset obtained from IDOT documents historical maintenance and rehabilitation contracts implemented across the highway network. Each record corresponds to a specific contract item and includes information such as contract identification, letting date, treatment type, cost, and associated location. This dataset supports further analysis of the deterioration of pavement functional characteristics over time under different pavement treatments. The most relevant fields include (i) contract ID, (ii) letting date, (iii) district, (iv) county, (v) inventory key route ID, (vi) begin mile, (vii) end mile, and (viii) description of work.

Safety Tiers Data

The Safety Tiers dataset provided by IDOT contains the results of Safety Tier analyses that rank roadway segments and intersections based on a standardized safety score on a scale from 1 to 5, where higher values indicate greater safety concern. These scores are derived from SPFs previously developed without incorporating friction data. Although this dataset was not directly incorporated into the safety analysis conducted in this project, it provides a statewide overview of general safety performance and may be enhanced through the integration of friction-related insights developed in this study.

DATA PROCESSING AND ORGANIZING

To support the development of SPFs and subsequent safety analyses, a comprehensive and internally consistent friction-related database was constructed. Multiple datasets were collected from different sources and integrated into a unified database. Significant effort was devoted to ensuring compatibility across datasets and establishing reliable linkages using common identifiers and spatial relationships. Two primary approaches were considered for merging datasets:

1. Attribute-based merging: This method uses the inventory key route ID in combination with the begin mile and end mile fields. Together, these attributes uniquely define roadway segments in Illinois and enable precise location referencing along a given route.

2. Spatial-based merging: This method uses geometric information from GIS shapefiles to perform spatial joins between datasets.

Because most datasets contain complete geographic information, while some datasets (e.g., LWST friction data and crash data) do not consistently include the inventory key route ID, a hybrid merging strategy was adopted. All datasets with reliable geometric information were first spatially joined to the roadway inventory database. The preservation history dataset was subsequently merged using the inventory key route ID together with overlapping begin-end mile ranges.

Merging of Datasets

The roadway inventory database served as the reference backbone for all spatial integrations. All datasets with reliable geometric information were first projected to a consistent coordinate reference system and then spatially joined to the roadway segments. After the spatial join, friction data (both LWST and SCRIM) were aggregated at the segment level. Specifically, the average of the

lowest 25% of the friction measurements within each segment was computed and used to represent the “average friction number” for that segment. For crash data, the total number of crashes for each severity category was summarized for each segment by year. Preservation history data, which are referenced using the inventory key route ID with begin-end mile ranges, were merged using an attribute-based approach. For each contract record, overlapping mile ranges along the same inventory key route were identified, and the corresponding treatment information was assigned to the associated roadway segments.

The final output after the merging procedure is a roadway segment-level dataset, in which each roadway segment is associated with traffic load (AADT), geometric characteristics (lane width, etc.), number of crashes for each severity type at each year, friction condition (LWST, SCRIM, and macrotexture) each year, other pavement surface conditions (IRI and CRS), and preservation treatment records at each year. This unified database is the foundation for subsequent SPF development and safety analysis.

In the meantime, the same merging procedure was applied for intersection data to obtain intersection-level dataset. Intersection-specific crash assignment followed current Illinois standards: Crashes occurring within 250 ft of signalized intersections, 150 ft of rural stop-controlled intersections, and 50 ft of urban stop-controlled intersections were classified as intersection-related. Because intersection datasets do not directly contain geometric characteristics for major and minor approaches, these attributes were derived through spatial joins with the roadway inventory database. Major and minor roads were identified based on road name. In cases where a crash fell within the defined influence areas of two adjacent intersections, the crash was assigned to the geographically closer intersection to avoid double counting.

Formation of Peer Groups

SPFs for both roadway segments and intersections were developed separately within defined peer groups to ensure consistent modeling across facilities with similar operational and geometric characteristics. Peer groups are defined using key categorical variables, including functional classification, number of lanes, and area type (e.g., urban, rural). For intersections, seven peer groups are predefined under existing IDOT standards. These classifications were retained to maintain consistency with prior safety analyses. For roadway segments, 12 peer groups were defined following the same standard (Table 10).

Table 10. Peer Groups

Rural Peer Groups	Urban Peer Groups
Rural Freeway, Four Lanes	Urban Freeway, Four Lanes
Rural Freeway, Six+ Lanes	Urban Freeway, Six Lanes
Rural Multilane Divided Highway	Urban Freeway, Eight Lanes
Rural Multilane Undivided Highway	Urban Multilane Divided Highway
Rural Two-Lane Highway	Urban Multilane Undivided Highway
–	Urban One-Way Arterial
–	Urban Two-Lane Highway

CHAPTER 4: SAFETY ANALYSIS—SPFS AND CMFS

This chapter presents the development of safety performance functions (SPFs) and crash modification factors (CMFs) to quantify the safety impacts of pavement friction on roadway segments and intersections. The analysis aims to establish statistically robust relationships between crash frequency and pavement friction while controlling for traffic exposure and geometric characteristics. Separate models were developed for each roadway and intersection peer group and for each crash severity type (K, A, B, C, O). In addition to these five types, SPFs were developed for two special cases: (i) K+A as severe crashes and (ii) K+A+B+C+O as all crashes. Because crash data are count-based and typically exhibit over-dispersion, negative binomial regression is adopted as the primary modeling framework. To further improve estimation reliability and address the regression-to-the-mean phenomenon, the Empirical Bayes (EB) method is applied by combining model-predicted crashes with observed crash counts.

ROADWAY PEER GROUPS SAFETY ANALYSIS

Model Framework

For roadway segments, SPFs were formulated to estimate the expected number of crashes as a function of segment length, traffic volume (AADT), pavement friction, and other geometry-related variables. For each crash type j on segment i, the expected crash frequency per year μ_{ij} is expressed in Figure 14:

$$\mu_{ij} = (l_i)^{\alpha_{1j}} \cdot (AADT_i)^{\alpha_{2j}} \cdot \exp(\beta_{0j} f_i + \beta_{1j} X_{1i} + \cdots + \beta_{nj} X_{ni} + C)$$

Figure 14. Equation. Roadway SPFs.

Where l_i is the segment length in miles, $AADT_i$ is the traffic load of segment i, f_i is the pavement friction, X_{ni} denotes n geometry-related variables (e.g., lane width, shoulder width, median width, surface type, access control type). C is the intercept term and all α, β are regression parameters. This formula is used for each crash severity type and for each peer group.

Negative Binomial Regression with Empirical Bayes Estimates

Crash counts are modeled using a negative binomial distribution to account for the over-dispersion phenomenon, as the variance of crash counts typically exceeds the mean. Specifically, the model assumes the following variance structure (Figure 15):

$$V_{ij} = \mu_{ij} + \alpha_j \mu_{ij}^2$$

Figure 15. Equation. SPF over-dispersion estimation.

Where α_j represents the over-dispersion factor. When $\alpha_j > 0$, the variance increases quadratically with the mean, allowing the model to accommodate unobserved heterogeneity across sites. Model

goodness-of-fit is evaluated using log-likelihood values and Akaike information criterion (AIC). Feature selection is performed to retain statistically significant predictors.

A key issue in crash-based safety analysis is the regression-to-the-mean phenomenon, which occurs when sites are selected for analysis or treatment because they experienced unusually high crash counts during a short observation period. Due to natural random variation, crash frequencies tend to fluctuate from year to year. Consequently, a site that records an unusually high number of crashes in one period may show a reduction in subsequent years even if no safety treatment is implemented. When decisions are based solely on observed crash counts, locations with temporarily elevated crash frequencies may be incorrectly identified as high-risk. Any subsequent reduction in crashes may then be mistakenly attributed to the implemented treatment, leading to biased estimates of safety effectiveness. To address this issue, the EB method combines model-based predictions with observed crash counts (Figure 16 and Figure 17):

$$EB_{ij} = W_{ij}\mu_{ij} + (1 - W_{ij})y_{ij}$$

Figure 16. Equation. EB estimation.

$$W_{ij} = (1 + \mu_{ij}\alpha_j)^{-1}$$

Figure 17. Equation. Weights' estimation.

Where EB_{ij} is the expected crash frequency calibrated from the EB method, y_{ij} is the observed type-i crash count at segment j, and W_{ij} is the weight determined by the reliability of the model prediction. The EB estimate represents a weighted average of predicted and observed crashes. When crash data are highly variable (large α_j), greater weight is placed on the model prediction. When observed crash counts are stable and based on longer observation periods, more weight is assigned to the observed data.

CMFs are derived directly from the estimated coefficients of the SPFs. For any explanatory variable included in the model, the CMF represents the multiplicative change in expected crash frequency associated with a specified change in that variable. Under the log-link function used in negative binomial regression, the expected crash frequency can be expressed in exponential form. Therefore, for a continuous variable X_k with coefficient β_k, the CMF corresponding to a change $\Delta X_k$is as follows (Figure 18):

$$CMF = \exp(\beta_k \cdot \Delta X_k)$$

Figure 18. Equation. CMF calculation for continuous explanatory variable.

If $CMF < 1$, the change is associated with a reduction in expected crashes. If $CMF > 1$, the change is associated with an increase in expected crashes. For categorical variables (e.g., access control, surface type), the CMF is computed as follows (Figure 19):

$$CMF = \exp(\beta_k)$$

Figure 19. Equation. CMF calculation for categorical explanatory variable.

Which represents the multiplicative effect relative to the reference category. The percentage change in crashes can be calculated as follows (Figure 20):

$$\%\ \text{Change} = (CMF - 1) \times 100\%$$

Figure 20. Equation. Percentage change in crashes from CMFs.

This formulation provides a consistent and interpretable way to translate regression coefficients into practical safety effects. Importantly, CMFs reflect relative changes in expected crash frequency, not absolute crash reductions. The magnitude of absolute crash reduction depends on the baseline crash frequency of the facility under consideration.

Safety Analysis Results

This section presents descriptive statistics for the urban two-lane highway peer group, which contains 43,682 observations covering 2012–2022. Independent variables include exposure measures (segment length and AADT), pavement friction, access control indicator, pavement surface type, and geometry-related variables such as median width and shoulder widths (Table 11). Crash severity distributions indicate that the majority of crashes are property damage only, while severe crashes (fatal and A-injury) account for a small proportion of total crashes (Table 12).

Table 11. Summary Statistics of Independent Variables (Urban Two-Lane Highway)

Feature	Mean	Std	Min	Max
log(Length)	-2.0339	1.1421	-4.6052	1.4563
log(AADT)	8.7807	0.7519	2.9957	10.24
Access Control	0.0989	0.2986	0	1
Median Width (ft)	1.3724	4.0614	0	42
Surface Type	0.0116	0.1072	0	1
Shoulder Outside 1	3.8218	3.2122	0	20
Shoulder Outside 2	1.0692	1.9430	0	10
Shoulder Inside 1	0.0173	0.3058	0	10
Friction	35.3907	7.8503	7	88

Table 12. Crash Frequency Statistics by Severity (Urban Two-Lane Highway)

Crash Type	Mean	Std	Min	Max	Portion
Fatal (K)	0.002816	0.05342	0	2	0.7%
A-Injury	0.013507	0.119716	0	2	3.6%
B-Injury	0.040864	0.222169	0	4	10.8%
C-Injury	0.031844	0.197782	0	4	8.4%
No Injury (PDO)	0.288197	0.905266	0	23	76.4%

Negative binomial regression models were estimated separately for each crash severity type. The figures below present illustrative results for fatal (Figure 21), A-injury (Figure 22), and property damage only (Figure 23) crashes.

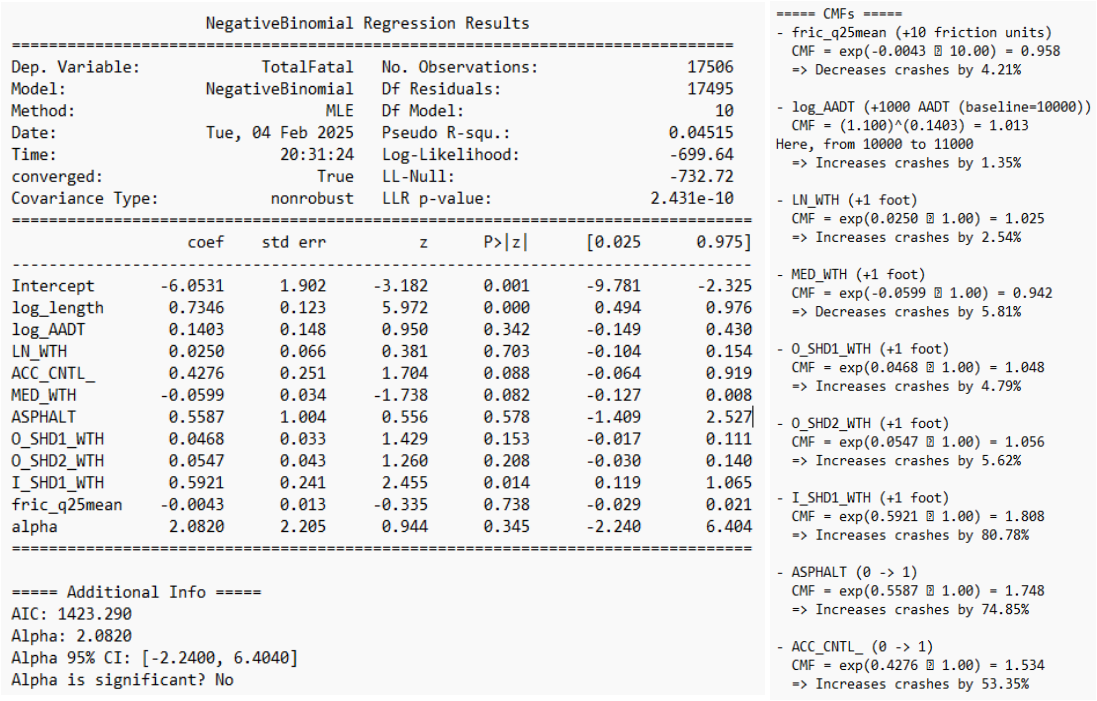

NegativeBinomial Regression Results

Dep. Variable:	TotalFatal	No. Observations:	17506
Model:	NegativeBinomial	Df Residuals:	17495
Method:	MLE	Df Model:	10
Date:	Tue, 04 Feb 2025	Pseudo R-squ.:	0.04515
Time:	20:31:24	Log-Likelihood:	-699.64
converged:	True	LL-Null:	-732.72
Covariance Type:	nonrobust	LLR p-value:	2.431e-10

	coef	std err	z	P>|z|	[0.025	0.975]
Intercept	-6.0531	1.902	-3.182	0.001	-9.781	-2.325
log_length	0.7346	0.123	5.972	0.000	0.494	0.976
log_AADT	0.1403	0.148	0.950	0.342	-0.149	0.430
LN_WTH	0.0250	0.066	0.381	0.703	-0.104	0.154
ACC_CNTL_	0.4276	0.251	1.704	0.088	-0.064	0.919
MED_WTH	-0.0599	0.034	-1.738	0.082	-0.127	0.008
ASPHALT	0.5587	1.004	0.556	0.578	-1.409	2.527
O_SHD1_WTH	0.0468	0.033	1.429	0.153	-0.017	0.111
O_SHD2_WTH	0.0547	0.043	1.260	0.208	-0.030	0.140
I_SHD1_WTH	0.5921	0.241	2.455	0.014	0.119	1.065
fric_q25mean	-0.0043	0.013	-0.335	0.738	-0.029	0.021
alpha	2.0820	2.205	0.944	0.345	-2.240	6.404

```
===== Additional Info =====
AIC: 1423.290
Alpha: 2.0820
Alpha 95% CI: [-2.2400, 6.4040]
Alpha is significant? No
```

```
===== CMFs =====
- fric_q25mean (+10 friction units)
  CMF = exp(-0.0043 × 10.00) = 0.958
  => Decreases crashes by 4.21%

- log_AADT (+1000 AADT (baseline=10000))
  CMF = (1.100)^(0.1403) = 1.013
Here, from 10000 to 11000
  => Increases crashes by 1.35%

- LN_WTH (+1 foot)
  CMF = exp(0.0250 × 1.00) = 1.025
  => Increases crashes by 2.54%

- MED_WTH (+1 foot)
  CMF = exp(-0.0599 × 1.00) = 0.942
  => Decreases crashes by 5.81%

- O_SHD1_WTH (+1 foot)
  CMF = exp(0.0468 × 1.00) = 1.048
  => Increases crashes by 4.79%

- O_SHD2_WTH (+1 foot)
  CMF = exp(0.0547 × 1.00) = 1.056
  => Increases crashes by 5.62%

- I_SHD1_WTH (+1 foot)
  CMF = exp(0.5921 × 1.00) = 1.808
  => Increases crashes by 80.78%

- ASPHALT (0 -> 1)
  CMF = exp(0.5587 × 1.00) = 1.748
  => Increases crashes by 74.85%

- ACC_CNTL_ (0 -> 1)
  CMF = exp(0.4276 × 1.00) = 1.534
  => Increases crashes by 53.35%
```

Figure 21. Graph. Safety analysis results—fatal crashes (urban two-lane highway).

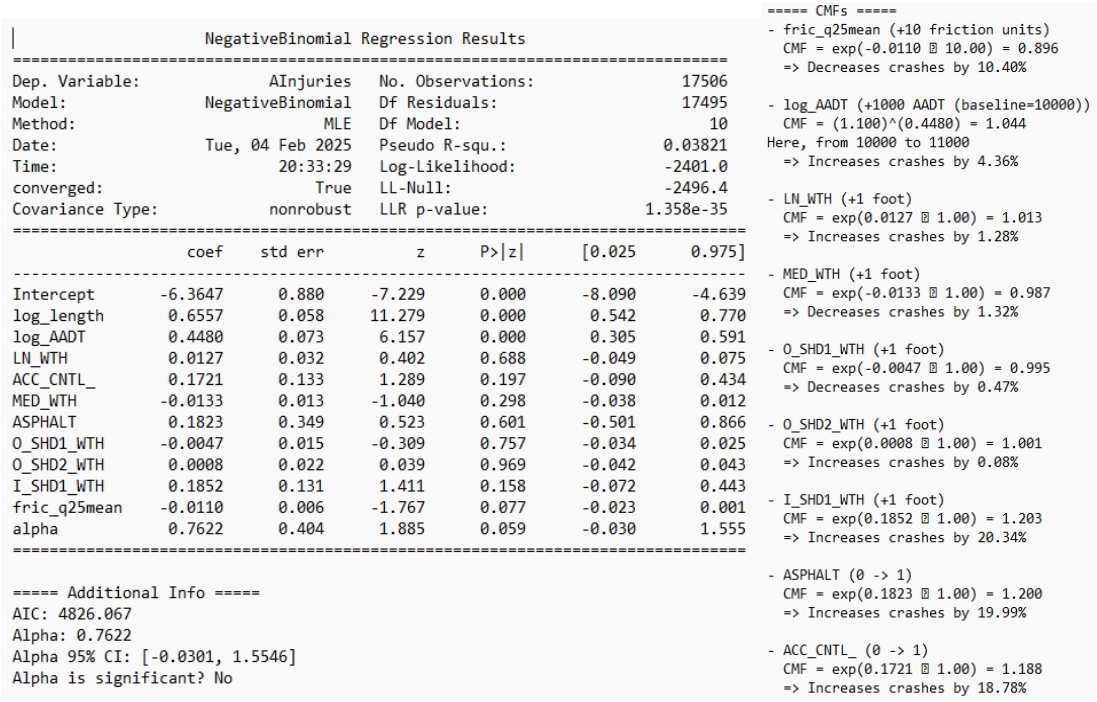

NegativeBinomial Regression Results

Dep. Variable:	AInjuries	No. Observations:	17506
Model:	NegativeBinomial	Df Residuals:	17495
Method:	MLE	Df Model:	10
Date:	Tue, 04 Feb 2025	Pseudo R-squ.:	0.03821
Time:	20:33:29	Log-Likelihood:	-2401.0
converged:	True	LL-Null:	-2496.4
Covariance Type:	nonrobust	LLR p-value:	1.358e-35

	coef	std err	z	P>|z|	[0.025	0.975]
Intercept	-6.3647	0.880	-7.229	0.000	-8.090	-4.639
log_length	0.6557	0.058	11.279	0.000	0.542	0.770
log_AADT	0.4480	0.073	6.157	0.000	0.305	0.591
LN_WTH	0.0127	0.032	0.402	0.688	-0.049	0.075
ACC_CNTL_	0.1721	0.133	1.289	0.197	-0.090	0.434
MED_WTH	-0.0133	0.013	-1.040	0.298	-0.038	0.012
ASPHALT	0.1823	0.349	0.523	0.601	-0.501	0.866
O_SHD1_WTH	-0.0047	0.015	-0.309	0.757	-0.034	0.025
O_SHD2_WTH	0.0008	0.022	0.039	0.969	-0.042	0.043
I_SHD1_WTH	0.1852	0.131	1.411	0.158	-0.072	0.443
fric_q25mean	-0.0110	0.006	-1.767	0.077	-0.023	0.001
alpha	0.7622	0.404	1.885	0.059	-0.030	1.555

```
===== Additional Info =====
AIC: 4826.067
Alpha: 0.7622
Alpha 95% CI: [-0.0301, 1.5546]
Alpha is significant? No
```

```
===== CMFs =====
- fric_q25mean (+10 friction units)
  CMF = exp(-0.0110 × 10.00) = 0.896
  => Decreases crashes by 10.40%

- log_AADT (+1000 AADT (baseline=10000))
  CMF = (1.100)^(0.4480) = 1.044
Here, from 10000 to 11000
  => Increases crashes by 4.36%

- LN_WTH (+1 foot)
  CMF = exp(0.0127 × 1.00) = 1.013
  => Increases crashes by 1.28%

- MED_WTH (+1 foot)
  CMF = exp(-0.0133 × 1.00) = 0.987
  => Decreases crashes by 1.32%

- O_SHD1_WTH (+1 foot)
  CMF = exp(-0.0047 × 1.00) = 0.995
  => Decreases crashes by 0.47%

- O_SHD2_WTH (+1 foot)
  CMF = exp(0.0008 × 1.00) = 1.001
  => Increases crashes by 0.08%

- I_SHD1_WTH (+1 foot)
  CMF = exp(0.1852 × 1.00) = 1.203
  => Increases crashes by 20.34%

- ASPHALT (0 -> 1)
  CMF = exp(0.1823 × 1.00) = 1.200
  => Increases crashes by 19.99%

- ACC_CNTL_ (0 -> 1)
  CMF = exp(0.1721 × 1.00) = 1.188
  => Increases crashes by 18.78%
```

Figure 22. Graph. Safety analysis results—A-injury crashes (urban two-lane highway).

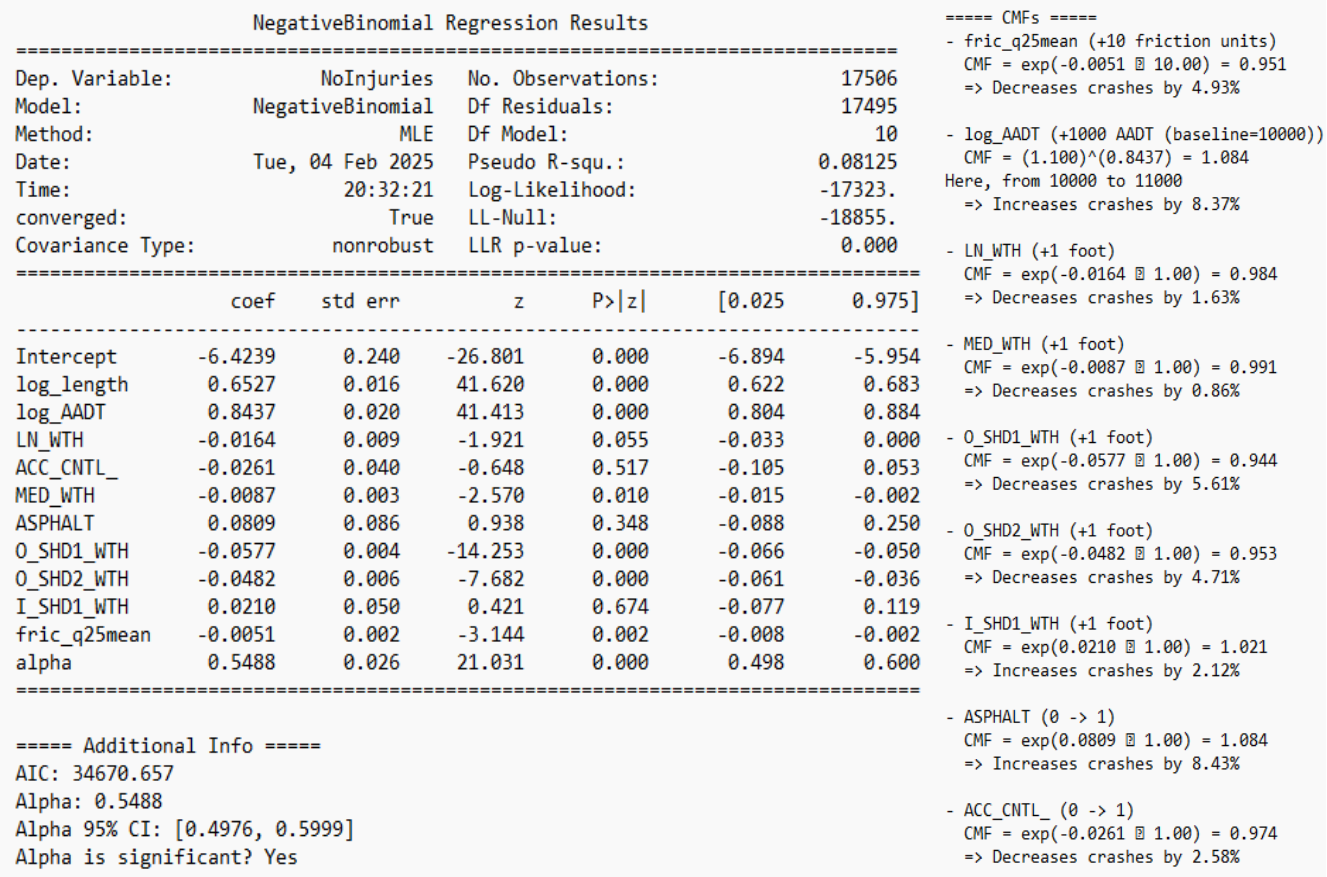

```
                    NegativeBinomial Regression Results
==============================================================================
Dep. Variable:             NoInjuries   No. Observations:                17506
Model:                NegativeBinomial   Df Residuals:                    17495
Method:                           MLE   Df Model:                           10
Date:                Tue, 04 Feb 2025   Pseudo R-squ.:                0.08125
Time:                        20:32:21   Log-Likelihood:                -17323.
converged:                       True   LL-Null:                       -18855.
Covariance Type:            nonrobust   LLR p-value:                     0.000
==============================================================================
                 coef    std err          z      P>|z|      [0.025      0.975]
------------------------------------------------------------------------------
Intercept      -6.4239      0.240    -26.801      0.000      -6.894      -5.954
log_length      0.6527      0.016     41.620      0.000       0.622       0.683
log_AADT        0.8437      0.020     41.413      0.000       0.804       0.884
LN_WTH         -0.0164      0.009     -1.921      0.055      -0.033       0.000
ACC_CNTL_      -0.0261      0.040     -0.648      0.517      -0.105       0.053
MED_WTH        -0.0087      0.003     -2.570      0.010      -0.015      -0.002
ASPHALT         0.0809      0.086      0.938      0.348      -0.088       0.250
O_SHD1_WTH     -0.0577      0.004    -14.253      0.000      -0.066      -0.050
O_SHD2_WTH     -0.0482      0.006     -7.682      0.000      -0.061      -0.036
I_SHD1_WTH      0.0210      0.050      0.421      0.674      -0.077       0.119
fric_q25mean   -0.0051      0.002     -3.144      0.002      -0.008      -0.002
alpha           0.5488      0.026     21.031      0.000       0.498       0.600
==============================================================================

===== Additional Info =====
AIC: 34670.657
Alpha: 0.5488
Alpha 95% CI: [0.4976, 0.5999]
Alpha is significant? Yes

===== CMFs =====
- fric_q25mean (+10 friction units)
  CMF = exp(-0.0051 × 10.00) = 0.951
  => Decreases crashes by 4.93%

- log_AADT (+1000 AADT (baseline=10000))
  CMF = (1.100)^(0.8437) = 1.084
Here, from 10000 to 11000
  => Increases crashes by 8.37%

- LN_WTH (+1 foot)
  CMF = exp(-0.0164 × 1.00) = 0.984
  => Decreases crashes by 1.63%

- MED_WTH (+1 foot)
  CMF = exp(-0.0087 × 1.00) = 0.991
  => Decreases crashes by 0.86%

- O_SHD1_WTH (+1 foot)
  CMF = exp(-0.0577 × 1.00) = 0.944
  => Decreases crashes by 5.61%

- O_SHD2_WTH (+1 foot)
  CMF = exp(-0.0482 × 1.00) = 0.953
  => Decreases crashes by 4.71%

- I_SHD1_WTH (+1 foot)
  CMF = exp(0.0210 × 1.00) = 1.021
  => Increases crashes by 2.12%

- ASPHALT (0 -> 1)
  CMF = exp(0.0809 × 1.00) = 1.084
  => Increases crashes by 8.43%

- ACC_CNTL_ (0 -> 1)
  CMF = exp(-0.0261 × 1.00) = 0.974
  => Decreases crashes by 2.58%
```

Figure 23. Graph. Safety analysis results—no injury crashes (urban two-lane highway).

Overall, the signs and magnitudes of the key coefficients are consistent with theoretical expectations. Segment length and AADT are consistently positive and statistically significant across crash types, indicating that higher exposure is associated with increased expected crash frequency. Some geometric variables, such as median width, also exhibit consistent effects across severity levels, with wider medians generally associated with lower crash frequencies. Pavement friction exhibits a negative coefficient across all crash types, suggesting that higher friction levels reduce the expected crash frequency. However, the statistical significance varies by severity level. The effect of friction appears more pronounced for lower-severity crashes (e.g., PDO) than for severe crashes (e.g., fatal crashes), likely due to the limited number of severe crash observations. Based on the estimated coefficients, a 10-unit increase in friction corresponds to an approximate 5%–10% reduction in crashes across severity types. Although the absolute reduction in severe crashes is numerically small, it remains meaningful relative to their low baseline frequency. The CMF further illustrate that increasing friction consistently lowers the expected crash frequency across severity levels, with stronger relative effects observed for moderate-severity crashes. The results for other crash severity types and roadway peer groups are provided in Appendix D.

INTERSECTION PEER GROUPS SAFETY ANALYSIS

For intersection peer groups, the historical LWST friction data provide sparse, point-based friction measurements that are primarily collected along roadway segments and are not consistently available within defined intersection influence areas. To ensure adequate observations and maintain consistency in the intersection safety analysis, the 2025 SCRIM dataset was used. As an illustrative example, results for the urban signalized intersection peer group for A-injury crashes are presented in Figure 24. For A-injury crashes, a negative binomial specification was adopted due to evidence of over-dispersion, whereas for no-injury crashes (Figure 25) a Poisson model was considered sufficient based on dispersion diagnostics. In both cases, friction exhibits a negative coefficient, indicating that higher friction levels are associated with lower expected crash frequencies at intersections. The derived CMFs suggest that a 10-unit increase in friction corresponds to a larger reduction in injury crashes and a moderate reduction in PDO crashes.

```
Peer group: Urban_Signalized_Intersection
DV: AInjuries
Model: GLM_NB
Poisson dispersion (Pearson chi2/df): 1.7081
Alpha (NB only): 0.070170
AIC: 186.8374323340082
LogLik (llf): -81.4187161670041

===== MODEL SUMMARY =====
                 Generalized Linear Model Regression Results
==============================================================================
Dep. Variable:              AInjuries   No. Observations:                 2613
Model:                            GLM   Df Residuals:                     2601
Model Family:        NegativeBinomial   Df Model:                           11
Link Function:                    Log   Scale:                          1.0000
Method:                          IRLS   Log-Likelihood:                -81.419
Date:                Tue, 20 Jan 2026   Deviance:                       129.06
Time:                        22:16:38   Pearson chi2:                 4.41e+03
No. Iterations:                    17   Pseudo R-squ. (CS):           0.01655
Covariance Type:            nonrobust
==============================================================================
                 coef    std err          z      P>|z|      [0.025      0.975]
------------------------------------------------------------------------------
Intercept      1.3835      2.261      0.612      0.541      -3.048       5.816
lnAADT_major  -0.7417      0.194     -3.822      0.000      -1.122      -0.361
lnAADT_minor   0.3662      0.278      1.316      0.188      -0.179       0.911
ma_MED_WTH    -0.2008      0.460     -0.436      0.663      -1.103       0.701
ma_I_SHD_1     0.4395      0.432      1.018      0.309      -0.407       1.286
ma_LN_WTH     -0.1233      0.117     -1.058      0.290      -0.352       0.105
ma_LNS         0.1923      0.536      0.359      0.720      -0.859       1.243
ma_O_SHD_1    -0.1359      0.280     -0.486      0.627      -0.684       0.412
mi_MED_WTH     0.0748      0.071      1.058      0.290      -0.064       0.213
mi_LN_WTH      0.5636      0.215      2.625      0.009       0.143       0.984
mi_O_SHD_1    -0.0133      0.221     -0.060      0.952      -0.447       0.420
Q25_Avg_FN    -0.0719      0.026     -2.777      0.005      -0.123      -0.021
==============================================================================
```

```
===== CMF CALCULATIONS =====
- Q25_Avg_FN (+10 friction)
  CMF = exp(-0.071944 × 10.00) = 0.4870
  => Decrease 51.30%
- lnAADT_major (+1000 AADT)
  CMF = (1.10)^(-0.741732) = 0.9317
  (From 10000 to 11000 AADT)
  => Decrease 6.83%
- lnAADT_minor (+1000 AADT)
  CMF = (1.10)^(0.366158) = 1.0355
  (From 10000 to 11000 AADT)
  => Increase 3.55%
- ma_MED_WTH (+1 ft)
  CMF = exp(-0.200849 × 1.00) = 0.8180
  => Decrease 18.20%
- ma_LN_WTH (+1 ft)
  CMF = exp(-0.123287 × 1.00) = 0.8840
  => Decrease 11.60%
- ma_O_SHD_1 (+1 ft)
  CMF = exp(-0.135905 × 1.00) = 0.8729
  => Decrease 12.71%
- ma_I_SHD_1 (+1 ft)
  CMF = exp(0.439482 × 1.00) = 1.5519
  => Increase 55.19%
- mi_MED_WTH (+1 ft)
  CMF = exp(0.074805 × 1.00) = 1.0777
  => Increase 7.77%
- mi_LN_WTH (+1 ft)
  CMF = exp(0.563555 × 1.00) = 1.7569
  => Increase 75.69%
- mi_O_SHD_1 (+1 ft)
  CMF = exp(-0.013304 × 1.00) = 0.9868
  => Decrease 1.32%
```

Figure 24. Graph. Safety analysis results—A-injury crashes (urban signalized intersection).

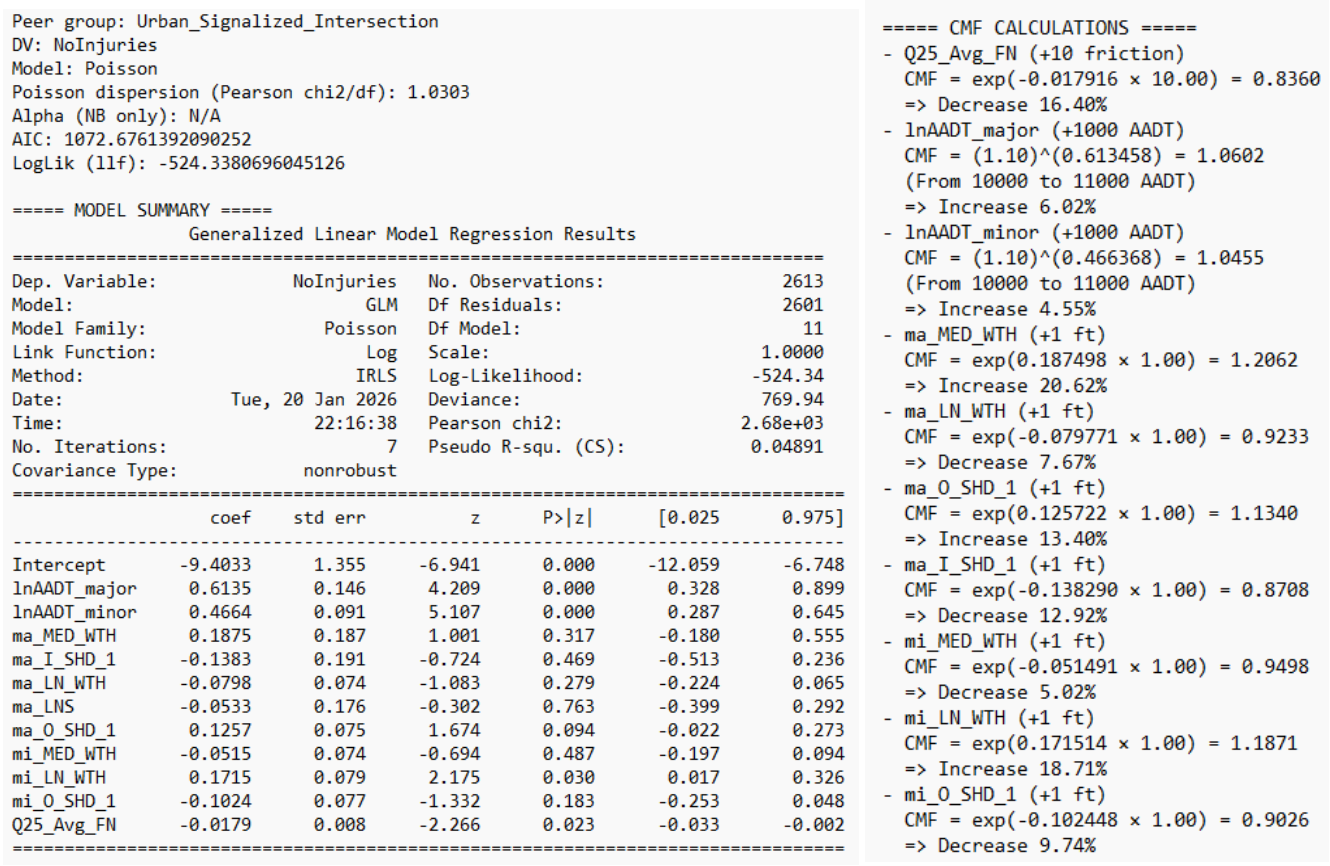

```
Peer group: Urban_Signalized_Intersection
DV: NoInjuries
Model: Poisson
Poisson dispersion (Pearson chi2/df): 1.0303
Alpha (NB only): N/A
AIC: 1072.6761392090252
LogLik (llf): -524.3380696045126

===== MODEL SUMMARY =====
                 Generalized Linear Model Regression Results
==============================================================================
Dep. Variable:             NoInjuries   No. Observations:                 2613
Model:                            GLM   Df Residuals:                     2601
Model Family:                 Poisson   Df Model:                           11
Link Function:                    Log   Scale:                          1.0000
Method:                          IRLS   Log-Likelihood:                -524.34
Date:                Tue, 20 Jan 2026   Deviance:                       769.94
Time:                        22:16:38   Pearson chi2:                 2.68e+03
No. Iterations:                     7   Pseudo R-squ. (CS):            0.04891
Covariance Type:            nonrobust
==============================================================================
                 coef    std err          z      P>|z|      [0.025      0.975]
------------------------------------------------------------------------------
Intercept      -9.4033      1.355     -6.941      0.000     -12.059      -6.748
lnAADT_major    0.6135      0.146      4.209      0.000       0.328       0.899
lnAADT_minor    0.4664      0.091      5.107      0.000       0.287       0.645
ma_MED_WTH      0.1875      0.187      1.001      0.317      -0.180       0.555
ma_I_SHD_1     -0.1383      0.191     -0.724      0.469      -0.513       0.236
ma_LN_WTH      -0.0798      0.074     -1.083      0.279      -0.224       0.065
ma_LNS         -0.0533      0.176     -0.302      0.763      -0.399       0.292
ma_O_SHD_1      0.1257      0.075      1.674      0.094      -0.022       0.273
mi_MED_WTH     -0.0515      0.074     -0.694      0.487      -0.197       0.094
mi_LN_WTH       0.1715      0.079      2.175      0.030       0.017       0.326
mi_O_SHD_1     -0.1024      0.077     -1.332      0.183      -0.253       0.048
Q25_Avg_FN     -0.0179      0.008     -2.266      0.023      -0.033      -0.002
==============================================================================
```

```
===== CMF CALCULATIONS =====
- Q25_Avg_FN (+10 friction)
  CMF = exp(-0.017916 × 10.00) = 0.8360
  => Decrease 16.40%
- lnAADT_major (+1000 AADT)
  CMF = (1.10)^(0.613458) = 1.0602
  (From 10000 to 11000 AADT)
  => Increase 6.02%
- lnAADT_minor (+1000 AADT)
  CMF = (1.10)^(0.466368) = 1.0455
  (From 10000 to 11000 AADT)
  => Increase 4.55%
- ma_MED_WTH (+1 ft)
  CMF = exp(0.187498 × 1.00) = 1.2062
  => Increase 20.62%
- ma_LN_WTH (+1 ft)
  CMF = exp(-0.079771 × 1.00) = 0.9233
  => Decrease 7.67%
- ma_O_SHD_1 (+1 ft)
  CMF = exp(0.125722 × 1.00) = 1.1340
  => Increase 13.40%
- ma_I_SHD_1 (+1 ft)
  CMF = exp(-0.138290 × 1.00) = 0.8708
  => Decrease 12.92%
- mi_MED_WTH (+1 ft)
  CMF = exp(-0.051491 × 1.00) = 0.9498
  => Decrease 5.02%
- mi_LN_WTH (+1 ft)
  CMF = exp(0.171514 × 1.00) = 1.1871
  => Increase 18.71%
- mi_O_SHD_1 (+1 ft)
  CMF = exp(-0.102448 × 1.00) = 0.9026
  => Decrease 9.74%
```

Figure 25. Graph. Safety analysis results—no injury crashes (urban signalized intersection).

From a modeling perspective, SCRIM-based friction data demonstrate improved statistical performance in intersection SPFs. Compared with models using LWST data, SCRIM-based models exhibit more stable coefficient estimates, narrower confidence intervals, and stronger statistical significance of the friction variable. This improvement is likely attributable to the higher spatial resolution of SCRIM measurements and their better alignment with intersection functional areas. In addition, SCRIM captures friction variation across the entire approach and conflict areas rather than at isolated test points, providing a more representative characterization of the friction conditions experienced by vehicles during braking and turning maneuvers.

CHAPTER 5: DECISION TREES FOR SITE SCREENING AND TREATMENT PRIORITIZATION

MOTIVATION AND PROBLEM STATEMENT

Chapter 4 established a set of safety performance functions (SPFs) that quantify crash risk as a function of pavement friction, traffic load, and geometric characteristics. These models provide a foundation for estimating expected crash frequency across the highway network. However, SPF results alone do not directly translate into actionable treatment planning decisions at the network level. In current practice, traditional pavement management decisions are primarily driven by structural and functional condition indices and ride quality indicators, such as IDOT's Condition Rating Survey (CRS) and the International Roughness Index (IRI). Treatment selection and prioritization are typically based on threshold-based screening procedures and economic evaluation methods, including benefit-cost ratio (BCR) methods and life cycle cost analysis (LCCA). The objective of these frameworks is to maintain serviceability, while minimizing agency costs, or to minimize total societal costs over a defined planning horizon.

However, pavement friction is rarely treated as an explicit decision variable in traditional pavement management systems. Although several transportation agencies have begun incorporating friction investigatory thresholds and friction-oriented programming, a comprehensive methodological framework that integrates friction into network-level planning remains underdeveloped. A fundamental challenge is that friction represents a distinct performance dimension that is not consistently correlated with structural or ride-quality indicators. A pavement segment may exhibit acceptable CRS or IRI while having inadequate skid resistance, or conversely may have structural deterioration but still maintain sufficient friction. Moreover, different treatments vary in their effectiveness in improving safety (friction improvement) and serviceability (CRS/IRI restoration).

As a result, relying solely on serviceability-driven frameworks may overlook safety deficiencies, while friction-focused approaches do not consider long-term structural performance and associated cost implications. This disconnect motivates the development of an integrated decision framework that jointly considers safety risk, pavement condition, treatment effectiveness, and life cycle costs in a unified network-level planning model.

Relationship between Pavement Friction and Other Pavement Condition Measures

As mentioned above, a key motivation for developing an integrated decision-making framework lies in the observed relationship between pavement friction and CRS based on real Illinois data. While CRS is widely used by IDOT in pavement management to represent overall pavement condition, it does not directly capture skid resistance performance, which is closely linked to roadway safety. The scatter plots of Illinois data in Figure 26 show that friction and CRS exhibit strong variablity across roadway segments and, therefore, are not apparently correlated. CRS primarily reflects condition and ride quality, whereas friction reflects surface texture and skid resistance characteristics. Deterioration mechanisms also differ: CRS degradation is typically associated with cracking, rutting, and structural fatigue, while friction deterioration is related to aggregate polishing, surface wear, and

environmental effects. From a treatment perspective, many surface treatments (e.g., HMA overlay, microsurfacing, ultra-thin bonded wearing course) can improve both CRS and friction. Some friction-oriented treatments (e.g., high friction surface treatment), however, offer minor improvements to CRS but greatly improve friction. The magnitude and longevity of improvements may differ across the two dimensions. In some cases, friction may decline more rapidly than CRS, or vice versa. Consequently, selecting treatments based solely on CRS thresholds may fail to identify segments with safety-related friction deficiencies.

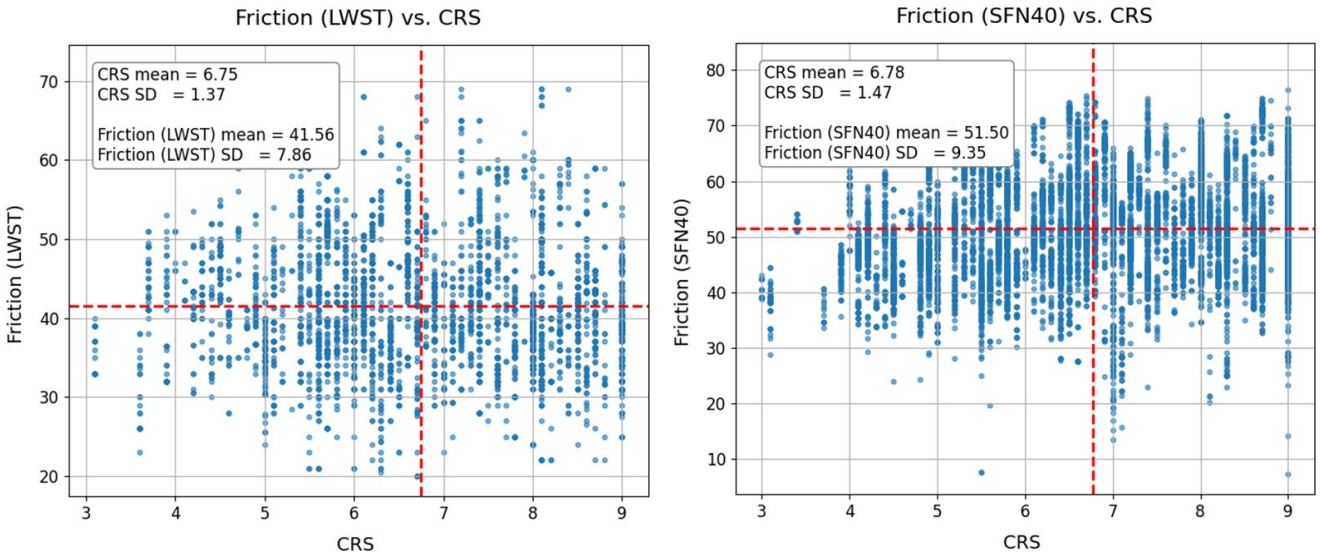

Figure 26. Graph. Joint distribution of Illinois CRS and friction data.

Limitation of Existing Screening and Prioritization Methods

Existing site screening and treatment prioritization approaches are usually limited and impractical for network-level treatment proritization. In practice, agencies often rely on safety tiers, friction investigatory thresholds, or condition-based triggers (e.g., CRS or IRI cutoffs) to identify candidate sites. Economic evaluation is frequently conducted using a BCR framework, as shown in Figure 27. Many implementation practices, however, emphasize either safety cost reduction alone or serviceability improvement alone, rather than jointly evaluating both dimensions. Moreover, traditional BCR analyses often rely on short analysis periods (e.g., 3–7 years for safety impacts) and may not fully capture long-term deterioration and rehabilitation cycles (Flintsch et al., 2023). As a result, decisions can become biased toward low-cost treatments that yield high short-term BCRs, potentially overlooking preventive strategies or long-term structural needs. In addition, many implementation practices operate at the project or spot-treatment level, without embedding decisions within a consistent network-level life-cycle optimization framework. These limitations highlight the need for an integrated approach that simultaneously accounts for safety risk, pavement performance, treatment effectiveness, and long-term cost performance.

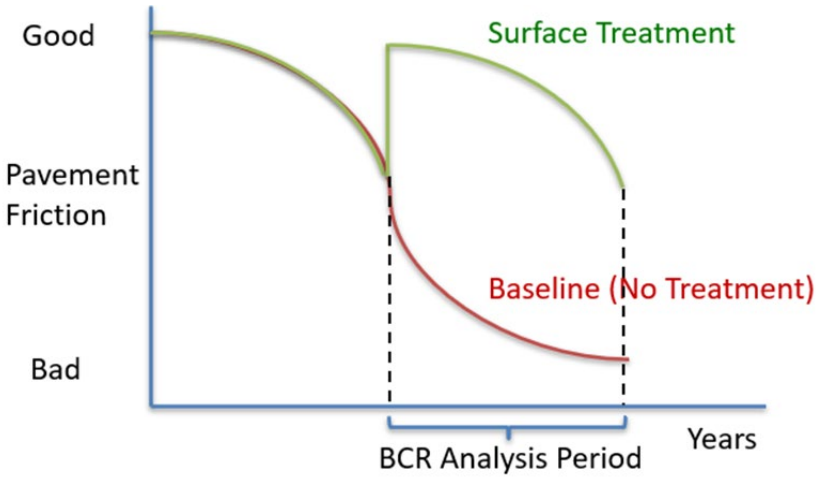

Figure 27. Illustration. Benefit-cost ratio method.

LIFE-CYCLE COST ANALYSIS FRAMEWORK

To overcome the limitations of traditional screening and prioritization methods, a LCCA framework is developed to jointly model pavement friction and structural condition within a unified optimization structure. The key idea is to translate both safety performance (friction-related crash risk) and serviceability performance (CRS-related user cost) into comparable monetary cost components, enabling integrated decision-making. Rather than evaluating projects over a short planning horizon, the framework adopts an infinite-horizon perspective to capture long-term deterioration, treatment cycles, and intertemporal trade-offs. Each pavement segment is characterized by its peer group, traffic load, and current condition state, defined by both CRS and friction. Treatments differ in cost and in their effectiveness in restoring these two condition dimensions. The objective is to identify treatment strategies that minimize the total discounted cost, including safety cost, user serviceability cost, and agency construction cost.

Model Formulation

We consider one lane-mile of a specific pavement facility (e.g., urban two-lane highway with hot-mix asphalt surface) serving traffic load q. Pavement condition is represented by a 2D state vector $\phi = (s, f)$, where $s \in (0,9]$ denotes the CRS value, and $f \in (0,100)$ denotes the pavement friction number.

At the beginning of each discrete decision epoch τ (e.g., fiscal year), the agency selects a treatment r from a finite set R, which includes all feasible treatments (e.g., HMA overlay, ultra-thin bonded wearing course [UTBWC], chip seal, microsurfacing, HFST) as well as the special action "do-nothing" ($r = 0$). Each treatment $r \in R$ has an agency construction cost M_r, which can bring thr current CRS condition to the post-treatment state $s^+ = S_r(s)$, and bring friction to the post-treatment state $f^+ = H_r(f)$. Based on ICT-IDOT project R27-150 (Ozer et al., 2018), CRS deterioration is modeled linearly with time and depends on traffic load q, truck percentage, and post-treament CRS. The CRS evolution is expressed as the following equation in Figure 28:

$$s(t) = 9.0 - m\left(\alpha_q \ln(q) - \alpha_{s^+} s^+ + \alpha_{Tr} Tr + \beta\right) \cdot t, \qquad \forall\, q, t \in (\tau, \tau + 1)$$

Figure 28. Equation. CRS deterioration model (Ozer et al., 2018).

Where $S(t)$ is the CRS value at time t, Tr is truck percentage, and $m, \alpha_q, \alpha_{s^+}, \alpha_{Tr}, \beta$ are treatment-specific parameters. Thus, each treatment produces a distinct CRS deterioration trajectory depending on traffic and treatment-specific characteristics. Meanwhile, the friction number after each treatment increases to a constant value $H_r(f) = h_r \geq 0$. The deterioration process of friction follows a constant rate depending on pavement characteristics and traffic load (Figure 29):

$$\frac{df(t)}{dt} = \begin{cases} -(a_1 + a_{2\hat{r}}\, q), & f(t) > f_{min} \\ 0, & f(t) = f_{min} \end{cases}, \quad \forall q, t \in (\tau, \tau + 1)$$

Figure 29. Equation. Friction deterioration model.

Where $a_1, a_{2\hat{r}}$ captures the sensitivity with respect to facility type, traffic load, and last applied treatment $\hat{r}$. The exact forms of $S_r(\cdot),\ s(t),\ H_r(\cdot), f(t)$ may vary by traffic, climate, materials, and construction quality across different states, and can be calibrated using agency-specific data.

In the life cycle cost framework, three cost components are considered: safety cost, derived from the SPF-based expected crash frequency $c_2 \cdot SPF(f(t))$; serviceability (user) cost, modeled as a linear function of CRS: $q(c_0 + c_1 s(t))$; and agency cost, represented by one-time treatment cost M_r. The total discounted life cycle cost is defined in Figure 30:

$$\min \sum_{\tau=0}^{\infty} \left[\int_{\tau}^{\tau+1} ((c_0 + c_1 s(t)) \cdot \mathrm{q} + c_2 SPF(f(t))) e^{-vt} dt + M_{r_\tau} e^{-v\tau} \right]$$

Figure 30. Equation. Total discounted LCCA objective.

where v is annual discount rate, and r_τ is treatment chosen at decision epoch τ. The objective minimizes the net present value of total societal cost over an infinite horizon.

Solution Structure and Policy Interpretation

Because treatment decisions are made at discrete decision epochs while CRS and friction evolve continuously between epochs, the life cycle optimization problem can be formulated either as a mixed-integer programming model or, more naturally, as a Markov Decision Process. By discretizing the 2D state space (s, f) and applying dynamic programming methods such as value iteration or policy iteration, we obtain an optimal stationary policy of the form (Figure 31):

$$r^*: = \pi^*(s, f, q),$$

Figure 31. Equation. Optimal treatment mapping.

which maps every feasible combination of CRS, friction, and traffic load to the least-cost treatment. The solution exhibits a clear structure in the 2D state space: Regions of high CRS and high friction correspond to a "do-nothing" or preventive maintenance action; regions with low friction but acceptable CRS favor friction-oriented treatments (e.g., chip seal, HFST, microsurfacing); regions with slightly worse CRS but moderate friction favor structural treatments (e.g., overlay or UTBWC); and states where both CRS and friction are low trigger major rehabilitation.

In the Illinois case study, the model inputs consist of treatment-specific CRS deterioration parameters (Table 13) and a treatment toolbox (Table 14) that specifies construction cost, post-treatment CRS s^+, and post-treatment friction h_r for each available treatment (e.g., HMA overlay, UTBWC, chip seal, microsurfacing, HFST). The CRS deterioration coefficients reflect how quickly structural condition declines under different traffic and truck-loading conditions, while the treatment toolbox defines the immediate restoration levels and agency costs. These are currently based on data from the CRS and preservation databases but will be updated once network-level data are available over more years on preservation treatments.

Table 13. CRS Deterioration Parameters by Treatment

Treatment	m	α_q	α_{s^+}	α_{Tr}	β
9.5 mm microsurfacing	0.90	0.028	0.064	0.17	0.889
0.5 in. chip seal	1.13	0.046	0.088	0.32	0.920
20 mm UTBWC	0.60	0.082	0.253	1.02	1.873
1.5 in. HMA overlay	0.38	0.042	0.118	0.74	1.493
HFST	1.01	0.138	0.257	1.31	1.05

Table 14. Treatment Cost and Effectiveness

Treatment r	M_r $(10^3$ \$$/lane - mi)$	s^+	h_r
1.5 in. HMA overlay	120.0	8.0	60
20 mm UTBWC	48.0	7.2	60
0.5 in. chip seal	15.0	6.5	52
9.5 mm microsurfacing	25.0	7.0	58
HFST	220.0	5.0	80

Table 15. Friction Deterioration Parameters by Treatment for Each Pavement Facility Type

Pavement Facility Type i	1.5 in. HMA Overlay	20 mm UTBWC	0.5 in. Chip Seal	9.5 mm Microsurfacing	HFST
Urban Multilane Undivided Hwy	5.940e-04	7.560e-04	1.080e-03	8.640e-04	3.240e-04
Urban Two-Lane Highway	5.692e-04	7.245e-04	1.035e-03	8.280e-04	3.105e-04
Urban Multilane Divided Hwy	5.445e-04	6.930e-04	9.900e-04	7.920e-04	2.970e-04
Urban Freeways 6+ Lanes	5.198e-04	6.615e-04	9.450e-04	7.560e-04	2.835e-04
Rural Freeways 8+ Lanes	4.702e-04	5.985e-04	8.550e-04	6.840e-04	2.565e-04
Rural Two-Lane Highway	4.455e-04	5.670e-04	8.100e-04	6.480e-04	2.430e-04

Using these calibrated inputs, the optimization model produces a 2D policy map for any representative facility (e.g., an urban two-lane highway under a specified AADT in Figure 32). We assume a safety cost coefficient 169 k$/generic crash and CRS (user) cost of 4e-6 k$/veh-mi/CRS. The resulting policy plot partitions the CRS-friction state space into distinct treatment regions. For instance, when CRS remains relatively high but friction drops below a critical range, friction-oriented treatments such as chip seal or microsurfacing become optimal. When CRS deteriorates substantially, structural treatments such as UTBWC or HMA overlay dominate, even if friction is moderate. In states where both CRS and friction are satisfactory, the model recommends do-nothing, reflecting the cost of premature intervention. The boundaries between these regions align closely with economically rational thresholds implied by life cycle cost trade-offs, rather than pre-defined investigatory limits. This case study demonstrates how the integrated framework translates calibrated deterioration models and treatment effectiveness data into transparent, state-dependent treatment rules.

The Illinois case study illustrates how these policy maps vary systematically with traffic level and facility type. For example, for urban two-lane highways under lower AADT, chip seal frequently emerges as the optimal friction-oriented treatment in low-friction states. As traffic increases, the optimal region shifts toward microsurfacing or overlay treatments due to faster deterioration and higher safety costs. Similarly, for rural freeways with higher traffic loads, structural treatments appear earlier in the state space. These variations confirm that the model adapts quantitatively to differing operational conditions rather than relying on fixed thresholds. The optimal policy results for other peer groups and traffic load levels are in Appendix E.

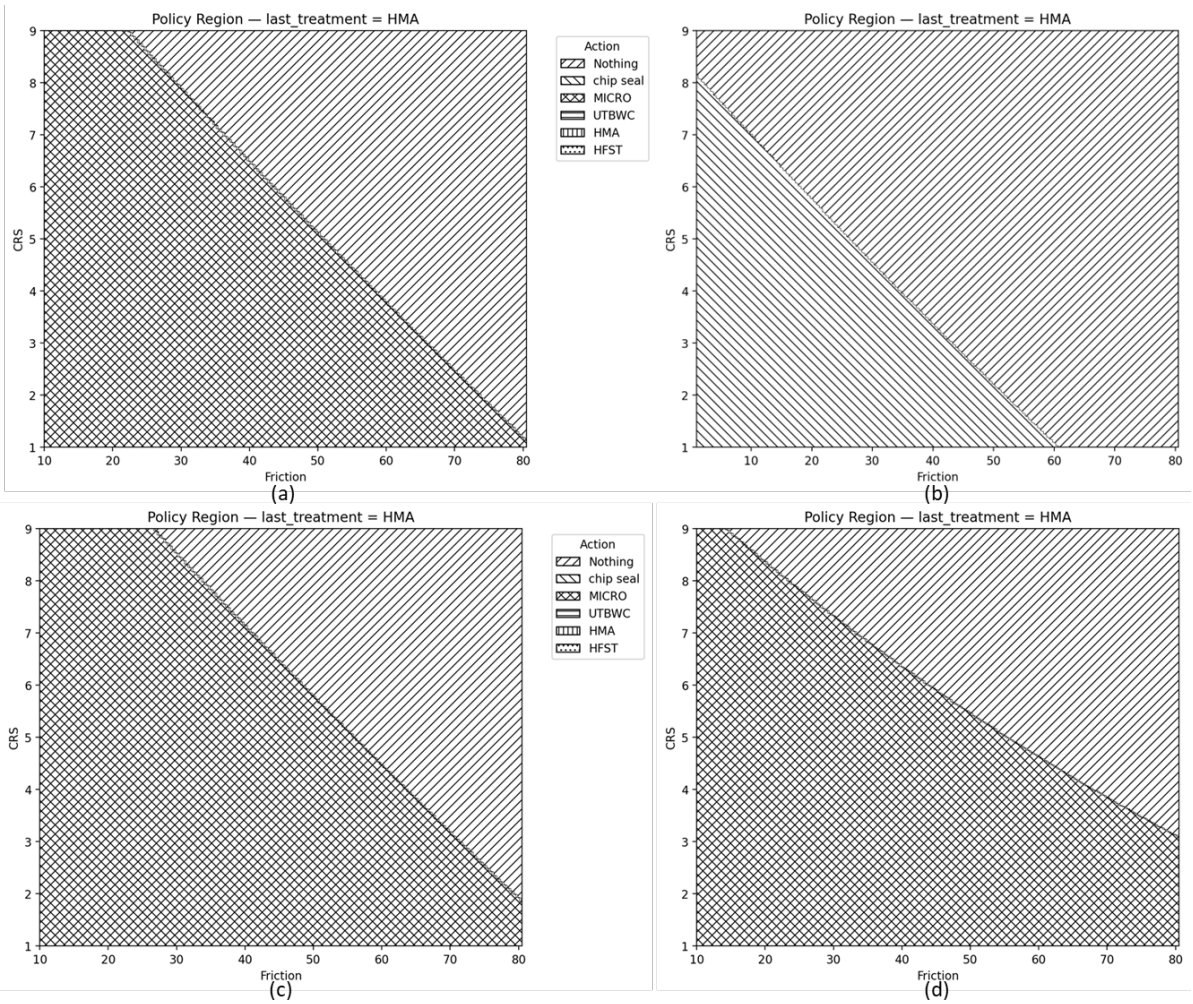

Figure 32. Graph. Optimal policies for urban two-lane highway segment under (a) 3,500 AADT/lane; (b) 1,000 AADT/lane; (c) 5,000 AADT/lane; (d) rural freeways, six+ lanes under 5,500 AADT/lane.

DECISION TREES FOR NETWORK SCREENING AND TREATMENT PRIORITIZATION

For network-level implementation, the dynamic programming (DP) model developed for a single pavement segment can be generalized in a straightforward and scalable manner. The key observation is that the single-segment problem depends only on a limited set of characteristics: peer group i, traffic load q, and the 2D state (s, f). Therefore, by solving the DP problem once for each representative peer group and traffic level, we obtain a complete 2D policy map that assigns an optimal treatment to every feasible CRS-friction combination. These policy maps naturally form the basis of decision trees for site screening and treatment selection.

In practice, network screening proceeds in three steps, illustrated in Figure 33 and Figure 34. First, each pavement segment is classified into its corresponding peer group and traffic category. Second, its current CRS and friction values are identified. Third, the segment's state is located on the pre-computed policy map, which immediately yields the optimal treatment decision. Because each peer group–traffic combination has a unique mapping, the resulting decision structure is consistent and

transparent across the entire network. This screening procedure creates a hierarchical decision structure: network – peer group – traffic load level – CRS-friction state – optimal policy. The advantage of this decision tree architecture is that the LCCA optimization framework is performed offline and real-time screening becomes a straightforward rule-based lookup. As a result, the network-level implementation remains computationally efficient and scalable. Treatment decisions across thousands of segments can be obtained and prioritized.

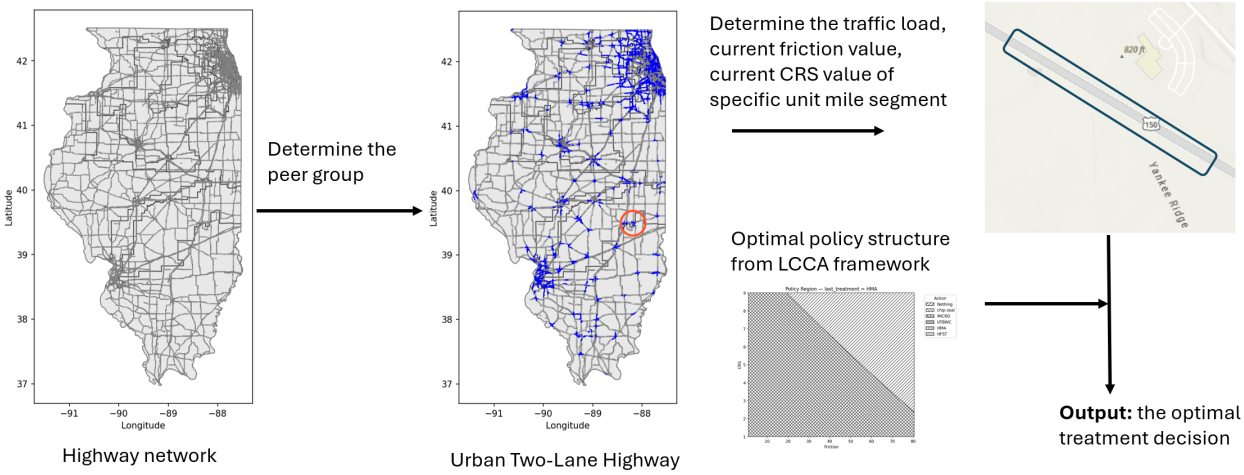

Figure 33. Illustation. Network treatment screening procedure.

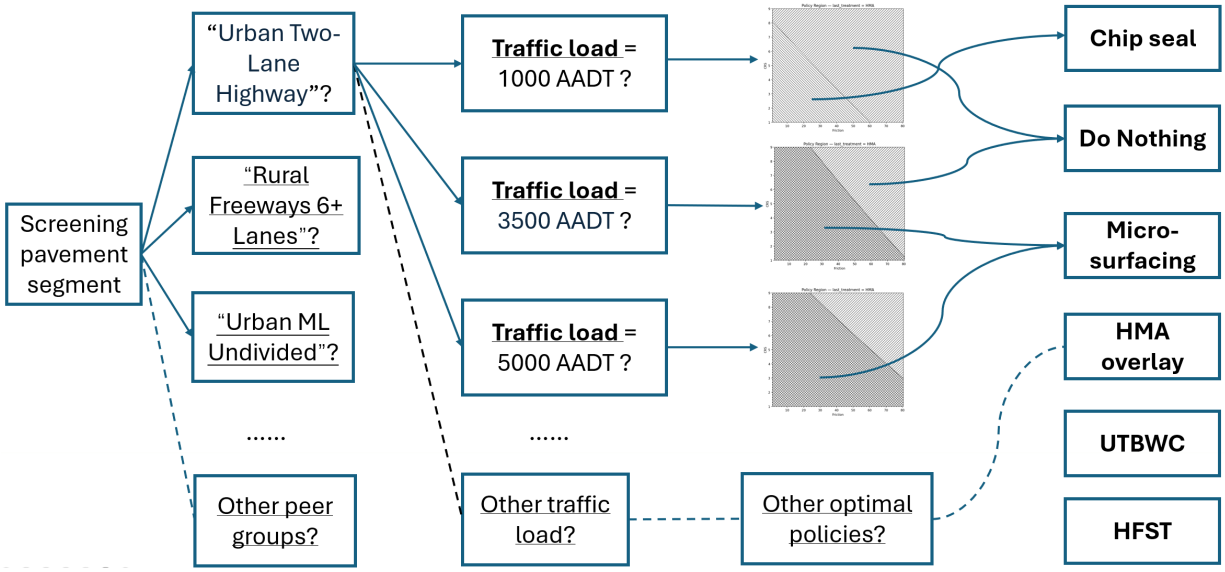

Figure 34. Illustation. Decision-tree framework for network treatment selection.

The trajectory plots in Figure 35 further demonstrate how pavement states evolve over time under the optimized policy. Starting from an initial CRS-friction condition, the pavement gradually deteriorates toward lower CRS and friction values. When the trajectory crosses a threshold boundary into a treatment region, the model recommends an intervention decision (e.g., chip seal, microsurfacing, etc.), which restores the state to a higher CRS and/or friction condition level, as

indicated by the upward and rightward shifts in the trajectory. Across different traffic levels (panels a–c), the system exhibits cyclic preservation behavior over a sufficiently long horizon and without budget constraints, which reflects a preventive maintenance strategy in practice. Higher traffic levels lead to faster deterioration and more frequent treatment interventions, resulting in shorter cycles between treatments.

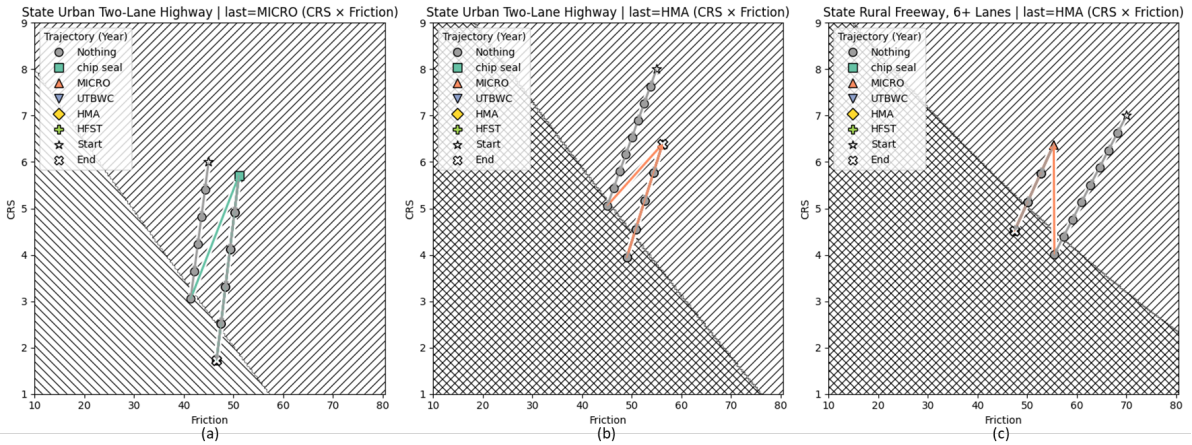

Figure 35. Graph. Sample evolution of urban two-lane highway segment under (a) 1,000 AADT/lane, (b) 2,500 AADT/lane, and (c) 3,667 AADT/lane.

Finally, a cost comparison over a 30-year horizon between the optimized policy and a simple threshold-based rule (e.g., treat when friction < 40 or CRS < 4) shows that the optimized life cycle policy consistently achieves lower average annual cost (Figure 36). This improvement arises because the LCCA framework balances short-term intervention costs with long-term deterioration dynamics, rather than triggering treatments based solely on static thresholds. These results demonstrate that the single-segment DP model provides a scalable and economically consistent foundation for network-level site screening, trajectory analysis, and treatment prioritization.

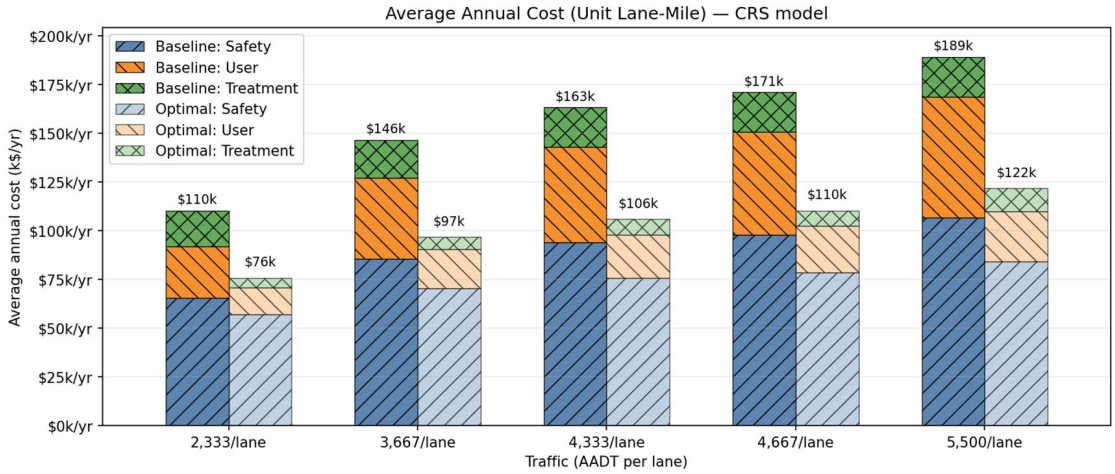

Figure 36. Graph. Average total cost compared between LCCA-optimized policy and traditional threshold-based policy.

CHAPTER 6: REFINEMENT OF FRICTION AGGREGATE POLICY

Conventional asphalt mixture design focuses primarily on volumetric parameters and mechanical performance (Cominsky, 1994). The prediction of surface texture and friction at the material selection and mixture design stage has not been widely practiced. However, integrating friction performance into the design phase, rather than evaluating it only post-construction, offers a proactive path to improving pavement safety outcomes and informing aggregate specification policies.

Digital image processing (DIP) techniques, particularly the Aggregate Imaging Measurement System (AIMS), have proven instrumental in advancing this area. AIMS enables quantitative characterization of aggregate angularity and surface texture at multiple scales through gradient and wavelet analysis methods, respectively (Al-Rousan et al., 2005). By tracking changes in these morphological indices across Micro-Deval polishing intervals, the technique provides both the initial aggregate shape characteristics and their rate of degradation under simulated traffic wear, key inputs for friction prediction frameworks.

AGGREGATE PROPERTIES FOR FRICTION PREDICTION

HMA Friction

Masad et al. (2007) pioneered the use of AIMS and Micro-Deval (MD) testing to evaluate the relationship between coarse aggregate surface texture and tire-pavement friction. In the study, 62 aggregate samples, including gravel, sandstone, and limestone, were characterized before and after MD polishing. Wavelet-based AIMS texture indices were correlated with field skid numbers (SN) measured on nine dense-graded asphalt test sections in Texas. Analysis of variance (ANOVA) indicated that aggregate mineralogy was the sole statistically significant factor governing SN values under similar gradation structures. Quartzite aggregates showed the most rapid texture loss under polishing, while sandstone and siliceous gravel maintained their texture properties more effectively despite lower initial values.

Building on this framework, Masad et al. (2009) aimed to predict tire-pavement friction based on aggregate characteristics and gradation. They prepared laboratory slabs using five aggregate types (including sandstone, limestone, dolomite, and granite) and different gradations. Friction and texture characteristics were evaluated using the Sand Patch (SP), British Pendulum (BP), Dynamic Friction Tester (DFT), and Circular Texture Meter (CTMeter) after various polishing intervals using a wheel-polishing device developed by the National Center for Asphalt Technology. The proposed model predicts the International Friction Index (IFI) as a function of aggregate surface texture (before and after MD polishing) and gradation. Aggregate surface texture evolution with MD polishing time was described by a three-parameter exponential decay function ($AIMS_{texture}$) (Figure 37), where a_{agg} represents the terminal surface texture, $a_{agg} + b_{agg}$ the initial surface texture, and c_{agg} the rate of change in texture for a certain polishing time (t), in minutes. Gradation was incorporated using a two-parameter the Weibull distribution (Figure 38), where the cumulative aggregate gradation percent passing (F) is a function of the aggregate size, in mm (x), and the shape (κ) and scale (λ) parameters.

$$AIMS_{texture} = a_{agg} + b_{agg} \times e^{(-c_{agg} \times t)}$$

Figure 37. Equation. Exponential decay model (AIMS texture index).

$$F(x, k, \lambda) = 1 - e^{-(x/\lambda)^k}$$

Figure 38. Equation. Cumulative Weibull distribution.

The introduction of a traffic parameter was proposed by Masad et al. (2011), improving the model developed by relating traffic to friction loss. Instead of a "polishing time," the authors developed a variable of "number of loading cycles" (*N*), based on a traffic multiplication factor (TMF), which is in turn a function of the AADT, and the decay rate (c_{mix}) of the aggregate-gradation combination. The authors captured the influence of traffic (*N*) into a mean profile depth (MPD) prediction equation. Kassem et al. (2013) significantly expanded the Masad et al. (2009) framework by incorporating both aggregate surface texture and angularity evolution into the prediction model developed. Using one asphalt binder, three aggregate sources (two limestones and one sandstone), and four gradations, the study produced slab specimens that were polished in increments up to 100,000 cycles using a three-wheel pneumatic device applying a 105 lb load (50 psi) tire pressure under continuous water spray to simulate wet traffic condition. AIMS quantified both texture and angularity indices at each polishing interval using exponential decay functions analogous to Figure 37. Initial and terminal friction, as well as the friction decay rate, were calibrated as a function of the terminal surface texture after polishing in MD (AMD), the Weibull gradation parameters, as well as the texture and angularity exponential coefficients. The model achieved $R^2 = 0.92$ between predicted and measured IFI, confirming that laboratory-derived aggregate morphology data can be directly linked to mixture-level friction performance and its degradation with polishing. This study established that both texture and angularity evolution are necessary predictors of long-term friction.

Chowdhury et al. (2017) extended the laboratory-based framework to a large-scale field validation and expanded it to include a friction prediction model for chip seal surfaces, in addition to typical HMA. The study evaluated 70 pavement sections distributed across multiple climatic regions of Texas (35 HMA sections and 35 chip seal sections), encompassing dense-graded, stone-matrix asphalt (SMA), porous friction course, and multiple seal coat grades. Field measurements included a locked-wheel skid trailer (SN at 50 mph), DFT, and CTMeter, and aggregate samples were characterized using the AIMS surface texture and angularity parameters at different polishing times in the MD equipment. The predictive equations for HMA and chip seal were formulated following the previous structure, expressing a_{mix}, ($a_{mix} + b_{mix}$), and c_{mix} as functions of aggregate texture and angularity evolution and Weibull gradation parameters, but separately calibrated for each surface type. The model achieved $R^2 \approx 0.67$ for IFI and $R^2 \approx 0.59$–0.63 for skid number across both surface types. Predictive equations were recalibrated for macrotexture (MPD) as a function of Weibull gradation parameters and cumulative traffic cycles. Key findings from this study are as follows. Seal coat surfaces generally exhibit higher initial friction than dense-graded HMA, though this advantage is strongly dependent on construction factors such as aggregate embedment and binder application

rate. Coarser aggregate gradations, reflected by larger Weibull scale parameters, consistently produce higher MPD values and initial friction. Friction loss follows an exponential decay pattern in which the rate and long-term equilibrium are both governed by traffic level. The authors noted that calibration was based on Texas materials and conditions, and that direct transferability to other regions, such as Illinois, would require local recalibration.

Siriphun et al. (2016) proposed a pre-construction friction index (IFI) prediction model calibrated on 106 asphalt pavement sections in Thailand. The model relates it to a polishing indicator derived from the polished stone value (PSV), MTD, and Weibull gradation parameters. A key variable, PSV_{diff}, representing the difference in PSV before and after polishing, was a statistically significant predictor of friction and serves as a practical microtexture durability parameter when AIMS equipment is not available. In a follow-up study, Siriphun et al. (2019) incorporated cumulative traffic volume (CTV) to capture friction degradation over time. They found the nominal maximum aggregate size (NMAS) of the mixture influences friction reduction only up to approximately 300,000 passenger car units of cumulative traffic. Beyond this threshold, NMAS was no longer statistically significant. This finding implies that aggregate nominal size governs early-life friction behavior, whereas long-term friction is dominated by polishing resistance and gradation characteristics.

Chen et al. (2015) and Chen et al. (2019) linked mixture design information to asphalt surface texture and friction behavior through a spectral analysis approach. Three-dimensional mixture surfaces were reconstructed from RGB images using the 3D-ITAM tool, and discrete Fourier transforms were used to compute texture levels in fractional-octave bands. A multivariate regression model predicted texture level at each central wavelength from mixture volumetrics (void structure) and gradation descriptors (fractal dimension, aggregate orientation, and contact characteristics). With adjusted R^2 values of approximately 0.67–0.72 across octave bands, this approach showed that mixture design variables can forecast not only overall macrotexture, but also the wavelength-by-wavelength distribution of texture energy. This provides a design-stage route from gradation and volumetrics to friction and noise surface texture spectra.

El-Ashwah and Abdelrahman (2025) evaluated seven HMA mixtures (five SMA and two dense-graded) with a three-wheel polishing device (TWPD) at multiple intervals up to 100,000 cycles, with friction and texture measured by a DFT and CTMeter, respectively. For asphalt mixtures, friction evolution under TWPD exhibited a two-stage pattern: an initial increase as binder films were removed from aggregate surfaces, followed by a gradual decrease toward a terminal value as aggregate microtexture polished. This behavior was captured by a comprehensive model decomposing mixture friction into three components: (1) peak mixture friction expressed as a linear function of initial aggregate ring DFT ($R^2 \approx 0.90$); (2) terminal mixture expressed as a linear function of aggregate DFT measured after 105 or 180 minutes of MD polishing ($R^2 \approx 0.88$–0.90); and (3) friction decay rate (c_{mix}) expressed as a linear function of the aggregate-level polishing rate coefficient ($R^2 \approx 0.97$). An IFI prediction model incorporating AIMS texture and angularity indices alongside three-parameter gradation model coefficients achieved $R^2 \approx 0.93$. Random forest analysis confirmed that TWPD polishing cycles were the most influential predictor of friction loss, followed by the percent loss of aggregate friction with DFT and terminal texture index. This analysis confirmed that aggregate polishing resistance and terminal friction, rather than initial friction values, are the dominant controls

on long-term mixture skid resistance, and supported incorporating polishing-based aggregate durability metrics into mix design and friction management policies.

Surface Treatment Friction

Heitzman and Moore (2017) conducted a controlled laboratory comparison of 11 aggregate types for HFST applications, with the TWPD as a conditioning mechanism. Aggregate types ranged from calcined bauxite to basalt, copper slag, flint rock, calcined kaolin products, quartz sands, and feldspathic materials. Testing at up to 140,000 polishing cycles revealed substantial variability in terminal friction values. Calcined bauxite exhibited the highest friction retention, confirming its role as the benchmark HFST aggregate. Flint rock and certain calcined kaolin products showed comparatively high performance, while basalt demonstrated strong polish resistance despite lower initial friction. Quartz sands and feldspathic materials exhibited the lowest terminal friction.

Woodward and Friel (2017) addressed the high cost and limited availability of calcined bauxite (high-quality aggregate for providing high friction) by developing a blending methodology for HFST applications. Using the wear test, a laboratory procedure applying 100,000 wheel passes to simulate heavy traffic, they demonstrated that the skid resistance of blended aggregates follows a Rule of Mixtures: The performance of a binary blend can be estimated as a weighted average of the independently tested constituent skid resistance values. Although no natural aggregate matches the performance of 100% calcined bauxite, blends containing approximately 50% bauxite and 50% high-PSV natural aggregate provided friction levels appropriate for intermediate-risk sites, offering a practical framework for cost-effective material selection.

El-Ashwah et al. (2023) evaluated six aggregate sources for HFST applications—calcined bauxite (control), Meramec River gravel, flint chat, earthwork, steel slag, and rhyolite trap rock—using the British Pendulum Tester, DFT, and TWPD at up to 140,000 cycles. Among local alternatives, flint chat exhibited friction performance closest to calcined bauxite, followed by steel slag and rhyolite trap rock. Crucially, the study found that British Pendulum Number (BPN) alone was insufficient to rank aggregate friction under dynamic sliding conditions, since BPN and DFT_{20} rankings diverged for certain aggregates. This confirms the importance of using device-appropriate metrics and polishing protocols for friction-based aggregate screening. Roshan and Abdelrahman (2024) investigated the specific and independent contributions of aggregate angularity and surface texture to skid resistance in surface treatment applications, using a regression model of the form $SN = \alpha(TI) + \beta(AI) + \gamma$, where *TI* and *AI* are the AIMS texture index and angularity index, respectively, and α, β, γ are regression coefficients. A central finding of the study is the crossover effect: In the early life of a chip seal, angularity is the dominant predictor of skid resistance, as fresh aggregate edges penetrate tire rubber effectively. Over time, polishing removes these sharp corners, and surface texture (*TI*) becomes the primary long-term predictor.

Microsurfacing Friction

Cui et al. (2020) examined the replacement of basalt with basic oxygen furnace steel slag in Type II microsurfacing and quantified the resulting surface texture improvements using AIMS, high-resolution laser scanning, and British pendulum testing. Steel slag exhibited substantially higher angularity and 2D form values than basalt, leading to increased positive texture and peak dominance

in reconstructed 3D surface profiles. Laser-derived MPD, MTD, and arithmetic roughness (R_a) all increased when coarse basalt was replaced with coarse steel slag, while fine slag replacement contributed minimally to macrotexture. British Pendulum Numbers increased from approximately 54 (basalt only) to nearly 68 (full steel slag replacement). Regression analysis showed strong correlations between skid resistance and R_a ($R^2 \approx 0.95$), suggesting full-profile roughness captures friction potential more comprehensively than MPD alone. Cui et al. (2022) advanced a data-driven prediction framework for microsurfacing texture degradation using a back-propagation artificial neural network (BP-ANN). The model incorporated aggregate gradient angularity, steel slag replacement ratio, oil-stone ratio, and gradation type as inputs, with sensitivity analysis revealing that fine-aggregate angularity dominates microtexture retention and gradation controls macrotexture development. The machine-learning model captured nonlinear texture decay under simulated traffic loading (MMLS3), providing a practical tool for forecasting microsurfacing friction performance from mixture design variables.

Alavi et al. (2025) examined the role of aggregate gradation and layer thickness on skid resistance and theoretical crash rates in microsurfacing applications. Laboratory samples were assessed using the British Pendulum Tester and sand patch test (MTD). The Penn State model was applied to convert these physical measurements into friction coefficients at various vehicle speeds for different gradation curves. Finer gradations yielded higher BPN values, indicating better low-speed friction from increased contact area, while coarser gradations produced higher MTD values, providing better drainage at highway speeds. Predictions showed that coarser gradation microsurfacing reduces braking distance more effectively at speeds above 90 km/h (56 mph). Layer thickness (single vs. variable overlap) had negligible impact on friction compared to the dominant influence of aggregate gradation.

Influences of Mineralogy and Chemical Composition

Huang et al. (2025) investigated aggregate mineralogy, specifically oxide chemistry quantified by X-ray fluorescence analysis, as an alternative to physical polishing tests for predicting terminal friction in asphalt surface mixtures. Silica dioxide (SiO_2) and iron oxide (Fe_2O_3) contents were quantified on aggregate fractions passing the #3/8 sieve and retained on the #4 sieve. Further characterization used AIMS, MD, and British Pendulum testing. Specimens were subjected up to 150,000 cycles in the TWPD, and friction evolution was monitored using DFT and CTMeter, with field validation via LWST. A multivariate regression model ($R^2 = 0.88$) related the terminal friction coefficient to combined silica-iron content and the percentage of polish-resistant aggregates. A combined $SiO_2 + Fe_2O_3$ content of at least 50% was necessary to sustain a friction coefficient ≥ 0.35, provided the mixture contained approximately 75% polish-resistant aggregates. Slag aggregates rich in Fe_2O_3 demonstrated that iron oxide contributes comparably to silica in preserving skid resistance. The study provides a screening tool that complements AIMS-based morphological characterization and could reduce laboratory burden for routine aggregate qualifications.

METHODOLOGY

Overview

This study presents a screening methodology to support friction aggregate selection in Illinois by leveraging existing DIP data and accelerated polishing results. First, aggregate morphology data are measured using AIMS, including repeated measurements across MD polishing intervals for selected aggregate sources. The data are used to quantify (i) initial aggregate shape characteristics (angularity and surface texture) and (ii) their durability (rate and magnitude of change with polishing in Micro-Deval). The aggregate indicators are then combined with mixture design information (NMAS, gradation descriptors, binder content, volumetrics, and mixture type) and applied through prediction models available in the literature to estimate friction performance metrics, such as IFI_{60}.

Because dense-graded HMA has been the primary basis for many published friction prediction frameworks, model suitability is expected to be strongest for dense-graded mixtures. For surface treatments and friction courses (chip seals, microsurfacing, ultra-thin overlays, high-friction surface treatments), future projects need to focus on the validation of treatment-specific field and laboratory friction data. Predicted friction performance is interpreted within the framework of roadway friction demand, explicitly recognizing that minimum friction requirements are governed by vehicle-pavement interaction under specific operating conditions. Scenario-based friction thresholds—such as those derived from the Deceleration Rate to Avoid Crash (DRAC) parameter—define the minimum surface friction necessary to prevent skidding during emergency braking, especially under wet conditions. These thresholds vary as a function of traffic level, operating speed, geometric characteristics (curves, intersections, downgrade sections), and crash exposure risk.

Friction Demand—Target Deceleration Level

In many operational scenarios, vehicles do not brake to a full stop but decelerate to a target speed because of a vehicular conflict or speed compliance, for example. A practical friction-demand formulation can therefore be based on a target longitudinal deceleration a_x (m/s²), rather than on stopping distance alone. This approach is also convenient for friction-demand categorization because it directly maps friction needs to typical maneuver severity. On a level tangent segment, if braking is friction-limited, the achievable longitudinal deceleration can be approximated as in Figure 39:

$$a_x \approx \eta_{ABS}\,\mu\,g$$

Figure 39. Equation. Longitudinal deceleration.

Where a_x is the achievable longitudinal deceleration (m/s²), η_{ABS} is the braking force utilization factor (typically 0.8 to 0.95 for ABS-equipped vehicles), μ is the pavement friction coefficient, and g is gravitational acceleration (9.81 m/s²). The minimum friction required to achieve a target deceleration on a tangent (Figure 40) is therefore:

$$\mu_{\text{min,tangent}} = \frac{a_x}{\eta_{\text{ABS}}\, g}$$

Figure 40. Equation. Minimum friction requirement.

As an example, using g = 9.81 m/s² and η_{ABS} = 0.9, the minimum friction required for target decelerations spanning 1 to 6 m/s² varies from 0.11 to 0.68 (Table 16). On horizontal curves, longitudinal and lateral tire forces must share the available adhesion potential. According to the friction ellipse (or friction circle in the isotropic case) concept, the combined force utilization is bounded by the tire-pavement friction capacity. On a curve, part of the available friction capacity is consumed by lateral demand (cornering). For pure longitudinal solicitation (straight-line braking/acceleration), the tire force increases up to a maximum value defined by the longitudinal friction capacity, and similarly for pure lateral solicitation (cornering), as shown in Figure 41, where F_z is the normal load, μ_x is the longitudinal friction coefficient, and μ_y is the lateral friction coefficient (Lenzo, 2022).

$$F_{x,\text{max}} = \mu_x F_z \quad F_{y,\text{max}} = \mu_y F_z$$

Figure 41. Equations. Representation of longitudinal and lateral forces.

When cornering while braking or accelerating, the longitudinal and lateral forces share the same friction potential, so the maximum values cannot be reached simultaneously. This coupling is commonly represented by a friction ellipse (anisotropic case) or, under the simplifying assumption of isotropic friction ($\mu_x \approx \mu_y \equiv \mu$), by the friction-circle concept (Figure 42), which leads to the saturation constraints depicted in Figure 43.

$$\left(\frac{F_x}{\mu F_z}\right)^2 + \left(\frac{F_y}{\mu F_z}\right)^2 \leq 1$$

Figure 42. Equation. Friction-circle bond limitation for curves.

$$F_x \leq \sqrt{(\mu F_z)^2 - F_y^2} \quad F_y \leq \sqrt{(\mu F_z)^2 - F_x^2}$$

Figure 43. Equations. Lateral force limits for curves.

On a horizontal curve, the vehicle is simultaneously subjected to lateral demand, represented by a dimensionless side-friction requirement (f), which depends on operating speed and curve radius (Garber & Hoel, 2009). Under combined braking and cornering, the minimum total friction coefficient required to simultaneously support both longitudinal and lateral demands is shown in Figure 44.

$$\mu_{\text{min,curve}} = \sqrt{\left(\frac{a_x}{\eta_{\text{ABS}}\, g}\right)^2 + f^2}$$

Figure 44. Equation. Minimum friction requirement for curves considering side-friction demand.

The available friction on curves must exceed the quadratic combination of braking and cornering demands. Thus, increasing lateral demand reduces the friction margin available for longitudinal deceleration, which is particularly critical under wet-weather or safety-sensitive operating conditions. Typical side-friction demand values used in practice range from 0.1 to 0.2 (Garber & Hoel, 2009), reflecting comfort and safety considerations required in AASHTO design standards. Locations with high combined-demand events—curves, ramps, intersections, and downgrades—require higher friction margins than low-demand tangents. Table 16 shows the friction demand for target decelerations of 1–6 m/s² with assumed $\eta_{ans} = 0.9$. Curve lateral demand is represented by side friction $f = 0.14$ (50 mph) and $f = 0.10$ (70 mph).

Table 16. Minimum Peak Friction Required for Target Deceleration Levels on Tangents and Curves

Target ax (m/s²)	μ_{min} tangent	μ_{min} curve ($f = 0.14$)	μ_{min} curve ($f = 0.10$)
1	0.11	0.18	0.15
2	0.23	0.27	0.25
3	0.34	0.37	0.35
4	0.45	0.47	0.46
5	0.57	0.58	0.58
6	0.68	0.70	0.69

Friction Prediction Method Overview

Prediction models reported in the literature (Aldagari et al., 2022; Chowdhury et al., 2017; Kassem et al., 2013) were identified as suitable for a first-level, general aggregate screening exercise. Illinois aggregate characteristics were previously quantified using AIMS indices measured at multiple MD polishing times. These measurements were condensed into durability indicators by fitting time-evolution functions. Gradation descriptors can be compiled to ensure that predictions also account for the surface type rather than aggregate properties alone. These indicators serve as inputs to the models for estimating initial friction and friction loss trends. For a long-term perspective, the applicability of the selected models needs to be validated and calibrated using available field or laboratory friction data. The policy refinement should account for the determination of friction demand categories based on traffic level, operating speed, and safety context, such as tangent/curves, intersections, and wet-weather crash risks. Collectively, predicted friction levels and durability are compared with demand thresholds to classify aggregate sources and selected gradations as appropriate for each surface type and demand category (Maia, Hajj, et al., 2024), and the results can be gathered in a statewide database structure to support continuous improvement of model calibration and policy guidance. Figure 45 summarizes the proposed workflow for friction-focused aggregate screening.

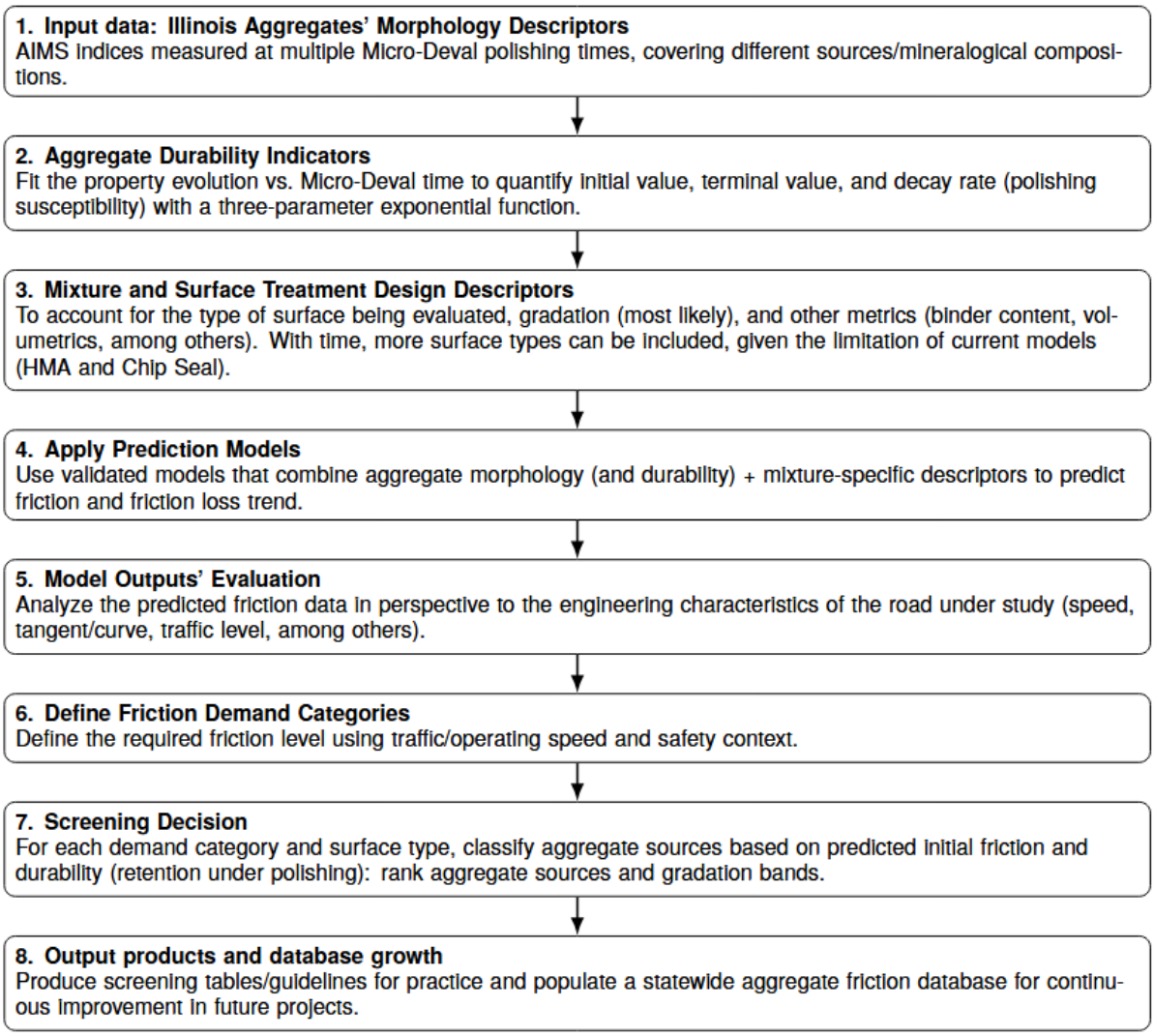

Figure 45. Graph. Proposed workflow for friction-focused aggregate screening using AIMS/Micro-Deval data, mixture design descriptors, and friction prediction models.

Aggregate Characterization—Morphology

Moaveni et al. (2014) and Mahmoud and Ortiz (2014) evaluated the effectiveness of two advanced aggregate imaging systems, AIMS-II and the enhanced University of Illinois Aggregate Image Analyzer (E-UIAIA), for quantifying changes in aggregate morphology caused by Micro-Deval polishing. Eleven coarse aggregates representing typical Illinois and neighboring-state sources (three limestones, two dolomites, two gravels, one steel slag, one air-cooled blast furnace slag, one quartzite, and one sandstone) were tested in a modified MD procedure using a single size fraction (passing 12.5 mm, retained on 9.5 mm, using 750 g of aggregate, 5,000 g steel balls, and 2 L of water). More than 26,000 particles were scanned at multiple polishing durations between 0 and 210 minutes, and angularity index (AI), surface texture index (STI), and flat-and-elongated ratio (FER)/sphericity were computed at each interval for both devices. Table 17 summarizes the aggregate sources evaluated in this study.

Table 17. Aggregate Sources, Geology, and Micro-Deval Configuration for Illinois Materials

ID	Description	Geology
FP1	Limestone	Pennsylvanian–Bond–Millersville
FP2	Limestone	Mississippian–Salem
FP3	Limestone	Ordovician–Galena
FP4	Silurian Dolomite	Silurian–Racine
FP5	Silurian Dolomite	Silurian–Racine–Joliet
FP6	Crushed Gravel	Henry Fm. Wisconsin glacial till
FP7	Chert Gravel (99% chert)	Maramec River gravel
FP8	Steel Slag	Steel slag
FP9	ACBF Slag	Air-cooled blast furnace slag
FP10	Quartzite	Lower Proterozoic quartzite (Baraboo Fm.)
FP11	Sandstone	Mississippian–Rosiclare sandstone

For all 11 aggregates, both imaging systems showed a decreasing trend in AI and STI with increasing MD time, with a marked reduction rate up to about 105 minutes followed by a slower approach to a terminal value. Steel and ACBF slags (FP8, FP9) exhibited minimal or no texture loss in AIMS-II results, consistent with their known high polishing resistance, whereas carbonates and limestones showed rapid angularity and texture loss. The three-parameter exponential decay function was fitted to all angularity and surface texture data (analog to Figure 37). In this equation, *a* represents the terminal (asymptotic) shape value, *b* corresponds to the difference between the initial and terminal values, and *c* is the rate parameter governing the speed of degradation. The model demonstrated high goodness-of-fit, with coefficients of determination typically ranging from $R^2 = 0.85$ to 0.99 for most aggregate sources. The Micro-Deval weight loss was combined with imaging-based percent changes in AI and STI at 105 minutes of polishing to classify aggregates into performance zones characterized by high or low abrasion and high or low polishing susceptibility. Table 18 summarizes these classifications.

Table 18. Aggregate Classification Based on Abrasion-Breakage (Angularity) and Polishing-Breakage (Surface Texture) Framework

Aggregate	Abrasion–Breakage (Angularity)	Polishing–Breakage (Surface Texture)
FP1	High Abrasion – Low Breakage	High Polishing – Low Breakage
FP2	High Abrasion – Low Breakage	High Polishing – Low Breakage
FP3	High Abrasion – High Breakage	High Polishing – High Breakage
FP4	High Abrasion – Low Breakage	High Polishing – Low Breakage
FP5	High Abrasion – High Breakage	Low Polishing – High Breakage
FP6	Low Abrasion – High Breakage	High Polishing – High Breakage
FP7	Low Abrasion – Low Breakage	Gained Texture – Low Breakage
FP8	Low Abrasion – Low Breakage	Gained Texture – Low Breakage
FP9	High Abrasion – High Breakage	Low Polishing – High Breakage
FP10	Low Abrasion – Low Breakage	Low Polishing – Low Breakage
FP11	High Abrasion – High Breakage	Gained Texture – High Breakage

Mahmoud and Ortiz (2014) extended this work into an implementation procedure for IDOT, focusing on AIMS. Using the same 11 aggregate sources, they performed staged MD testing (15–210 minutes) and concluded, based on confidence-interval analysis of AIMS texture data, that all aggregates reached terminal texture and angularity by approximately 210 minutes. They then applied the same exponential model to texture evolution. A full polishing curve can be adequately captured using AIMS measurements at only three points (0, 105, and 210 minutes), with an optional 60-minute point for improved precision. This led to a recommended AIMS and MD standard procedure for Illinois. The exponential model characterization of these aggregates resulted in the parameters shown in Table 19 and Table 20. The model demonstrated high goodness-of-fit, with coefficients of determination typically ranging (R^2) from 0.85–0.99.

Table 19. Three-Parameter Exponential Models for Angularity Loss under Micro-Deval

ID	E-UIAIA AI model			AIMS-II AI model		
	a	b	c	a	b	c
FP1	321.5	258.8	0.0057	1,492	1,185	0.0174
FP2	329.9	208.4	0.0094	1,433	1,232	0.0140
FP3	253.7	237.6	0.0152	1,384	1,189	0.0155
FP4	278.9	286.4	0.0041	1,877	1,053	0.0185
FP5	255.2	223.9	0.0276	1,443	1,331	0.0186
FP6	371.0	−0.1	0.0265	1,924	560.6	0.0529
FP7	360.2	45.1	0.0446	2,618	274.4	0.0239
FP8	326.7	169.2	0.0110	2,112	1,144	0.0114
FP9	328.5	172.5	0.0570	1,590	1,635	0.0248
FP10	348.8	127.8	0.0169	2,098	730.0	0.0190
FP11	343.1	153.8	0.0370	1,130	1,323	0.0209

*Angularity Index = $a + b\, e^{-ct}$.

Table 20. Three-Parameter Exponential Models for Surface Texture Loss under Micro-Deval

ID	E-UIAIA STI model			AIMS-II STI model		
	a	b	c	a	b	c
FP1	2.03	0.93	0.0285	120.8	137.6	0.0266
FP2	2.02	1.01	0.0154	151.1	162.1	0.0256
FP3	1.32	1.14	0.0170	93.27	92.70	0.0304
FP4	2.00	0.73	0.0140	97.16	65.95	0.0095
FP5	0.98	1.10	0.0340	53.34	14.83	0.0341
FP6	1.46	≈0	−1.5760	164.7	64.50	0.0256
FP7	1.15	0.15	0.0540	204.1	−49.39	0.0866
FP8	1.30	0.68	0.0260	437.7	−16.49	−0.0030
FP9	1.50	0.80	0.0237	659.1	29.18	0.9935
FP10	1.72	0.73	0.0220	436.8	161.8	0.0176
FP11	1.93	0.79	0.0400	353.8	−16.31	2.4130

*Texture Index = $a + b\, e^{-ct}$. Negative b or anomalous c values reflect negligible STI loss.

Figure 46 and Figure 47 present the evolution of angularity and surface texture with polishing time. Aggregate sources such as FP7, FP8, and FP10 exhibit relatively low abrasion and polishing susceptibility, maintaining higher morphology indices throughout the test. After 210 minutes of MD polishing, FP7 (chert gravel) and FP8 (steel slag) display the highest retained angularity values. In terms of surface texture, FP8 (steel slag), FP9 (air-cooled blast furnace slag), FP10 (quartzite), and FP11 (sandstone) maintain comparatively elevated texture indices at the end of the polishing period, suggesting improved resistance to micro-texture degradation.

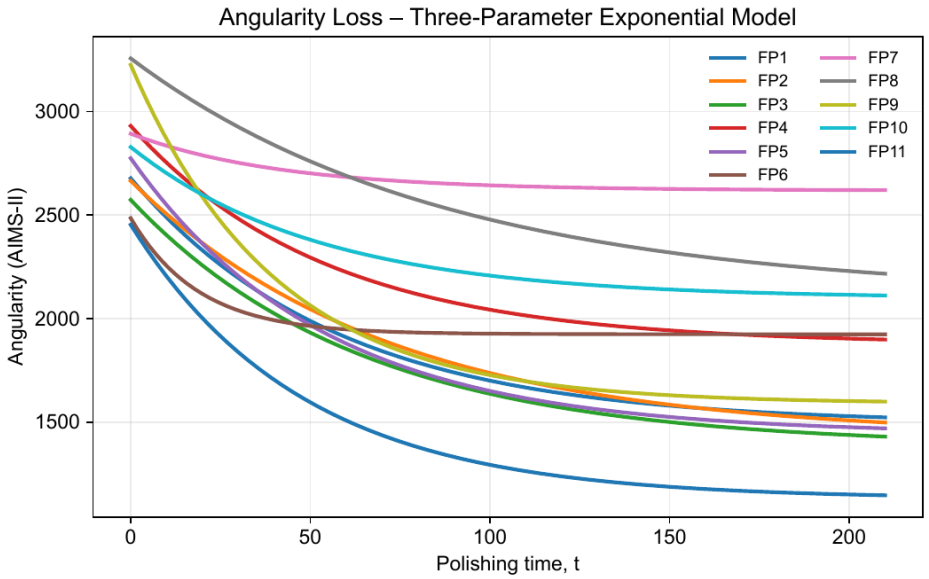

Figure 46. Graph. Abrasion resistance—angularity evolution with MD polishing time for Illinois aggregates.

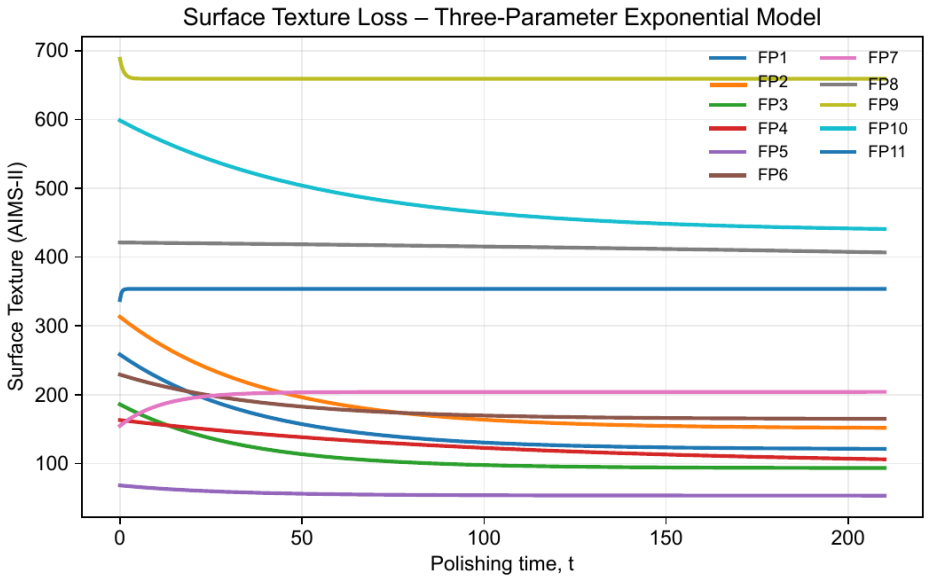

Figure 47. Graph. Polishing resistance—surface texture evolution with MD polishing time for Illinois aggregates.

HMA Gradation

Aggregate gradation requirements were obtained from IDOT's (2022) *Standard Specifications for Road and Bridge Construction* (Section 406—Hot-Mix Asphalt; Table 406-2). The following gradations are permitted for surface courses: IL-9.5FG, IL-9.5, IL-9.5L, SMA-9.5, and SMA-12.5. To further explore different gradation structures on Weibull representation, additional mixes were considered, including IL-19.0, IL-19.0L, and IL-4.75. Table 21 and Table 22 present the specified gradation bands for the primary IDOT surface course mixes and additional non-surface mixes selected for analysis, respectively.

Table 21. Mixture Composition Limits (% Passing) for Extracted IDOT Surface Mixes

Sieve Size	IL-9.5FG		IL-9.5		IL-9.5L		SMA-9.5		SMA-12.5	
	Min	Max	Min	Max	Min	Max	Min	Max	Min	Max
37.5 mm	–	–	–	–	–	–	–	–	–	–
25 mm	–	–	–	–	–	–	–	–	–	–
19 mm	–	–	–	–	–	–	–	–	100	–
12.5 mm	–	100	–	100	–	100	95	100	90	99
9.5 mm	90	100	90	100	95	100	70	95	50	85
4.75 mm	60	75	32	69	52	80	30	50	20	40
2.36 mm	45	60	32	52	38	65	20	30	16	24
1.18 mm	25	40	10	32	–	–	–	21	–	–
600 µm	15	30	–	–	–	–	–	18	–	–
300 µm	8	15	4	15	–	–	–	15	–	–
150 µm	6	10	3	10	–	–	–	–	–	–
75 µm	4	6.5	4	6	4	8	8	11	8	11
20 µm	–	–	–	–	–	–	–	3	–	3
Dust/Asphalt Binder Ratio	–	1	–	1	–	1	–	–	–	–

Table 22. Mixture Composition Limits (% Passing) for IL-19.0, IL-19.0L, and IL-4.75 Mixes

Sieve Size	IL-19.0		IL-19.0L		IL-4.75	
	Min	Max	Min	Max	Min	Max
37.5 mm	–	–	–	–	–	–
25 mm		100	–	100	–	–
19 mm	90	100	95	100	–	–
12.5 mm	75	89	–	–	–	100
9.5 mm	–	–	–	–	–	100
4.75 mm	40	60	38	65	90	100
2.36 mm	26	42	–	–	70	90
1.18 mm	15	30	–	–	50	65
600 µm	–	–	–	–	–	–
300 µm	6	15	–	–	15	30
150 µm	4	9	–	–	10	18
75 µm	3.0	6.0	3.0	7.0	7.0	9.0
20 µm	–	–	–	–	–	–
Dust/Asphalt Binder Ratio	–	1.0	–	1.0	–	1.0

Gradations were represented using a two-parameter Weibull cumulative distribution (Figure 48). The parameters were estimated independently for each upper and lower specification band using nonlinear least-squares regression applied to the specified percent passing limits.

$$F(x,k,\lambda) = 1 - e^{-(x/\lambda)^k}$$

Figure 48. Equation. Cumulative Weibull distribution.

where x = aggregate size (mm), k = shape parameter, λ = scale parameter (mm), and $F(x)$ represents the cumulative percent passing expressed as a fraction. Only sieve sizes with defined specification limits were included in the regression. A weighted nonlinear regression approach was adopted in which sieve sizes in the coarse fraction ($x \geq 4.75$ mm) were assigned higher weights to ensure adequate representation of the structural portion of the gradation.

Table 23 presents the optimized Weibull parameters for all IDOT HMA gradation bands. IL-19.0, IL-19.0L, and IL-4.75 are not specified for surface HMA courses in IDOT practice but were included for comparative evaluation.

Table 23. Weibull Parameters for IDOT HMA Gradation Bands

Mix	Band	k	λ	RMSE (%)
IL-9.5FG	Upper	0.851	2.802	4.60
IL-9.5FG	Lower	1.039	4.753	3.35
IL-9.5	Upper	1.075	3.659	5.59
IL-9.5	Lower	2.420	6.852	6.01
IL-9.5L	Upper	0.955	2.675	3.29
IL-9.5L	Lower	1.755	5.465	4.71
SMA-9.5	Upper	1.790	5.583	5.95
SMA-9.5	Lower	1.969	8.157	4.50
SMA-12.5	Upper	1.911	6.672	3.03
SMA-12.5	Lower	2.545	10.015	7.62
IL-19.0	Upper	0.878	4.962	2.94
IL-19.0	Lower	1.032	8.918	1.51
IL-19.0L	Upper	1.111	4.537	1.51
IL-19.0L	Lower	1.323	8.296	0.68
IL-4.75	Upper	0.918	0.988	1.72
IL-4.75	Lower	0.900	1.877	0.98

The weighted Weibull fits demonstrate that IDOT gradation envelopes can be represented using a compact two-parameter formulation while preserving accuracy in the structurally relevant coarse fraction ($x \geq 4.75$ mm). The shape parameter k governs the curvature of the cumulative distribution. Lower k values correspond to more gradual transitions in percent passing (smoother gradations), whereas higher k values indicate steeper transitions and more concentrated particle size distributions. Gap-graded SMA mixtures generally exhibited larger curvature variability, reflecting their discontinuous gradation structure. The scale parameter λ is directly related to the characteristic

particle size controlling the inflection region of the distribution. Mixtures with larger NMAS tend to exhibit larger λ values, consistent with physical expectations. Overall, the weighted regression approach provided stable parameter estimation across dense-, fine-, and gap-graded mixtures without requiring distribution truncation.

Chip Seal Gradation

For chip seal applications in Illinois, aggregate gradations and quality requirements are governed by IDOT's *Standard Specifications for Road and Bridge Construction* (Section 1004) and the corresponding Special Provisions for Bituminous Surface Treatments. IDOT specifies that aggregates used in chip seal applications shall conform to designated coarse aggregate gradations, including CA14, CA15, CA16, and CA20 (Table 24). These gradations are intentionally open graded to promote proper embedment, surface macrotexture development, and effective drainage. IDOT discourages the use of well-graded aggregates in chip seal treatments because particle size variability can reduce uniform tire contact, leading to partial friction loss. Larger particles may become dislodged under traffic or snowplowing operations, while excessively fine aggregates may become overly embedded in the binder, increasing the risk of bleeding. Coarse aggregates must also satisfy minimum quality criteria defined in Section 1004, including limits on sodium sulfate soundness loss, LA abrasion loss, deleterious materials content, and percent passing the No. 200 sieve.

Table 24. IDOT Coarse Aggregate Gradation Bands for Chip Seal Applications (% Passing)

Gradation	12.5 mm	9.5 mm	4.75 mm	2.36 mm	1.18 mm
CA14	90 ± 10	45 ± 20	3 ± 3	–	–
CA15	100	75 ± 15	7 ± 7	–	2 ± 2
CA16	100	97 ± 3	30 ± 15	–	2 ± 2
CA20	100	92 ± 8	20 ± 10	5 ± 5	3 ± 3

To provide a continuous analytical representation of the chip seal aggregate gradation bands, a two-parameter Weibull cumulative distribution was fitted to the coarse-side control points (12.5, 9.5, and 4.75 mm) for both the upper and lower limits of each IDOT gradation. The Weibull parameters λ and k were obtained through nonlinear least-squares optimization, with the fitting restricted to sieve sizes ≥ 4.75 mm to ensure accurate representation of the coarse fraction governing macrotexture and embedment behavior in chip seal applications (Table 25).

Table 25. Weibull Parameters for IDOT Chip Seal Gradation Bands

Gradation	Band	k	λ	RMSE (%)
CA14	Upper	4.616	9.36	1.64
CA14	Lower	6.278	11.59	0.16
CA15	Upper	3.932	7.68	0.01
CA15	Lower	9.829	9.58	0.06
CA16	Upper	3.530	5.50	0.06
CA16	Lower	4.114	7.39	0.05
CA20	Upper	4.276	6.05	0.06
CA20	Lower	4.124	8.20	0.14

Application of the Friction Prediction Model

The IFI value for any aggregate-gradation combination was predicted using the analytical framework proposed by Aldagari et al. (2022), which expresses mixture friction behavior as a function of aggregate texture evolution, angularity evolution, and gradation characteristics. The model also uses a traffic-related parameter (*N*, based on a traffic multiplication factor) to estimate initial and final MPD values. The model defines three mixture-level parameters: terminal friction value (a_{mix}), the initial friction value ($a_{mix} + b_{mix}$), and friction decay rate (c_{mix}). Model parameters for HMA are defined in Figure 49 to Figure 51 and for chip coat surfaces in Figure 52 to Figure 54.

$$a_{mix} = \frac{49.3144 + \lambda}{351.289 - 0.00193(AMD)^2}$$

Figure 49. Equation. Terminal IFI for HMA surfaces.

$$a_{mix} + b_{mix} = 0.33 \ln\left(\frac{1.43757(a_{TX} + b_{TX}) + 46.8933\lambda + 333.491k}{2.42031(a_{GA} + b_{GA})}\right) + 1.00801$$

Figure 50. Equation. Initial IFI for HMA surfaces.

$$c_{mix} = 0.018 + 1.654\, c_{TX} + 1.346\, c_{GA}$$

Figure 51. Equation. Decay rate in IFI for HMA surfaces.

$$a_{mix} = \frac{40.493 + \lambda}{330 - 0.0011(AMD)^2}$$

Figure 52. Equation. Terminal IFI for chip seal surfaces.

$$a_{mix} + b_{mix} = 0.4 \ln\left(\frac{1.43757(a_{TX} + b_{TX}) + 46.8933\lambda + 3343.491k}{2.02031(a_{GA} + b_{GA})}\right)$$

Figure 53. Equation. Initial IFI for chip seal surfaces.

$$c_{mix} = 2.654\, c_{TX} + 1.346\, c_{GA}$$

Figure 54. Equation. Decay rate in IFI for chip seal surfaces.

The parameters are derived from aggregate morphology descriptors obtained from AIMS: surface texture exponential coefficients (a_{TX}, b_{TX}, c_{TX}), angularity exponential coefficients (a_{GA}, b_{GA}, c_{GA}), the aggregate surface texture expected at 150 minutes of Micro-Deval polishing (AMD), and gradation characteristics encoded via the Weibull scale (λ) and shape (k) parameters. Table 26 presents the final stored AIMS-II aggregate parameters and computed AMD values used as inputs to the friction model.

For FP7, FP8, and FP11, texture loss during MD polishing was negligible, so $b_{TX} = 0$ and $c_{TX} = 0$ were adopted, resulting in time-invariant texture values.

Table 26. AIMS-II Aggregate Parameters and Computed AMD Values for Friction Modeling

ID	a_{TX}	b_{TX}	c_{TX}	a_{GA}	b_{GA}	c_{GA}	AMD
FP1	120.8	137.6	0.0266	1492	1185	0.0174	123.35
FP2	151.1	162.1	0.0256	1433	1232	0.0140	154.58
FP3	93.27	92.70	0.0304	1384	1189	0.0155	94.24
FP4	97.16	65.95	0.0095	1877	1053	0.0185	113.02
FP5	53.34	14.83	0.0341	1443	1331	0.0186	53.43
FP6	164.7	64.50	0.0256	1924	560.6	0.0529	166.09
FP7	204.1	0.00	0.00	2618	274.4	0.0239	204.10
FP8	437.7	0.00	0.00	2112	1144	0.0114	437.70
FP9	659.1	29.18	0.9935	1590	1635	0.0248	659.10
FP10	436.8	161.8	0.0176	2098	730.0	0.0190	448.35
FP11	353.8	0.00	0.00	1130	1323	0.0209	353.80

RESULTS

HMA Friction Prediction

The predicted initial IFI values showed dependence on both gradation structure and aggregate mineralogy. Coarser gradations (higher λ values), such as IL 19 mm and SMA-type bands, consistently produced higher initial friction values compared to finer gradations (e.g., IL 4.75 mm). This behavior is expected, as coarser structures enhance macrotexture, which contributes to hysteresis mechanisms and improved water drainage at the tire-pavement interface. The coarser limits of IL-9.5 and IL-12.5 gradations also demonstrate good performance in terms of predicted IFI. Aggregate mineralogy exerted a similarly strong influence on predicted friction. Steel slag (FP8), quartzite (FP10), chert gravel (FP7), and air-cooled blast furnace slag (FP9) exhibited the highest initial IFI values across most gradation bands. These materials are characterized by high angularity indices, strong resistance to polishing, and durable microtexture retention. Steel slag demonstrated superior performance, likely due to its high specific gravity and highly angular particle structure. Quartzite and chert also performed favorably due to their hardness and resistance to surface polishing.

In contrast, limestone sources (FP1–FP3) generally produced lower predicted initial IFI values, particularly when combined with finer gradations, as shown in Figure 55. This trend is consistent with the smoother surface texture and greater polishing susceptibility typically associated with carbonate aggregates. Silurian dolomites (FP4 and FP5), crushed gravel (FP6), and sandstone (FP11) exhibited intermediate performance, indicating that acceptable friction levels can be achieved with these materials when paired with sufficiently coarse gradations. Overall, the results confirm that friction performance is governed by the coupled interaction between aggregate microtexture durability, angularity retention, and gradation-controlled macrotexture. The generated friction matrix provides a rational screening tool for identifying aggregate-mix combinations suitable for high-demand surface applications, particularly in high-speed or high-traffic environments where sustained friction performance is critical.

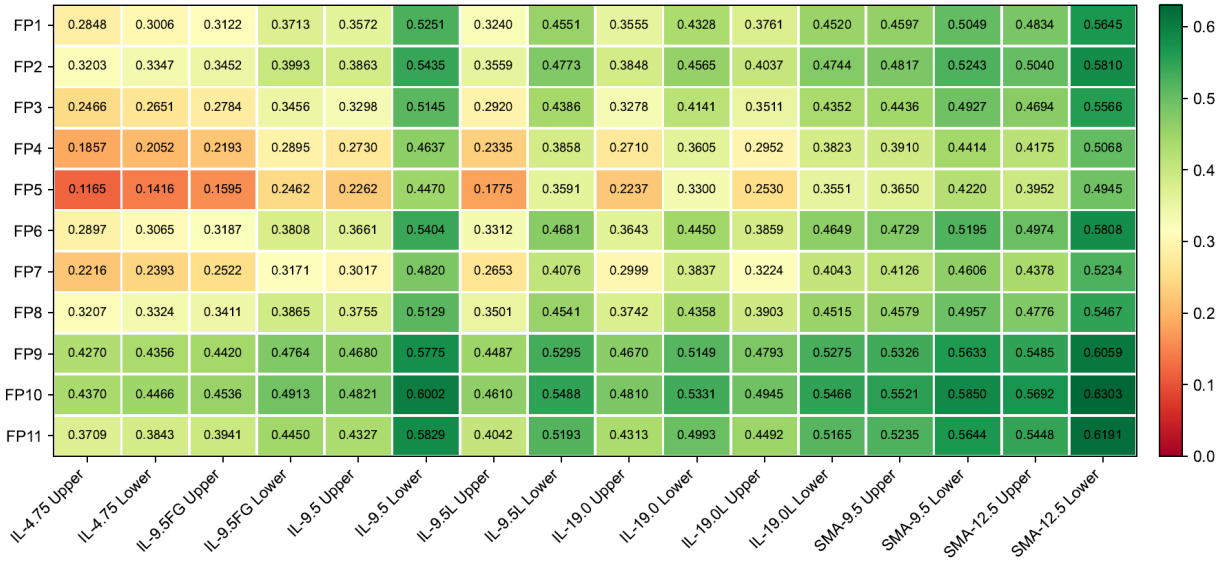

Figure 55. Graph. Predicted initial IFI (a_{mix}+b_{mix}) for all HMA aggregate-gradation combinations.

In the IFI friction model, the parameter a_{mix} represents the long-term, asymptotic friction value approached by a pavement surface after extensive traffic polishing. Physically, it characterizes the lower bound of surface friction once the texture most susceptible to polishing has been removed. The denominator of the a_{mix} equation decreases as AMD increases, making it highly sensitive to aggregate morphology. When AMD exceeds approximately 426.7, the threshold at which the denominator becomes zero, the expression becomes undefined or negative. This behavior indicates that the gradation-based asymptote alone is insufficient to represent the long-term friction performance of highly textured aggregates. In such cases, following the convention adopted in the predictive model, a_{mix} was replaced by (a_{mix} + b_{mix}), treating the initial post-construction friction as the applicable friction reference. Among the 11 aggregates evaluated, FP8, FP9, and FP10 exceeded this AMD threshold.

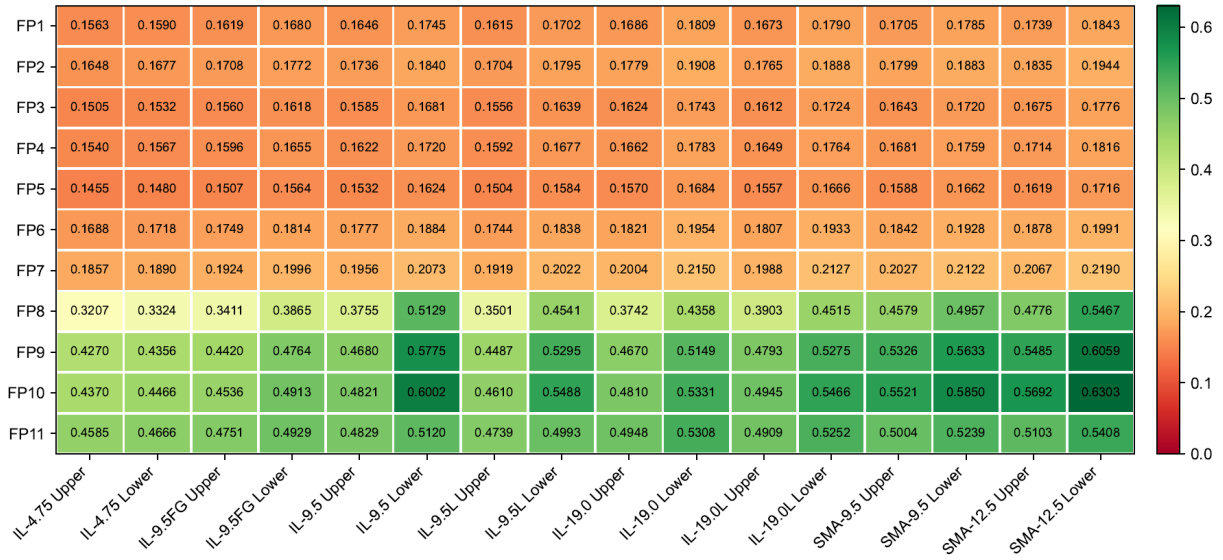

Figure 56. Graph. Predicted final IFI (a_{mix}) for all HMA aggregate-gradation combinations.

Chip Seal Friction Prediction

The predicted initial IFI ($a_{mix} + b_{mix}$) for chip seal surface treatments is presented in Figure 57. The results show a gradation-driven trend, with the CA15 band (lower limit) consistently producing the highest initial IFI values across nearly all aggregate sources. CA15 Lower combinations typically fall within the upper performance range (approximately 0.69–0.77), followed by CA14 Lower. In contrast, CA16 and CA20 grades generally yield lower initial IFI values. The superior performance of CA15 Lower is associated with its larger Weibull parameters (λ and κ), which promote enhanced macrotexture development. Because the model formulation increases initial IFI with increasing gradation scale and shape parameters, gradations with more coarser fractions exhibit improved friction potential.

Aggregate mineralogy further differentiates performance within each gradation band. Quartzite (FP10), steel slag (FP8), and sandstone (FP11) consistently produce higher predicted initial IFI values, especially when paired with CA15 Lower. These materials are characterized by high angularity and durable microtexture retention, which enhance the numerator term of the friction model. Limestone (FP1–FP3) and dolomite (FP4–FP5) sources generally show lower terminal predicted friction values, reflecting their comparatively smoother surface texture and greater susceptibility to polishing. The terminal friction parameter (a_{mix}), shown in Figure 58, exhibits a similar but less amplified pattern. While gradation influence remains evident, variability across bands is reduced relative to the initial IFI results. Hard, polish-resistant aggregates such as quartzite and steel slag maintain the highest terminal friction levels, indicating sustained long-term friction potential. Limestone and dolomite aggregates demonstrate lower terminal values, suggesting more deterioration susceptibility in terms of long-term polishing effects.

Notably, the differences between gradation bands are more pronounced in the initial friction parameter than in the terminal friction term. This indicates that gradation primarily influences early-life macrotexture contribution, whereas long-term friction is more strongly governed by aggregate microtexture durability. Overall, the chip seal analysis confirms that optimal friction performance requires a favorable gradation band—particularly CA15 Lower—and a hard, polish-resistant aggregate such as quartzite, steel slag, or sandstone. These combinations provide high initial friction and sustained terminal friction, supporting their suitability for high-demand chip seal applications.

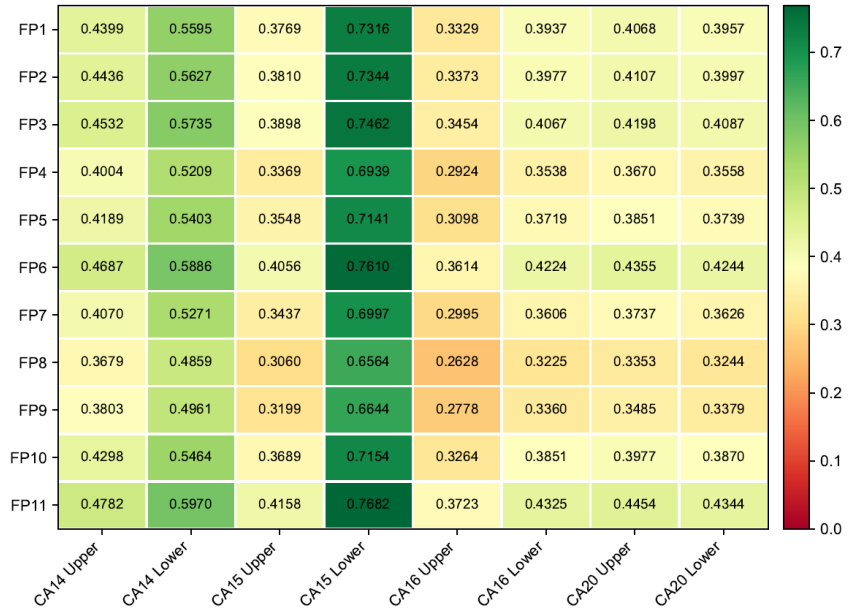

Figure 57. Graph. Predicted initial IFI (a_{mix} + b_{mix}) for all chip seal aggregate-gradation combinations.

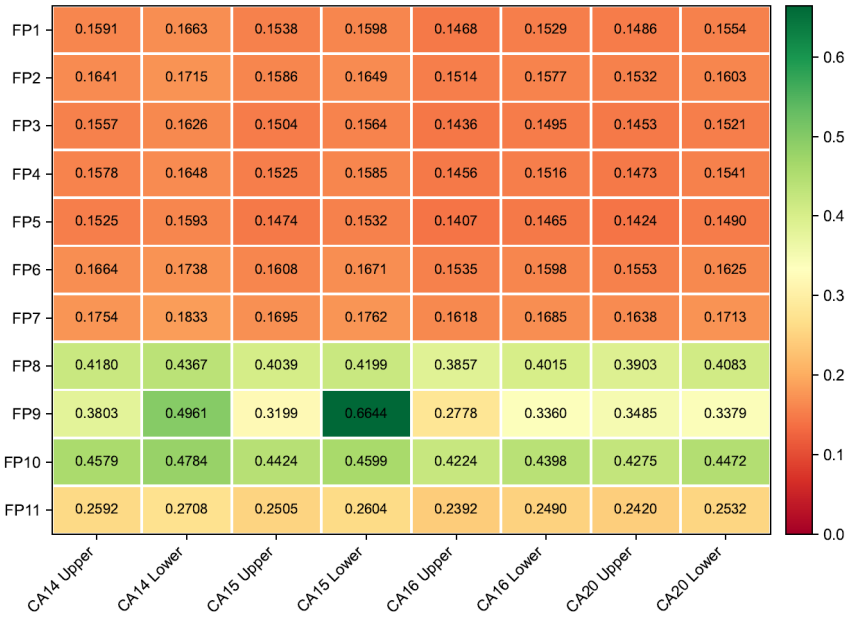

Figure 58. Graph. Predicted final IFI (a_{mix}) for all chip seal aggregate-gradation combinations.

For chip seals, PUC (performance-based uniformity coefficient) is a gradation-uniformity index computed from the aggregate size distribution, evaluated at two standardized points around the median size (M): 0.7M and 1.4M. They quantify how tightly clustered the aggregate sizes are around the median. If the gradation is uniform, a large fraction of particles falls near M, so the distribution "jumps" quickly through that region, yielding a small ratio F(0.7M)/F(1.4M), leading to PUC values closer to zero. The closer PUC is to zero, the more uniform the aggregate gradation, optimizing the performance against aggregate loss (raveling) and bleeding.

Table 27. Uniformity Coefficients for the Different Gradation Bands Used for Chip Seal in Illinois

Gradation	Band	k	λ	M (mm)	F(0.7M)	F(1.4M)	PUC
CA14	Upper	4.616	9.36	8.646	0.125058	0.962223	0.129967
CA14	Lower	6.278	11.59	10.933	0.071189	0.996756	0.071421
CA15	Upper	3.932	7.68	6.996	0.156766	0.925916	0.169309
CA15	Lower	9.829	9.58	9.229	0.020596	1.000000	0.020596
CA16	Upper	3.530	5.50	4.958	0.178644	0.897029	0.199151
CA16	Lower	4.114	7.39	6.760	0.147680	0.937145	0.157585
CA20	Upper	4.276	6.05	5.553	0.139999	0.946170	0.147964
CA20	Lower	4.124	8.20	7.503	0.147195	0.937728	0.156970

Macrotexture Prediction

The MPD predictions confirm that gradation is the dominant driver of macrotexture for both HMA and chip seal surfaces, with traffic governing the rate of decline through polishing. For HMA, the heatmaps at low, medium, high, and very high traffic (Appendix G) illustrate a strong horizontal gradient, indicating that mix type controls the magnitude of MPD across all aggregates. Coarser gradations, particularly SMA-12.5 Lower and IL-9.5 Lower, consistently occupy the highest texture tier at every traffic level, while fine dense-graded mixes such as IL-4.75 and IL-9.5FG Upper remain in the lowest MPD range. As traffic increases, the overall color intensity shifts downward, but the ranking between mix types remains stable, reinforcing the primary influence of the Weibull scale parameter (λ) on macrotexture depth. Aggregate effects in HMA are secondary but still observable. Aggregates with low polishing rates (e.g., FP8, FP11, FP7) maintain higher MPD retention across traffic levels. However, even at very high traffic, the difference attributable to aggregate source remains substantially smaller than the spread introduced by gradation selection. This confirms that, for HMA applications, mix design decisions outweigh aggregate polishing characteristics in determining long-term macrotexture performance.

For chip seals, the gradation effect is similarly dominant, but the aggregate effect is more visually pronounced in the heatmaps (Appendix G). CA14 Lower and CA14 Upper consistently produce the highest MPD values across all traffic levels, reflecting their larger Weibull scale parameters and coarser particle size distributions. The chip seal color scheme further emphasizes that values around 1.0 mm represent typical performance, while only values approaching 2.0 mm transition into the highest texture classification. As traffic increases, CA14 Lower remains within the upper macrotexture tier, whereas CA16 Upper and CA20 Upper progressively shift toward lower MPD ranges, particularly when paired with more polish-sensitive aggregates. Aggregate influence is more evident in chip seal than in HMA because the texture is directly governed by the exposed single-size aggregate layer. FP8, FP11, and FP7 consistently appear in higher MPD tiers across traffic levels, while FP9 (high abrasion aggregate), FP6, and FP5 trend lower, particularly under very high traffic. Nevertheless, even in chip seal applications, the choice of gradation remains the first-order decision variable. Overall, the results demonstrate strong internal consistency between gradation-driven texture predictions and polishing-rate effects, while highlighting that optimal macrotexture performance must ultimately be balanced with mechanical durability and constructability considerations discussed previously.

SUMMARY AND FUTURE WORK

The findings from this chapter indicate the potential modifications to Illinois aggregate policies that could improve pavement friction overall. Aggregate source plays a substantial role, as indicated by the models and current aggregate policy, for both chip seal and HMA. A major limitation is the limited number of sources tested for each aggregate. Even in the preliminary study, there is some variation between different sources, such as for limestone, in terms of the friction they can provide. Future work should assess the uncertainty depending on quarry source and incorporate this into the friction aggregate policy. In addition, utilizing coarser fractions of gradation bands results in better texture and friction, as expected. Currently, there is no friction index for HMA included in the mix design process, so refinement of gradation policies for surface mixes should be considered in areas where the friction demand is high. Meanwhile, SMA gradations provide much more definitive friction due to more restrictive gradation bands and aggregate requirements. This is even more important for chip seals, as the allowed aggregate gradation is largely based on engineering judgement. Friction and uniformity-based coefficients can therefore be a factor in the decision of which aggregate gradation to select.

CHAPTER 7: SUMMARY AND RECOMMENDATIONS

SUMMARY OF RESEARCH

This research provides a comprehensive foundation for the development of an Illinois friction management program by integrating safety analysis, pavement performance modeling, life cycle optimization, data architecture design, and implementation strategy. The project reviewed literature on pavement friction management, pavement treatment, pavement aggregate policies, safety performance functions (SPFs), benefit-cost analysis frameworks, and friction management practices adopted by other state transportation agencies and Federal Highway Administration guidance. The review identified a critical gap in current practice: Although friction is directly linked to crash risk, it is rarely integrated into pavement management systems in a systematic and economically optimized manner. A detailed assessment of current Illinois Department of Transportation practice was conducted, including analysis of roadway inventory data, locked-wheel skid tester (LWST) friction databases, SCRIM (sideway-force coefficient routine investigation machine) continuous measurements, preservation records, crash data, traffic exposure datasets, and macrotexture measurements. This effort revealed inconsistencies in data identifiers, partial coverage across years, and the absence of a unified geo-database linking friction, safety, and serviceability information. These findings motivated the design of a structured friction geo-database architecture to support long-term implementation.

From an analytical perspective, the study established SPFs that quantify crash risk as a function of friction, traffic load, and geometric characteristics for both roadway segments and intersections. Continuous 2025 SCRIM data were incorporated to enhance spatial coverage and improve intersection-level safety modeling.

Building upon the safety analysis, a life cycle cost analysis framework was developed to jointly model pavement friction (safety dimension) and Condition Rating Survey (serviceability dimension). The model integrates deterioration processes, treatment effectiveness functions, agency construction costs, user serviceability costs, and crash-related safety costs into a unified dynamic optimization structure. The framework generates optimal stationary treatment policies that map 2D pavement states (CRS, friction) to cost-minimizing treatment decisions.

The resulting solution exhibits a decision-tree structure that is intuitive, transparent, and scalable. For each peer group and traffic category, a unique policy map is generated, enabling straightforward network-level site screening and treatment prioritization. A case study in Illinois demonstrates that optimized life cycle policies outperform traditional threshold-based approaches over long horizons, particularly in balancing short-term intervention costs with long-term deterioration dynamics.

Finally, a prototype architectural plan for an Illinois friction management program was proposed, including the design of a friction geo-database integrating roadway inventory, friction measurements (LWST and SCRIM), crash data, preservation records, and treatment effectiveness parameters. This data infrastructure supports consistent safety modeling, decision-tree implementation, and program-level monitoring.

ARCHITECTURAL PLAN OF AN ILLINOIS FRICTION MANAGEMENT PROGRAM

The implementation of a statewide friction management program requires more than analytical models. It also demands a well-structured database capable of integrating heterogeneous data sources and assisting operational decision-making. Building upon the modeling framework, including SPFs, life cycle cost optimization, and decision-tree-based screening, this chapter presents the architectural design and prototype development of an Illinois Friction Geo-Database. The objective of the geo-database is to serve as the central data backbone for the Illinois pavement friction management program. It integrates roadway inventory data, discrete and continuous friction measurements, preservation history, crash records, traffic exposure data, macrotexture measurements, and treatment effectiveness information into a unified spatial framework. By linking safety, serviceability, and treatment information at the segment and site levels, the database enables consistent network-level screening, performance monitoring, and benefit-cost evaluation (Figure 59).

The architectural design follows three guiding principles:

1. Integration across condition dimensions: Friction, CRS, traffic, crash data, and treatment history are linked through common spatial and attribute identifiers (e.g., inventory key route ID, begin-end mileposts, coordinates) to ensure compatibility across datasets.

2. Scalability and maintainability: The structure supports periodic updates from IDOT databases, continuous pavement friction measurement across years, preservation records, and real-time traffic/crash sources.

3. Decision support readiness: The database is structured to directly interface with SPF estimation outputs, Empirical Bayes estimations, life cycle cost calculations, and optimal policy mappings derived in earlier chapters.

The geo-database architecture incorporates the following major components:

1. Roadway inventory layer (IRIS-based), serving as the spatial backbone.

2. Friction data layer, including both LWST measurements and continuous pavement friction measurement records.

3. Preservation and treatment layer, documenting treatment types, costs, and post-treatment performance.

4. Crash and traffic exposure layer, supporting safety performance estimation and identifying high-risk locations.

5. Macrotexture and geometric attributes, enriching surface and geometric characterization.

Special attention is given to identifier harmonization, including the use of inventory key route ID, begin and end mile references, and spatial joints where necessary. The design also anticipates future enhancements, such as incorporating curvature and superelevation.

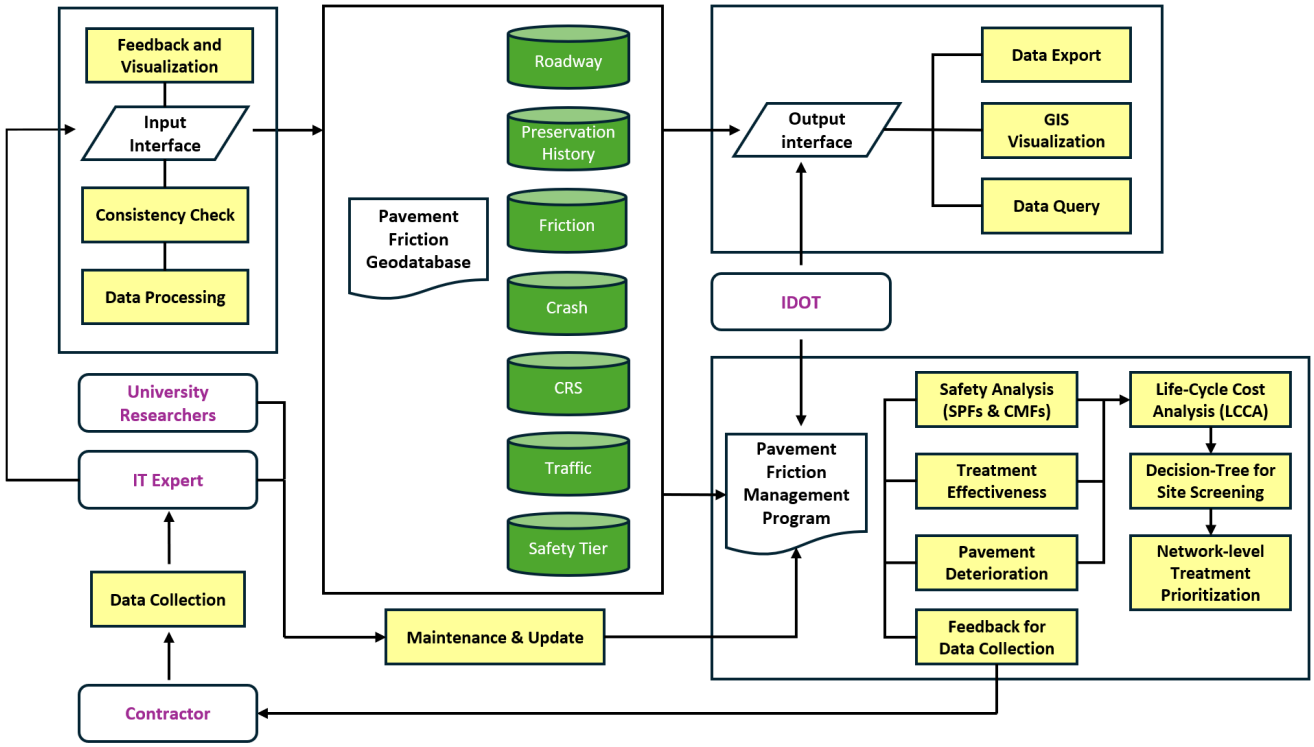

Figure 59. Graph. Proposed architecture for the Illinois friction management program.

LIMITATIONS OF WORK

Despite the comprehensive scope of this research, several limitations remain. First, the deterioration models for CRS and friction rely on empirical formulations calibrated from available data. Although grounded in prior Illinois Center for Transportation research, real-world deterioration may vary due to climate, material variability, traffic composition, and construction practices. Continued calibration with expanded longitudinal datasets is necessary. Second, treatment effectiveness functions are simplified representations of complex field performance. The interaction between friction and structural restoration is not fully understood, and laboratory validation or controlled field studies would improve confidence in parameter estimates. Third, although pilot continuous pavement friction measurements were done in 2025 in IDOT District 6, friction data scarcity is still a big challenge that limits the accuracy and reliability of our safety analysis. While SCRIM data enhance spatial coverage, historical depth remains limited. Harmonizing SCRIM and LWST measurements for long-term consistency remains another ongoing challenge. Fourth, the life cycle optimization framework assumes deterministic deterioration and representative traffic categories. Future work may incorporate uncertainty, stochastic deterioration, and more granular traffic forecasting.

FUTURE DEVELOPMENTS

Several future developments are recommended to facilitate implementation and improve model robustness. First, an integrated decision-support system should be developed to automate network-level screening, safety analysis, and treatment selection by embedding the proposed SPFs and LCCA

framework into IDOT's pavement management system. Such a system would allow IDOT to input roadway characteristics, observed crash data and collected friction data, automatically compute predicted crash frequencies, estimate expected safety benefits, and generate prioritized treatment recommendations under budget constraints. Second, improvements in data integration and crash-location accuracy are necessary. Because roadway, crash, traffic, and friction datasets originate from different sources and may contain spatial inconsistencies, future work should enhance identifier harmonization (e.g., inventory key route ID, begin-end mile alignment) and improve geometric information accuracies that would reduce estimation bias in safety models. Third, expanded longitudinal SCRIM data collection and correlation with historical LWST measurements would strengthen the accuracy and reliability of safety analysis. Fourth, systematic field and laboratory investigations should be conducted to quantify how aggregate characteristics, mix type, surface texture, and treatment selection influence friction deterioration, enabling more precise modeling and policy optimization. Finally, uncertainty modeling—such as stochastic deterioration, traffic growth variability, and treatment performance uncertainty—should be incorporated into the life cycle framework to support risk-informed capital planning. Together, these advancements would transition the proposed framework from a research prototype to a fully operational Illinois friction management program.

REFERENCES

Abdul Kadir, A. I., Rais, N. M., & Mohd-Towel, R. (2020). Micro Surfacing Asphalt Pavement as a Mitigation Measure at Accident's Prone Area along East Coast Expressway Phase 2 (ECE 2). *Journal of the Society of Automotive Engineers Malaysia*, *4*(3), 378–393. https://doi.org/10.56381/jsaem.v4i3.31

Abdullah, W. A. R. (2020). *Quantifying the relationship between skid resistance and crashes for Iowa roadways: A framework for a skid resistance policy*. Iowa State University.

Ahammed, M. A., & Tighe, S. L. (2008). Concrete pavement surface textures and multivariables frictional performance analysis: a North American case study. *Canadian Journal of Civil Engineering*, *35*(7), 727–738. https://doi.org/10.1139/L08-025

Alavi, M. Z., Ahmadi, A., & Movahed, F. V. (2025). How aggregate gradation and layer thickness influence asphalt microsurfacing texture and skid resistance. *Construction and Building Materials*, *481*, 141482. https://doi.org/https://doi.org/10.1016/j.conbuildmat.2025.141482

Aldagari, S., Al-Assi, M., Kassem, E., Chowdhury, A., & Masad, E. (2022). Development of predictive models for skid resistance of asphalt pavements and seal coat. *International Journal of Pavement Engineering*, *23*(3), 695–707. https://doi.org/10.1080/10298436.2020.1766685

Alhasan, A., Smadi, O., Bou-Saab, G., Hernandez, N., & Cochran, E. (2018). Pavement Friction Modeling using Texture Measurements and Pendulum Skid Tester. *Transportation Research Record*, *2672*(40), 440–451. https://doi.org/10.1177/0361198118774165

Al-Rousan, T., Masad, E., Myers, L., & Speigelman, C. (2005). New Methodology for Shape Classification of Aggregates. *Transportation Research Record*, *1913*(1), 11–23. https://doi.org/10.1177/0361198105191300102

Alsheyab, M. A., & Khasawneh, M. A. (2024). Statistical Modeling of Asphalt Pavement Surface Friction Based on Aggregate Fineness Modulus and Asphalt Mix Volumetrics. *International Journal of Pavement Research and Technology*, *17*(5), 1093–1111. https://doi.org/10.1007/s42947-023-00289-9

American Association of State Highway and Transportation Officials (AASHTO). (2008). *Guide for Pavement Friction*. AASHTO Joint Technical Committee on Pavements.

Anupam, K., Srirangam, S. K., Scarpas, A., & Kasbergen, C. (2013). Influence of Temperature on Tire–Pavement Friction: Analyses. *Transportation Research Record*, *2369*(1), 114–124. https://doi.org/10.3141/2369-13

Ban, I., Deluka-Tibljaš, A., & Ružić, I. (2024). Skid Resistance Performance Assessment by a PLS Regression-Based Predictive Model with Non-Standard Texture Parameters. *Lubricants*, *12*(1). https://doi.org/10.3390/lubricants12010023

Bao, J., Jiang, Y., & Li, S. (2023). Determination of Safety-Oriented Pavement-Friction Performance Ratings at Network Level Using a Hybrid Clustering Algorithm. *Lubricants*, *11*(7). https://doi.org/10.3390/lubricants11070275

Bennert, T., Blight, R., Ganji, V., Tulanowski, D., & Gresavage, S. (2021). Development of High Friction

Surface Treatment Prescreening Protocols and an Alternative Friction Application. *Transportation Research Record*, *2675*(5), 345–355. https://doi.org/10.1177/0361198121990027

Bhargava, N., Siddagangaiah, A. K., & Ryntathiang, T. L. (2020). State of the art review on design and performance of microsurfacing. *Road Materials and Pavement Design*, *21*(8), 2091–2125. https://doi.org/10.1080/14680629.2019.1607771

Buddhavarapu, P., de Fortier Smit, A., Banerjee, A., Trevino, M., & Prozzi, J. A. (2013). Evaluation of the Benefits of Diamond Grinding of a Continuously Reinforced Concrete Pavement. *Transportation Research Record*, *2369*(1), 59–67. https://doi.org/10.3141/2369-07

Buddhavarapu, P., Smit, A. F., & Prozzi, J. A. (2015). A fully Bayesian before–after analysis of permeable friction course (PFC) pavement wet weather safety. *Accident Analysis & Prevention*, *80*, 89–96. https://doi.org/https://doi.org/10.1016/j.aap.2015.04.003

Buss, A., Guirgui, M., & Gransberg, D. (2018). Chip seal aggregate evaluation and successful roads preservation. *Construction and Building Materials*, *180*, 396–404. https://doi.org/10.1016/J.CONBUILDMAT.2018.05.255

Cafiso, S., Montella, A., D'Agostino, C., Mauriello, F., & Galante, F. (2021). Crash modification functions for pavement surface condition and geometric design indicators. *Accident Analysis & Prevention*, *149*, 105887. https://doi.org/https://doi.org/10.1016/j.aap.2020.105887

Cerezo, V., Do, M. T., Prevost, D., & Bouteldja, M. (2014). Friction/water depth relationship—In situ observations and its integration in tire/road friction models. *Proceedings of the Institution of Mechanical Engineers, Part J: Journal of Engineering Tribology*, *228*(11), 1285–1297. https://doi.org/10.1177/1350650114544533

Chang, J. J., Yeih, W., Chung, T. J., & Huang, R. (2016). Properties of pervious concrete made with electric arc furnace slag and alkali-activated slag cement. *Construction and Building Materials*, *109*, 34–40. https://doi.org/10.1016/J.CONBUILDMAT.2016.01.049

Chen, D., Han, S., Ling, C., & Su, Q. (2019). Prediction of asphalt mixture surface texture level and its distributions using mixture design parameters. *International Journal of Pavement Engineering*, *20*(5), 557–565. https://doi.org/10.1080/10298436.2017.1316644

Chen, D., Sefidmazgi, N. R., & Bahia, H. (2015). Exploring the feasibility of evaluating asphalt pavement surface macro-texture using image-based texture analysis method. *Road Materials and Pavement Design*, *16*(2), 405–420. https://doi.org/10.1080/14680629.2015.1016547

Chen, D.-H., & Hong, F. (2015). Long-Term Performance of Diamond Grinding. *Journal of Performance of Constructed Facilities*, *29*(1), 6014006. https://doi.org/10.1061/(ASCE)CF.1943-5509.0000578

Chen, X., Zhu, H., Dong, Q., & Huang, B. (2017). Case study: performance effectiveness and cost-benefit analyses of open-graded friction course pavements in Tennessee. *International Journal of Pavement Engineering*, *18*(11), 957–970. https://doi.org/10.1080/10298436.2016.1138112

Choubane, B., Holzschuher, C. R., Gokhale, S., & Fletcher, J. (2006). Precision of Smooth and Ribbed Tire Locked Wheel Testers for Measurement of Roadway Surface Friction Characteristics. *Transportation Research Record: Journal of the Transportation Research Board*, (1949), 137–147.

Chowdhury, A., Kassem, E., Aldagari, S., & Masad, E. (2017). *Validation of Asphalt Mixture Pavement Skid Prediction Model and Development of Skid Prediction Model for Surface Treatments* (Number FHWA/TX-17/0-6746-01-1). http://tti.tamu.edu/documents/0-6746-01-1.pdf

Chu, L., Guo, W., & Fwa, T. F. (2022). Theoretical and practical engineering significance of British pendulum test. *International Journal of Pavement Engineering*, *23*(1), 1–8. https://doi.org/10.1080/10298436.2020.1726351

Cominsky, R. J. (1994). *The Superpave Mix Design Manual for New Construction and Overlays* (Number SHRP-A-407).

Cui, P., Wu, S., Liu, Q., & Wang, F. (2022). Artificial neural network modeling for predicting surface texture and its attenuation of micro-surfacing containing steel slag aggregates. *Construction and Building Materials*, *346*, 128504. https://doi.org/https://doi.org/10.1016/j.conbuildmat.2022.128504

Cui, P., Wu, S., Xiao, Y., Yang, C., & Wang, F. (2020). Enhancement mechanism of skid resistance in preventive maintenance of asphalt pavement by steel slag based on micro-surfacing. *Construction and Building Materials*, *239*, 117870. https://doi.org/10.1016/j.conbuildmat.2019.117870

de León Izeppi, E., Flintsch, G. W., & McGhee, K. (2010). *Field Performance of High Friction Surfaces* (Number FHWA/VTRC 10-CR6).

de León Izeppi, E., Katicha, S. W., Flintsch, G. W., McCarthy, R., & McGhee, K. K. (2016). *Continuous Friction Measurement Equipment as a Tool for Improving Crash Rate Prediction: A Pilot Study* (Number VTRC 16-R8).

de León Izeppi, E., Flintsch, G., & McCarthy, R. (2017). *Evaluation of Methods for Pavement Surface Friction Testing on Non-Tangent Roadways and Segments* (Number FHWA/NC/2017-02).

de León Izeppi, E., Flintsch, G., Katicha, S., McGhee, K., & McCarthy, R. (2019). *Locked-Wheel and Sideway-Force CFME Friction Testing Equipment Comparison and Evaluation Report* (Number FHWA-RC-19-001).

De Rose, M., Iuele, T., Perri, G., & Vaiana, R. (2025). On the Mix Design Advances in Microsurfacing: A Systematic Surface Performance-Oriented Literature Review. *International Journal of Pavement Research and Technology*, *18*(5), 1083–1102. https://doi.org/10.1007/s42947-023-00407-7

Deng, Q., Zhan, Y., Liu, C., Qiu, Y., & Zhang, A. (2021). Multiscale power spectrum analysis of 3D surface texture for prediction of asphalt pavement friction. *Construction and Building Materials*, *293*, 123506. https://doi.org/https://doi.org/10.1016/j.conbuildmat.2021.123506

Du, Z., Skar, A., Pettinari, M., & Zhu, X. (2023). Pavement Friction Evaluation Based on Vehicle Dynamics and Vision Data Using a Multi-Feature Fusion Network. *Transportation Research Record*, *2677*(11), 219–236. https://doi.org/10.1177/03611981231165029

Dupont, P., & Bauduin, A. (2005). La nouvelle circulaire adhérence de la Direction des routes nationales de France. *Bulletin Des Laboratoires Des Ponts et Chaussées*, (255), 159–168.

El-Ashwah, A. S., & Abdelrahman, M. (2025). Relating aggregate friction properties to asphalt pavement friction loss through laboratory testing, statistical analysis, and machine learning

insights. *International Journal of Pavement Engineering*, *26*(1), 2456739. https://doi.org/10.1080/10298436.2025.2456739

El-Ashwah, A. S., Broaddus, K., & Abdelrahman, M. (2023). Predicting the Friction Coefficient of High-Friction Surface Treatment Application Aggregates Using the Aggregates' Characteristics. *Journal of Materials in Civil Engineering*, *35*(5), 4023089. https://doi.org/10.1061/(ASCE)MT.1943-5533.0004739

Elkhazindar, A., Hafez, M., & Ksaibati, K. (2022). Incorporating Pavement Friction Management into Pavement Asset Management Systems: State Department of Transportation Experience. *CivilEng*, *3*(2), 541–561. https://doi.org/10.3390/civileng3020032

Erwin, T. C. (2007). *Safety Effects of Microsurfacing and Resurfacing Treatments: A Case Study* [University of Waterloo]. http://hdl.handle.net/10012/3257

Federal Highway Administration. (2017). *Pavement Friction Management Safety Benefits*. https://highways.dot.gov/

Federal Highway Administration. (2023). *Characterizing Road Safety Performance Using Pavement Friction* (Number FHWA-SA-23-006). https://highways.dot.gov/sites/fhwa.dot.gov/files/2023-06/FHWA%20Characterizing%20Road%20Safety%20Performance%20Using%20Pavement%20Friction.pdf

Flintsch, G., de León Izeppi, E., McCarthy, R., Katicha, S., Persaud, B., Guo, F., Medina, A., & Tobias, P. (2023). *Characterizing Road Safety Performance Using Pavement Friction* (Number FHWA-SA-23-006).

Friel, S., & Woodward, D. (2019). High Friction Surfacing Systems Using Blends of Natural Aggregate and Calcined Bauxite. *Coatings*, *9*(3). https://doi.org/10.3390/coatings9030177

Fwa, T. F. (2017). Skid resistance determination for pavement management and wet-weather road safety. *International Journal of Transportation Science and Technology*, *6*(3), 217–227. https://doi.org/https://doi.org/10.1016/j.ijtst.2017.08.001

Garber, N. J., & Hoel, L. A. (2009). *Traffic and Highway Engineering* (4th ed.). Cengage Learning.

Geedipally, S. R., Pratt, M. P., & Lord, D. (2019). Effects of geometry and pavement friction on horizontal curve crash frequency. *Journal of Transportation Safety & Security*, *11*(2), 167–188. https://doi.org/10.1080/19439962.2017.1365317

Giles, C. G., Sabey, B. E., & Cardew, K. H. F. (1965). Development and Performance of the Portable Skid Resistance Tester. *Rubber Chemistry and Technology*, *38*(4), 840–862. https://doi.org/10.5254/1.3535703

Gransberg, D. D., & James, D. M. B. (2005). *Chip Seal Best Practices* (Number 342). https://nap.nationalacademies.org/catalog/13814

Gu, F., Chen, C., Heitzman, M., Potter, R., & Powell, B. (2023). Evaluation of locked-wheel skid trailer and SCRIM friction measurements at NCAT test track. *International Journal of Pavement Engineering*, *24*(2), 2124249. https://doi.org/10.1080/10298436.2022.2124249

Gu, F., Lo Presti, D., Heitzman, M., Powell, B., & Allison, V. (2022). Feasibility of using more polishable

aggregates in dense-graded asphalt surface mixture: Case study of dolomite. *Construction and Building Materials*, *342*, 127915. https://doi.org/https://doi.org/10.1016/j.conbuildmat.2022.127915

Gu, F., Watson, D., Moore, J., & Tran, N. (2018). Evaluation of the benefits of open graded friction course: Case study. *Construction and Building Materials*, *189*, 131–143. https://doi.org/10.1016/J.CONBUILDMAT.2018.08.185

Guo, F., Pei, J., Huang, G., Hu, Z., Niu, Z., & Cannone Falchetto, A. (2023). Evolution of tire-pavement friction with the regular surface macro-texture characteristics and environmental factors using three-dimensional (3D) printing technology. *Journal of Cleaner Production*, *382*, 135293. https://doi.org/https://doi.org/10.1016/j.jclepro.2022.135293

Guo, F., Pei, J., Zhang, J., Li, R., Zhou, B., & Chen, Z. (2021). Study on the skid resistance of asphalt pavement: A state-of-the-art review and future prospective. *Construction and Building Materials*, *303*, 124411. https://doi.org/https://doi.org/10.1016/j.conbuildmat.2021.124411

Hacker, D., Ashurst Kean H., Jr., & Graves, C. (2023). *Friction and Texture Equipment Correlation Study* (Number KTC-24-04).

Hajj, R., Filonzi, A., Bhasin, A., Dormohammadi, A., Zhu, C., & Tandon, V. (2018). *Design and Construction of Ultra Thin Overlays as an Alternative to Seal Coats* (Number FHWA/TX-18/0-6857-1).

Hajj, R., Filonzi, A., Smit, A., & Bhasin, A. (2019). Design and Performance of Mixes for Use as Ultrathin Overlay. *Journal of Transportation Engineering, Part B: Pavements*, *145*(3), 4019026. https://doi.org/10.1061/JPEODX.0000130

Hall, J. W., Smith, K. L., Titus-Glover, L., Wambold, J. C., Yager, T. J., & Rado, Z. (2009). *Guide for Pavement Friction* (Number Project 01-43). https://doi.org/10.17226/23038

Hamilton, I., & Coley, D. (2021). *Kentucky's Network Screening Process* (Number FHWA-SA-21-015).

Hanson, D. I. (2001). Construction and Performance of an Ultrathin Bonded Hot-Mix Asphalt Wearing Course. *Transportation Research Record*, *1749*(1), 53–59. https://doi.org/10.3141/1749-08

Hauer, E. (1992). Empirical bayes approach to the estimation of "unsafety": The multivariate regression method. *Accident Analysis & Prevention*, *24*(5), 457–477. https://doi.org/https://doi.org/10.1016/0001-4575(92)90056-O

Hauer, E., Harwood, D. W., Council, F. M., & Griffith, M. S. (2002). Estimating Safety by the Empirical Bayes Method: A Tutorial. *Transportation Research Record*, *1784*(1), 126–131. https://doi.org/10.3141/1784-16

Hauer, E., Terry, D., & Griffith, M. S. (1994). Effect of Resurfacing on Safety of Two-Lane Rural Roads in New York State. *Transportation Research Record*, (1467), 30–37. https://onlinepubs.trb.org/Onlinepubs/trr/1994/1467/1467-005.pdf

Heitzman, M., & Moore, J. (2017). *Evaluation of Laboratory Friction Performance of Aggregates for High Friction Surface Treatments* (Number NCAT Report 17-01).

Henry, J. J. (2000). *Evaluation of Pavement Friction Characteristics: A Synthesis of Highway Practice*

(Number NCHRP Synthesis 291). National Academy Press.

Hu, Y., Sun, Z., Han, Y., Li, W., & Pei, L. (2022). Evaluate Pavement Skid Resistance Performance Based on Bayesian-LightGBM Using 3D Surface Macrotexture Data. *Materials*, *15*(15). https://doi.org/10.3390/ma15155275

Huang, B., Zhong, J., Huang, K., Ma, Y., & Polaczyk, P. (2025). *Investigating the Long-term Frictional Properties and Establishing Aggregate Polishness Guidelines for Asphalt Surface Mixtures in Tennessee* (Numbers RES2023-15). https://rosap.ntl.bts.gov/view/dot/82912

Illinois Department of Transportation. (2022). *Standard specifications for road and bridge construction*. IDOT.

Ivan, J. N., Ravishanker, N., Jackson, E., Aronov, B., & Guo, S. (2012). A Statistical Analysis of the Effect of Wet-Pavement Friction on Highway Traffic Safety. *Journal of Transportation Safety & Security*, *4*(2), 116–136. https://doi.org/10.1080/19439962.2011.620218

Jain, S., Das, A., & Venkatesh, K. S. (2021). Automated and contactless approaches for pavement surface texture measurement and analysis – A review. *Construction and Building Materials*, *301*, 124235. https://doi.org/https://doi.org/10.1016/j.conbuildmat.2021.124235

Kamel, N., & Gartshore, T. (1982). Ontario's Wet Pavement Accident Reduction Program. In *Pavement Surface Characteristics and Materials*. ASTM International. https://doi.org/10.1520/STP28465S

Kassem, E., Awed, A., Masad, E. A., & Little, D. N. (2013). Development of Predictive Model for Skid Loss of Asphalt Pavements. *Transportation Research Record*, *2372*(1), 83–96. https://doi.org/10.3141/2372-10

Katicha, S., & Flintsch, G. (2022). Estimating the effect of friction on crash risk: Reducing the effect of omitted variable bias that results from spatial correlation. *Accident Analysis & Prevention*, *170*, 106642. https://doi.org/https://doi.org/10.1016/j.aap.2022.106642

Khaleghian, S., Emami, A., & Taheri, S. (2017). A technical survey on tire-road friction estimation. *Friction*, *5*(2), 123–146. https://doi.org/10.1007/s40544-017-0151-0

Khaleghian, S., Ghasemalizadeh, O., Taheri, S., & Flintsch, G. (2019). A Combination of Intelligent Tire and Vehicle Dynamic Based Algorithm to Estimate the Tire-Road Friction. *SAE International Journal of Passenger Cars - Mechanical Systems*, *12*(2), 81–97. https://doi.org/https://doi.org/10.4271/06-12-02-0007

Khanjari, M., Abdi Kordani, A., & Zarei, M. (2022). Simulation and Modelling of Safety of Roadways in Reverse Horizontal Curves (RHCs): With Focus on Lateral Acceleration. *Advances in Civil Engineering*, *2022*(1), 5442515. https://doi.org/https://doi.org/10.1155/2022/5442515

Khasawneh, M. (2015). The Prediction of LWST Values from DFT and CTM Measurements Using Linear and Nonlinear Regression Analyses. *Jordan Journal of Civil Engineering*, *9*, 487–498. https://doi.org/10.14525/jjce.9.4.3121

King, W. Jr., Kabir, M. S., Cooper, S. B. Jr., & Abadie, C. (2013). *Evaluation of Open Graded Friction Course (OGFC) Mixtures* (Number FHWA/LA.13/513).

Kogbara, R. B., Masad, E. A., Kassem, E., Scarpas, A. (Tom), & Anupam, K. (2016). A state-of-the-art

review of parameters influencing measurement and modeling of skid resistance of asphalt pavements. *Construction and Building Materials*, *114*, 602–617. https://doi.org/https://doi.org/10.1016/j.conbuildmat.2016.04.002

Kogbara, R. B., Masad, E. A., Woodward, D., & Millar, P. (2018). Relating surface texture parameters from close range photogrammetry to Grip-Tester pavement friction measurements. *Construction and Building Materials*, *166*, 227–240. https://doi.org/10.1016/j.conbuildmat.2018.01.102

Komaragiri, S., Amirkhanian, A., & Bhasin, A. (2020). Friction and Texture Retention of Concrete Pavements. *Transportation Research Record*, *2674*(6), 457–465. https://doi.org/10.1177/0361198120919397

Kouchaki, S., Roshani, H., Prozzi, J. A., Garcia, N. Z., & Hernandez, J. B. (2018). Field Investigation of Relationship between Pavement Surface Texture and Friction. *Transportation Research Record*, *2672*(40), 395–407. https://doi.org/10.1177/0361198118777384

Kováč, M., Brna, M., & Decký, M. (2021). Pavement Friction Prediction Using 3D Texture Parameters. *Coatings*, *11*(10). https://doi.org/10.3390/coatings11101180

Larson, R. M., Hoerner, T. E., Smith, K. D., & Wolters, A. S. (2008). *Relationship Between Skid Resistance Numbers Measured with Ribbed and Smooth Tire and Wet Accident Locations* (Number State Job No. 134323). http://worldcat.org/arcviewer/1/OHI/2009/04/10/H1239376456705/viewer/file1.pdf

Leandri, P., & Losa, M. (2015). Peak Friction Prediction Model Based on Surface Texture Characteristics. *Transportation Research Record*, *2525*(1), 91–99. https://doi.org/10.3141/2525-10

Lee, J. S., & Kim, Y. R. (2009). Performance-Based Uniformity Coefficient of Chip Seal Aggregate. *Transportation Research Record*, *2108*(1), 53–60. https://doi.org/10.3141/2108-06

Lei, J., Zheng, N., Chen, X., Bi, J., & Wu, X. (2022). Research on the relationship between anti-skid performance and various aggregate micro texture based on laser scanning confocal microscope. *Construction and Building Materials*, *316*, 125984. https://doi.org/10.1016/J.CONBUILDMAT.2021.125984

Lenzo, B. (2022). *Vehicle Dynamics - Fundamentals and Ultimate Trends* (1st ed., Vol. 603). Springer. https://doi.org/10.1007/978-3-030-75884-4

Leu, M. C., & Henry, J. J. (1978). Prediction of Skid Resistance as a Function of Speed from Pavement Texture Measurements. *Transportation Research Record*, (666), 7–13. http://onlinepubs.trb.org/Onlinepubs/trr/1978/666/666-002.pdf

Li, Q. J., Zhan, Y., Yang, G., & Wang, K. C. P. (2020). Pavement skid resistance as a function of pavement surface and aggregate texture properties. *International Journal of Pavement Engineering*, *21*(10), 1159–1169. https://doi.org/10.1080/10298436.2018.1525489

Li, S., Cong, P., Yu, D., Xiong, R., & Jiang, Y. (2019). Laboratory and Field Evaluation of Single Layer and Double Layer High Friction Surface Treatments. *Transportation Research Record*, *2673*(2), 552–561. https://doi.org/10.1177/0361198119826078

Li, S., Harris, D., & Wells, T. (2016). Surface texture and friction characteristics of diamond-ground concrete and asphalt pavements. *Journal of Traffic and Transportation Engineering (English Edition)*, *3*(5), 475–482. https://doi.org/10.1016/J.JTTE.2016.08.001

Li, S., Shields, T., Noureldin, S., & Jiang, Y. (2012). Field Evaluation of Surface Friction Performance of Chip Seals in Indiana. *Transportation Research Record*, *2295*(1), 11–18. https://doi.org/10.3141/2295-02

Li, S., Xiong, R., Yu, D., Zhao, G., Cong, P., & Jiang, Y. (2017). *Friction Surface Treatment Selection: Aggregate Properties, Surface Characteristics, Alternative Treatments, and Safety Effects* (Number FHWA/IN/JTRP-2017/09).

Lu, J., Pan, B., Liu, Q., Sun, M., Liu, P., & Oeser, M. (2022). A novel noncontact method for the pavement skid resistance evaluation based on surface texture. *Tribology International*, *165*, 107311. https://doi.org/https://doi.org/10.1016/j.triboint.2021.107311

Lyon, C., & Persaud, B. (2008). Safety Effects of Targeted Program to Improve Skid Resistance. *Transportation Research Record*, *2068*(1), 135–140. https://doi.org/10.3141/2068-15

Lyon, C., Persaud, B., & Merritt, D. (2018). Quantifying the safety effects of pavement friction improvements – results from a large-scale study. *International Journal of Pavement Engineering*, *19*(2), 145–152. https://doi.org/10.1080/10298436.2016.1172709

Ma, Z., Wang, H., Zhang, Y., Jelagin, D., & Li, Y. (2025). Effects of aggregate shape on the macrotexture and performance of chip seal: a laboratory study. *Road Materials and Pavement Design*, *26*(1), 181–202. https://doi.org/10.1080/14680629.2024.2340862

Mahboob Kanafi, M., & Tuononen, A. J. (2017). Top topography surface roughness power spectrum for pavement friction evaluation. *Tribology International*, *107*, 240–249. https://doi.org/https://doi.org/10.1016/j.triboint.2016.11.038

Mahmoud, E., & Ortiz, E. (2014). *Implementation of AIMS in Measuring Aggregate Resistance to Polishing, Abrasion, and Breakage* (Number FHWA-ICT-14-014).

Maia, R. S., Hajj, R. M., Cunto, F. J. C., & Branco, V. T. F. C. (2024). Safety-oriented urban pavement design and evaluation: integrating microscopic simulation and tyre-pavement friction. *International Journal of Pavement Engineering*, *25*(1), 2345138. https://doi.org/10.1080/10298436.2024.2345138

Maia, R. S., Lu, Y., & Hajj, R. (2024). Porous asphalt mixture performance in cold regions: Case study of Chicago. *Case Studies in Construction Materials*, *20*. https://doi.org/10.1016/j.cscm.2024.e03250

Masad, E., Luce, A., Mahmoud, E., & Chowdhury, A. (2007). *Relationship of Aggregate Texture to Asphalt Pavement Skid Resistance Using Image Analysis of Aggregate Shape* (Number Highway IDEA Project 114).

Masad, E., Rezaei, A., & Chowdhury, A. (2011). *Field Evaluation of Asphalt Mixture Skid Resistance and Its Relationship to Aggregate Characteristics* (Number FHWA/TX-11/0-5627-3). http://tti.tamu.edu/documents/0-5627-3.pdf

Masad, E., Rezaei, A., Chowdhury, A., & Harris, P. (2009). *Predicting Asphalt Mixture Skid Resistance Based on Aggregate Characteristics* (Number FHWA/TX-09/0-5627-1). http://tti.tamu.edu/documents/0-5627-1.pdf

Mataei, B., Zakeri, H., Zahedi, M., & Moghadas Nejad, F. (2016). Pavement Friction and Skid Resistance Measurement Methods: A Literature Review. *Open Journal of Civil Engineering*, *6*, 537–565. https://doi.org/10.4236/ojce.2016.64046

McCarthy, R., Flintsch, G., Katicha, S., Izeppi, E. de L., & Guo, F. (2022). Determining investigatory levels of friction with crash modelling. *International Journal of Pavement Engineering*, *23*(9), 3236–3243. https://doi.org/10.1080/10298436.2021.1888089

McCullough, B. F., & Hankins, K. D. (1966). *Skid Resistance Guidelines for Surface Improvements on Texas Highways* (Numbers 45–2).

McGovern, C., Rusch, P., & Noyce, D. A. (2011). *State Practices to Reduce Wet Weather Skidding Crashes* (Number FHWA-SA-11-21).

Meegoda, J. N., & Gao, S. (2015). Evaluation of pavement skid resistance using high speed texture measurement. *Journal of Traffic and Transportation Engineering (English Edition)*, *2*(6), 382–390. https://doi.org/https://doi.org/10.1016/j.jtte.2015.09.001

Milton, J. C., Shankar, V. N., & Mannering, F. L. (2008). Highway accident severities and the mixed logit model: An exploratory empirical analysis. *Accident Analysis & Prevention*, *40*(1), 260–266. https://doi.org/https://doi.org/10.1016/j.aap.2007.06.006

Moaveni, M., Mahmoud, E., Ortiz, E. M., Tutumluer, E., & Beshears, S. (2014). Use of Advanced Aggregate Imaging Systems to Evaluate Aggregate Resistance to Breakage, Abrasion, and Polishing. *Transportation Research Record*, *2401*(1), 1–10. https://doi.org/10.3141/2401-01

Musey, K., & Park, S. (2016). Pavement Skid Number and Horizontal Curve Safety. *Procedia Engineering*, *145*, 828–835. https://doi.org/https://doi.org/10.1016/j.proeng.2016.04.108

Najafi, S., Flintsch, G. W., & Khaleghian, S. (2019). Pavement friction management – artificial neural network approach. *International Journal of Pavement Engineering*, *20*(2), 125–135. https://doi.org/10.1080/10298436.2016.1264221

Najafi, S., Shetty, S., Flintsch, G. W., Scofield, L., & Katicha, S. (2012). Evaluation of the Effect of Diamond Grinding and Grooving on Surface Characteristics of Concrete Pavements. *Transportation Research Board Annual Meeting*.

Noyce, D. A., Bahia, H. U., Yambo, J., Chapman, J., & Bill, A. (2007). *Incorporating Road Safety into Pavement Management: Maximizing Surface Friction for Road Safety Improvements* (Number MRUTC 04-04). http://www.mrutc.org/research/0404/

Onyango, M., & Woods, M. (2017). Analysis of the Utilization of Open-Graded Friction Course (OGFC) in the United States. In *Airfield and Highway Pavements 2017: Pavement Innovation and Sustainability - Proceedings of the International Conference on Highway Pavements and Airfield Technology 2017* (pp. 137–147). ASCE. https://doi.org/10.1061/9780784480946.013

Pardillo Mayora, J. M., & Jurado Piña, R. (2009). An assessment of the skid resistance effect on traffic

safety under wet-pavement conditions. *Accident Analysis & Prevention*, *41*(4), 881–886. https://doi.org/https://doi.org/10.1016/j.aap.2009.05.004

Peng, J., Chu, L., Wang, T., & Fwa, T. F. (2021). Analysis of vehicle skidding potential on horizontal curves. *Accident Analysis & Prevention*, *152*, 105960. https://doi.org/https://doi.org/10.1016/j.aap.2020.105960

Piyatrapoomi, N., Weligamage, J., Kumar, A., & Bunker, J. (2008). Identifying Relationship Between Skid Resistance and Road Crashes Using Probability-Based Approach. In M. Owen, R. Wills, J. Smart, A. Jones, S. Child, & J. Barton (Eds.), *Proceedings of the 2nd International Safer Roads Conference* (pp. 1–12). Safe Roads Organisation.

Pranjić, I., & Deluka-Tibljaš, A. (2022). Pavement Texture–Friction Relationship Establishment via Image Analysis Methods. *Materials*, *15*(3). https://doi.org/10.3390/ma15030846

Prowell, B. D., & Hanson, D. I. (2005). Evaluation of Circular Texture Meter for Measuring Surface Texture of Pavements. *Transportation Research Record*, *1929*(1), 88–96. https://doi.org/10.1177/0361198105192900111

Quiros, S. B., Flintsch, G. W., de León Izeppi, E., & McGhee, K. K. (2018). Interconversion of Locked-Wheel and Continuous Friction Measurement Equipment (CFME) Friction Measurements. *Transportation Research Record*, *2672*(40), 452–462. https://doi.org/10.1177/0361198118797455

Rao, S., Yu, H. T., Khazanovich, L., Darter, M. I., & Mack, J. W. (1999). Longevity of Diamond-Ground Concrete Pavements. *Transportation Research Record*, *1684*(1), 128–136. https://doi.org/10.3141/1684-15

Rasol, M., Schmidt, F., & Ientile, S. (2023). FriC-PM: Machine Learning-based road surface friction coefficient predictive model using intelligent sensor data. *Construction and Building Materials*, *370*, 130567. https://doi.org/https://doi.org/10.1016/j.conbuildmat.2023.130567

Reed, C. M. (1992). *The Performance Evaluation of Single Pass Thin Lift Bituminous Overlays* (Number FHWA/IL/PR-110). https://rosap.ntl.bts.gov/view/dot/13412

Reed, C. M. (1994). Seven-Year Performance Evaluation of Single Pass, Thin Lift Bituminous Concrete Overlays. *Transportation Research Record*, *1454*, 23–27. https://onlinepubs.trb.org/Onlinepubs/trr/1994/1454/1454-004.pdf

Rizenbergs, R. L., Burchett, J. L., & Napier, C. T. (1973). *Accidents on Rural Interstate and Parkway Roads and Their Relation to Pavement Friction: Interim Report* (Number KYHPR-64-24, HPR-1(9), Part II).

Roshan, A., & Abdelrahman, M. (2024). Influence of Aggregate Properties on Skid Resistance of Pavement Surface Treatments. *Coatings*, *14*(8). https://doi.org/10.3390/coatings14081037

Roy, U., Farid, A., & Ksaibati, K. (2023). Effects of Pavement Friction and Geometry on Traffic Crash Frequencies: A Case Study in Wyoming. *International Journal of Pavement Research and Technology*, *16*(6), 1468–1481. https://doi.org/10.1007/s42947-022-00208-4

Sabey, B. E., & Lupton, G. N. (1964). Friction on Wet Surfaces of Tire-Tread-Type Vulcanizates. *Rubber Chemistry and Technology*, *37*(4), 878–893. https://doi.org/10.5254/1.3540385

Saghafi, M., Abdallah, I. N., & Nazarian, S. (2022). Practical Specimen Preparation and Testing Protocol for Evaluation of Friction Performance of Asphalt Pavement Aggregates with Three-Wheel Polishing Device. *Journal of Materials in Civil Engineering*, *34*(1), 4021397. https://doi.org/10.1061/(ASCE)MT.1943-5533.0004018

Saito, K., Horiguchi, T., Kasahara, A., Abe, H., & Henry, J. J. (1996). Development of Portable Tester for Measuring Skid Resistance and Its Speed Dependency on Pavement Surfaces. *Transportation Research Record*, *1536*(1), 45–51. https://doi.org/10.1177/0361198196153600107

Salt, G. F. (1977). Research on Skid-Resistance at the Transport and Road Research Laboratory (1927–1977). *Transportation Research Record*, (622), 26–38. http://onlinepubs.trb.org/Onlinepubs/trr/1976/622/622-002.pdf

Serigos, P. A., Smit, A. D. F., & Prozzi, J. A. (2014). Incorporating Surface Microtexture in the Prediction of Skid Resistance of Flexible Pavements. *Transportation Research Record*, *2457*(1), 105–113. https://doi.org/10.3141/2457-11

Sharafeldin, M., Albatayneh, O., Farid, A., & Ksaibati, K. (2022). A Bayesian Approach to Examine the Impact of Pavement Friction on Intersection Safety. *Sustainability*, *14*(19). https://doi.org/10.3390/su141912495

Shoenberger, J. E., & Vollor, T. W. (1990). *Hot In-Place Recycling of Asphalt Pavements* (Number WES/TR/GL-90-22). https://doi.org/10.21236/ADA228983

Siriphun, S., Chotisakul, S., & Horpibulsuk, S. (2016). Skid Resistance of Asphalt Concrete at the Construction Stage Based on Thai Aggregates. *Journal of Materials in Civil Engineering*, *28*(12), 4016145. https://doi.org/10.1061/(ASCE)MT.1943-5533.0001662

Siriphun, S., Horpibulsuk, S., Chotisakul, S., Suddeepong, A., Chinkulkijniwat, A., & Arulrajah, A. (2019). Effect of cumulative traffic and statistical predictive modelling of field skid resistance. *Road Materials and Pavement Design*, *20*(2), 426–439. https://doi.org/10.1080/14680629.2017.1385511

Snyder, M. B. (2019). *Concrete Pavement Texturing* (Number FHWA-HIF-17-011). https://rosap.ntl.bts.gov/view/dot/43538/dot_43538_DS1.pdf

Solaimanian, M., & Kennedy, T. W. (1998). *Evaluation of the Cape Seal Process as a Pavement Rehabilitation Alternative* (Number FHWA/TX-99/1788-S). https://rosap.ntl.bts.gov/view/dot/14902

Song, W., Gong, H., Zeng, S., Cong, L., Sun, Y., Wu, H., & Huang, B. (2021). Field performance evaluation of open-graded asphalt friction courses: A survival data analysis. *Construction and Building Materials*, *306*, 124745. https://doi.org/10.1016/J.CONBUILDMAT.2021.124745

Speir, R., Puzin, T., Barcena, R., & Desaraju, P. (2009). *Development of Friction Improvement Policies and Guidelines for the Maryland State Highway Administration* (Number MD-07-SP708B4F).

Tegge, R. A., Jo, J., & Ouyang, Y. (2010). *Development and Application of Safety Performance Functions for Illinois*.

Tegge, R. A., & Ouyang, Y. (2009). Correcting erroneous crash locations in transportation safety

analysis. *Accident Analysis and Prevention*, *41*(1), 202–209. https://doi.org/10.1016/j.aap.2008.10.013

Tighe, Susan, Li, Ningyuan, Falls, Lynne Cowe, & Haas, Ralph. (2000). Incorporating Road Safety into Pavement Management. *Transportation Research Record*, *1699*(1), 1–10. https://doi.org/10.3141/1699-01

Tobias, P. (2023). *CPFM stakeholder interviews - FHWA (WDM discussion notes)*.

Tobias, P., de León Izeppi, E., Flintsch, G., Katicha, S., & McCarthy, R. (2023). *Pavement Friction for Road Safety: Primer on Friction Measurement and Management Methods* (Number FHWA-SA-23-007).

Torbic, D. J., Harwood, D. W., Gilmore, D. K., Pfefer, R., Neuman, T. R., Slack, K. L., & Hardy, K. K. (2004). *Guidance for Implementation of the AASHTO Strategic Highway Safety Plan. Volume 7: A Guide for Reducing Collisions on Horizontal Curves* (Vol. 7, Number 500). Transportation Research Board.

Ueckermann, A., Wang, D., Oeser, M., & Steinauer, B. (2015). A contribution to non-contact skid resistance measurement. *International Journal of Pavement Engineering*, *16*(7), 646–659. https://doi.org/10.1080/10298436.2014.943216

Underwood, B. S., Castorena, C., Goenaga, B., Munywoki, B., & Rogers, P. (2023). *Development of Friction Performance Models* (Number FHWA/NC/2022-05).

Uzarowski, L., Maher, M., & Farrington, G. (2005). Thin Surfacing: Effective Way of Improving Road Safety Within Scarce Road Maintenance Budget. *Transportation – Investing in Our Future*, 13.

Vaiana, R., De Rose, M., & Perri, G. (2023). Microsurfacing: a predictive macrotexture model from mix design parameters. *Construction and Building Materials*, *409*, 133961. https://doi.org/10.1016/J.CONBUILDMAT.2023.133961

Vargas-Nordcbeck, A. (2023). Performance of Cape Seal Treatments Used for Pavement Preservation. *Transportation Research Circular E-C283: 13th International Conference on Low-Volume Roads*, 61–68.

Viner, H. E., Sinhal, R., & Parry, A. R. (2005). Linking Road Traffic Accidents with Skid Resistance – Recent UK Developments. *Proceedings of the International Conference on Surface Friction*, 1–4.

Vollor, T. W., Hanson, D. I., & Brown, R. (2006). *Development of Laboratory Procedure for Measuring Friction of HMA Mixtures: Phase I* (Numbers 06–06).

Wallman, C.-G., & Aaström, H. (2001). *Friction Measurement Methods and the Correlation Between Road Friction and Traffic Safety: A Literature Review* (Number 911A).

Wallman, C.-G., Wretling, P., & Öberg, G. (1997). *Effects of Winter Road Maintenance: State of the Art* (Number 423A).

Wambold, J. C., Antle, C. E., Henry, J. J., & Rado, Z. (1995). *International PIARC Experiment to Compare and Harmonize Texture and Skid Resistance Measurements*.

Wambold, J. C., Henry, J. J., & Radó, Z. (2000). Friction Measurement Techniques for Snow and Ice Road Operations. *Proceedings of the Fourth International Symposium on Pavement Surface*

Characteristics of Roads and Airfields: SURF, 143–152.

Wang, D., Chen, X., Oeser, M., Stanjek, H., & Steinauer, B. (2014). Study of micro-texture and skid resistance change of granite slabs during the polishing with the Aachen Polishing Machine. *Wear*, *318*(1), 1–11. https://doi.org/https://doi.org/10.1016/j.wear.2014.06.005

Wang, D., Zhang, Z., Kollmann, J., & Oeser, M. (2020). Development of aggregate micro-texture during polishing and correlation with skid resistance. *International Journal of Pavement Engineering*, *21*(5), 629–641. https://doi.org/10.1080/10298436.2018.1502436

Watson, D. E., & Heitzman, M. (2014). *Thin Asphalt Concrete Overlays: A Synthesis of Highway Practice* (National Cooperative Highway Research Program (NCHRP) Synthesis 464).

Wilson, B. T., & Mukhopadhyay, A. (2016). *Alternative Aggregates and Materials for High Friction Surface Treatments* (Numbers BDR74-977–05).

Woodward, D., & Friel, S. (2017). Predicting the Wear of High Friction Surfacing Aggregate. *Coatings*, *7*(5). https://doi.org/10.3390/coatings7050071

Xiao, J., Kulakowski, B. T., & EI-Gindy, M. (2000). Prediction of Risk of Wet-Pavement Accidents: Fuzzy Logic Model. *Transportation Research Record*, *1717*(1), 28–36. https://doi.org/10.3141/1717-05

Xu, G., Lin, X., Wang, S., Zhan, Y., Liu, J., & Huang, H. (2024). Incep-FrictionNet-Based Pavement Texture Friction Level Classification Prediction Method. *Lubricants*, *12*(1). https://doi.org/10.3390/lubricants12010008

Yang, G., Li, Q. J., Zhan, Y., Yu, W., Wang, K. C. P., & Peng, Y. (2019). Field performance evaluation of high friction surface treatments (HFST) in Oklahoma. *Canadian Journal of Civil Engineering*, *46*(12), 1142–1150. https://doi.org/10.1139/cjce-2018-0521

Yang, G., Yu, W., Li, Q. J., Wang, K., Peng, Y., & Zhang, A. (2021). Random Forest-Based Pavement Surface Friction Prediction Using High-Resolution 3D Image Data. *Journal of Testing and Evaluation*, *49*(2), 1141–1152. https://doi.org/10.1520/JTE20180937

Yang, G., Zhang, A. A., Wang, K. C. P., Li, J. Q., Liu, W., & Liu, Y. (2023). Deep-learning based non-contact method for assessing pavement skid resistance using 3D laser imaging technology. *International Journal of Pavement Engineering*, *24*(2), 2147520. https://doi.org/10.1080/10298436.2022.2147520

Yu, M., You, Z., Wu, G., Kong, L., Liu, C., & Gao, J. (2020). Measurement and modeling of skid resistance of asphalt pavement: A review. *Construction and Building Materials*, *260*, 119878. https://doi.org/https://doi.org/10.1016/j.conbuildmat.2020.119878

Zhan, Y., Li, J. Q., Liu, C., Wang, K. C. P., Pittenger, D. M., & Musharraf, Z. (2021). Effect of aggregate properties on asphalt pavement friction based on random forest analysis. *Construction and Building Materials*, *292*, 123467. https://doi.org/10.1016/J.CONBUILDMAT.2021.123467

Zhan, Y., Liu, C., Deng, Q., Feng, Q., Qiu, Y., Zhang, A., & He, X. (2022). Integrated FFT and XGBoost framework to predict pavement skid resistance using automatic 3D texture measurement. *Measurement*, *188*, 110638. https://doi.org/https://doi.org/10.1016/j.measurement.2021.110638

Zhang, K., & Kevern, J. (2021). Review of porous asphalt pavements in cold regions: the state of practice and case study repository in design, construction, and maintenance. In *Journal of Infrastructure Preservation and Resilience* (Vol. 2, Number 1). Springer Nature. https://doi.org/10.1186/s43065-021-00017-2

Zhao, G., Jiang, Y., Li, S., & Tighe, S. (2022). Exploring implicit relationships between pavement surface friction and vehicle crash severity using interpretable extreme gradient boosting method. *Canadian Journal of Civil Engineering*, *49*(7), 1206–1219. https://doi.org/10.1139/cjce-2021-0337

Zhao, G., Liu, L., Li, S., & Tighe, S. (2021). Assessing Pavement Friction Need for Safe Integration of Autonomous Vehicles into Current Road System. *Journal of Infrastructure Systems*, *27*(2), 4021007. https://doi.org/10.1061/(ASCE)IS.1943-555X.0000615

Zheng, N., Bi, J., Dong, S., Lei, J., He, Y., Cui, Z., & Chen, L. (2022). Testing and evaluation for long-term skid resistance of asphalt pavement composite seal using texture characteristics. *Construction and Building Materials*, *356*, 129241. https://doi.org/https://doi.org/10.1016/j.conbuildmat.2022.129241

Zhu, X., Yang, Y., Zhao, H., Jelagin, D., Chen, F., Gilabert, F. A., & Guarin, A. (2021). Effects of surface texture deterioration and wet surface conditions on asphalt runway skid resistance. *Tribology International*, *153*, 106589. https://doi.org/https://doi.org/10.1016/j.triboint.2020.106589

Zong, Y., Li, S., Zhang, J., Zhai, J., Li, C., Ji, K., Feng, B., Zhao, H., Guan, B., & Xiong, R. (2021). Effect of aggregate type and polishing level on the long-term skid resistance of thin friction course. *Construction and Building Materials*, *282*, 122730. https://doi.org/10.1016/J.CONBUILDMAT.2021.122730

Zou, Y., Yang, G., & Cao, M. (2022). Neural network-based prediction of sideway force coefficient for asphalt pavement using high-resolution 3D texture data. *International Journal of Pavement Engineering*, *23*(9), 3157–3166. https://doi.org/10.1080/10298436.2021.1884862

APPENDIX A: LITERATURE REVIEW

Pavement friction is a primary functional surface property governing tire–pavement interaction and, therefore, vehicle control during braking and steering, particularly under wet conditions where available friction is reduced and friction demand increases. Consequently, maintaining adequate friction is a core pavement safety objective and a recognized element of highway agencies' safety and pavement management practices (Federal Highway Administration, 2023; Hall et al., 2009; Henry, 2000; Wambold et al., 1995). Given its importance, the measurement and use of friction data in pavement management systems have evolved greatly over the last 15 years, and the integration of friction and safety data is an emerging and rapidly evolving field.

PAVEMENT FRICTION-RELATED PRESERVATION TREATMENTS

Many agencies have been using preservation treatments for the specific purpose of improving friction over the last two decades. A summary of these treatments and recent studies involving these treatments and their effectiveness is provided in this report. It is important to distinguish between functional surface treatments and structural rehabilitation strategies. Friction-related treatments are intended to restore surface functionality, primarily skid resistance and macrotexture, without contributing to the structural capacity of the pavement system. When both frictional and mechanical performance have deteriorated, structural rehabilitation is required. In such cases, HMA overlays remain the most common practice, as they restore structural integrity while simultaneously exposing fresh, unworn aggregate surfaces that enhance friction characteristics.

Open graded friction course (OGFC) is one of the most common pavement surface treatments in some states. However, the use of this practice is mixed, with a recent survey reporting that of the 42 states who responded, 45% use OGFC, 42% used to but no longer use OGFC, and 13% have never used OGFC (Onyango & Woods, 2017), and most of the states using it concentrated in the southern part of the country. This treatment uses an open-graded asphalt mixture gradation, producing a porous layer to improve drainage, reduce noise, and improve friction (Gu et al., 2018; King et al., 2013). Friction is of utmost importance, as some studies have shown that friction number is the primary factor controlling service life of OGFC layers (Song et al., 2021)A recent Tennessee DOT study indicated that OGFC did not have a statistically significant effect on overall crash rates but did significantly decrease wet-crash rates (X. Chen et al., 2017). Despite their potential safety and drainage benefits, the implementation of porous mixtures remains challenging in cold climates such as Illinois, where moisture infiltration and repeated freeze–thaw cycles can accelerate deterioration and compromise durability (Maia, Lu, et al., 2024; Zhang & Kevern, 2021).

High Friction Surface Treatments (HFST) consist of a thin layer of durable, polish-resistant aggregate bonded to the prepared pavement using a polymer or epoxy resin binder. When sufficient binder is applied to mitigate aggregate loss, HFST can reduce crashes by up to 90%, with the best performance on tight curves (Wilson & Mukhopadhyay, 2016). Aggregate selection is a critical component of HFST performance. Calcined bauxite is commonly specified due to its superior polish resistance and durability, although alternative aggregate sources have been investigated in the literature (Friel & Woodward, 2019). A recent Missouri DOT study examined the importance of aggregate properties for

HFSTs, showing that angularity, surface texture, and polishing resistance could serve as inputs to predict friction coefficients for this type of treatment (El-Ashwah et al., 2023). S. Li et al. (2017) developed a comprehensive framework for selecting pavement surface treatments for the Indiana DOT, integrating aggregate properties, surface characteristics, and safety outcomes to bridge the gap between high-cost HFST and conventional preservation techniques. Aggregates evaluated included dolomite, limestone, quartzite, sandstone, blast furnace slag, steel slag, and calcined bauxite. Laboratory polishing was performed with a circular polishing device and friction monitored with the British Pendulum Tester to generate friction exponential decay curves. Field friction was validated with locked-wheel skid trailer measurements. A statewide safety analysis using crash data from 2010–2015 quantified CMFs for various treatments. Calcined bauxite HFST reduced total crashes by more than 70% and wet-pavement crashes by over 80% at high-risk horizontal curves. Alternative treatments incorporating steel slag or quartzite achieved wet-crash reductions of approximately 30–50%, demonstrating meaningful safety benefits at substantially lower cost. Based on these results, the authors proposed a tiered friction management strategy: Tier 1 applications (critical curves and ramps) require calcined bauxite HFST; Tier 2 locations (moderate curves, intersection approaches) can utilize steel slag or sandstone in HFST or ultrathin bonded wearing course (UTBWC) systems; and Tier 3 network-level applications may rely on conventional dense-graded mixtures with adequate macrotexture. This study underscored that friction management should be demand-based rather than uniform across the network. A recent Indiana DOT study found HFST to be as effective in a single layer as a double layer and suggested using surface friction or MPD for quality assurance of HFST, if aggregate properties were well-controlled (S. Li et al., 2019).

Many agencies have also noticed premature deterioration of HFST, and some have used a “high friction chip seal” as an alternative, where asphalt binder is the binding agent as opposed to epoxy asphalt, but the same types of coarse aggregates are used (Bennert et al., 2021). A recent study in Missouri also showed this method, combined with the optimization of aggregate type, could provide similar friction performance while reducing life cycle costs (Roshan & Abdelrahman, 2024).

Chip seals or bituminous surface treatments are treatments where a layer of asphalt binder is applied, and then a layer of aggregate “chips” is embedded in this binder to improve friction and mitigate moisture infiltration into the pavement structure (Gransberg & James, 2005). Indiana DOT has conducted thorough study of their chip sealed roads over the last decade and determined that aggregate type has a somewhat substantial impact early on, but less over the life of the chip seal. Their study also showed the potential use of chip seals on high traffic roads (S. Li et al., 2012). QC/QA for chip seals is also very critical to ensure the mitigation of bleeding or raveling (Buss et al., 2018). However, at the design stage, care can also be taken to select aggregates which have the proper shape properties to achieve good embedment (Ma et al., 2025). For chip seals, proper aggregate gradation is essential. The aggregate must achieve sufficient embedment to ensure retention and durability, while maintaining exposed surface texture. Oversized or poorly graded particles may cause raveling due to inadequate bonding, whereas undersized particles can promote binder bleeding and compromise friction performance (Lee & Kim, 2009).

Cape seals consist of a chip seal overlaid with slurry seal or microsurfacing, forming an integrated surface system rather than two independent layers. Beyond structural preservation benefits, cape

seals play a relevant role in maintaining functional surface characteristics directly linked to safety performance. The chip seal layer provides macrotexture through exposed coarse aggregate, while the slurry or microsurfacing layer partially fills voids and enhances aggregate retention. Compared with single-layer chip seals, cape seals generally provide a denser and more uniform surface, reducing the likelihood of bleeding or aggregate loss that could negatively impact skid resistance. In contrast to thin HMA overlays, cape seals maintain higher macrotexture due to their surface treatment nature, which can be beneficial under wet-weather conditions where water drainage and tire–pavement contact are critical. Granite and other high-quality crushed aggregates are often specified to ensure long-term microtexture retention, especially in low-volume roads where traffic polishing is slower but environmental exposure may still affect durability (Solaimanian & Kennedy, 1998; Vargas-Nordcbeck, 2023).

Ultra-thin overlays are another alternative to chip seals (Hajj et al., 2019). Ultra-thin overlays are generally asphalt overlays which are placed at 0.5 to 1-inch in thickness, as solely a surface correction and not a structural layer. These overlays can provide improved friction as one important factor, and in some cases are economical compared to chip seals (Hajj et al., 2018). These overlays are often called ultra-thin bonded wearing course (UTBWC). Typically, a membrane or thick layer of asphalt emulsion is placed between the existing pavement surface and a UTBWC (Hanson, 2001). According to a survey conducted by NCHRP, it is not ideal to use ultra-thin overlays when there is existing cracking or rutting on the pavement surface, as these treatments are intended for structurally sound pavements and are unlikely to perform adequately when applied over distresses indicative of underlying structural deficiencies (Watson & Heitzman, 2014).

Microsurfacing is a mix prepared on-site consisting of high-quality aggregate of sizes typically below 9.5 mm, polymer-modified emulsified asphalt, mineral filler, water, and chemicals which control the breaking time. Its use for improving friction has been shown to be highly effective (De Rose et al., 2025). The microsurfacing mix is designed to seal the pavement from water infiltration, restore smoothness, increase resistance to surface deformation, and improve overall friction (Uzarowski et al., 2005). Despite this treatment being widely used, a recent review uncovered some further research needs which would help improve the implementation of microsurfacing mixes including: examining the effect on cure of environmental conditions, identification of clear tolerance limits, assessing moisture damage and aging resistance, and examining the influence of pre-compaction, which is not typically done (Bhargava et al., 2020). Some recent research has also examined the impact of mix design parameters on texture of microsurfacing, showing gradation-based parameters defined as weighted deviations from an optimal gradation curve are robust predictors of macrotexture, achieving excellent R^2 values, especially when combined with an exponential representation of bitumen content (Vaiana et al., 2023).

In addition to surface treatments, thin asphalt overlay strategies were previously implemented as cost-effective rehabilitation alternatives. IDOT introduced the Surface Maintenance at the Right Time (SMART) program in the mid-1980s, consisting of single-pass thin lift bituminous overlays aimed at preserving rural highways before severe deterioration occurred. Performance evaluations showed that SMART projects maintained or improved Condition Rating Survey (CRS) values and ride quality beyond initial expectations over a five-year monitoring period (Reed, 1992, 1994). In cases where

surface friction loss is associated with aged binder or material shortages, hot in-place recycling (HIPR) provides an alternative rehabilitation strategy by reheating, scarifying, rejuvenating, and recompacting the existing asphalt layer, thereby restoring surface texture and correcting distresses such as rutting and low-friction conditions without requiring full material replacement (Shoenberger & Vollor, 1990).

For concrete pavements, diamond grinding has been shown to be an effective treatment to restore both smoothness (when faulting has occurred) and friction (Rao et al., 1999). Diamond grinding has also been used for asphalt pavements and has been shown to be effective in improving friction and mitigating rutting (S. Li et al., 2016). Recent studies have indicated that diamond grinding can provide long-lasting friction and texture improvement (Ahammed & Tighe, 2008; Buddhavarapu et al., 2013; D.-H. Chen & Hong, 2015). Diamond grooving is another technique which can be used in conjunction with diamond grinding to improve friction of concrete pavements (Najafi et al., 2012). Other techniques which can improve concrete surface texture are tining, brooming, and the Next Generation Concrete Surface, which basically acts as a hybrid between grinding and grooving (Snyder, 2019).

PAVEMENT FRICTION EVALUATION METHODS

Locked-wheel skid trailer (LWST) testing, the primary friction evaluation device used in Illinois and most state DOTs, remains widely implemented due to its standardized methodology, repeatability, and compatibility with network-level pavement management and safety assessment programs. LWST operates by accelerating the test vehicle towing the trailer to an acceptable speed, spraying water ahead of the trailer tire (to capture wet friction), and locking the test tire to measure skid between tire and pavement. The results of LWST testing are reported in terms of skid number (SN), which is defined as the coefficient of friction between the tire and the pavement multiplied by 100 (Rizenbergs et al., 1973). However, it is crucial to note that this measured SN is not comparable to other friction number (FN) measurements by default because different normal forces are applied when different devices are used.

One of the major benefits of LWST is that it can use either a smooth or ribbed tire, or both. The smooth tire measurement is mostly related to pavement macrotexture, while ribbed tire measurements are more related to microtexture of the pavement surface. Choubane et al. (2006) demonstrated that, although both tires exhibited high repeatability and reproducibility across open- and dense-graded surfaces, the smooth tire was significantly more sensitive to water film thickness and surface texture variations, whereas the ribbed tire was comparatively insensitive to water film effects. This confirms that smooth tire results better reflect macrotexture-related drainage characteristics, while ribbed tire measurements are more representative of microtexture-controlled friction mechanisms under wet testing conditions. A second major benefit of using LWST is its ability to capture both wheel paths. Finally, the test is relatively quick. One disadvantage includes that the test averages friction over more than 50 feet, so it cannot investigate very specific spots. A second disadvantage is that the test cannot be used on any segments which are not straight, which excludes critical locations for safety such as ramps and curves (Hall et al., 2009). Third, measurements can only be conducted at one speed, which can be a drawback if the pavement friction at different speeds is

desired, which would require multiple passes at different speeds over the same section (Saito et al., 1996). Finally, while LWST can be used at typical traffic speeds, it is limited in terms of its ability to continuously measure pavement friction because measurements can only be done once the wheels are locked and full slip is achieved.

A survey of state agencies conducted in the early 2000s as part of NCHRP 1-43 (Hall et al., 2009) indicated that of 46 agencies surveyed, 41 were using LWST based on ASTM E274, 3 were not conducting friction measurements in the field, and one agency was using a modified version of the Dynatest Runway Friction Tester called the Highway Friction Tester (HFT), which can measure friction continuously using a single wheel attached to the device. Although new equipment has become available over the last several years, LWST remains widely used. A recent Wyoming DOT study indicated that 90% of the 32 state DOTs who responded to a survey reported using LWST for friction investigation (Elkhazindar et al., 2022). An alternative to using the LWST method, when very granular data is required at very specific spots, is the use of the Dynamic Friction Tester (DFT) (Saito et al., 1996). In the above-mentioned Wyoming DOT study, the DFT was indicated to be the second most widely used equipment among the states surveyed (Elkhazindar et al., 2022).

The DFT is a portable device with a rotating wheel placed parallel to the ground with diameter of 28.4 cm and three rubber pads on the bottom. While the wheel rotates up to a designated speed (typically 80 km/h), water is sprayed on the surface, then the wheel is dropped to allow the three pads to contact the pavement surface, and the coefficient of friction between the rubber pads and pavement surface is measured. The speed is reduced (typically to 20 km/h at a constant rate) to obtain measurements at a range of speeds until the test is stopped. The introduction of the test demonstrated ability to predict the friction component at 60 km/h (F60) of the International Friction Index. To compliment DFT measurements, the Circular Texture Meter (CTM) can be used with the same diameter to capture mean profile depth (MPD) (Prowell & Hanson, 2005), which forms the texture component of the IFI. These devices can also be combined with laboratory friction assessment methods, such as the use of the Three Wheel Polishing Device (TWPD) (Vollor et al., 2006) for measurement of degradation of materials over time (Hajj et al., 2018; Komaragiri et al., 2020; Saghafi et al., 2022; Zong et al., 2021). It has also been shown that DFT/CTM measurements correlate well with components of LWST measurements and IFI (Khasawneh, 2015). The main drawbacks of these methods are that they measure only over very small areas, which can be misleading, and that they require lane closure and traffic control.

Internationally, and occasionally in the United States, simple and low-cost measures are used such as the British Pendulum Test (BPT) (Chang et al., 2016; Chu et al., 2022; Serigos et al., 2014). This test was developed by the United Kingdom's Road Research Laboratory (RRL) as one of the early friction tests (Salt, 1977). The test is simple, as a pendulum is dropped from a known height, is allowed to skid across the pavement or material specimen, and the height at which it swings back up to is measured and reported as British Pendulum Number (BPN), a proxy for the skid resistance of the surface. Generally, this test is seen as a good assessment tool for micro-texture (Chu et al., 2022), but it provides a very small area of measurement and cannot practically be used in pavement management applications. Nonetheless, clear relationships have been shown between BPN and

friction coefficients (Leu & Henry, 1978; Sabey & Lupton, 1964), and it is a powerful tool for lab-scale assessment of materials, especially when evaluating different aggregate types.

In terms of continuous friction measurement (CFM), more attention has been paid over the last few years to the potential advantages which are provided. These can broadly be classified into three categories (Mataei et al., 2016; Yu et al., 2020): (i) sideway force measurements where a tire at a yaw angle is used to measure friction, (ii) fixed slip measurements where a straight tire that is slipping at a constant level is used to measure friction, ad (iii) variable slip measurements where a straight tire can be programmed to slip at any level to measure friction. Among sideway force measurement techniques, two major devices are commonly used, the Sideway-force Coefficient Routine Investigation Machine (SCRIM) and the Mu-Meter. These devices work based on a simple principle: because the tire measuring friction is placed at a yaw angle, the side force can be directly measured while the vehicle moves forward, even while the measurement wheel is allowed to rotate, which directly indicates the friction provided by the pavement. The SCRIM does this at an angle of 20^{o} while the Mu-Meter uses two wheels, each at an angle of 7.5^{o}. Recent efforts have been made to "harmonize" measurements between the SCRIM device and LWST so that data can be used by state DOTs by converting friction numbers (FN) measured using SCRIM (based on the SCRIM Reading (SR)) to SN. Some studies have also looked at doing this through the IFI (Quiros et al., 2018). However, it should be noted that good relationships have only been found for the ribbed tire LWST measurements compared to the SCRIM, because of the SCRIM's limitations in terms of capturing the effect of macrotexture (which all the above CFM techniques share) (de León Izeppi et al., 2019). A recent study from the National Center for Asphalt Technology (NCAT) also showed good relationship between SCRIM and LWST results and indicated that SCRIM repeatability is best at 50 mph and for tangent sections (Gu et al., 2023).

Among fixed slip testing methods, many devices exist, each with tires which must meet ASTM E1551: Standard Specification for Special Purpose, Smooth-Tread Tire, Operated on Fixed Braking Slip Continuous Friction Measuring Equipment (Yu et al., 2020). This includes the Dynatest device mentioned above which Arizona uses for routine friction investigation, as well as the commonly used GripTester. One drawback of these testing methods consists in the differences observed between the test and actual braking and the specified slip ratio allowed (for example 14% using the HFT), especially for snowy or icy conditions (Yu et al., 2020).

The last category are devices which can conduct variable slip measurements to obtain a range of FN for a given pavement based on the changing slip. One example of such a device is the Road Analyzer and Recorder (ROAR), a device which can perform both fixed and variable slip, which was developed as part of a joint project between the Norwegian road agency and Minnesota DOT in the mid-90s (Wambold et al., 2000). The SALTAR device, which can also be added to snowplows or salt trucks was developed as a part of this apparatus for friction measurement (Wambold et al., 2000). Despite the benefits of these devices, it should be noted that they have a major drawback of high costs for maintenance and operation of the equipment, and a complex analysis (Yu et al., 2020).

The above contact-based methods, while widely used and fairly reliable, do have some drawbacks in terms of repeatability of measurements due to factors such as temperature (Anupam et al., 2013)

and the presence of water (Cerezo et al., 2014), which can make the consistency of network-level friction measurements challenging (Yang et al., 2023). As an alternative, contactless approaches have been evaluated (Jain et al., 2021). Although it is well-known that texture cannot directly predict friction (de León Izeppi et al., 2017), some studies have directly correlated 2D texture to friction using empirical models (Kouchaki et al., 2018; Leandri & Losa, 2015; Meegoda & Gao, 2015; Pranjić & Deluka-Tibljaš, 2022) or mechanistic techniques (Ueckermann et al., 2015).

Recently, many researchers have attempted to reconstruct 3D texture models to predict friction. Kogbara et al. (2018) utilized close-range photogrammetry (CRP) to obtain 3D texture and found a good relationship between the top 2 mm of the pavement surface texture using this method with the friction measured using the GripTester. These findings align with those of Mahboob Kanafi & Tuononen (2017), who observed the top 20% of roughness measurements for smooth roads had a good relationship with friction. To further harmonize texture and friction measurements, Alhasan et al. (2018) developed a relationship between Mean Profile Depth (MPD) and friction using a specific model, although it should be noted that this relationship was only for dry friction as measurements utilized the BPT. Deng et al. (2021) utilized a similar approach based on mechanistic power spectrum analysis of 3D texture data, which was found to effectively predict BPT results. To evaluate the contribution of microtexture specifically, Guo et al. (2023) utilized 3D printed aggregate specimens combined with Atomic Force Microscopy to predict friction. There have also been several other empirical studies converting 3D texture to friction in recent years (Ban et al., 2024; Guo et al., 2021; Kováč et al., 2021; Q. J. Li et al., 2020). Finally, one very novel approach is to use a combination of vehicle dynamics data and vision data to predict friction coefficients (Du et al., 2023), while some have proposed using only vehicle dynamics (Khaleghian et al., 2019) or sensors embedded in the pavement (Rasol et al., 2023), although the latter approach is not practical for network-level study.

Machine learning has also become an increasingly powerful tool for converting image data to friction based on texture and other features. Yang et al. (2021) conducted a comprehensive study of the impacts of 3D texture data and found that at high speeds, macro- and micro-texture could mostly predict friction together, but that at low speeds macro-texture was much more important and that temperature had more impact than micro-texture). Lu et al. (2022) used a convolutional neural network to assess the impact of different texture aspects on friction and determined that wavelengths above 2.4 mm were most critical for wet friction. Zou et al. (2022) later used image processing and 3D texture data combined with neural networks to predict friction results from SCRIM testing. The same group later utilized 1D images as the inputs and predicted friction values from the GripTester, although it was mentioned that their future work will focus on using higher resolution measurements based on laser data (Yang et al., 2023), which is an approach taken by other researchers (Hu et al., 2022; Xu et al., 2024; Zhan et al., 2022).

STUDIES RELATING FRICTION TO TRAFFIC SAFETY

One of the most important aspects of studying friction is understanding its relationship to traffic safety. Some of the earliest studies were conducted by researchers in Finland and uncovered that stopping distance has a clear relationship to pavement friction (Wallman et al., 1997). In these studies, a clear low friction point was observed at which friction had substantial impact on crash rate.

Many of the early studies in the United States and United Kingdom, synthesized by (Hall et al., 2009), were consistent with these, showing that at high levels of friction, there is not a strong relationship with crash rates, but that crash rates increased rapidly once friction deteriorated beyond a certain level (Giles et al., 1965; McCullough & Hankins, 1966; Rizenbergs et al., 1973). Subsequent studies evaluated the importance of friction by performing before-after studies of sections where friction was increased and observing crash reductions (Kamel & Gartshore, 1982; Wallman & Aaström, 2001) or predicted crash reduction (Xiao et al., 2000). Some studies also observed direct empirical relationships between friction and crash rates (Hall et al., 2009). However, correlative studies should be carefully considered, as sources of bias may appear in the data. For example, high friction treatments may be applied at areas where safety is a major concern for reasons unrelated to friction (Katicha & Flintsch, 2022).

One of the major challenges which remains for state DOTs is defining the thresholds at which friction treatments should be applied. A few preliminary studies were conducted on the best ways to integrate safety into pavement management systems (Tighe et al., 2000), but it was not until the last two decades when this began receiving more attention. Most agencies set investigatory and intervention levels based on the friction level at which a section should be monitored and included in planning and the level at which a section should receive a treatment (McGovern et al., 2011). The following three methods were defined by Hall et al. (2009) as part of the above-mentioned NCHRP project:

1. Using historical data to set the investigatory (level at which skid resistance deteriorates significantly) and intervention (level at which a specific percent of investigatory level) levels.

2. Combine historical skid resistance data with crash rates and follow a similar approach to the one above.

3. Set the investigatory skid resistance level equal to the level at which wet-to-dry crash ratio begins to increase substantially and the intervention level to the minimum allowable wet-to-dry crash ratio, both a set number of standard deviations below the average skid resistance levels.

However, having set values for thresholds using these methods comes with the major drawback of only considering a single speed and water film thickness, which can vary as drivers travel the road (Fwa, 2017). To consider the effect of speed, two major models exist, the model developed at Penn State University (Leu & Henry, 1978) and the IFI model developed by the Permanent International Association of Road Congresses (Wambold et al., 1995). Some researchers have also used probability-based approaches to link the probability of a crash with the skid resistance (Piyatrapoomi et al., 2008). Recently, Fwa (2017) developed a finite element model which could represent the effects of both water film thickness and speed on skid number (SN), which could provide better insights into wet-to-dry crash ratios in different conditions. A similar study was conducted for airfield runways by Zhu et al. (2021), which considered more factors including the properties of the rubber tire and slip ratio in addition to speed and water film thickness (Zhu et al., 2021). A full review of road-tire friction models and their development can be found in Khaleghian et al. (2017).

Recent studies have explored the relationship between friction and safety in more detail. McCarthy et al. (2022) utilized a statistical approach to determine investigatory thresholds for three countries based on crash and friction data and found them generally to be similar in magnitude (McCarthy et al., 2022). A recent Texas Transportation Institute (TTI) study developed Crash Modification Factors (CMFs) for horizonal curves which included the impact of pavement friction and found it to be very important for wet-weather crashes (Geedipally et al., 2019). In Italy, Cafiso et al. developed SPFs and CMFs for roads in their network based on many factors, including Grip Number and International Roughness Index (IRI) (Cafiso et al., 2021). Abdullah analyzed the relationship between friction and crash rates on Iowa roads and observed a dependency on the type of crash and roadway (Abdullah, 2020).

Ivan et al. (2012) determined, in a Connecticut DOT study, that friction reduction had the most impact at intersections on non-isolated curves on undivided roads and on mild curves on rural divided roads (Ivan et al., 2012), which could partially be explained by driver sight or driver behavior, respectively. Curves are of specific interest to many state DOTs, with Musey & Park (2016) recently developing CMFs which consider horizontal curvature and friction levels and found that friction had a particularly critical impact on wet crashes on horizontal curve. Some studies have also been conducted to develop computational models for the effect of friction on horizontal curves (Khanjari et al., 2022; Peng et al., 2021). In addition to curves, an area of increasing interest to state DOTs are intersections. A recent Wyoming DOT study examined crash data for intersections and indicated that higher friction reduced the likelihood of serious injury from intersection accidents (Sharafeldin et al., 2022).

Roy et al. (2023) observed the importance of friction for both wet- and dry-road crashes by developing SPFs for Wyoming DOT with the goal of identifying “hotspots” where low friction could cause excessive crashes and equivalent property-damage-only (EPDO) crashes. Crash severity has also recently been linked to friction levels (Bao et al., 2023; Zhao et al., 2022). In addition, many researchers have used machine learning to predict crash rates based on many factors, which include pavement friction (Najafi et al., 2019). Finally, one new concern may be the impact of pavement friction on crash rates when autonomous vehicles are involved. A recent study used Indiana DOT data and determined that current Indiana road friction levels are sufficient to prevent an increase in accidents due to the driving of autonomous vehicles (Zhao et al., 2021).

IMPACT OF PAVEMENT MATERIALS ON FRICTION AND SAFETY

Several studies have recently been conducted with the objective of linking pavement friction to the materials used in the pavement. Noyce et al. (2007) conducted a thorough study of asphalt mix design factors and their impact on mean texture depth (MTD), but could not identify a direct relationship between texture and friction. In general, it is well-known that aggregate gradation and coarse aggregate properties play significant roles in friction through macro- and micro-texture respectively. Zhan et al. (2021). conducted a study for Oklahoma DOT in which the importance of different aggregate characteristics and other features on friction was examined by testing aggregate sampled from quarries in parallel with GripTester friction testing and 3D laser-based imaging of field sites. Their findings indicated loss of texture was the most important aggregate-related issue, while

AADT was the most important issue overall. Lei et al. (2022) conducted a study of different aggregate types and their polishing resistance by examining them under two types of microscopes and found that sandstone had the best resistance to polishing and limestone had the worst. Alsheyab & Khasawneh (2024) performed a study of lab specimens in which they used the sand path test and BPT and determined that fineness modulus had the most impact on both MTD and BPN. A recent study of West Virginia indicated that using dolomite could have detrimental effects on friction if more than 50% was used, but also identified shotblasting as an effective treatment to restore friction of such roads (Gu et al., 2022).

One recent study examined the effect of aggregate type when diamond grinding was used and found slightly better friction retention when siliceous aggregates were used compared to limestone, but that the trend was minor and that limestone was in some cases slightly better (Komaragiri et al., 2020).

IMPACT OF PAVEMENT SURFACE TREATMENTS ON FRICTION AND SAFETY

Several studies have demonstrated the impact of applying pavement surface treatments on friction and, correspondingly, reduction in crashes. One of the early studies from Spain determined that improvement in SCRIM number from below 50 to above 60 resulted in an average wet-crash reduction of 68% (Pardillo Mayora & Jurado Piña, 2009).

One of the early Empirical Bayes (EB) studies indicated that newly resurfaced pavements in New York were causing an increase in crashes if compensatory safety improvements were not used (Hauer et al., 1994). Milton et al. (2008) observed mixed results depending on the type of crashes which were observed. In those where property damage only and injuries occurred, increased friction resulted in increased accidents, while possible injury accidents were decreased (Milton et al., 2008). This may be in part due to speed adaptation, which was observed by Lyon et al. in a more recent study, where dry-road crashes increased over four states for some treatments including thin HMA overlays and open graded friction course (OGFC) on two lane roads and OGFC and chip seals on multi-lane roads. However, benefits were observed in terms of dry-road crash reduction for ultra-thin bonded wearing course (UTBWC), chip seals, slurry seals, and diamond grinding on different road types (Lyon et al., 2018). Wet-road crash rates were also reduced for most treatment types, although no major benefit was observed for HMA on two lane roads or OGFC for two lane and multi-lane roads. Buddhavarapu et al. (2015) also found similar findings on the lack of effectiveness of OGFC in reducing wet-weather crashes, for the state of Texas overall (Buddhavarapu et al., 2015).

In terms of specific treatment types, de León Izeppi et al. (2010) investigated the use of high friction surface treatment (HFST) in Wisconsin and observed that the reductions in costs due to crashes were 2-8 times the costs of the treatments, and that these treatments had very high initial friction, although traditional IFI models did not apply to these (de León Izeppi et al., 2010). Yang et al. (2019) observed major reductions in crash rates where HFST was applied, and higher numbers where calcined bauxite aggregates were used, although they did observe some distresses (Yang et al., 2019).

There are considerably fewer studies on the effects of microsurfacing. Erwin (2007) observed that by analyzing before-and-after crash rates for microsurfacing projects, significant effects were observed

in reducing crashes based on this treatment, including 32% reduction in wet-weather crashes (Erwin, 2007). One other study in Malaysia also identified a reduction in crashes and increase in friction after the application of microsurfacing (Abdul Kadir et al., 2020). As part of NCHRP 17-25, microsurfacing was one treatment investigated, along with a 1.5-inch HMA overlay, which showed substantial improvement when Safety Performance Functions (SPF) were used (Lyon & Persaud, 2008).

One lab study examined the effect of a composite fog seal on top of chip seal and observed that this material had an overall better BPN over time as well as MTD (Zheng et al., 2022). Diamond grooving has also been shown to significantly reduce wet-weather crashes by 55%-72% in a range of studies reviewed as part of an NCHRP study (Torbic et al., 2004).

APPENDIX B: ILLINOIS FRICTION DATA ANALYSIS

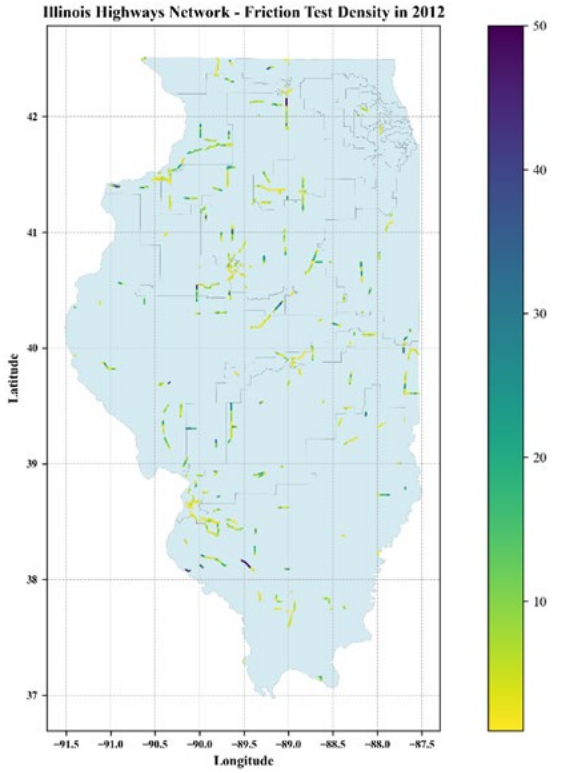

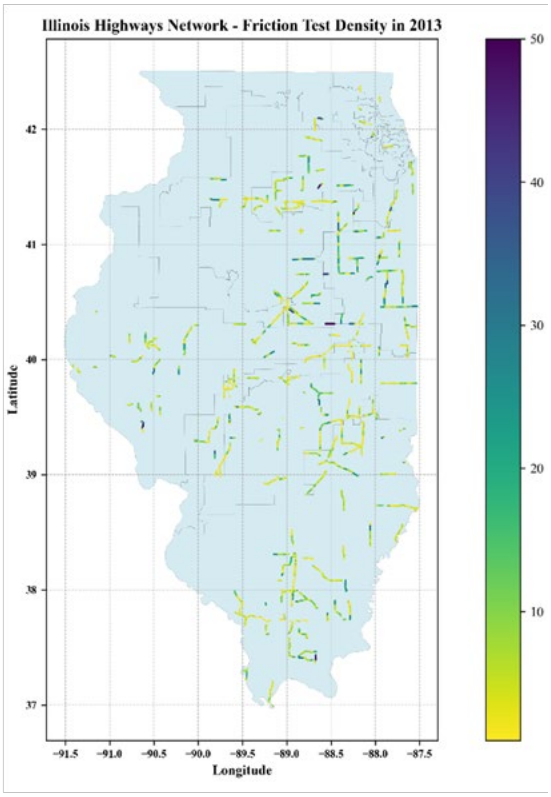

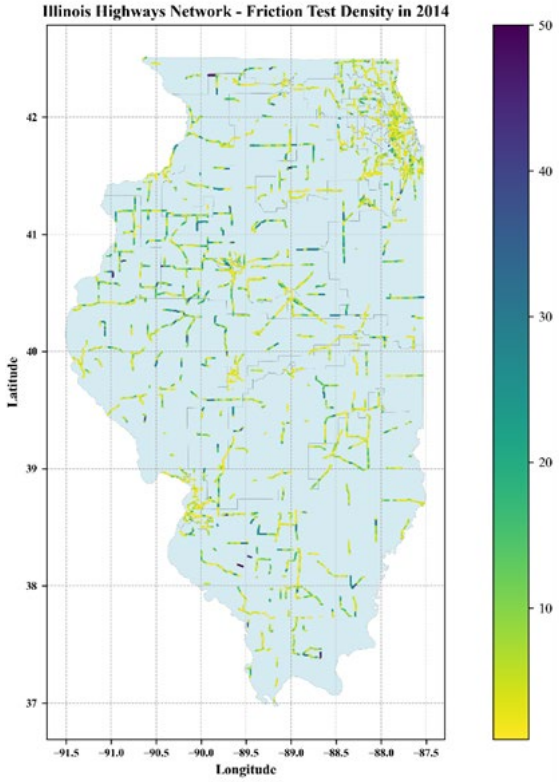

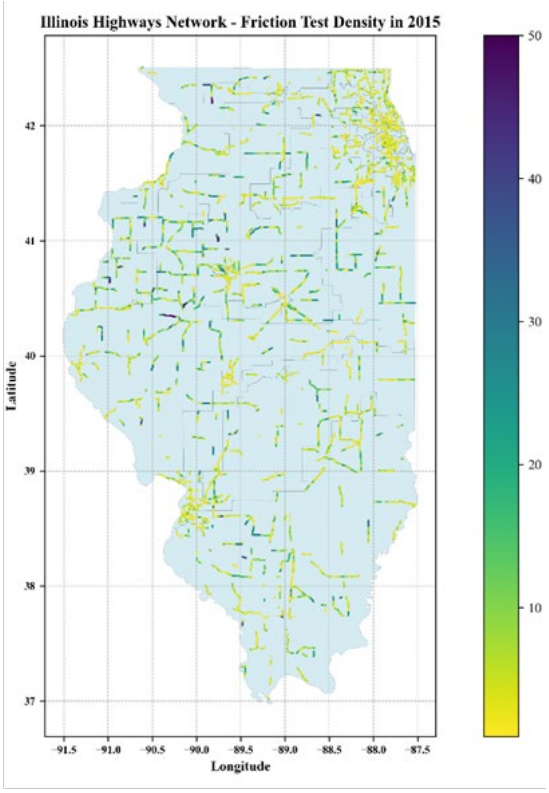

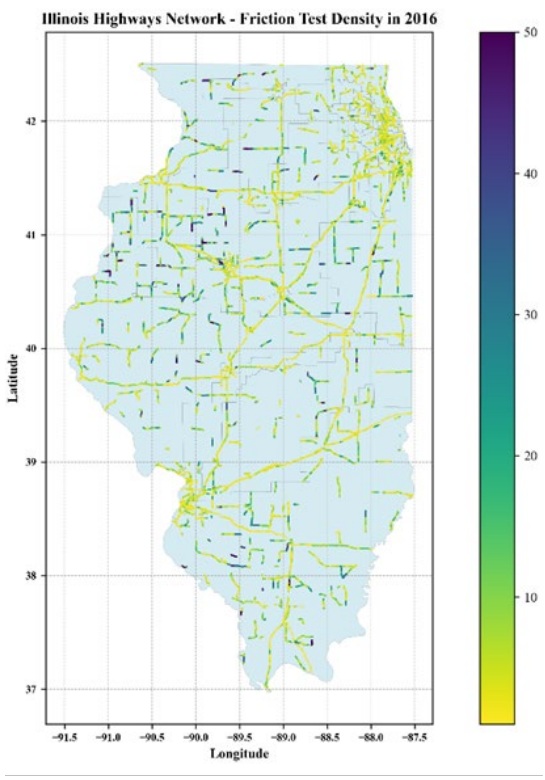
Illinois Highways Network - Friction Test Density in 2016
Latitude
Longitude
42
41
40
39
38
37
−91.5
−91.0
−90.5
−90.0
−89.5
−89.0
−88.5
−88.0
−87.5
50
40
30
20
10

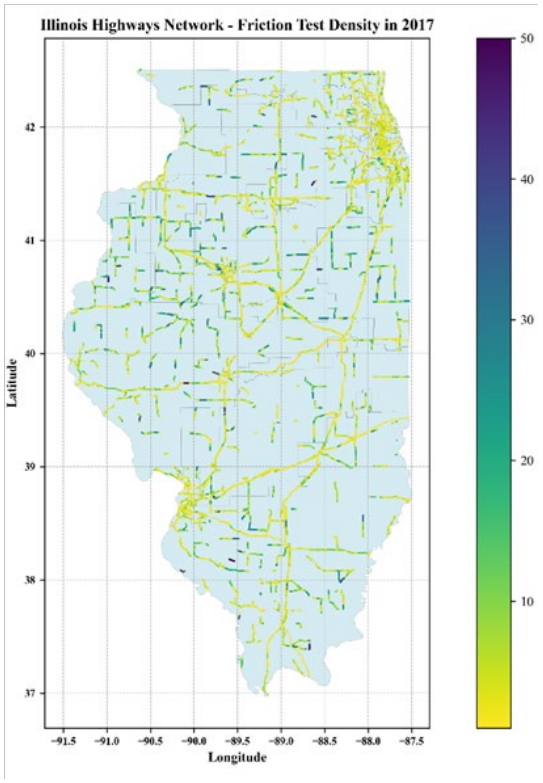
Illinois Highways Network - Friction Test Density in 2017
Latitude
Longitude
42
41
40
39
38
37
−91.5
−91.0
−90.5
−90.0
−89.5
−89.0
−88.5
−88.0
−87.5
50
40
30
20
10

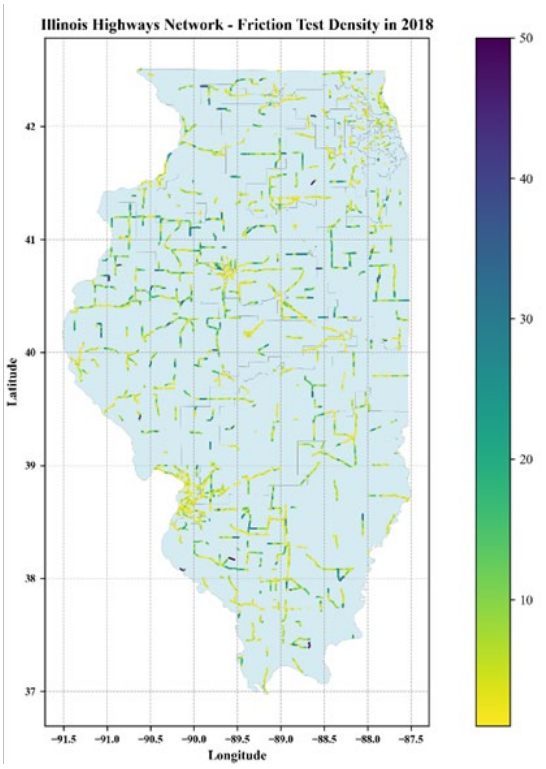
Illinois Highways Network - Friction Test Density in 2018
Latitude
Longitude
42
41
40
39
38
37
−91.5
−91.0
−90.5
−90.0
−89.5
−89.0
−88.5
−88.0
−87.5
50
40
30
20
10

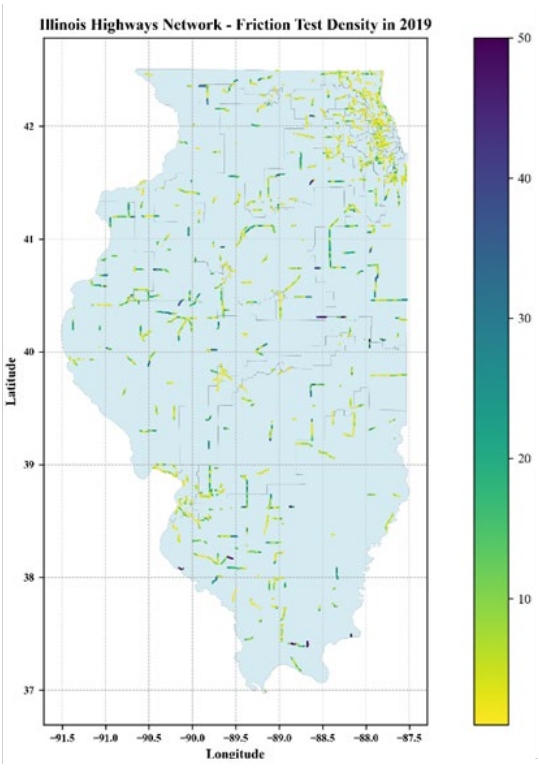
Illinois Highways Network - Friction Test Density in 2019
Latitude
Longitude
42
41
40
39
38
37
−91.5
−91.0
−90.5
−90.0
−89.5
−89.0
−88.5
−88.0
−87.5
50
40
30
20
10

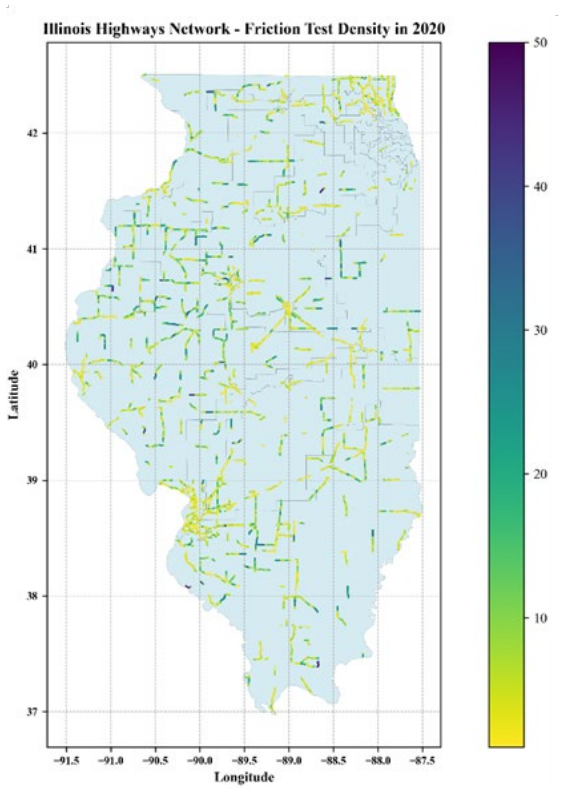
Illinois Highways Network - Friction Test Density in 2020
Latitude
Longitude
42
41
40
39
38
37
−91.5
−91.0
−90.5
−90.0
−89.5
−89.0
−88.5
−88.0
−87.5
50
40
30
20
10

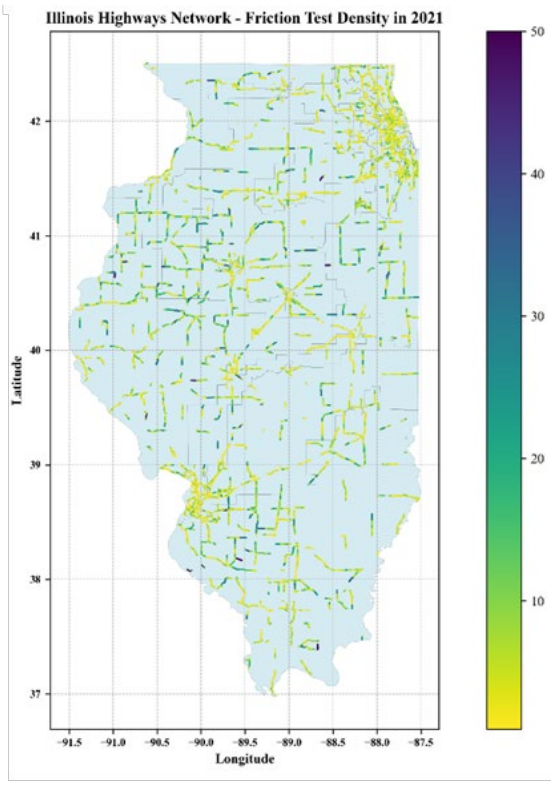
Illinois Highways Network - Friction Test Density in 2021
Latitude
Longitude
42
41
40
39
38
37
−91.5
−91.0
−90.5
−90.0
−89.5
−89.0
−88.5
−88.0
−87.5
50
40
30
20
10

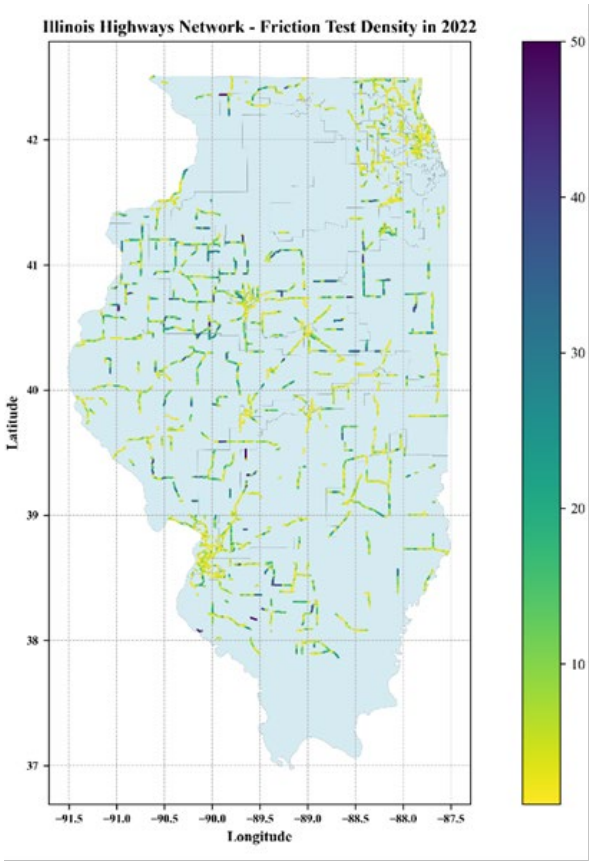
Illinois Highways Network - Friction Test Density in 2022
Latitude
Longitude
42
41
40
39
38
37
−91.5
−91.0
−90.5
−90.0
−89.5
−89.0
−88.5
−88.0
−87.5
50
40
30
20
10

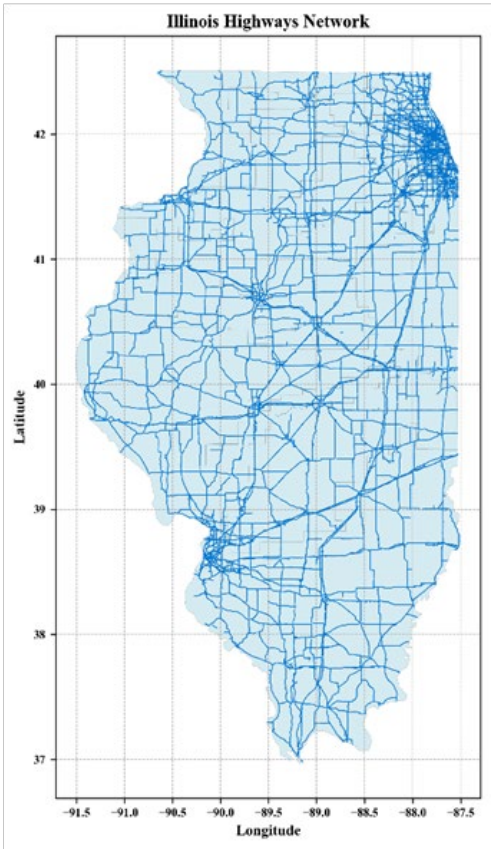
Illinois Highways Network
Latitude
Longitude
42
41
40
39
38
37
−91.5
−91.0
−90.5
−90.0
−89.5
−89.0
−88.5
−88.0
−87.5

APPENDIX C: ONLINE SURVEY

SURVEY FOR IDOT DISTRICT

Part 1. Pavement friction management program

Q1.1 Does your district have a pavement friction management program?

- Yes
- No

Q1.2 If yes, how long has the program been in use?

- Less than 2 years
- 3 to 5 years
- 5 to 10 years
- More than 10 years

Q1.3 Does your district collect network-level pavement friction data? If yes, how does your jurisdiction measure network-level pavement friction data (e.g., measuring equipment)? If not, indicate the main reasons why your jurisdiction has not started network-level pavement friction data.

- Yes, _____
- No, _____

Q1.4 Which of the data types are regularly collected (e.g., pavement friction, macrotexture (mean profile depth), curve radius, grade etc.)?

[Short answer]

Q1.5 What is the frequency of your pavement friction data collection?

[Short answer]

Q1.6 What does your district do with the pavement friction data (e.g., estimate crashes)?

[Short answer]

Q1.7 Do you have any additional ideas or information (e.g., lessons learned) to share about deploying your pavement friction management program?

- Yes, _____

  _____
- No

Part 2. Pavement treatments

Q2.1 What are major considerations (e.g., friction, roadway facility types, cost, traffic volume, lifecycle) in selecting specific pavement treatments for specific pavement types? And which one triggers the implementation of treatments?

[Short answer]

Q2.2 What types of pavement friction treatments does your district use for pavement rehabilitation, preservation, and enhancement (e.g., chip seal, micro-surfacing, diamond grinding, etc.) and what is the average frequency/expected service life of those treatments?

Pavement Friction Treatment	Average Frequency/Expected Service Life

Q2.3 How does your district determine the investigatory threshold for applying pavement treatments?

[Short answer]

Q2.4 Has your district conducted before-and-after analysis to quantify these treatments' effectiveness in crash reduction?

- Yes, _____

  _____
- No

Q2.5 Has your district conducted assessments to find out if treated roadway sections are under-performing or over-performing in terms of providing friction?

- Yes, _____

  _____
- No

Q2.6 Has your district established a policy or procedure to do decision making processes about selections of pavement friction treatments? If yes, describe how your policy or procedure works.

- Yes, _____

  _____
- No

Q2.7 Does your district have a computer program or decision-tree software to do cost-benefit analysis of pavement friction treatments? If yes, explain it briefly.

- Yes, _____

  _____

- No

Q2.8 Does your district have a computer program or decision-tree software to assist you with decisions on whether and which pavement treatment is recommended for certain roadways? If yes, explain it briefly.

- Yes, _____

  _____

- No

SURVEY FOR IDOT DISTRICT

Part 1. Pavement friction management program

Q1.1 Does your state have a pavement friction management program?

- Yes
- No

Q1.2 If yes, how long has the program been in use?

- Less than 2 years
- 3 to 5 years
- 5 to 10 years
- More than 10 years

Q1.3 Does your state collect network-level pavement friction data? If yes, how does your state measure network-level pavement friction data (e.g., measuring equipment)? If not, indicate the main reasons why your state has not started network-level pavement friction data.

- Yes, _____
- No, _____

Q1.4 Which of the data types are regularly collected (e.g., pavement friction, macrotexture (mean profile depth), curve radius, grade etc.)?

[Short answer]

Q1.5 What is the frequency of your pavement friction data collection?

[Short answer]

Q1.6 Does the friction test program vary across the roadway functional class? And how does your state select which lane to test?

[Short answer]

Q1.7 Does your state use contractors for pavement friction data collection, or does your state do it in-house?

[Short answer]

Q1.8 Does your state have a program/database/App to store and manage all the collected pavement friction data?

[Short answer]

- Yes, _____

  _____

- No

Q1.9 If your state collects continuous pavement friction data, how do you see your data correlated with discrete pavement friction data (i.e., collected by locked-wheel tester trailer)?

[Long answer]

Q1.10 Does your state have any experience to share in collecting and processing the continuous pavement friction data (e.g., data cleaning, storage, analysis, and reporting)?

- Yes, _____

  _____

- No

Q1.11 Has your state categorized different roadway facility types (e.g., freeway, multi-lane highway, rural 2-lane roadway etc.) and site types (e.g., intersections, segment, curves) while collecting pavement friction data?

- Yes, _____

  _____

- No

Q1.12 Has your state used pavement friction data to develop safety Performance Functions (SPFs) and Crash Modification Factors (CMFs)? If yes, which pavement characters (e.g., curvature, lane width etc.) are considered in the development of SPFs and CMFs?

- Yes, _____

  _____

- No

Q1.13 Has your state used pavement friction data to analyze network level traffic safety issues (i.e., crash risks) and to develop investigatory or intervention levels of frictions to reduce crash risks?

- Yes, _____

  _____

- No

Q1.14 Has your state integrated the pavement friction data analysis results into your project prioritization processes (e.g., safety engineering, pavement preservation)?

- Yes, _____

  _____

- No

Q1.15 Has your state integrated the pavement friction data into your asset management processes?

- Yes, _____

  _____

- No

Q1.16 Do you have any additional ideas or information (e.g., lessons learned) to share about deploying your pavement friction management program?

- Yes, _____

  _____

- No

Part 2. Pavement treatments

Q2.1 What are major considerations (e.g., friction, roadway facility types, cost, traffic volume, lifecycle) in selecting specific pavement treatments for specific pavement types? And which one triggers the implementation of treatments?

[Short answer]

Q2.2 What types of pavement friction treatments does your state use for pavement rehabilitation, preservation, and enhancement (e.g., chip seal, micro-surfacing, diamond grinding, etc.) and what is the average frequency/expected service life of those treatments?

Pavement Friction Treatment	Average Frequency/Expected Service Life

Q2.3 How does your state determine the investigatory threshold for applying pavement treatments?

[Short answer]

Q2.4 Has your state conducted before-and-after analysis to quantify these treatments' effectiveness in crash reduction?

- Yes, _____

  _____

- No

Q2.5 Has your state conducted assessments to find out if treated roadway sections are under-performing or over-performing in terms of providing friction?

- Yes, _____

  _____

- No

Q2.6 Has your state established a policy or procedure to do decision making processes about selections of pavement friction treatments? If yes, describe how your policy or procedure works.

- Yes, _____

  _____

- No

Q2.7 Does your state have a computer program or decision-tree software to do cost-benefit analysis of pavement friction treatments? If yes, explain it briefly.

- Yes, _____

  _____

- No

Q2.8 Does your state have a computer program or decision-tree software to assist you with decisions on whether and which pavement treatment is recommended for certain roadways? If yes, explain it briefly.

- Yes, _____

  _____

- No

APPENDIX D: SAFETY ANALYSIS RESULTS

This appendix summarizes the estimated Safety Performance Function (SPF) models developed for roadway segments and intersections using Illinois LWST and SCRIM friction data. The tables report the estimated regression coefficients (coef), associated p-values, and corresponding Crash Modification Factors (CMFs) for different crash severity categories and roadway peer groups.

For roadway-level SPFs, the explanatory variables include roadway exposure, geometric characteristics, pavement friction, and cross-sectional features. Specifically, log_length represents the natural logarithm of segment length, log_AADT represents the natural logarithm of Annual Average Daily Traffic (AADT), and fric_q25mean denotes the average lower-quartile pavement friction measurement obtained from LWST data. The remaining variables describe roadway geometry and cross-sectional characteristics, including lane width (LN_WTH), median width (MED_WTH), pavement surface type (ASPHALT), access control indicator (ACC_CNTL_), inside shoulder width (I_SHD1_WTH), and outside shoulder widths (O_SHD1_WTH and O_SHD2_WTH).

For intersection-level SPFs developed using SCRIM friction data, the variables include major-road and minor-road traffic exposure (lnAADT_major, lnAADT_minor), average friction measurement (Q25_Avg_FN), and roadway geometric variables associated with both major and minor approaches. Variables prefixed with ma_ correspond to major-road characteristics, while variables prefixed with mi_ correspond to minor-road characteristics. These include median width (MED_WTH), lane width (LN_WTH), number of lanes (LNS), inside shoulder width (I_SHD_1), and outside shoulder width (O_SHD_1).

Blank cells indicate that a variable was not included in the final SPF specification for that specific peer group. During model development, variables with weak statistical significance, negligible contribution to model fit, multicollinearity concerns, or unstable coefficient estimates were excluded through an iterative model refinement process to improve interpretability and robustness of the final models.

ROADWAY PEER GROUPS WITH LWST FRICTION DATA

Roadway SPF Results for Fatal (K) Crashes

Peer group	Metric	log_length	log_AADT	fric_q25mean	LN_WTH	MED_WTH	ASPHALT	ACC_CNTL_	I_SHD1_WTH	O_SHD1_WTH	O_SHD2_WTH
State Rural Freeway, 4 Lanes	coef	0.7697	2.1133	0.0121		0.0040	-0.3258			-0.0563	-0.0171
	p-value	0.000	0.000	0.430		0.002	0.590			0.689	0.851
	CMF	--	1.223	1.128		1.004	0.722			0.945	0.983
State Rural Multilane Divided Highway	coef	1.1914	1.5098	-0.0489		-0.0292		0.5308		-0.2314	0.0522
	p-value	0.002	0.038	0.279		0.043		0.404		0.007	0.662
	CMF	--	1.155	0.613		0.971		1.700		0.793	1.054
State Rural Multiplane Undivided Highway	coef	1.0100	0.7538	0.0762			-1.7854			0.0105	
	p-value	0.401	0.593	0.539			0.342			0.962	
	CMF	--	1.074	2.142			--			1.011	
State Rural Two-Lane Highway	coef	1.4081	0.7486	-0.0089	0.0443	-0.1097	-0.7750	0.0199		-0.0032	-0.0288
	p-value	0.000	0.000	0.276	0.481	0.048	0.222	0.926		0.903	0.365
	CMF	--	1.074	0.915	1.045	0.896	0.461	1.020		0.997	0.972
State Urban Freeway, 4 Lanes	coef	0.4472	-0.0037	-0.0069	-0.2188	-0.0004		0.0570		-0.0411	0.0651
	p-value	0.005	0.992	0.689	0.672	0.833		0.959		0.672	0.614
	CMF	--	1.000	0.933	0.804	1.000		1.059		0.960	1.067
State Urban Freeway, 6 Lanes	coef	0.6400	-0.1231	-0.0001		-0.0017				-0.0596	-0.0723
	p-value	0.003	0.805	0.995		0.748				0.734	0.684
	CMF	--	0.988	0.999		0.998				0.942	0.930
State Urban Freeway, 8+ Lanes	coef	1.2054	2.7682	0.0018		0.0046	-1.4918				
	p-value	0.048	0.109	0.968		0.037	0.258				
	CMF	--	1.302	1.018		1.005	0.225				
State Urban Multilane Divided Highway	coef	1.0957	0.4631	-0.0055	-0.2447	-0.0044	0.3960	-0.0615	-0.0595	-0.0416	-0.0752
	p-value	0.000	0.044	0.724	0.267	0.687	0.592	0.847	0.366	0.268	0.481
	CMF	--	1.045	0.946	0.783	0.996	1.486	0.940	0.942	0.959	0.928
State Urban Multilane Undivided Highway	coef	1.2870	0.4146	-0.0097	0.0364	0.0551		-0.3545		-0.0418	0.2266
	p-value	0.000	0.134	0.598	0.735	0.033		0.564		0.398	0.001
	CMF	--	1.040	0.908	1.037	1.057		0.701		0.959	1.254
State Urban One-Way Arterial	coef	1.3481	0.0997	-0.0518	0.0987		-1.6250	0.2870			
	p-value	0.044	0.871	0.403	0.562		0.156	0.811			
	CMF	--	1.010	0.596	1.104		0.197	1.332			
State Urban Two-Lane Highway	coef	0.7346	0.1403	-0.0043	0.0250	-0.0599	0.5587	0.4276	0.5921	0.0468	0.0547
	p-value	0.000	0.342	0.738	0.703	0.082	0.578	0.088	0.014	0.153	0.208
	CMF	--	1.013	0.958	1.025	0.942	1.748	1.534	1.808	1.048	1.056

Roadway SPF Results for A-Injury Crashes

Peer group	Metric	log_length	log_AADT	fric_q25mean	LN_WTH	MED_WTH	ASPHALT	ACC_CNTL_	I_SHD1_WTH	O_SHD1_WTH	O_SHD2_WTH
State Rural Freeway, 4 Lanes	coef	0.9771	1.3157	-0.0024	0.0827	-0.0013	-0.2565			0.1454	-0.0258
	p-value	0.000	0.000	0.734	0.141	0.325	0.338			0.020	0.530
	CMF	--	1.134	0.977	1.086	0.999	0.774			1.157	0.975
State Rural Freeway, 6+ Lanes	coef	0.4571	2.3162	0.0243		-0.0133	-0.3594				0.0782
	p-value	0.239	0.245	0.435		0.649	0.876				0.611
	CMF	--	1.247	1.275		0.987	0.698				1.081
State Rural Multilane Divided Highway	coef	0.5994	0.6778	-0.0448		0.0002		0.4614		-0.0579	0.1149
	p-value	0.001	0.043	0.039		0.977		0.149		0.265	0.106
	CMF	--	1.067	0.639		1.000		1.586		0.944	1.122
State Rural Multiplane Undivided Highway	coef	1.1625	1.2193	0.2246						0.0316	
	p-value	0.183	0.287	0.061						0.852	
	CMF	--	1.123	9.446						1.032	
State Rural Two-Lane Highway	coef	1.3317	0.9171	-0.0026	-0.0937	0.0181	-0.1982	-0.1157		-0.0373	-0.0581
	p-value	0.000	0.000	0.545	0.004	0.034	0.602	0.327		0.009	0.001
	CMF	--	1.091	0.974	0.911	1.018	0.820	0.891		0.963	0.944
State Urban Freeway, 4 Lanes	coef	0.4026	0.5924	-0.0119	0.1420	0.0007		-0.5539		-0.0396	-0.0413
	p-value	0.000	0.000	0.092	0.359	0.160		0.166		0.283	0.460
	CMF	--	1.058	0.888	1.153	1.001		0.575		0.961	0.960
State Urban Freeway, 6 Lanes	coef	0.5433	0.2057	-0.0104		-0.0015				0.0286	-0.1247
	p-value	0.000	0.260	0.127		0.368				0.608	0.081
	CMF	--	1.020	0.901		0.999				1.029	0.883
State Urban Freeway, 8+ Lanes	coef	1.1987	0.6171	-0.0003		0.0009	-0.8586				-8.866e-05
	p-value	0.000	0.296	0.986		0.311	0.105				1.000
	CMF	--	1.061	0.997		1.001	0.424				1.000
State Urban Multilane Divided Highway	coef	0.8746	0.6399	-0.0077	-0.0551	0.0005	-0.0767	-0.0550	0.0279	-0.0850	-0.1849
	p-value	0.000	0.000	0.257	0.521	0.610	0.764	0.702	0.258	0.000	0.001
	CMF	--	1.063	0.926	0.946	1.001	0.926	0.947	1.028	0.919	0.831
State Urban Multilane Undivided Highway	coef	0.7769	0.6282	-0.0059	-0.0033	-0.0184	-0.4221	-0.0430	0.0146	-0.0353	0.1324
	p-value	0.000	0.000	0.449	0.953	0.330	0.316	0.888	0.873	0.137	0.001
	CMF	--	1.062	0.943	0.997	0.982	0.656	0.958	1.015	0.965	1.142
State Urban One-Way Arterial	coef	1.0000	0.4798	-0.0262	-0.0854		-0.6302	-0.4648		0.0478	
	p-value	0.003	0.135	0.309	0.185		0.426	0.562		0.519	
	CMF	--	1.047	0.770	0.918		0.532	0.628		1.049	
State Urban Two-Lane Highway	coef	0.6557	0.4480	-0.0110	0.0127	-0.0133	0.1823	0.1721	0.1852	-0.0047	0.0008
	p-value	0.000	0.000	0.077	0.688	0.298	0.601	0.197	0.158	0.757	0.969
	CMF	--	1.044	0.896	1.013	0.987	1.200	1.188	1.203	0.995	1.001

Roadway SPF Results for B-Injury Crashes

Peer group	Metric	log_length	log_AADT	fric_q25mean	LN_WTH	MED_WTH	ASPHALT	ACC_CNTL_	I_SHD1_WTH	O_SHD1_WTH	O_SHD2_WTH
State Rural Freeway, 4 Lanes	coef	0.9354	0.8968	-0.0013	-0.0627	-0.0016	-0.1351			0.0831	-0.0162
	p-value	0.000	0.000	0.795	0.444	0.113	0.500			0.069	0.596
	CMF	--	1.089	0.987	0.939	0.998	0.874			1.087	0.984
State Rural Freeway, 6+ Lanes	coef	0.9766	-0.8364	-0.0394		-0.0015	5.6531				-0.2996
	p-value	0.034	0.666	0.096		0.801	0.799				0.306
	CMF	--	0.923	0.674		0.998	285.188				0.741
State Rural Multilane Divided Highway	coef	0.9199	1.1529	0.0053		-0.0044		-0.2028		-0.0389	0.0283
	p-value	0.000	0.000	0.762		0.503		0.440		0.381	0.641
	CMF	--	1.116	1.054		0.996		0.816		0.962	1.029
State Rural Multiplane Undivided Highway	coef	1.3701	2.1030	-0.0666			-3.3555			0.0704	
	p-value	0.115	0.205	0.506			0.091			0.665	
	CMF	--	1.222	0.514			--			1.073	
State Rural Two-Lane Highway	coef	0.8771	0.9801	-0.0016	-0.0389	0.0028	-0.5626	-0.2430		-0.0262	-0.0676
	p-value	0.000	0.000	0.616	0.112	0.680	0.011	0.006		0.009	0.000
	CMF	--	1.098	0.985	0.962	1.003	0.570	0.784		0.974	0.935
State Urban Freeway, 4 Lanes	coef	0.8043	0.9549	-0.0005	0.0129	0.0004		-0.8091		-0.0808	-0.0596
	p-value	0.000	0.000	0.903	0.918	0.183		0.003		0.001	0.096
	CMF	--	1.095	0.995	1.013	1.000		0.445		0.922	0.942
State Urban Freeway, 6 Lanes	coef	0.8099	1.4204	-0.0034		-2.077e-05				-0.0316	-0.2194
	p-value	0.000	0.000	0.485		0.973				0.443	0.000
	CMF	--	1.145	0.967		1.000				0.969	0.803
State Urban Freeway, 8+ Lanes	coef	1.2007	2.1898	-0.0223		0.0024	0.3987				-0.4809
	p-value	0.000	0.000	0.036		0.000	0.214				0.210
	CMF	--	1.232	0.800		1.002	1.490				0.618
State Urban Multilane Divided Highway	coef	0.8298	0.9047	-0.0044	-0.1815	0.0013	-0.1768	0.0077	0.0148	-0.0927	-0.1238
	p-value	0.000	0.000	0.277	0.001	0.006	0.242	0.932	0.316	0.000	0.000
	CMF	--	1.090	0.957	0.834	1.001	0.838	1.008	1.015	0.911	0.884
State Urban Multilane Undivided Highway	coef	0.7392	0.9518	-0.0118	-0.1067	0.0092	0.0935	-0.1197	-0.1203	-0.0746	0.0711
	p-value	0.000	0.000	0.008	0.004	0.331	0.726	0.521	0.228	0.000	0.013
	CMF	--	1.095	0.889	0.899	1.009	1.098	0.887	0.887	0.928	1.074
State Urban One-Way Arterial	coef	0.8081	0.6063	-0.0008	-0.0886		0.4482	-0.0013		-0.0830	
	p-value	0.000	0.003	0.956	0.043		0.548	0.998		0.166	
	CMF	--	1.059	0.992	0.915		1.565	0.999		0.920	
State Urban Two-Lane Highway	coef	0.7065	0.7108	-0.0059	-0.0131	-0.0133	0.0761	-0.1747	0.1654	-0.0244	-0.0639
	p-value	0.000	0.000	0.112	0.518	0.083	0.689	0.059	0.062	0.007	0.000
	CMF	--	1.070	0.943	0.987	0.987	1.079	0.840	1.180	0.976	0.938

Roadway SPF Results for C-Injury Crashes

Peer group	Metric	log_length	log_AADT	fric_q25mean	LN_WTH	MED_WTH	ASPHALT	ACC_CNTL_	I_SHD1_WTH	O_SHD1_WTH	O_SHD2_WTH
State Rural Freeway, 4 Lanes	coef	0.9735	0.7886	-0.0017	-0.3995	-0.0007	-0.2578			-0.0217	-0.0440
	p-value	0.000	0.001	0.861	0.419	0.668	0.450			0.803	0.450
	CMF	--	1.078	0.983	0.671	0.999	0.773			0.979	0.957
State Rural Freeway, 6+ Lanes	coef	0.7513	1.8339	0.0371		-0.0064					-0.1913
	p-value	0.185	0.455	0.611		0.784					0.624
	CMF	--	1.191	1.449		0.994					0.826
State Rural Two-Lane Highway	coef	0.9078	1.0554	-0.0055	-0.0895	-0.0098	-0.6650	-0.0912		-0.0468	-0.0620
	p-value	0.000	0.000	0.291	0.027	0.499	0.075	0.523		0.006	0.002
	CMF	--	1.106	0.946	0.914	0.990	0.514	0.913		0.954	0.940
State Urban Freeway, 4 Lanes	coef	0.8486	0.9853	-0.0062	-0.0520	0.0004		-1.2931		-0.1292	-0.0704
	p-value	0.000	0.000	0.404	0.777	0.426		0.001		0.001	0.224
	CMF	--	1.098	0.940	0.949	1.000		0.274		0.879	0.932
State Urban Freeway, 6 Lanes	coef	0.8608	1.3403	-0.0179		0.0004				-0.0464	-0.1661
	p-value	0.000	0.000	0.012		0.608				0.462	0.040
	CMF	--	1.136	0.836		1.000				0.955	0.847
State Urban Freeway, 8+ Lanes	coef	1.4558	0.9097	-0.0056		0.0013	0.0935				-0.7558
	p-value	0.000	0.088	0.762		0.080	0.861				0.244
	CMF	--	1.091	0.946		1.001	1.098				0.470
State Urban Multilane Divided Highway	coef	0.7020	1.3836	-0.0189	-0.2220	0.0003	-0.1813	-0.0486	-0.0067	-0.0776	-0.1329
	p-value	0.000	0.000	0.000	0.000	0.706	0.231	0.604	0.673	0.000	0.000
	CMF	--	1.141	0.828	0.801	1.000	0.834	0.953	0.993	0.925	0.876
State Urban Multilane Undivided Highway	coef	0.7676	1.3595	-0.0206	-0.0622	0.0026	0.8671	-0.3713	0.0689	-0.0774	-0.0042
	p-value	0.000	0.000	0.000	0.092	0.800	0.021	0.062	0.217	0.000	0.902
	CMF	--	1.138	0.814	0.940	1.003	2.380	0.690	1.071	0.925	0.996
State Urban One-Way Arterial	coef	0.4832	0.8754	0.0072	-0.1210		0.7083	-1.2658		-0.0380	
	p-value	0.049	0.000	0.657	0.019		0.493	0.224		0.534	
	CMF	--	1.087	1.075	0.886		2.031	0.282		0.963	
State Urban Two-Lane Highway	coef	0.5014	1.2258	-0.0134	-0.0991	0.0034	0.4605	-0.0834	-0.1623	-0.0310	-0.0341
	p-value	0.000	0.000	0.002	0.000	0.673	0.049	0.431	0.327	0.002	0.035
	CMF	--	1.124	0.875	0.906	1.003	1.585	0.920	0.850	0.969	0.966

Roadway SPF Results for Non-Injury/PDO Crashes

Peer group	Metric	log_length	log_AADT	fric_q25mean	LN_WTH	MED_WTH	ASPHALT	ACC_CNTL_	I_SHD1_WTH	O_SHD1_WTH	O_SHD2_WTH
State Rural Freeway, 4 Lanes	coef	0.9857	0.7114	-3.59e-05		-0.0010	0.1861			0.0336	0.0097
	p-value	0.000	0.000	0.987		0.007	0.042			0.078	0.458
	CMF	--	1.070	1.000		0.999	1.205			1.034	1.010
State Rural Freeway, 6+ Lanes	coef	0.9698	0.0152	-0.0090		-0.0020	0.2540				-0.0474
	p-value	0.000	0.977	0.275		0.389	0.693				0.349
	CMF	--	1.001	0.914		0.998	1.289				0.954
State Rural Multilane Divided Highway	coef	1.0787	0.5078	0.0041		7.143e-05		0.0508		-0.0356	-0.0272
	p-value	0.000	0.000	0.497		0.975		0.597		0.028	0.237
	CMF	--	1.050	1.042		1.000		1.052		0.965	0.973
State Rural Multiplane Undivided Highway	coef	0.9318	1.2777	0.0832			-0.4132			0.1611	
	p-value	0.001	0.008	0.047			0.627			0.005	
	CMF	--	1.130	2.298			--			1.175	
State Rural Two-Lane Highway	coef	0.9811	0.6645	-0.0125	-0.0052	-0.0026	-0.1184	-0.2449		-0.0343	-0.0672
	p-value	0.000	0.000	0.000	0.582	0.444	0.325	0.000		0.000	0.000
	CMF	--	1.065	0.883	0.995	0.997	0.888	0.783		0.966	0.935
State Urban Freeway, 4 Lanes	coef	0.8350	1.0567	-0.0012	0.0699	0.0003		-0.2548		-0.0355	-0.0368
	p-value	0.000	0.000	0.558	0.298	0.178		0.105		0.001	0.036
	CMF	--	1.106	0.988	1.072	1.000		0.775		0.965	0.964
State Urban Freeway, 6 Lanes	coef	0.8841	1.5750	-0.0004		-0.0005				0.0239	-0.1207
	p-value	0.000	0.000	0.894		0.188				0.303	0.000
	CMF	--	1.162	0.996		1.000				1.024	0.886
State Urban Freeway, 8+ Lanes	coef	1.1655	1.9285	-0.0050		0.0022	-0.0110				-0.1712
	p-value	0.000	0.000	0.582		0.000	0.965				0.539
	CMF	--	1.202	0.951		1.002	0.989				0.843
State Urban Multilane Divided Highway	coef	0.7695	0.9401	-0.0058	-0.2106	0.0002	-0.2429	-0.0447	-0.0297	-0.0737	-0.1151
	p-value	0.000	0.000	0.002	0.000	0.462	0.001	0.293	0.000	0.000	0.000
	CMF	--	1.094	0.943	0.810	1.000	0.784	0.956	0.971	0.929	0.891
State Urban Multilane Undivided Highway	coef	0.7131	1.0540	-0.0055	-0.0973	-0.0065	0.2856	-0.1706	0.0307	-0.0447	0.0023
	p-value	0.000	0.000	0.010	0.000	0.203	0.057	0.062	0.308	0.000	0.885
	CMF	--	1.106	0.946	0.907	0.994	1.331	0.843	1.031	0.956	1.002
State Urban One-Way Arterial	coef	0.6921	0.7539	0.0074	-0.0251		0.1966	-0.2593		-0.0711	
	p-value	0.000	0.000	0.257	0.213		0.507	0.254		0.005	
	CMF	--	1.074	1.077	0.975		1.217	0.772		0.931	
State Urban Two-Lane Highway	coef	0.6527	0.8437	-0.0051	-0.0164	-0.0087	0.0809	-0.0261	0.0210	-0.0577	-0.0482
	p-value	0.000	0.000	0.002	0.055	0.010	0.348	0.517	0.674	0.000	0.000
	CMF	--	1.084	0.951	0.984	0.991	1.084	0.974	1.021	0.944	0.953

Roadway SPF Results for Severe (K+A) Crashes

Peer group	Metric	log_length	log_AADT	fric_q25mean	LN_WTH	MED_WTH	ASPHALT	ACC_CNTL_	I_SHD1_WTH	O_SHD1_WTH	O_SHD2_WTH
State Rural Freeway, 4 Lanes	coef	0.9489	1.4155	-0.0002	0.0673	0.0001	-0.2505			0.1150	-0.0290
	p-value	0.000	0.000	0.975	0.236	0.887	0.307			0.047	0.443
	CMF	--	1.144	0.998	1.070	1.000	0.778			1.122	0.971
State Rural Freeway, 6+ Lanes	coef	0.5746	2.8255	0.0281		-0.0166					0.1017
	p-value	0.115	0.155	0.284		0.553					0.188
	CMF	--	1.309	1.324		0.984					1.107
State Rural Multilane Divided Highway	coef	0.6945	0.8200	-0.0476		-0.0062		0.4679		-0.1031	0.0951
	p-value	0.000	0.009	0.020		0.342		0.113		0.024	0.135
	CMF	--	1.081	0.621		0.994		1.597		0.902	1.100
State Rural Multiplane Undivided Highway	coef	0.8903	1.6542	0.1680			-2.3245			0.0518	
	p-value	0.249	0.239	0.057			0.173			0.726	
	CMF	--	1.171	5.368			--			1.053	
State Rural Two-Lane Highway	coef	0.9495	0.8387	-0.0045	-0.0676	0.0101	-0.2883	-0.1080		-0.0329	-0.0490
	p-value	0.000	0.000	0.232	0.019	0.182	0.360	0.299		0.008	0.001
	CMF	--	1.083	0.956	0.935	1.010	0.750	0.898		0.968	0.952
State Urban Freeway, 4 Lanes	coef	0.4107	0.5096	-0.0112	0.1014	0.0006		-0.4807		-0.0405	-0.0263
	p-value	0.000	0.000	0.090	0.508	0.198		0.205		0.246	0.612
	CMF	--	1.050	0.894	1.107	1.001		0.618		0.960	0.974
State Urban Freeway, 6 Lanes	coef	0.5327	0.1879	-0.0095	0.4247	-0.0014				0.0120	-0.1219
	p-value	0.000	0.272	0.145	0.226	0.354				0.823	0.060
	CMF	--	1.018	0.910	1.529	0.999				1.012	0.885
State Urban Freeway, 8+ Lanes	coef	1.2027	0.8339	-0.0023		0.0014	-0.9412				0.0041
	p-value	0.000	0.135	0.894		0.066	0.058				0.994
	CMF	--	1.083	0.978		1.001	0.390				1.004
State Urban Multilane Divided Highway	coef	0.9082	0.6102	-0.0073	-0.0793	0.0004	-0.0184	-0.0624	0.0136	-0.0784	-0.1647
	p-value	0.000	0.000	0.246	0.324	0.743	0.940	0.637	0.556	0.000	0.001
	CMF	--	1.060	0.930	0.924	1.000	0.982	0.940	1.014	0.925	0.848
State Urban Multilane Undivided Highway	coef	0.8527	0.5964	-0.0062	0.0027	0.0003	-0.1329	-0.0778	-0.0198	-0.0364	0.1534
	p-value	0.000	0.000	0.387	0.958	0.984	0.746	0.777	0.826	0.087	0.000
	CMF	--	1.058	0.940	1.003	1.000	0.876	0.925	0.980	0.964	1.166
State Urban One-Way Arterial	coef	1.1132	0.3829	-0.0287	-0.0642		-0.7976	-0.0330		0.0074	-0.1226
	p-value	0.000	0.173	0.225	0.260		0.204	0.963		0.917	0.532
	CMF	--	1.037	0.751	0.938		0.450	0.968		1.007	0.885
State Urban Two-Lane Highway	coef	0.6714	0.3915	-0.0095	0.0139	-0.0203	0.2128	0.2235	0.2709	0.0038	0.0106
	p-value	0.000	0.000	0.091	0.627	0.092	0.520	0.061	0.015	0.785	0.590
	CMF	--	1.038	0.909	1.014	0.980	1.237	1.250	1.311	1.004	1.011

Roadway SPF Results for Severe (K+A) Crashes

Peer group	Metric	log_length	log_AADT	fric_q25mean	LN_WTH	MED_WTH	ASPHALT	ACC_CNTL_	I_SHD1_WTH	O_SHD1_WTH	O_SHD2_WTH
State Rural Freeway, 4 Lanes	coef	0.9858	0.7624	0.0001	-0.0207	-0.0010	0.1068			0.0435	0.0035
	p-value	0.000	0.000	0.959	0.395	0.004	0.201			0.014	0.773
	CMF	--	1.075	1.001	0.980	0.999	1.113			1.045	1.004
State Rural Freeway, 6+ Lanes	coef	0.9602	0.1866	-0.0063		-0.0014					-0.0497
	p-value	0.000	0.706	0.422		0.516					0.153
	CMF	--	1.018	0.939		0.999					0.951
State Rural Multilane Divided Highway	coef	1.0216	0.5958	0.0011		-0.0017		0.0511		-0.0463	-0.0131
	p-value	0.000	0.000	0.839		0.402		0.560		0.002	0.528
	CMF	--	1.058	1.011		0.998		1.052		0.955	0.987
State Rural Two-Lane Highway	coef	0.9669	0.7743	-0.0090	-0.0172	-0.0006	-0.2792	-0.3629		-0.0242	-0.0591
	p-value	0.000	0.000	0.000	0.048	0.834	0.008	0.000		0.000	0.000
	CMF	--	1.077	0.914	0.983	0.999	0.756	0.696		0.976	0.943
State Urban Freeway, 4 Lanes	coef	0.8182	1.0208	-0.0020	0.0653	0.0003		-0.3849		-0.0435	-0.0418
	p-value	0.000	0.000	0.299	0.302	0.107		0.009		0.000	0.013
	CMF	--	1.102	0.980	1.068	1.000		0.681		0.957	0.959
State Urban Freeway, 6 Lanes	coef	0.8857	1.5224	-0.0015		-0.0004				0.0217	-0.1284
	p-value	0.000	0.000	0.606		0.259				0.331	0.000
	CMF	--	1.156	0.985		1.000				1.022	0.880
State Urban Freeway, 8+ Lanes	coef	1.1659	1.8888	-0.0071		0.0022	0.0284				-0.2097
	p-value	0.000	0.000	0.427		0.000	0.908				0.453
	CMF	--	1.197	0.931		1.002	1.029				0.811
State Urban Multilane Divided Highway	coef	0.7677	0.9469	-0.0066	-0.1976	0.0004	-0.2211	-0.0359	-0.0218	-0.0766	-0.1200
	p-value	0.000	0.000	0.000	0.000	0.141	0.002	0.361	0.001	0.000	0.000
	CMF	--	1.094	0.936	0.821	1.000	0.802	0.965	0.978	0.926	0.887
State Urban Multilane Undivided Highway	coef	0.7288	1.0456	-0.0072	-0.0932	-0.0046	0.2509	-0.1742	0.0183	-0.0483	0.0124
	p-value	0.000	0.000	0.000	0.000	0.313	0.066	0.034	0.500	0.000	0.369
	CMF	--	1.105	0.930	0.911	0.995	1.285	0.840	1.018	0.953	1.012
State Urban One-Way Arterial	coef	0.7187	0.7404	0.0056	-0.0374		0.1885	-0.2667		-0.0629	-0.0023
	p-value	0.000	0.000	0.345	0.039		0.475	0.244		0.006	0.966
	CMF	--	1.073	1.058	0.963		1.207	0.766		0.939	0.998
State Urban Two-Lane Highway	coef	0.6544	0.8377	-0.0056	-0.0208	-0.0087	0.1177	-0.0331	0.0513	-0.0496	-0.0471
	p-value	0.000	0.000	0.000	0.007	0.004	0.135	0.360	0.217	0.000	0.000
	CMF	--	1.083	0.946	0.979	0.991	1.125	0.967	1.053	0.952	0.954

INTERSECTION PEER GROUPS WITH SCRIM DATA

Intersection SPF Results for A-Injury Crashes

Peer group	Metric	lnAADT_major	lnAADT_minor	Q25_Avg_FN	ma_MED_WTH	ma_LN_WTH	ma_LNS	ma_I_SHD_1	ma_O_SHD_1	mi_MED_WTH	mi_LN_WTH	mi_O_SHD_1
Rural Minor Leg Stop Control	coef	-0.7417	0.3662	-0.0719	-0.2008	-0.1233	0.1923	0.4395	-0.1359	0.0748	0.5636	-0.0133
	p-value	0.000	0.188	0.005	0.663	0.290	0.720	0.309	0.627	0.290	0.009	0.952
	CMF	0.9317	1.0355	0.4870	0.8180	0.8840	--	1.5519	0.8729	1.0777	1.7569	0.9868
Urban Multilane Minor Leg Stop Control	coef	-0.7417	0.3662	-0.0719	-0.2008	-0.1233	0.1923	0.4395	-0.1359	0.0748	0.5636	-0.0133
	p-value	0.000	0.188	0.005	0.663	0.290	0.720	0.309	0.627	0.290	0.009	0.952
	CMF	0.9317	1.0355	0.4870	0.8180	0.8840	--	1.5519	0.8729	1.0777	1.7569	0.9868
Urban Signalized Intersection	coef	-0.7417	0.3662	-0.0719	-0.2008	-0.1233	0.1923	0.4395	-0.1359	0.0748	0.5636	-0.0133
	p-value	0.000	0.188	0.005	0.663	0.290	0.720	0.309	0.627	0.290	0.009	0.952
	CMF	0.9317	1.0355	0.4870	0.8180	0.8840	--	1.5519	0.8729	1.0777	1.7569	0.9868
Urban Two Lane Minor Leg Stop Control	coef	-0.7417	0.3662	-0.0719	-0.2008	-0.1233	0.1923	0.4395	-0.1359	0.0748	0.5636	-0.0133
	p-value	0.000	0.188	0.005	0.663	0.290	0.720	0.309	0.627	0.290	0.009	0.952
	CMF	0.9317	1.0355	0.4870	0.8180	0.8840	--	1.5519	0.8729	1.0777	1.7569	0.9868

Intersection SPF Results for B-Injury Crashes

Peer group	Metric	lnAADT_major	lnAADT_minor	Q25_Avg_FN	ma_MED_WTH	ma_LN_WTH	ma_LNS	ma_I_SHD_1	ma_O_SHD_1	mi_MED_WTH	mi_LN_WTH	mi_O_SHD_1
Rural Minor Leg Stop Control	coef	0.5057	0.6625	-0.0424	-0.4697	-0.1379	0.5678	0.0965	0.2710	0.1628	0.1110	-0.0038
	p-value	0.160	0.004	0.045	0.204	0.406	0.060	0.734	0.126	0.003	0.593	0.983
	CMF	1.0494	1.0652	0.6544	0.6252	0.8712	--	1.1013	1.3112	1.1768	1.1174	0.9962
Urban Multilane Minor Leg Stop Control	coef	0.5057	0.6625	-0.0424	-0.4697	-0.1379	0.5678	0.0965	0.2710	0.1628	0.1110	-0.0038
	p-value	0.160	0.004	0.045	0.204	0.406	0.060	0.734	0.126	0.003	0.593	0.983
	CMF	1.0494	1.0652	0.6544	0.6252	0.8712	--	1.1013	1.3112	1.1768	1.1174	0.9962
Urban Signalized Intersection	coef	0.5057	0.6625	-0.0424	-0.4697	-0.1379	0.5678	0.0965	0.2710	0.1628	0.1110	-0.0038
	p-value	0.160	0.004	0.045	0.204	0.406	0.060	0.734	0.126	0.003	0.593	0.983
	CMF	1.0494	1.0652	0.6544	0.6252	0.8712	--	1.1013	1.3112	1.1768	1.1174	0.9962
Urban Two Lane Minor Leg Stop Control	coef	0.5057	0.6625	-0.0424	-0.4697	-0.1379	0.5678	0.0965	0.2710	0.1628	0.1110	-0.0038
	p-value	0.160	0.004	0.045	0.204	0.406	0.060	0.734	0.126	0.003	0.593	0.983
	CMF	1.0494	1.0652	0.6544	0.6252	0.8712	--	1.1013	1.3112	1.1768	1.1174	0.9962

Intersection SPF Results for C-Injury Crashes

Peer group	Metric	lnAADT_major	lnAADT_minor	Q25_Avg_FN	ma_MED_WTH	ma_LN_WTH	ma_LNS	ma_I_SHD_1	ma_O_SHD_1	mi_MED_WTH	mi_LN_WTH	mi_O_SHD_1
Rural Minor Leg Stop Control	coef	0.1107	0.5449	-0.0349	-0.0099	0.1898	0.1938	-0.0634	0.1336	-0.0272	0.1432	-0.0450
	p-value	0.743	0.032	0.105	0.984	0.305	0.607	0.888	0.505	0.875	0.516	0.824
	CMF	1.0106	1.0533	0.7052	0.9902	1.2090	--	0.9386	1.1429	0.9732	1.1540	0.9560
Urban Multilane Minor Leg Stop Control	coef	0.1107	0.5449	-0.0349	-0.0099	0.1898	0.1938	-0.0634	0.1336	-0.0272	0.1432	-0.0450
	p-value	0.743	0.032	0.105	0.984	0.305	0.607	0.888	0.505	0.875	0.516	0.824
	CMF	1.0106	1.0533	0.7052	0.9902	1.2090	--	0.9386	1.1429	0.9732	1.1540	0.9560
Urban Signalized Intersection	coef	0.1107	0.5449	-0.0349	-0.0099	0.1898	0.1938	-0.0634	0.1336	-0.0272	0.1432	-0.0450
	p-value	0.743	0.032	0.105	0.984	0.305	0.607	0.888	0.505	0.875	0.516	0.824
	CMF	1.0106	1.0533	0.7052	0.9902	1.2090	--	0.9386	1.1429	0.9732	1.1540	0.9560
Urban Two Lane Minor Leg Stop Control	coef	0.1107	0.5449	-0.0349	-0.0099	0.1898	0.1938	-0.0634	0.1336	-0.0272	0.1432	-0.0450
	p-value	0.743	0.032	0.105	0.984	0.305	0.607	0.888	0.505	0.875	0.516	0.824
	CMF	1.0106	1.0533	0.7052	0.9902	1.2090	--	0.9386	1.1429	0.9732	1.1540	0.9560

Intersection SPF Results for No-Injury/PDO Crashes

Peer group	Metric	lnAADT_major	lnAADT_minor	Q25_Avg_FN	ma_MED_WTH	ma_LN_WTH	ma_LNS	ma_I_SHD_1	ma_O_SHD_1	mi_MED_WTH	mi_LN_WTH	mi_O_SHD_1
Rural Minor Leg Stop Control	coef	0.6135	0.4664	-0.0179	0.1875	-0.0798	-0.0533	-0.1383	0.1257	-0.0515	0.1715	-0.1024
	p-value	0.000	0.000	0.023	0.317	0.279	0.763	0.469	0.094	0.487	0.030	0.183
	CMF	1.0602	1.0455	0.8360	1.2062	0.9233	--	0.8708	1.1340	0.9498	1.1871	0.9026
Urban Multilane Minor Leg Stop Control	coef	0.6135	0.4664	-0.0179	0.1875	-0.0798	-0.0533	-0.1383	0.1257	-0.0515	0.1715	-0.1024
	p-value	0.000	0.000	0.023	0.317	0.279	0.763	0.469	0.094	0.487	0.030	0.183
	CMF	1.0602	1.0455	0.8360	1.2062	0.9233	--	0.8708	1.1340	0.9498	1.1871	0.9026
Urban Signalized Intersection	coef	0.6135	0.4664	-0.0179	0.1875	-0.0798	-0.0533	-0.1383	0.1257	-0.0515	0.1715	-0.1024
	p-value	0.000	0.000	0.023	0.317	0.279	0.763	0.469	0.094	0.487	0.030	0.183
	CMF	1.0602	1.0455	0.8360	1.2062	0.9233	--	0.8708	1.1340	0.9498	1.1871	0.9026
Urban Two Lane Minor Leg Stop Control	coef	0.6135	0.4664	-0.0179	0.1875	-0.0798	-0.0533	-0.1383	0.1257	-0.0515	0.1715	-0.1024
	p-value	0.000	0.000	0.023	0.317	0.279	0.763	0.469	0.094	0.487	0.030	0.183
	CMF	1.0602	1.0455	0.8360	1.2062	0.9233	--	0.8708	1.1340	0.9498	1.1871	0.9026

APPENDIX E: OPTIMAL POLICIES FOR TREATMENT SELECTIONS

ROADWAY PEER GROUPS WITH LWST FRICTION DATA

This appendix summarizes the optimal policies for treatment selections. Each peer-group panel below shows the policy regions for all available AADT levels previously treated by HMA overlay. Each subpanel uses Friction on the x-axis and CRS on the y-axis; hatching indicates the optimal action according to the shared legend.

State Rural Freeway, 6+ Lanes

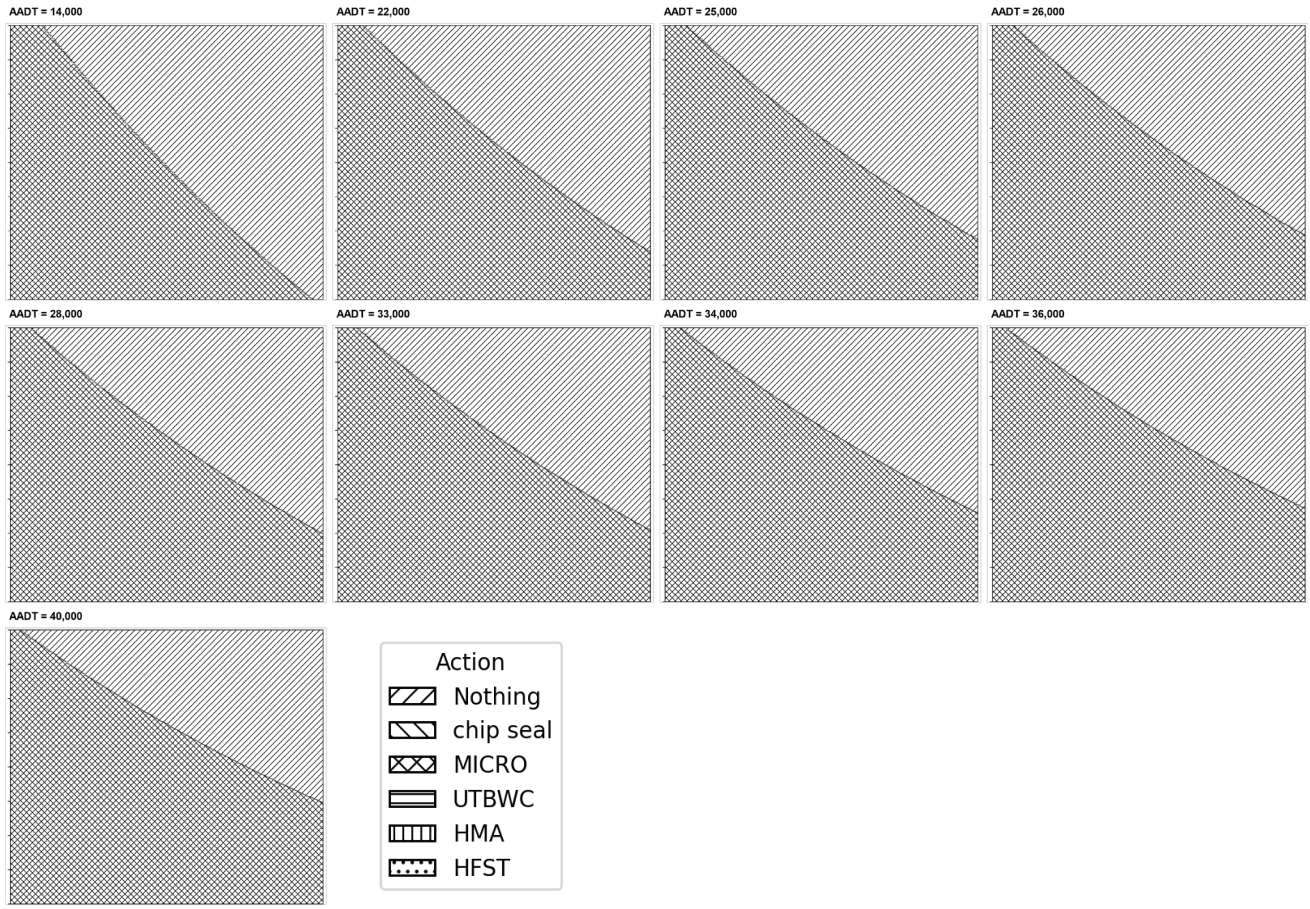

State Rural Two-Lane Highway, 6+ Lanes

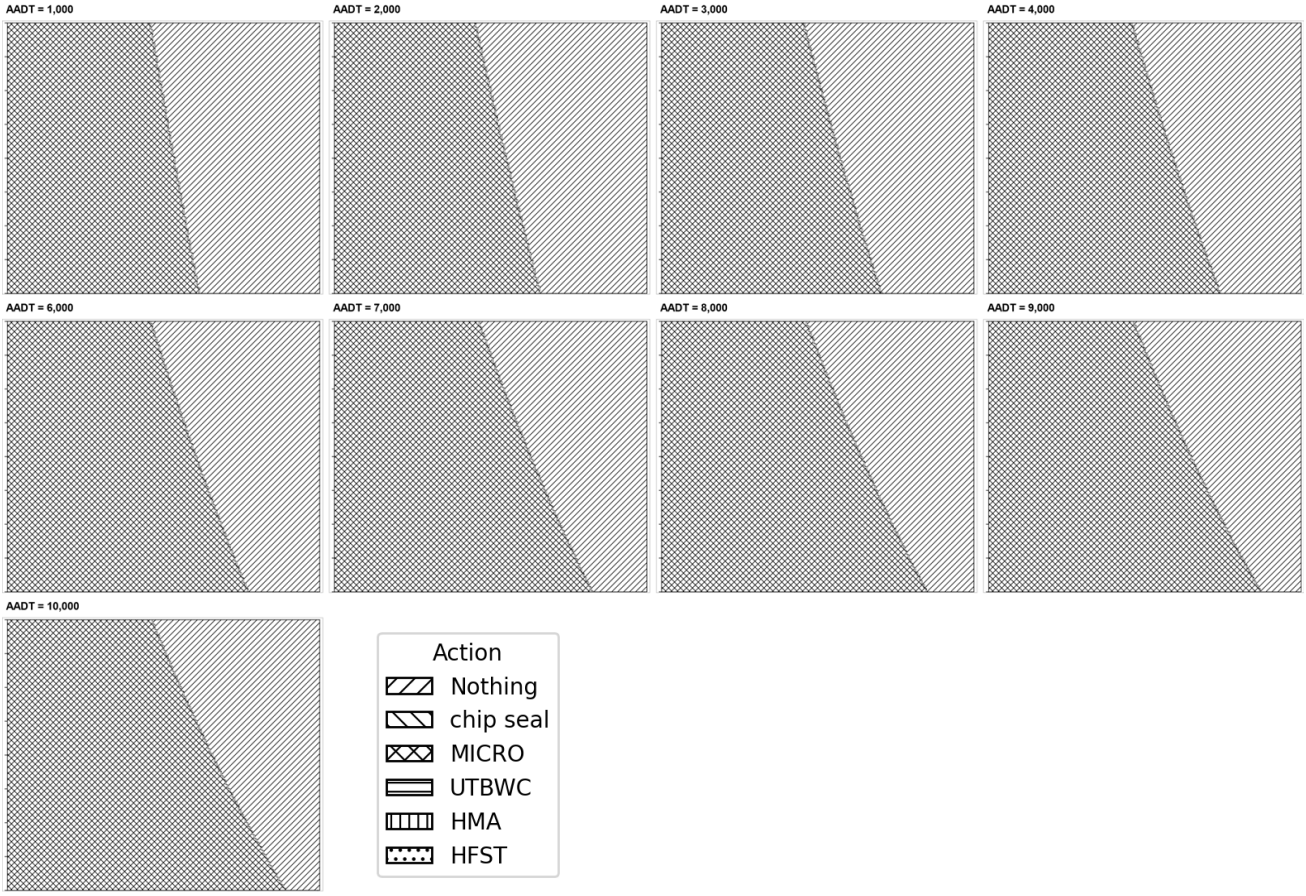

State Urban Freeway, 8+ Lanes

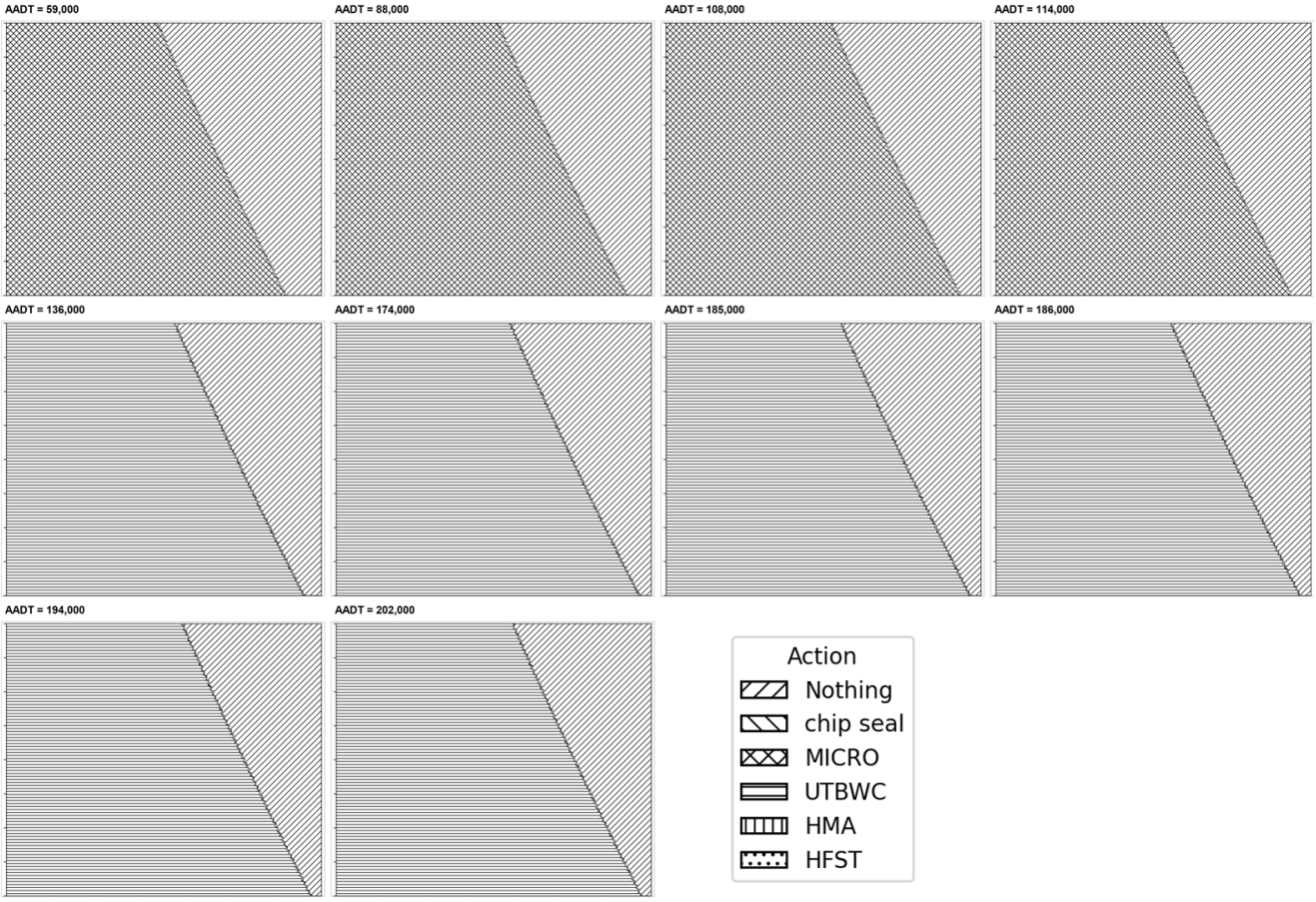

State Urban Multilane Divided Highway

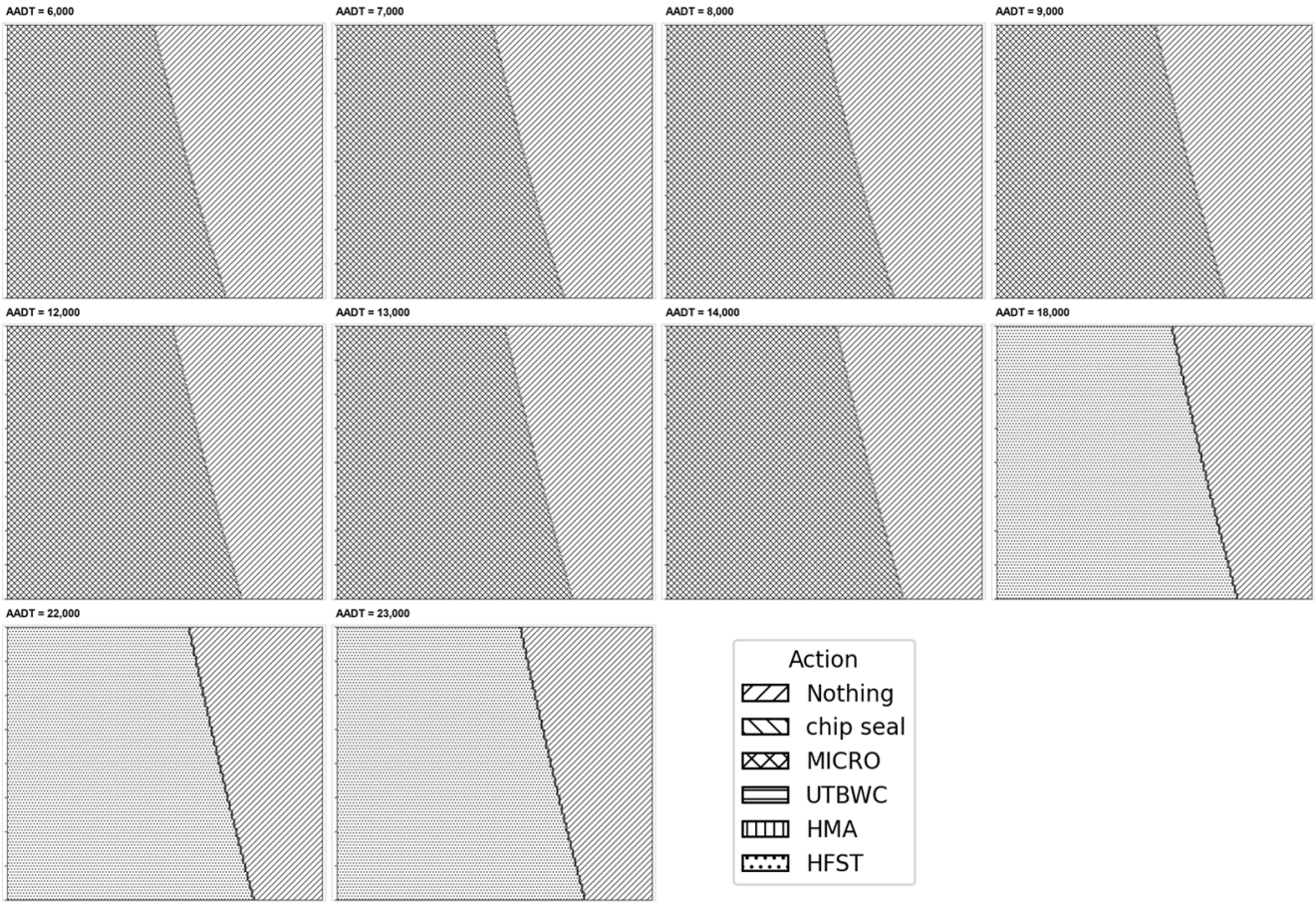

State Urban Multilane Undivided Highway

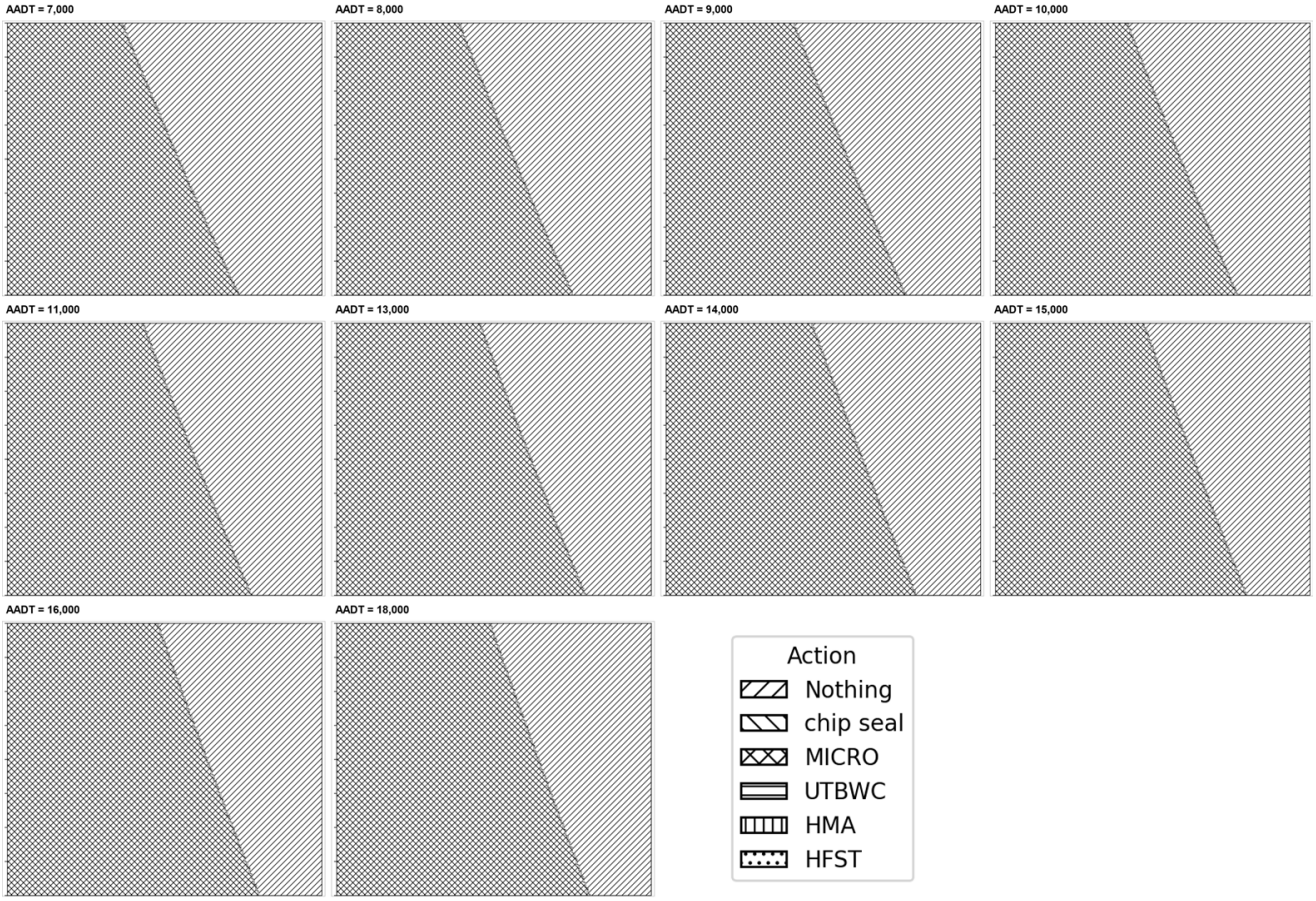

State Urban Two-Lane Highway

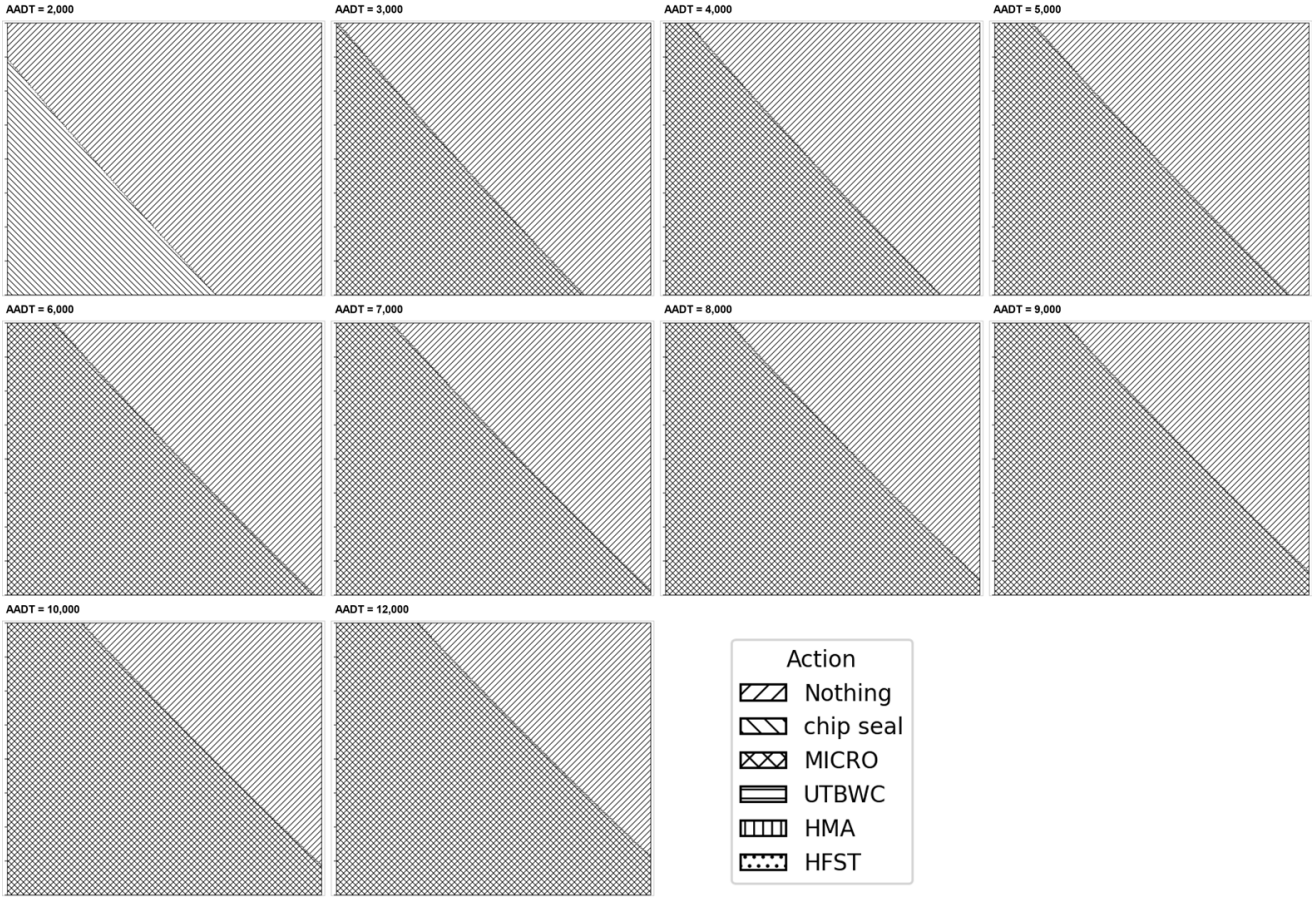

APPENDIX F: GRADATION FIT

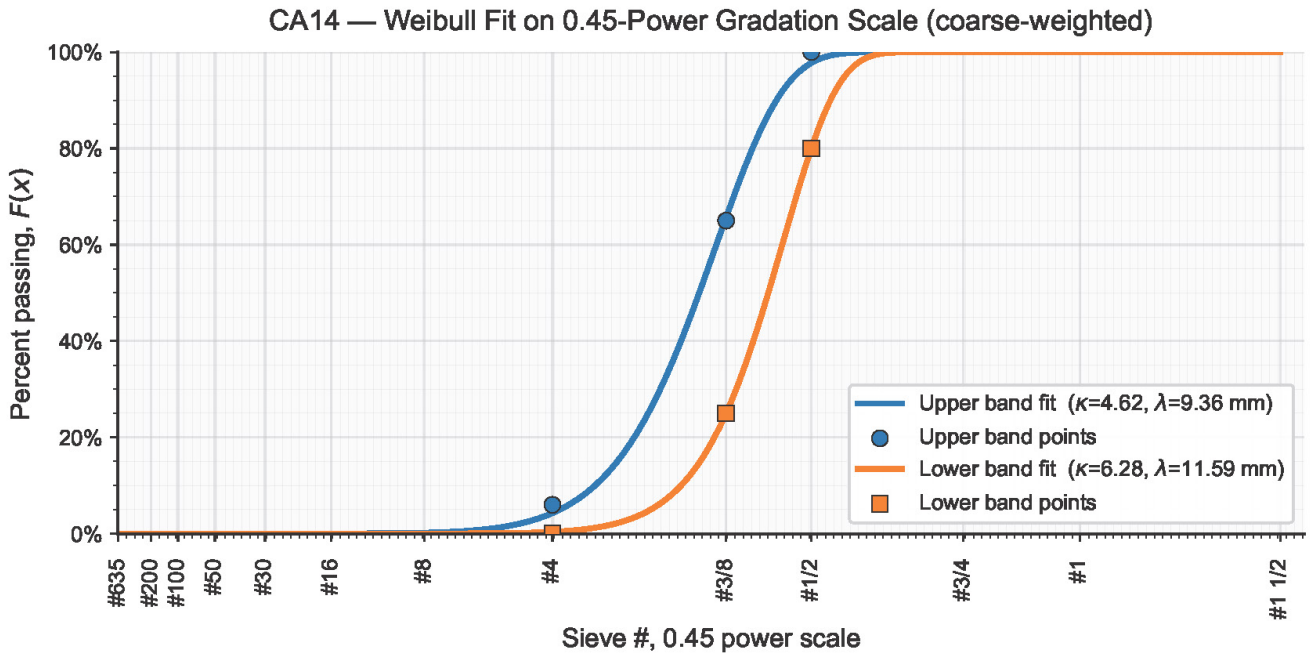

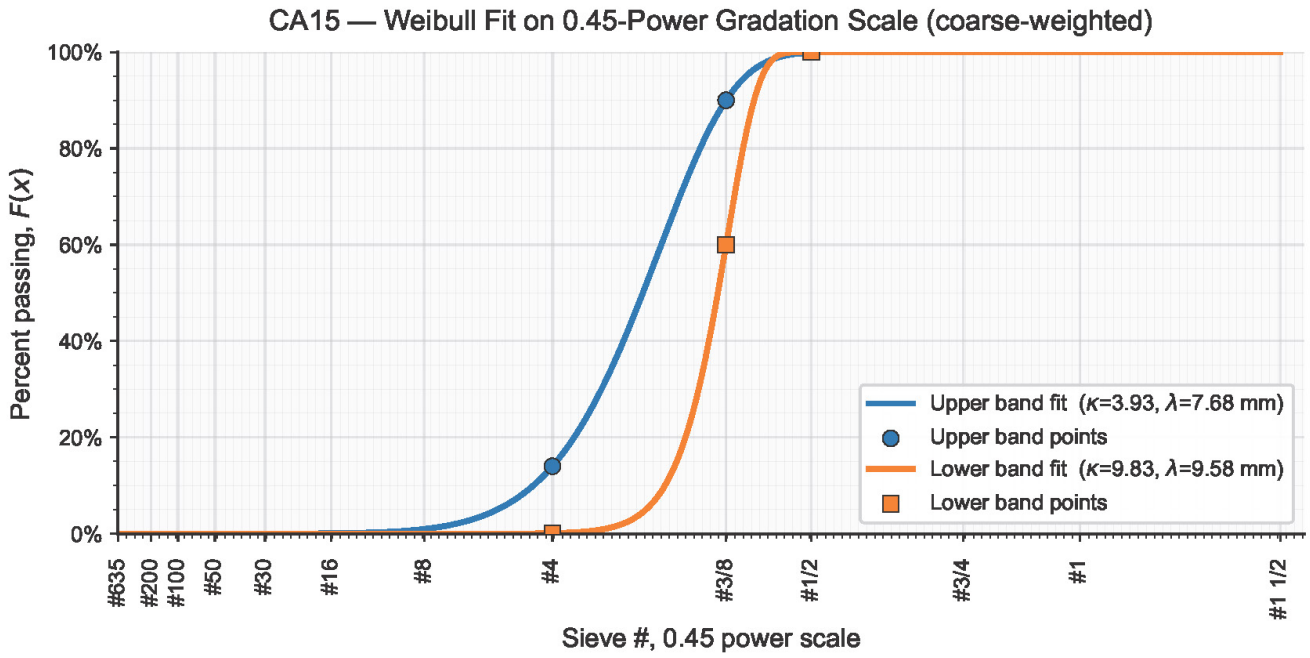

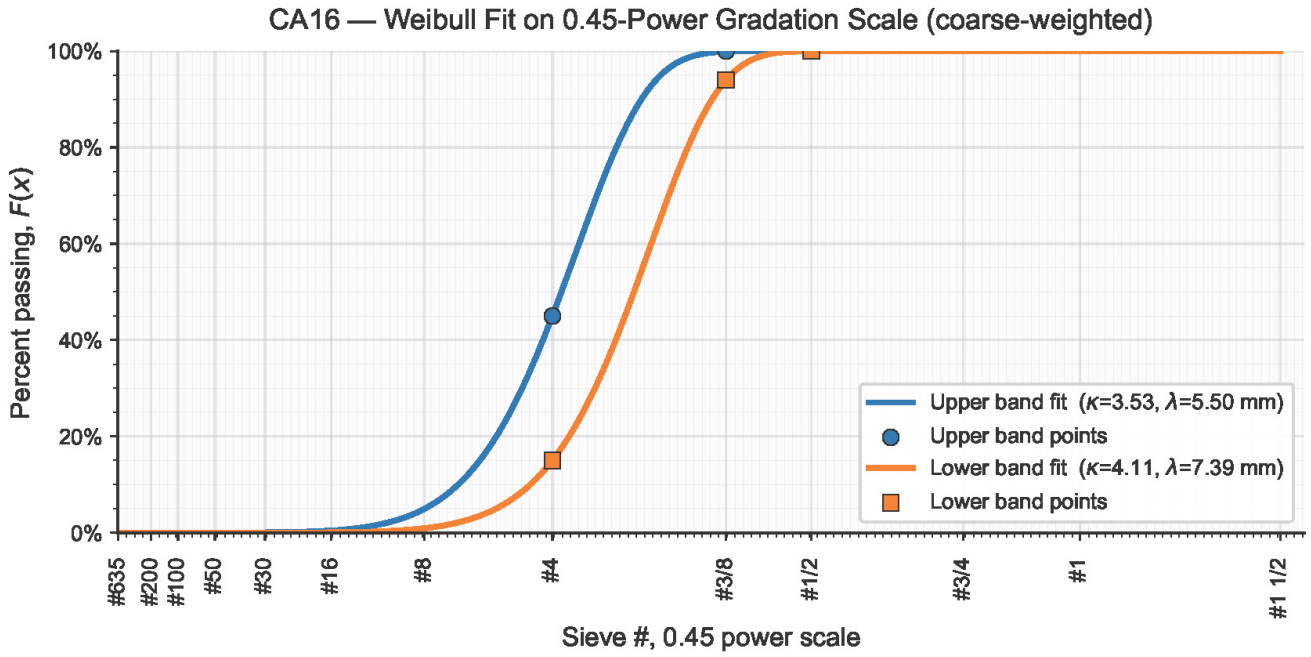
CA16 — Weibull Fit on 0.45-Power Gradation Scale (coarse-weighted)
Percent passing, F(x)
100%
80%
60%
40%
20%
0%
#635
#200
#100
#50
#30
#16
#8
#4
#3/8
#1/2
#3/4
#1
#1 1/2
Sieve #, 0.45 power scale
Upper band fit (κ=3.53, λ=5.50 mm)
Upper band points
Lower band fit (κ=4.11, λ=7.39 mm)
Lower band points

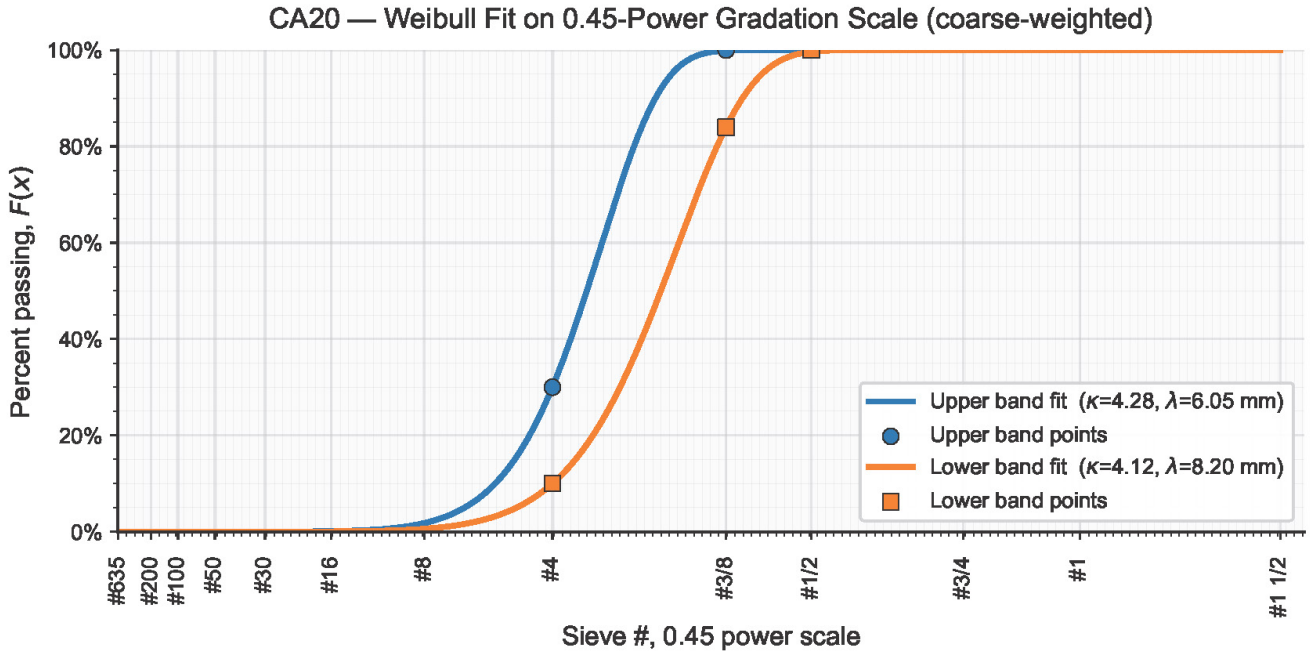
CA20 — Weibull Fit on 0.45-Power Gradation Scale (coarse-weighted)
Percent passing, F(x)
100%
80%
60%
40%
20%
0%
#635
#200
#100
#50
#30
#16
#8
#4
#3/8
#1/2
#3/4
#1
#1 1/2
Sieve #, 0.45 power scale
Upper band fit (κ=4.28, λ=6.05 mm)
Upper band points
Lower band fit (κ=4.12, λ=8.20 mm)
Lower band points

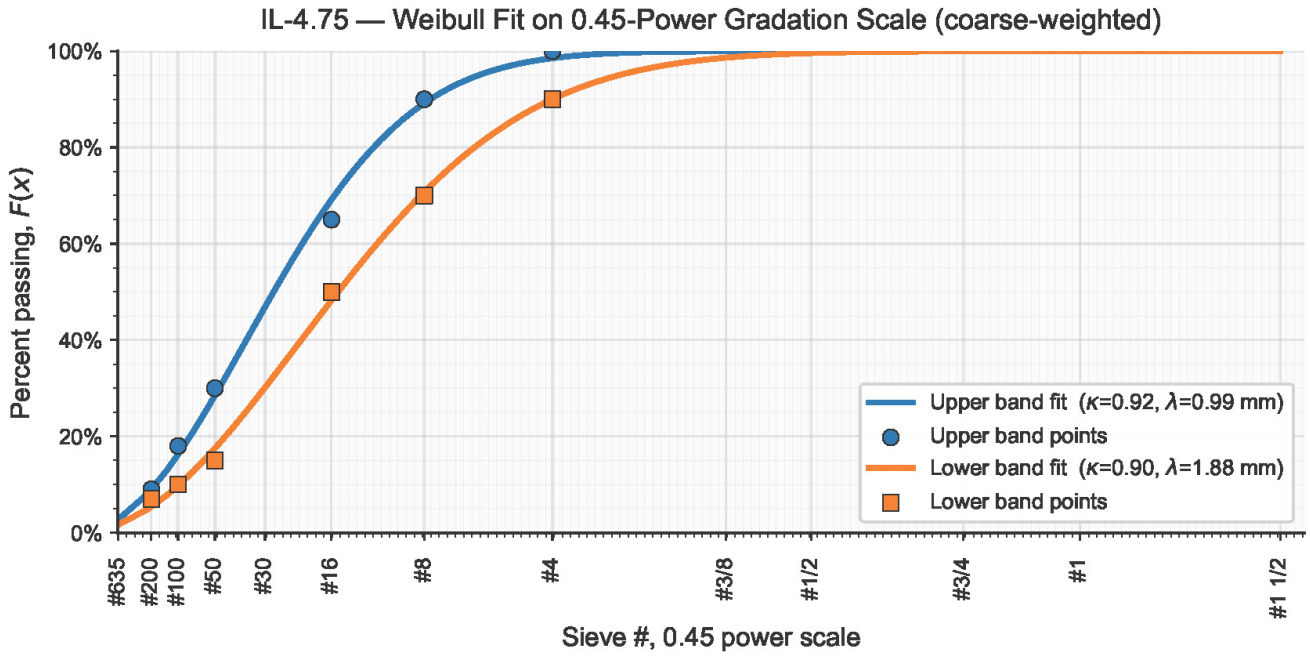
IL-4.75 — Weibull Fit on 0.45-Power Gradation Scale (coarse-weighted)
Percent passing, F(x)
100%
80%
60%
40%
20%
0%
#635
#200
#100
#50
#30
#16
#8
#4
#3/8
#1/2
#3/4
#1
#1 1/2
Sieve #, 0.45 power scale
Upper band fit (κ=0.92, λ=0.99 mm)
Upper band points
Lower band fit (κ=0.90, λ=1.88 mm)
Lower band points

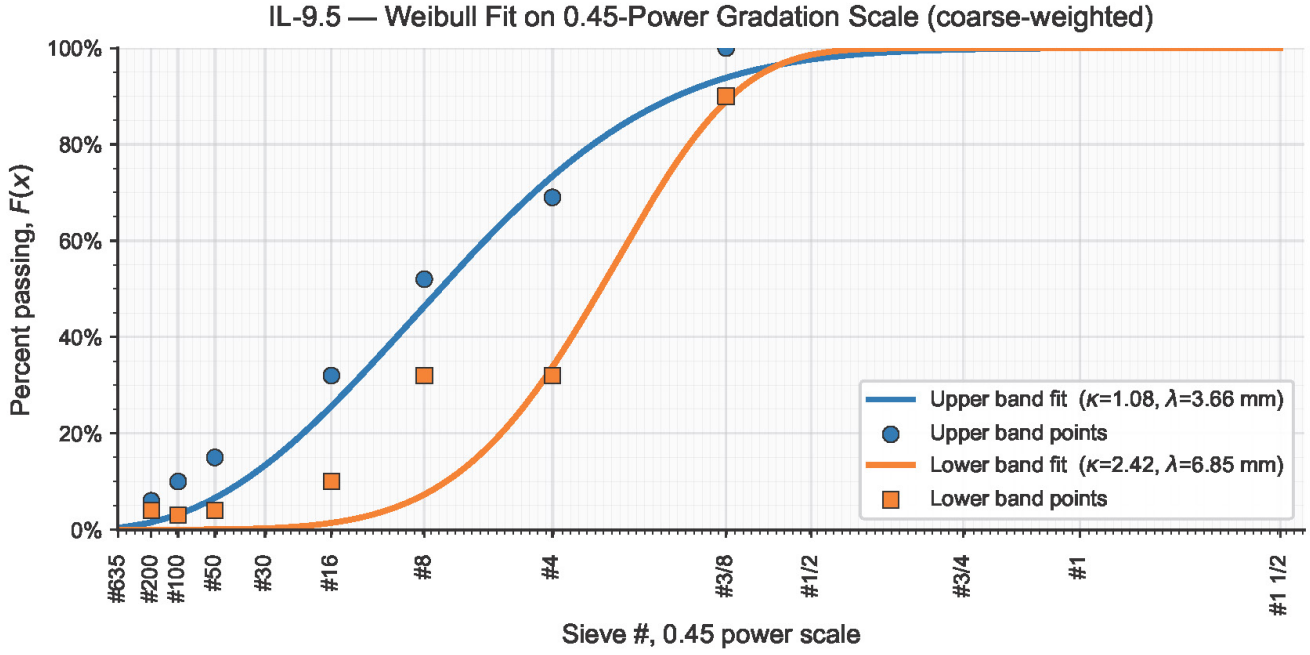
IL-9.5 — Weibull Fit on 0.45-Power Gradation Scale (coarse-weighted)
Percent passing, F(x)
100%
80%
60%
40%
20%
0%
#635
#200
#100
#50
#30
#16
#8
#4
#3/8
#1/2
#3/4
#1
#1 1/2
Sieve #, 0.45 power scale
Upper band fit (κ=1.08, λ=3.66 mm)
Upper band points
Lower band fit (κ=2.42, λ=6.85 mm)
Lower band points

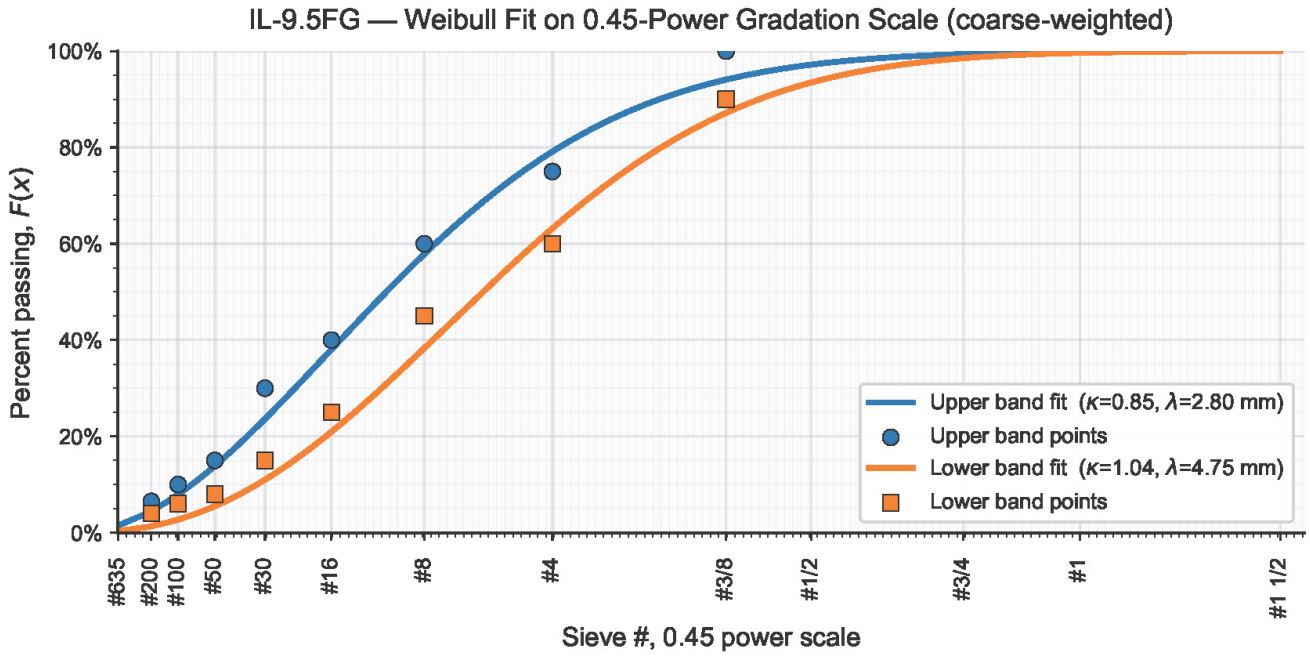
IL-9.5FG — Weibull Fit on 0.45-Power Gradation Scale (coarse-weighted)
Percent passing, F(x)
100%
80%
60%
40%
20%
0%
#635
#200
#100
#50
#30
#16
#8
#4
#3/8
#1/2
#3/4
#1
#1 1/2
Sieve #, 0.45 power scale
Upper band fit (κ=0.85, λ=2.80 mm)
Upper band points
Lower band fit (κ=1.04, λ=4.75 mm)
Lower band points

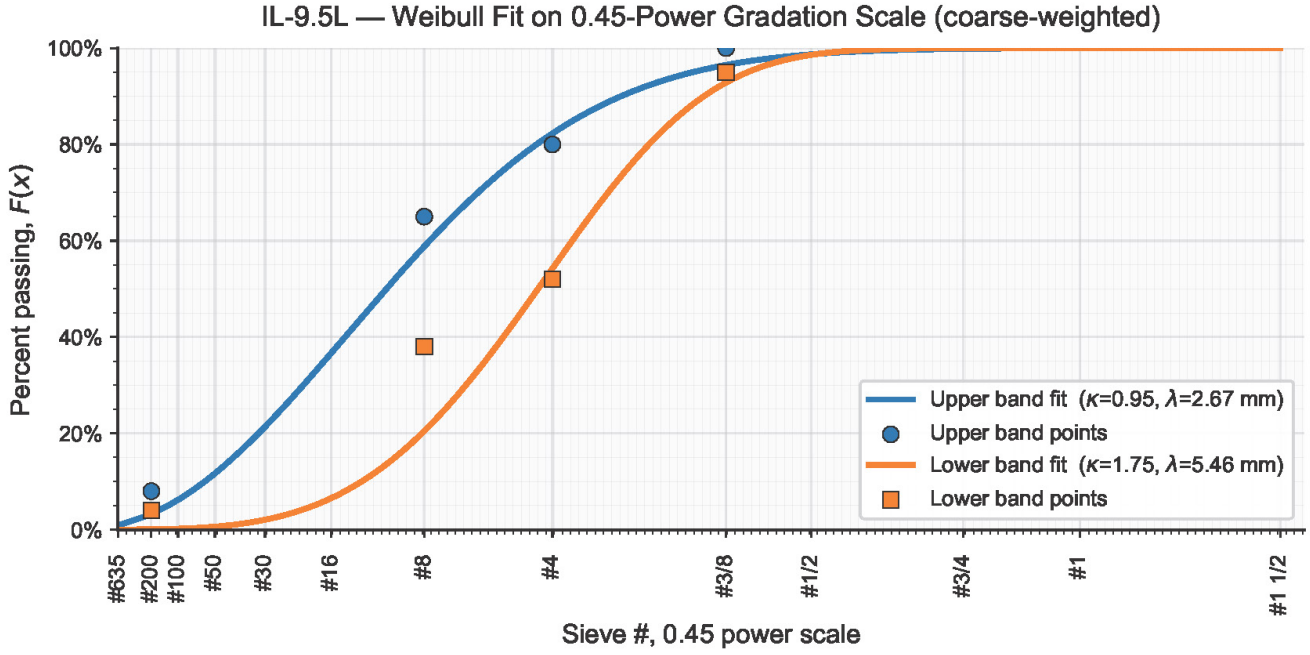
IL-9.5L — Weibull Fit on 0.45-Power Gradation Scale (coarse-weighted)
Percent passing, F(x)
100%
80%
60%
40%
20%
0%
#635
#200
#100
#50
#30
#16
#8
#4
#3/8
#1/2
#3/4
#1
#1 1/2
Sieve #, 0.45 power scale
Upper band fit (κ=0.95, λ=2.67 mm)
Upper band points
Lower band fit (κ=1.75, λ=5.46 mm)
Lower band points

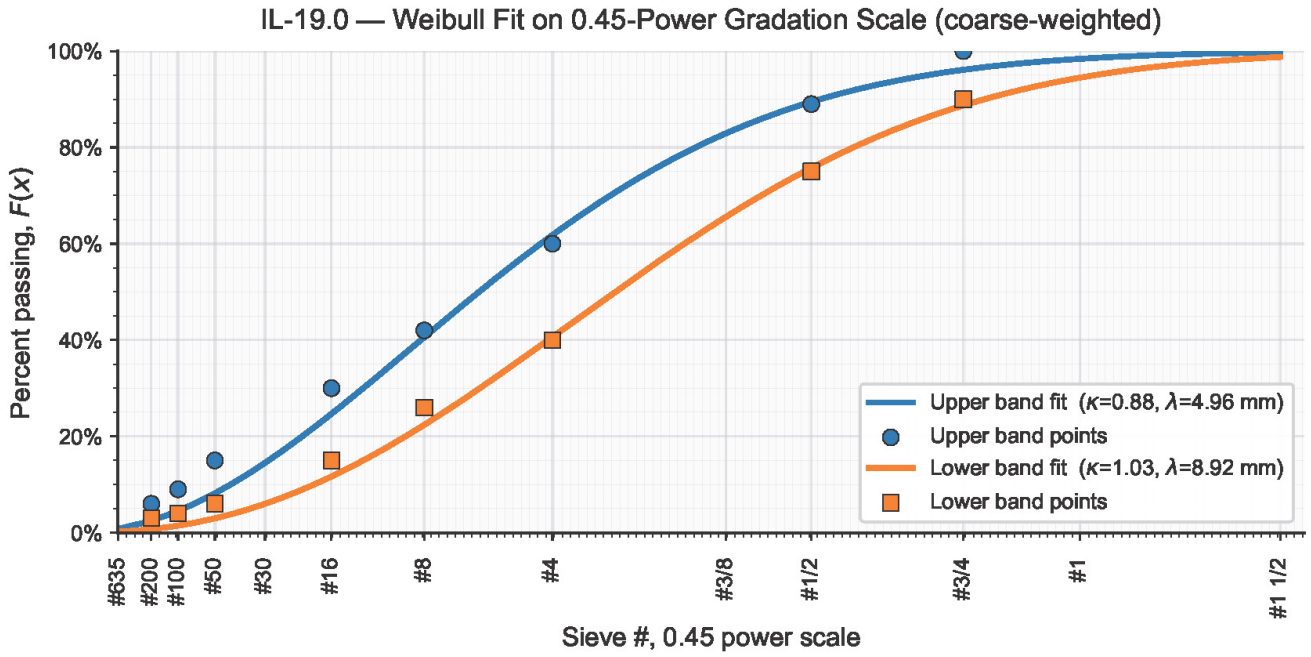
IL-19.0 — Weibull Fit on 0.45-Power Gradation Scale (coarse-weighted)
Percent passing, F(x)
100%
80%
60%
40%
20%
0%
#635
#200
#100
#50
#30
#16
#8
#4
#3/8
#1/2
#3/4
#1
#1 1/2
Sieve #, 0.45 power scale
Upper band fit (κ=0.88, λ=4.96 mm)
Upper band points
Lower band fit (κ=1.03, λ=8.92 mm)
Lower band points

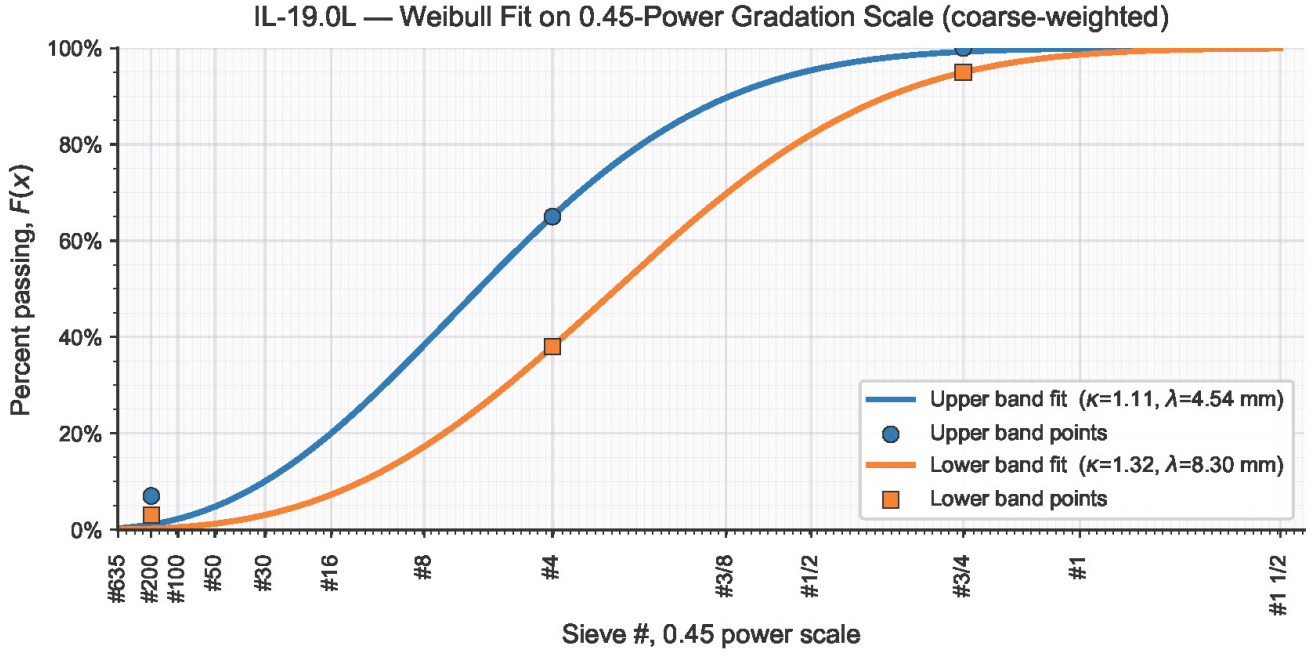
IL-19.0L — Weibull Fit on 0.45-Power Gradation Scale (coarse-weighted)
Percent passing, F(x)
100%
80%
60%
40%
20%
0%
#635
#200
#100
#50
#30
#16
#8
#4
#3/8
#1/2
#3/4
#1
#1 1/2
Sieve #, 0.45 power scale
Upper band fit (κ=1.11, λ=4.54 mm)
Upper band points
Lower band fit (κ=1.32, λ=8.30 mm)
Lower band points

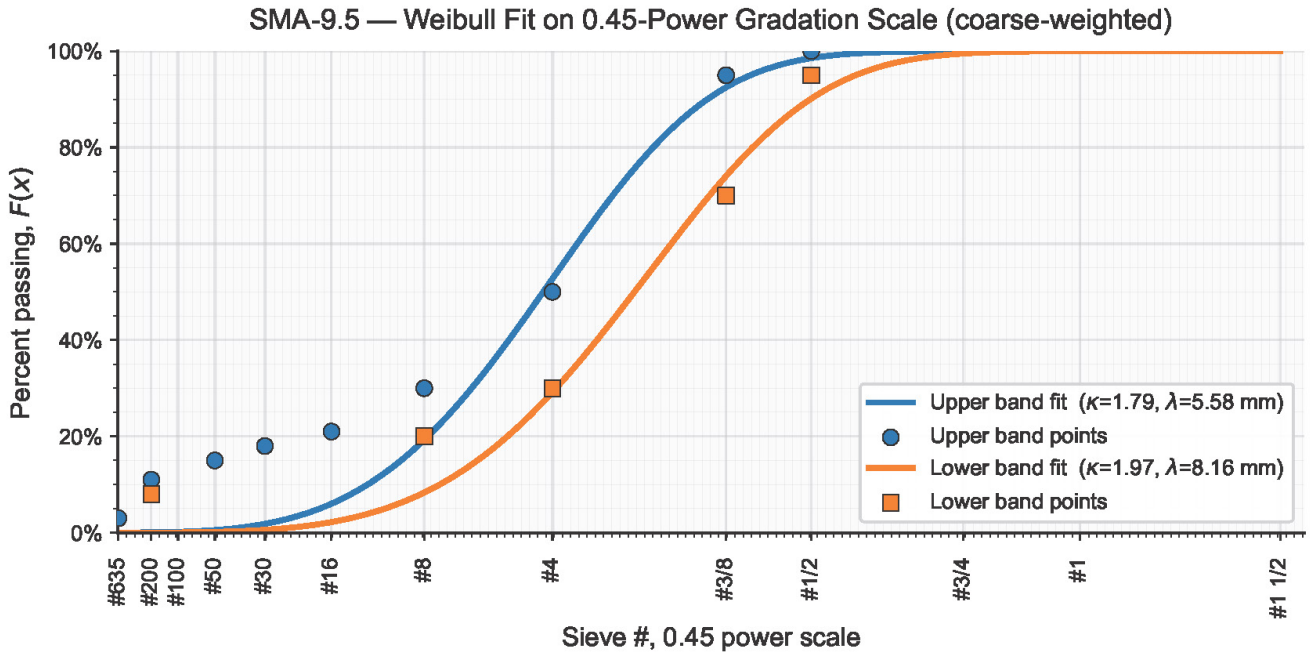
SMA-9.5 — Weibull Fit on 0.45-Power Gradation Scale (coarse-weighted)
Percent passing, F(x)
100%
80%
60%
40%
20%
0%
#635
#200
#100
#50
#30
#16
#8
#4
#3/8
#1/2
#3/4
#1
#1 1/2
Sieve #, 0.45 power scale
Upper band fit (κ=1.79, λ=5.58 mm)
Upper band points
Lower band fit (κ=1.97, λ=8.16 mm)
Lower band points

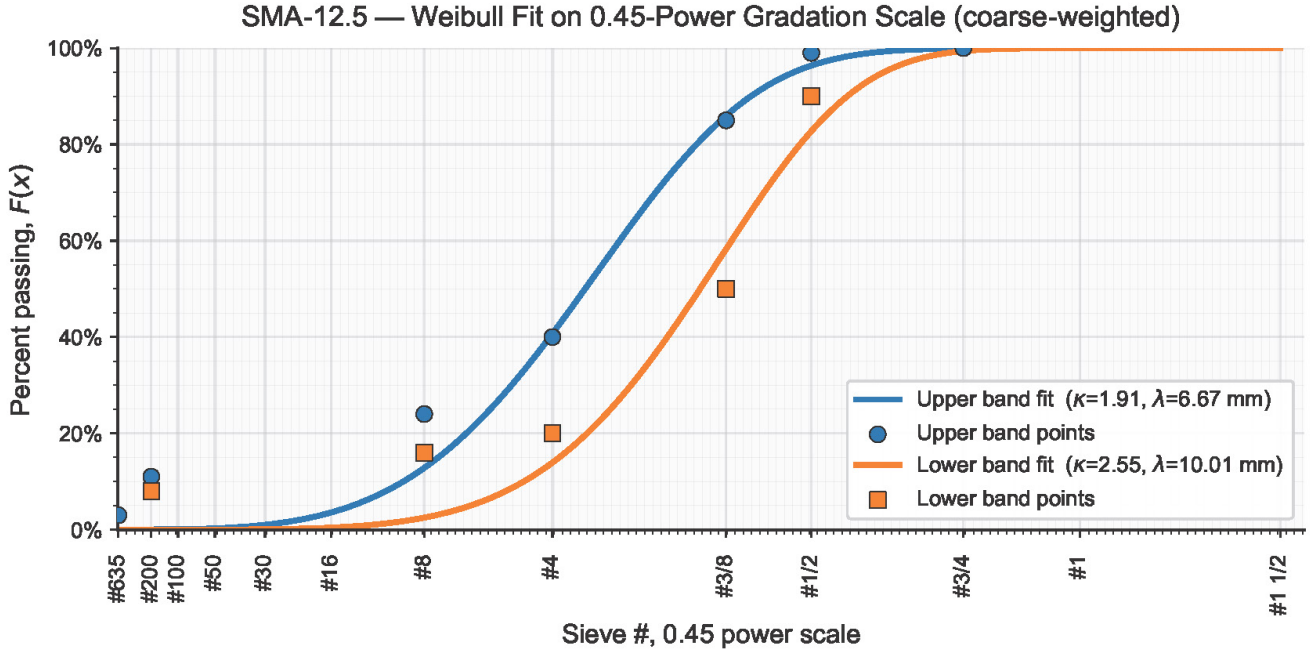
SMA-12.5 — Weibull Fit on 0.45-Power Gradation Scale (coarse-weighted)
Percent passing, F(x)
100%
80%
60%
40%
20%
0%
#635
#200
#100
#50
#30
#16
#8
#4
#3/8
#1/2
#3/4
#1
#1 1/2
Sieve #, 0.45 power scale
Upper band fit (κ=1.91, λ=6.67 mm)
Upper band points
Lower band fit (κ=2.55, λ=10.01 mm)
Lower band points

APPENDIX G: MPD ESTIMATION

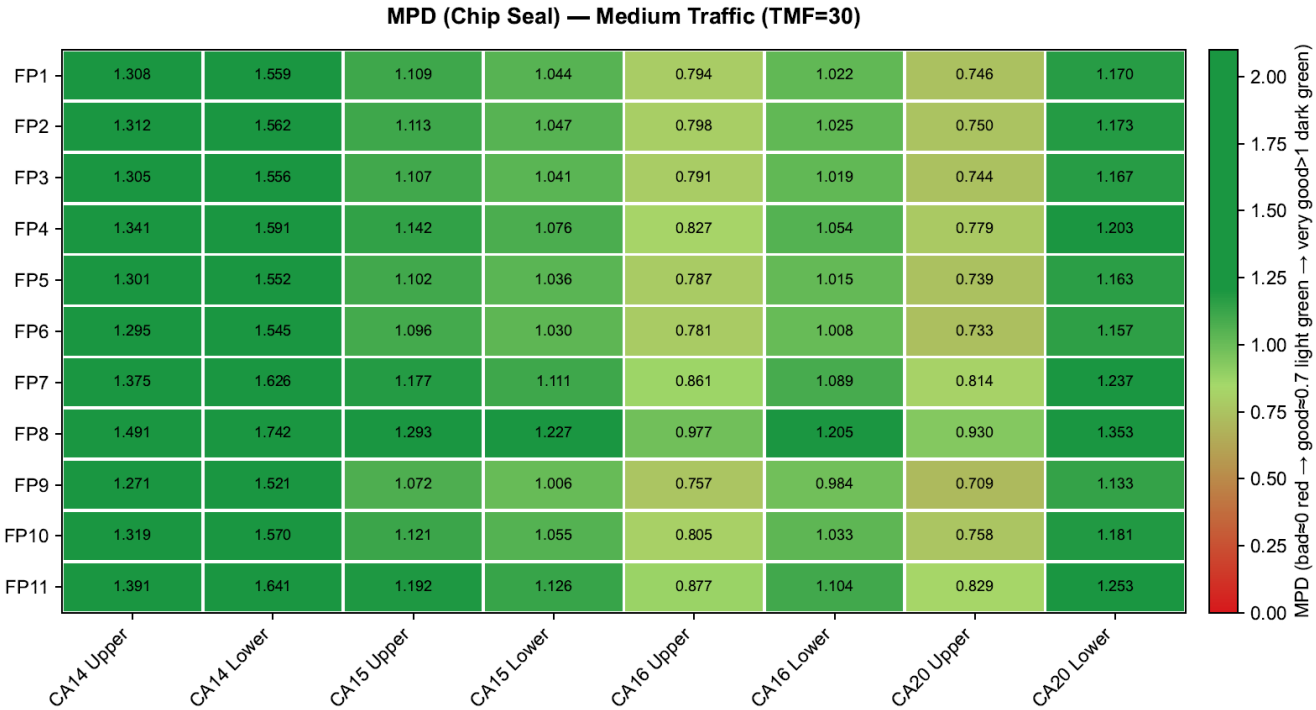

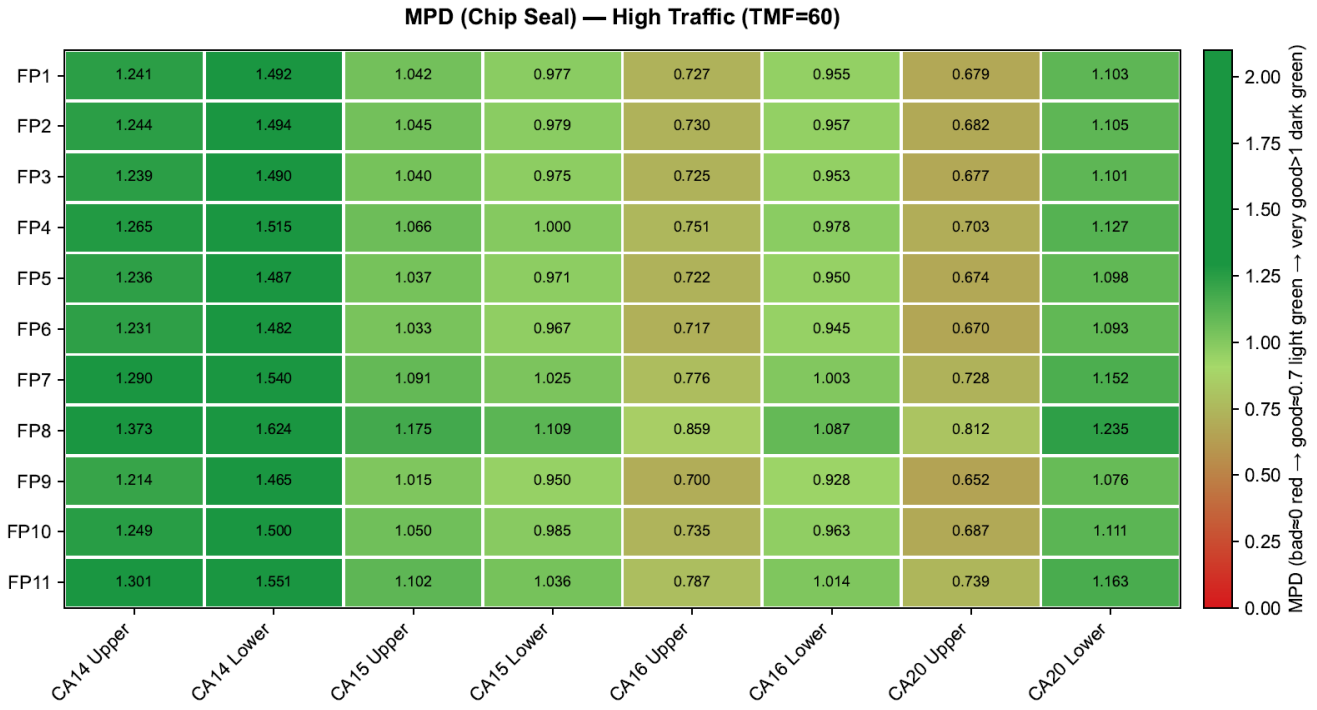
MPD (Chip Seal) — High Traffic (TMF=60)
FP1 1.241 1.492 1.042 0.977 0.727 0.955 0.679 1.103
FP2 1.244 1.494 1.045 0.979 0.730 0.957 0.682 1.105
FP3 1.239 1.490 1.040 0.975 0.725 0.953 0.677 1.101
FP4 1.265 1.515 1.066 1.000 0.751 0.978 0.703 1.127
FP5 1.236 1.487 1.037 0.971 0.722 0.950 0.674 1.098
FP6 1.231 1.482 1.033 0.967 0.717 0.945 0.670 1.093
FP7 1.290 1.540 1.091 1.025 0.776 1.003 0.728 1.152
FP8 1.373 1.624 1.175 1.109 0.859 1.087 0.812 1.235
FP9 1.214 1.465 1.015 0.950 0.700 0.928 0.652 1.076
FP10 1.249 1.500 1.050 0.985 0.735 0.963 0.687 1.111
FP11 1.301 1.551 1.102 1.036 0.787 1.014 0.739 1.163
CA14 Upper
CA14 Lower
CA15 Upper
CA15 Lower
CA16 Upper
CA16 Lower
CA20 Upper
CA20 Lower
MPD (bad≈0 red → good≈0.7 light green → very good>1 dark green)
2.00
1.75
1.50
1.25
1.00
0.75
0.50
0.25
0.00

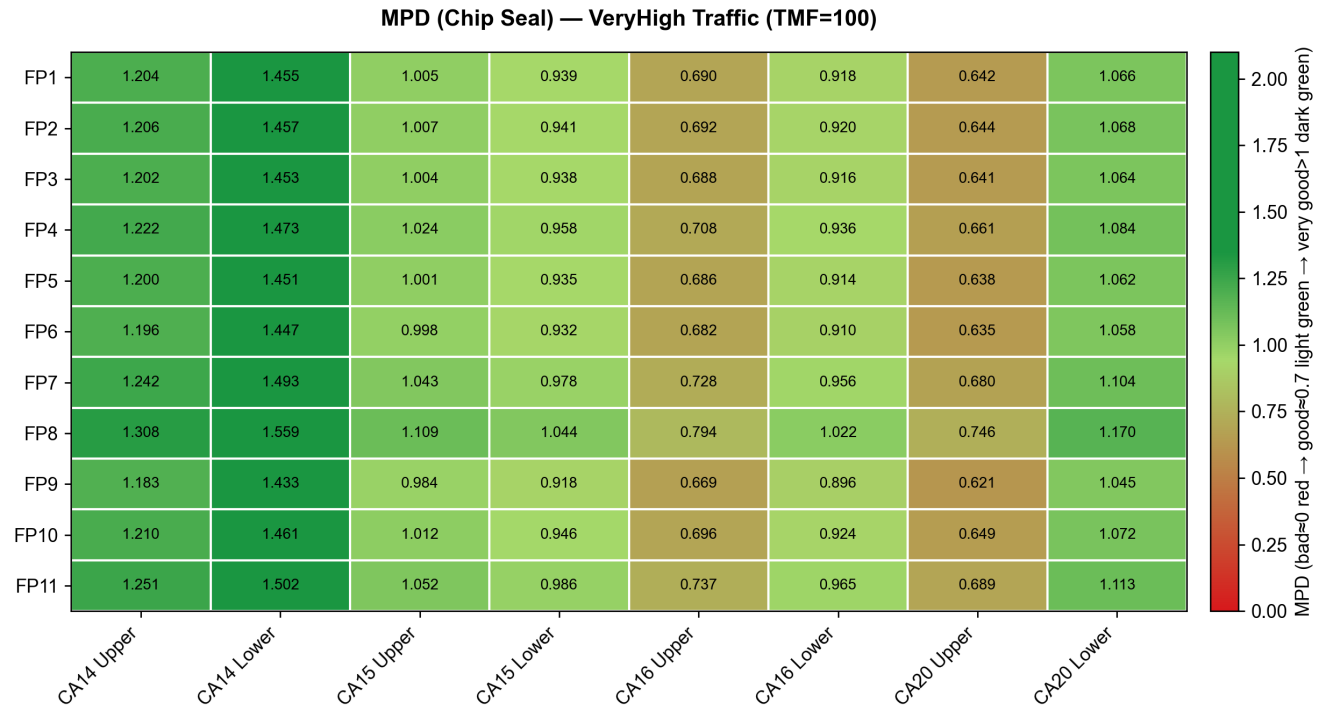
MPD (Chip Seal) — VeryHigh Traffic (TMF=100)
FP1 1.204 1.455 1.005 0.939 0.690 0.918 0.642 1.066
FP2 1.206 1.457 1.007 0.941 0.692 0.920 0.644 1.068
FP3 1.202 1.453 1.004 0.938 0.688 0.916 0.641 1.064
FP4 1.222 1.473 1.024 0.958 0.708 0.936 0.661 1.084
FP5 1.200 1.451 1.001 0.935 0.686 0.914 0.638 1.062
FP6 1.196 1.447 0.998 0.932 0.682 0.910 0.635 1.058
FP7 1.242 1.493 1.043 0.978 0.728 0.956 0.680 1.104
FP8 1.308 1.559 1.109 1.044 0.794 1.022 0.746 1.170
FP9 1.183 1.433 0.984 0.918 0.669 0.896 0.621 1.045
FP10 1.210 1.461 1.012 0.946 0.696 0.924 0.649 1.072
FP11 1.251 1.502 1.052 0.986 0.737 0.965 0.689 1.113
CA14 Upper
CA14 Lower
CA15 Upper
CA15 Lower
CA16 Upper
CA16 Lower
CA20 Upper
CA20 Lower
MPD (bad≈0 red → good≈0.7 light green → very good>1 dark green)
2.00
1.75
1.50
1.25
1.00
0.75
0.50
0.25
0.00

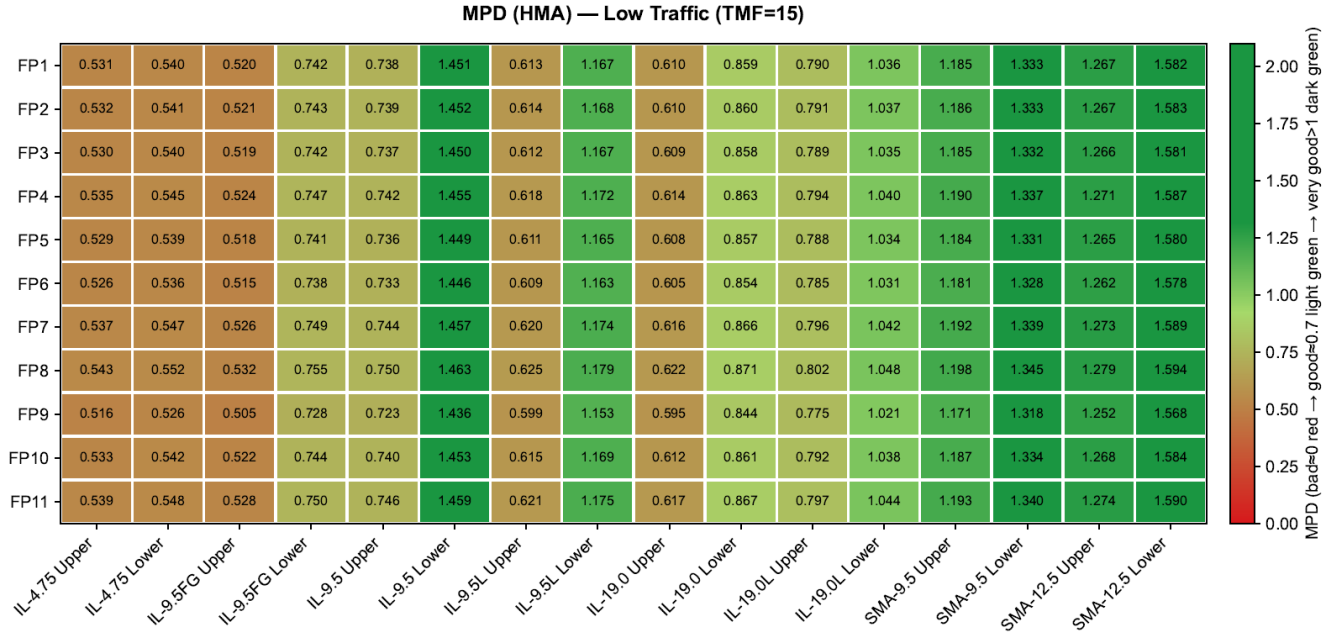
MPD (HMA) — Low Traffic (TMF=15)
FP1 0.531 0.540 0.520 0.742 0.738 1.451 0.613 1.167 0.610 0.859 0.790 1.036 1.185 1.333 1.267 1.582
FP2 0.532 0.541 0.521 0.743 0.739 1.452 0.614 1.168 0.610 0.860 0.791 1.037 1.186 1.333 1.267 1.583
FP3 0.530 0.540 0.519 0.742 0.737 1.450 0.612 1.167 0.609 0.858 0.789 1.035 1.185 1.332 1.266 1.581
FP4 0.535 0.545 0.524 0.747 0.742 1.455 0.618 1.172 0.614 0.863 0.794 1.040 1.190 1.337 1.271 1.587
FP5 0.529 0.539 0.518 0.741 0.736 1.449 0.611 1.165 0.608 0.857 0.788 1.034 1.184 1.331 1.265 1.580
FP6 0.526 0.536 0.515 0.738 0.733 1.446 0.609 1.163 0.605 0.854 0.785 1.031 1.181 1.328 1.262 1.578
FP7 0.537 0.547 0.526 0.749 0.744 1.457 0.620 1.174 0.616 0.866 0.796 1.042 1.192 1.339 1.273 1.589
FP8 0.543 0.552 0.532 0.755 0.750 1.463 0.625 1.179 0.622 0.871 0.802 1.048 1.198 1.345 1.279 1.594
FP9 0.516 0.526 0.505 0.728 0.723 1.436 0.599 1.153 0.595 0.844 0.775 1.021 1.171 1.318 1.252 1.568
FP10 0.533 0.542 0.522 0.744 0.740 1.453 0.615 1.169 0.612 0.861 0.792 1.038 1.187 1.334 1.268 1.584
FP11 0.539 0.548 0.528 0.750 0.746 1.459 0.621 1.175 0.617 0.867 0.797 1.044 1.193 1.340 1.274 1.590
IL-4.75 Upper
IL-4.75 Lower
IL-9.5FG Upper
IL-9.5FG Lower
IL-9.5 Upper
IL-9.5 Lower
IL-9.5L Upper
IL-9.5L Lower
IL-19.0 Upper
IL-19.0 Lower
IL-19.0L Upper
IL-19.0L Lower
SMA-9.5 Upper
SMA-9.5 Lower
SMA-12.5 Upper
SMA-12.5 Lower
2.00
1.75
1.50
1.25
1.00
0.75
0.50
0.25
0.00
MPD (bad=0 red → good=0.7 light green → very good>1 dark green)


MPD (HMA) — Medium Traffic (TMF=30)
FP1 0.501 0.511 0.490 0.713 0.708 1.421 0.583 1.138 0.580 0.829 0.760 1.006 1.156 1.303 1.237 1.552
FP2 0.503 0.512 0.492 0.715 0.710 1.423 0.585 1.139 0.582 0.831 0.762 1.008 1.158 1.305 1.239 1.554
FP3 0.500 0.510 0.489 0.712 0.707 1.420 0.582 1.137 0.579 0.828 0.759 1.005 1.155 1.302 1.236 1.551
FP4 0.510 0.520 0.499 0.722 0.717 1.430 0.593 1.147 0.589 0.839 0.769 1.015 1.165 1.312 1.246 1.562
FP5 0.498 0.507 0.487 0.710 0.705 1.418 0.580 1.134 0.577 0.826 0.757 1.003 1.153 1.300 1.234 1.549
FP6 0.492 0.502 0.481 0.704 0.699 1.412 0.575 1.129 0.571 0.820 0.751 0.997 1.147 1.294 1.228 1.544
FP7 0.515 0.524 0.504 0.726 0.722 1.435 0.597 1.151 0.593 0.843 0.773 1.020 1.169 1.316 1.250 1.566
FP8 0.526 0.535 0.515 0.737 0.733 1.446 0.608 1.162 0.604 0.854 0.785 1.031 1.180 1.327 1.261 1.577
FP9 0.472 0.482 0.461 0.684 0.679 1.392 0.555 1.109 0.551 0.800 0.731 0.977 1.127 1.274 1.208 1.524
FP10 0.505 0.514 0.494 0.717 0.712 1.425 0.587 1.141 0.584 0.833 0.764 1.010 1.160 1.307 1.241 1.556
FP11 0.517 0.526 0.506 0.728 0.724 1.437 0.599 1.153 0.596 0.845 0.776 1.022 1.172 1.319 1.253 1.568
IL-4.75 Upper
IL-4.75 Lower
IL-9.5FG Upper
IL-9.5FG Lower
IL-9.5 Upper
IL-9.5 Lower
IL-9.5L Upper
IL-9.5L Lower
IL-19.0 Upper
IL-19.0 Lower
IL-19.0L Upper
IL-19.0L Lower
SMA-9.5 Upper
SMA-9.5 Lower
SMA-12.5 Upper
SMA-12.5 Lower
2.00
1.75
1.50
1.25
1.00
0.75
0.50
0.25
0.00
MPD (bad=0 red → good=0.7 light green → very good>1 dark green)

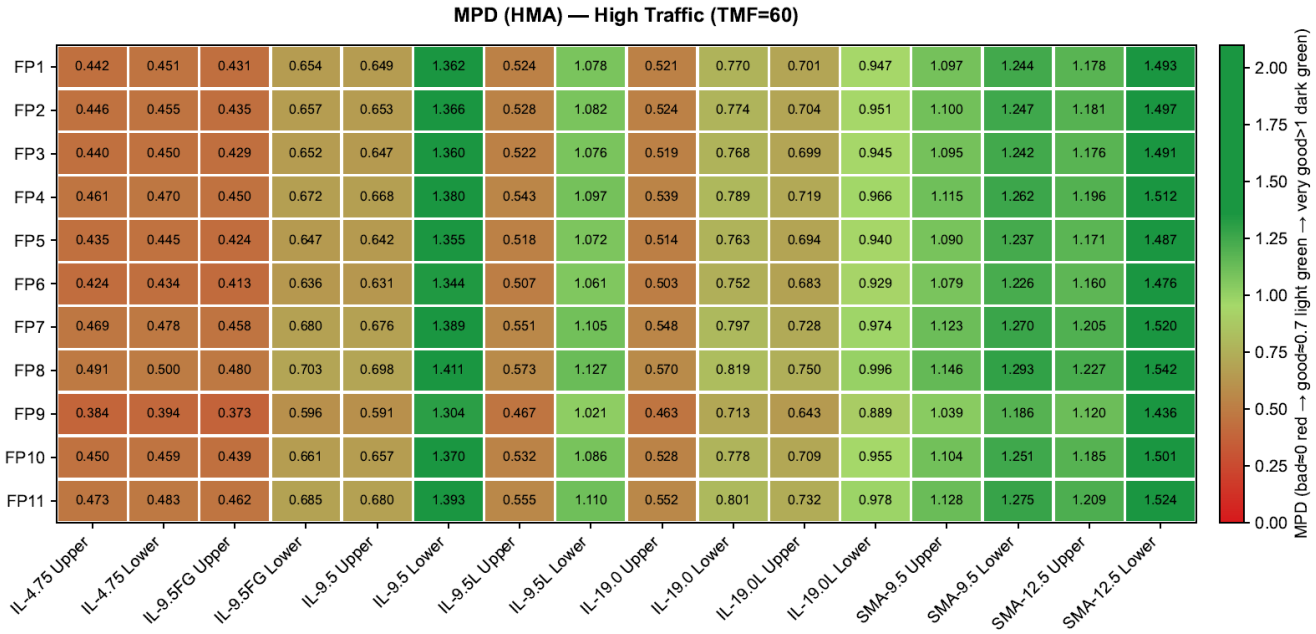
MPD (HMA) — High Traffic (TMF=60)
FP1 0.442 0.451 0.431 0.654 0.649 1.362 0.524 1.078 0.521 0.770 0.701 0.947 1.097 1.244 1.178 1.493
FP2 0.446 0.455 0.435 0.657 0.653 1.366 0.528 1.082 0.524 0.774 0.704 0.951 1.100 1.247 1.181 1.497
FP3 0.440 0.450 0.429 0.652 0.647 1.360 0.522 1.076 0.519 0.768 0.699 0.945 1.095 1.242 1.176 1.491
FP4 0.461 0.470 0.450 0.672 0.668 1.380 0.543 1.097 0.539 0.789 0.719 0.966 1.115 1.262 1.196 1.512
FP5 0.435 0.445 0.424 0.647 0.642 1.355 0.518 1.072 0.514 0.763 0.694 0.940 1.090 1.237 1.171 1.487
FP6 0.424 0.434 0.413 0.636 0.631 1.344 0.507 1.061 0.503 0.752 0.683 0.929 1.079 1.226 1.160 1.476
FP7 0.469 0.478 0.458 0.680 0.676 1.389 0.551 1.105 0.548 0.797 0.728 0.974 1.123 1.270 1.205 1.520
FP8 0.491 0.500 0.480 0.703 0.698 1.411 0.573 1.127 0.570 0.819 0.750 0.996 1.146 1.293 1.227 1.542
FP9 0.384 0.394 0.373 0.596 0.591 1.304 0.467 1.021 0.463 0.713 0.643 0.889 1.039 1.186 1.120 1.436
FP10 0.450 0.459 0.439 0.661 0.657 1.370 0.532 1.086 0.528 0.778 0.709 0.955 1.104 1.251 1.185 1.501
FP11 0.473 0.483 0.462 0.685 0.680 1.393 0.555 1.110 0.552 0.801 0.732 0.978 1.128 1.275 1.209 1.524
IL-4.75 Upper
IL-4.75 Lower
IL-9.5FG Upper
IL-9.5FG Lower
IL-9.5 Upper
IL-9.5 Lower
IL-9.5L Upper
IL-9.5L Lower
IL-19.0 Upper
IL-19.0 Lower
IL-19.0L Upper
IL-19.0L Lower
SMA-9.5 Upper
SMA-9.5 Lower
SMA-12.5 Upper
SMA-12.5 Lower
2.00
1.75
1.50
1.25
1.00
0.75
0.50
0.25
0.00
MPD (bad=0 red → good=0.7 light green → very good>1 dark green)

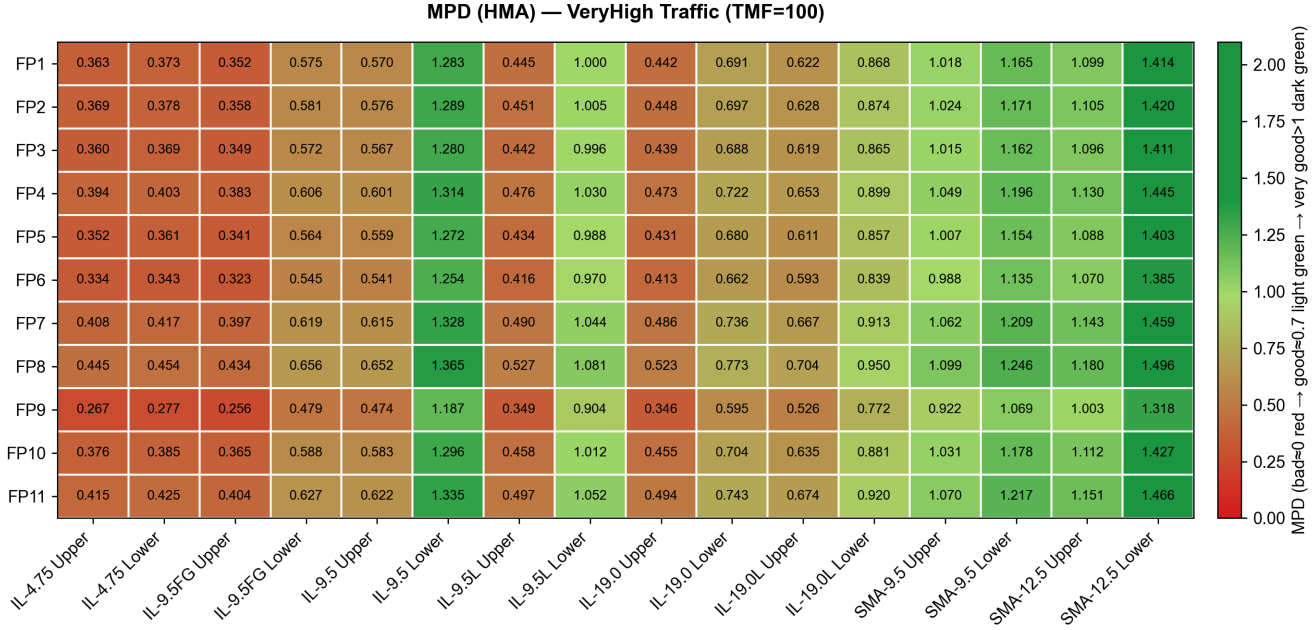
MPD (HMA) — VeryHigh Traffic (TMF=100)
FP1 0.363 0.373 0.352 0.575 0.570 1.283 0.445 1.000 0.442 0.691 0.622 0.868 1.018 1.165 1.099 1.414
FP2 0.369 0.378 0.358 0.581 0.576 1.289 0.451 1.005 0.448 0.697 0.628 0.874 1.024 1.171 1.105 1.420
FP3 0.360 0.369 0.349 0.572 0.567 1.280 0.442 0.996 0.439 0.688 0.619 0.865 1.015 1.162 1.096 1.411
FP4 0.394 0.403 0.383 0.606 0.601 1.314 0.476 1.030 0.473 0.722 0.653 0.899 1.049 1.196 1.130 1.445
FP5 0.352 0.361 0.341 0.564 0.559 1.272 0.434 0.988 0.431 0.680 0.611 0.857 1.007 1.154 1.088 1.403
FP6 0.334 0.343 0.323 0.545 0.541 1.254 0.416 0.970 0.413 0.662 0.593 0.839 0.988 1.135 1.070 1.385
FP7 0.408 0.417 0.397 0.619 0.615 1.328 0.490 1.044 0.486 0.736 0.667 0.913 1.062 1.209 1.143 1.459
FP8 0.445 0.454 0.434 0.656 0.652 1.365 0.527 1.081 0.523 0.773 0.704 0.950 1.099 1.246 1.180 1.496
FP9 0.267 0.277 0.256 0.479 0.474 1.187 0.349 0.904 0.346 0.595 0.526 0.772 0.922 1.069 1.003 1.318
FP10 0.376 0.385 0.365 0.588 0.583 1.296 0.458 1.012 0.455 0.704 0.635 0.881 1.031 1.178 1.112 1.427
FP11 0.415 0.425 0.404 0.627 0.622 1.335 0.497 1.052 0.494 0.743 0.674 0.920 1.070 1.217 1.151 1.466
IL-4.75 Upper
IL-4.75 Lower
IL-9.5FG Upper
IL-9.5FG Lower
IL-9.5 Upper
IL-9.5 Lower
IL-9.5L Upper
IL-9.5L Lower
IL-19.0 Upper
IL-19.0 Lower
IL-19.0L Upper
IL-19.0L Lower
SMA-9.5 Upper
SMA-9.5 Lower
SMA-12.5 Upper
SMA-12.5 Lower
2.00
1.75
1.50
1.25
1.00
0.75
0.50
0.25
0.00
MPD (bad=0 red → good=0.7 light green → very good>1 dark green)


Illinois Department
of Transportation


ILLINOIS